Title

In Vivo Characterization of CLR01, an Aggregation and Toxicity Inhibitor, with an Alzheimer's Disease Focus

Author

Attar, Aida

Publication Date

2013

Peer reviewed|Thesis/dissertation

UNIVERSITY OF CALIFORNIA

Los Angeles

In Vivo Characterization of CLR01, an Aggregation and Toxicity Inhibitor, with an Alzheimer's Disease Focus

A dissertation submitted in satisfaction of the requirements for

a Doctor of Philosophy degree

in Neuroscience

By

Aida Attar

2014

ABSTRACT OF THE DISSERTATION

In Vivo Characterization of CLR01, an Aggregation and Toxicity Inhibitor, with an Alzheimer's Disease Focus

By

Aida Attar

Doctor of Philosophy in Neuroscience

University of California-Los Angeles

2014

Professor Gal Bitan, Chair

Aberrant protein self-assembly underlies over 30 human diseases called amyloidoses, for which there are no cures. In these diseases, particular proteins misfold and self-assemble into toxic oligomers that disrupt cellular function, and proceed to form insoluble amyloid fibrils that deposit in specific tissues. A promising strategy for preventing and treating amyloidoses is inhibition or modulation of the self-assembly process to disrupt the formation of the toxic oligomers. In practice, this has proven immensely difficult because the oligomer structures are unknown, are metastable, and do not have distinct binding sites.

In this dissertation, three primary studies are presented that evaluate and characterize a small molecule, CLR01, which utilizes a novel strategy circumventing these challenges and has been found to be efficacious as an aggregation and toxicity inhibitor *in vitro* and *in vivo*. In the first study, CLR01 was evaluated for its ability to rescue synaptic toxicity in cell culture and brain slices. Additionally, it was tested in a transgenic mouse model of AD for its ability to reduce the pathological hallmarks of AD − amyloid plaques and neurofibrillary tangles. This study found positive results in all domains tested; a rescue from amyloid β-protein (Aβ)-induced depletion of synaptic spine density, a rescue of Aβ-induced disruption of basal synaptic transmission and long-term potentiation, and reduction of brain Aβ, hyperphosphorylated tau, and microglia burden. CLR01 also showed low propensity for causing metabolic toxicity or drug-drug interaction, indicating favorable drug-like characteristics.

In the second study, CLR01's safety and pharmacological profile were characterized in mice. CLR01 was found not to disrupt normal protein assembly, to have a high safety margin in mice, and to penetrate the blood-brain barrier (BBB) at 1−3%. Interestingly, brain levels of CLR01 remained stable for 72 hours following administration despite rapid clearance from the plasma. These results suggest a large safety margin for CLR01 and a pharmacokinetic profile that allows reaching high levels in the brain by administering relatively low doses.

The third study delineates a detailed optimization of behavioral testing of mice for detection of memory deficits using the Barnes maze, and validates for the first time memory deficits in a triple-transgenic mouse model of AD at the youngest age described in the literature. The study provides a framework for analysis of CLR01's influence on

learning and memory deficits in this triple transgenic model. Additionally, the study provides specific and detailed guidelines for optimizing both the performance and the analysis of the Barnes maze in a manner that increases the likelihood of detecting subtle changes in future studies using mouse models of AD. The work described in this dissertation provides a strong foundation supporting formal pre-clinical development of CLR01 as a promising disease-modifying therapeutic drug for AD.

COMMITTEE PAGE

The dissertation of Aida Attar is approved.

Marie-Francoise Chesselet

Joseph B Watson

Karen H Gylys

Edmond H Teng

Gal Bitan, Committee Chair

University of California, Los Angeles

2014

DEDICATION PAGE

This dissertation is dedicated to my mother, Parvin Deivari, and my father, Fereidoun Attar, for their courageous sacrifices to give up an established and comfortable life in Iran and start from scratch in the United States. Without their audacity, strength, and dedication to providing the best opportunities for their children, none of the countless opportunities that I have been afforded to allow me to reach this stage in my life would have been possible. They have my eternal gratitude.

TABLE OF CONTENTS

LIST OF FIGURES AND TABLES

Chapter 1: Alzheimer's Disease and Therapies

Chapter 2: Disrupting Self-Assembly and Toxicity of Amyloidogenic Protein Oligomers by "Molecular Tweezers" – from the Test Tube to Animal Model

Ch3: Protection of primary neurons and mouse brain from Alzheimer's pathology by molecular tweezers

Ch4: Safety and pharmacological characterization of the molecular tweezer CLR01

Ch5: A Shortened Barnes Maze Protocol Reveals Memory Deficits at 4-Months of Age in the Triple-Transgenic Mouse Model of Alzheimer's Disease

ABBREVIATIONS

3×Tg − triple-transgenic
^{3}H-CLR01 − tritium-labeled CLR01
Aβ – amyloid β-protein
Aβ40 − 40-residue isoform of amyloid β-protein
Aβ42 − 42-residue isoform of amyloid β-protein
AChEIs – acetylcholine esterase inhibitors
AD – Alzheimer's Disease
ALP – Alkaline phosphatase
AMPA − 2-amino-3-(5-methyl-3-oxo-1 2- oxazol-4-yl)propanoic acid
ANOVA – analysis of variance
APOE – apolipoprotein E
APP – amyloid β-protein precursor
ATP – adenosine triphosphate
BBB − blood-brain barrier
CA1 – *cornu ammonis* 1
CD – circular dichroism
CHC – central hydrophobic cluster
CNS – central nervous system
CPM – Counts per minute
CSF – cerebrospinal fluid
CTFs − C-terminal fragments
CYP450 − cytochrome P450
DLAM – Division of laboratory animal medicine
DLS – dynamic light scattering,
EGCG – epigallocatechin-3-gallate
EM – electron microscopy
EPSCs − excitatory postsynaptic currents
FDG – fluorodeoxyglucose
fEPSP – field excitatory postsynaptic potential
HFS – high-frequency stimulation
hpf – hours post fertilization
HS – holes searched
IAPP – islet amyloid polypeptide
Lac – lactacystin
IC_{50} – half-maximal inhibition concentration
IP – Intraperitoneal
IV – intravenous
LC-MS – liquid chromatography-mass spectrometry
LDH – lactate dehydrogenase
LTP – long-term potentiation
mAb – monoclonal antibody
MARK - microtubule affinity-regulating kinase
MCI – mild cognitive impairment
mEPSC – miniature excitatory postsynaptic currents
MRI – magnetic resonance imaging
MTs – molecular tweezers
MTT – 3-(4 5-dimethylthiazol-2-yl)-2 5-diphenyltetrazolium bromide
MWM – Morris water maze
NFTs – neurofibrillary tangles
NMDA – N-methyl-D-aspartate
p-tau − hyperphosphorylated-tau
PC-12 – rat pheochromocytoma
PD – Parkinson's disease
PET – positron emission tomography
PHF – paired helical filaments
PrP – prion protein
PSEN – presenilin
PXR − pregnane X receptor
ROS – reactive oxygen species
sAPP − soluble amyloid β-protein precursor
SC – subcutaneous
SDS-PAGE – sodium dodecyl sulphate-polyacrylamide gel electrophoresis
SEM – standard error of the mean
SI – *scyllo*-inositol
α-syn – α-synuclein
ThT – thioflavin T
UPS – 26S ubiquitin-proteasome system
WT – wild-type
ZF - zebrafish

ACKNOWLEDGEMENTS

People

I would like to express my deepest appreciation to my committee chair, mentor, and friend, Dr. Gal Bitan, whose ideas, guidance, and support over the last six years have been invaluable and absolutely indispensible. His endless patience, encouragement, trust, and accommodation for free and open discussion not only helped shape and strengthen my research but also promoted my personal growth. I feel so lucky and privileged to have had the opportunity to work with Gal on a project that we are both very passionate about.

I would like to thank my many collaborators, especially Sally Frautschy who was particularly vital early in my studies. Her generosity in placing her time, expertise, and resources at my disposal markedly strengthened the foundation of my professional work. Thanks to my Dissertation Committee members – Marie-Francoise Chesselet, Karen Gylys, Joseph Watson, and Edmond Teng – who provided valuable insight and support, which substantially has improved my dissertation.

I would next like to thank Dave Teplow and all the current and former members of the Bitan, Teplow, and Chesselet labs, especially Eric Hayden. They made themselves continuously available for discussion and provided insightful suggestions. In particular, Eric has graciously tolerated my presence at a distance of three feet for many years and ceaselessly surprises me with his spirit of benevolence. He literally has taught me everything from how to use my Mac to scientific methods to acro-yoga.

I would like to give special thanks to my friends and family, who provided ongoing moral support, encouragement, and necessary distraction from science. I could not have made it here today without them.

Papers

The following dissertation, while an individual work, draws on research done in collaboration with fellow scientists. Chapter 2 includes a shortened version of a review published in Current Pharmaceutical Design, *Disrupting Self-Assembly and Toxicity of Amyloidogenic Protein Oligomers by "Molecular Tweezers"- from the Test Tube to Animal Models* (A. Attar and G. Bitan, 2014, 20: in press; Bitan was the PI for this and all articles acknowledged below), and some of the associated figures are reproduced with kind permission from this source, Bentham Science. Chapter 3 is a version of a primary article published in the journal Brain, *Protection of Primary Neurons and Mouse Brain From Alzheimer's Pathology by Molecular Tweezers* (A. Attar, C. Ripoli*, E. Riccardi*, P. Maiti*, T. Liu*, M. R. Jones*, K. Lichti-Kaiser*, F. Yang*. G.D. Gale*, C. Tseng*, M. Tan*, C. Xie**, J. L. Straudinger**, F.-G. Klärner**, T. Schradr**, S. A. Frautschy**, C. Grassi**, and G. Bitan, 2012, 135(12): 3735-3748) and all of the associated figures and tables are reproduced with acknowledgement to the Oxford University Press. Chapter 4 is a version of a primary article that is in preparation for submission, *Safety and Pharmacological Characterization of the Molecular Tweezer CLR01* (A. Attar, W-T. C. Chan*, F.-G. Klärner**, T. Schrader**, and G. Bitan). Chapter 5 is a version of a primary article published in PLOS ONE, *A Shortened Barnes Maze Protocol Reveals Memory Deficits at 4-Months of Age in the Triple-Transgenic Mouse Model of Alzheimer's Disease* (A. Attar, T. Liu*, W-T. C. Chan*, J. Hayes*, M.

Nejad*, K. Lei*, and G. Bitan, 2013, 8 (11): e80355) and all of the associated figures and tables are reproduced with acknowledgement to PLOS ONE. My thanks to all my co-authors.

Note: * denotes contribution with designing and/or performing experiments, ** denotes contribution with supervision of projects and with conceptual discussion.

Funding Sources

Lastly, my gratitude to my funding sources, without which this work could not have been actualized. Financial support was provided by University of California-Los Angeles Jim Easton Consortium for Alzheimer's Drug Discovery and Biomarker Development (Bitan); American Health Assistance Foundation grant A2008-350 (Bitan); RJG Foundation grant 20095024 (Bitan); Cure Alzheimer's Fund grant (Bitan); Individual Pre-doctoral National Research Service Award 1F31AG037283 (Attar); National Institute of Health grant R01AG021975 (Frautschy); Veteran's Administration Merit Award (Frautschy); UCLA Morris K. Udall Parkinson Disease Research Center of Excellence P50 NS38367 (PI Chesselet, Co-PI Bitan); and Center for Gene-Environment in Parkinson's Disease: Pilot Research Award P01 ES016732 (Bitan).

VITA

EDUCATION:

2003−2007	B.Sc. *Summa cum laude*, University of Minnesota-Twin Cities Double Major: Neuroscience; Genetics, Cell Biology, and Development. GPA: 3.77/4.0
2007−2013	Ph.D. University of California-Los Angeles, Neuroscience Interdepartmental Ph.D. Program. GPA: 4.0/4.0 Advanced to candidacy: November 2011

ACADEMIC EXPERIENCE:

2007−2013	Graduate Student Researcher, laboratory of Dr. Gal Bitan, Department of Neurology, University of California-Los Angeles,
2012	Teaching Assistant, Introduction to Engaged Scholarship, UCLA
2009−2010	Teaching Assistant, Project Brainstorm, University of California-Los Angeles,
2006−2007	Research Assistant, Department of Physiology, University of Minnesota
2006−2007	Teaching Assistant, Animal Diversity Lab, University of Minnesota
2004−2006	Research Assistant, Department of Neuroscience, University of Minnesota
2005	Teaching Assistant, Biochemistry, University of Minnesota

PUBLICATIONS AND PRESENTATIONS:

Research Papers:

1. In preparation: F. Richter, S. R. Subramaniam, C. Zhu, **A. Attar,** N. Franich, G. Bitan, and M. F. Chesselet, *CLR01 Therapy for Parkinsosn's Disease*.
2. In preparation: D.H.J. Lopes, **A. Attar**, Z. Du, K. McDaniel, S. Dutt, K. Bravo-Rodriquez, J.M. Ramirez-Anguita, E. Sancez-Garcia, F.-G. Klärner, C. Wang, T. Schrader, and G. Bitan, *The molecular tweezer CLR01 inhibits islet amyloid polypeptide assembly and toxicity via an unexpected mechanism.*
3. Submitted: **A. Attar**, W-T. C. Chan, F.-G. Klärner, T. Schrader, and G. Bitan, *Safety and Pharmacological Characterization of the Molecular Tweezer CLR01.*
4. Submitted: N. Ferreira, A Pereira-Henriques, **A. Attar**, F.-G. Klärner, T. Schrader, G. Bitan, M. J. Saraiva, and M. R. Almeida, *Molecular Tweezers Targeting Transthyretin Amyloidosis*.
5. Submitted: S. Acharya, B. Safaie, **A. Attar**, M. Ivanova, F.-G. Klärner, T. Schrader, G. Bitan, and L.J. Lapidus, *Molecular Basis for Preventing α-synuclein Aggregation by Molecular Tweezers.*

6. **A. Attar**, T. Liu, W-T. C. Chan, J. Hayes, M. Nejad, K. Lei, and G. Bitan (2013) *Shortened Barnes Maze Protocol and Early Memory Deficits in Triple-Transgenic Mouse Model of Alzheimer's Disease.* **PLOS ONE**, 8 (11): e80355.
7. **A. Attar**, C. Ripoli, E. Riccardi, P. Maiti, T. Liu, M. R. Jones, K. Lichti-Kaiser, F. Yang. G.D. Gale, C. Tseng, M. Tan, C. Xie, J. L. Straudinger, F.-G. Klärner, T. Schradr, S. A. Frautschy, C. Grassi, and G. Bitan (2012) *Protection of primary neurons and mouse brain from Alzheimer's pathology by molecular tweezers*. **Brain,** 135: 3735-3748.
8. S. Prabhudesai, S. Sinha, **A. Attar**, A. Kotagiri, A.G. Fitzmaurice, R. Lakshmanan, M.I. Ivanova, J.A. Loo, F.-G. Klärner, T. Schrader, G. Bitan, and J. Bronstein (2012) *A Small-molecule Inhibitor of α-Synuclein Neurotoxicity.* **Neurotherapeutics**, 9: 464–476.
9. R. Romero-Calderón, E. D. O'Hare, N. A. Suthana, A. A. Scott-Van Zeeland, A. Rizk-Jackson, **A. Attar**, S. Madsen, C. A. Ghiani, C. J. Evans, and J. B. Watson (2011) *Project Brainstorm: Connecting College Students With School Children To Learn About Neuroscience.* **PLoS Biology**, 10 (4): e1001310.
10. J. Moskovitz, P. Maiti, D.H.J. Lopes, D.B. Oien, **A. Attar**, T. Liu, S. Mittal, J. Hayes, and G. Bitan (2011) *Induction of methionine-sulfoxide reductases protects neurons from amyloid β-protein insults in vitro and in vivo.* **Biochemistry**, 50: 10687–10697.

Book Chapters and Literature Reviews:

1. **A. Attar**, G. Bitan (2014) *Disrupting Self-Assembly and Toxicity of Amyloidogenic Protein Oligomers by "Molecular Tweezers" – from the Test Tube to Animal Models.* **Current Pharmaceutical Design**, 20: In Press.
2. **A. Attar**, D. Meral, B. Urbanc, G. Bitan (2013) Chapter 38: Assembly of amyloid β-protein variants containing familial Alzheimer's disease-linked amino acid substitutions. In: Uversky VN, Lyubchenko V, editors. Bionanoimaging: Protein Misfolding & Aggregation. USA: Elsevier. pp. 429-442.
3. **A. Attar**, F. Rahimi, and G. Bitan (2013) *Modulators of amyloid protein aggregation and toxicity – EGCG and CLR01.* **Translational Neuroscience**, 4 (4):385-409.

Invited Commentary

1. **A. Attar**, G. Bitan, and H. Li (2010) Invited comment by Alzforum on paper of the week by Ladiwala et al., in J. Biol. Chem. (Nov. 23rd 2010) *Aromatic small molecules remodel toxic soluble oligomers of amyloid β through three independent pathways*. Dec 29th, 2010.

Other

1. Undergraduate Honors Thesis, Department of Integrative Biology and Physiology, University of Minnesota. May 2007. Title: *Central administration of benzamil mitigates DOCA-salt hypertension by abating activity of the paraventricular nucleus.* Authors: **A. Attar**.

Abstracts:

1. Nov 2013, 43rd Annual Meeting of the Society for Neuroscience, San Diego, CA. Title: *Peripheral and central administration of the molecular tweezer CLR01 shows beneficial effects in mice overexpressing human wild-type α-synuclein.* Authors: F. Richter, C. Zhu, S. Subramaniam, N. Franich, N. Bove, P. Lee, K. De La Rosa, J.

Kwong, **A. Attar**, G. Bitan, M.-F. Chesselet.

2. Oct 2012, 42st Annual Meeting of the Society for Neuroscience, New Orleans, LA. Title: *Brain penetration of amyloid assembly and toxicity inhibitor, CLR01, in 12-month- and 24-month-old wild-type and transgenic mice.* Authors: **A. Attar**, G. Bitan. Presentation.
3. Oct 2012, 42st Annual Meeting of the Society for Neuroscience, New Orleans, LA. Title: *Molecular tweezers inhibit protein aggregation and toxicity in vitro and in vivo.* Authors: G. Bitan, **A. Attar**, S. Sinha, D. H. J. Lopes, P. Maiti, M. R. Jones, F. Yang, S. A. Frautchy, S. Prabhudesai, J. M. Bronstein, F. Richter, M. Chesselet, Z. Du, C. Wang, C. Ripoli, E. Riccardi, C. Grassi, F.-G. Klärner, T. Schrader.
4. July 2012, 15th Meeting of the Alzheimer's Association International Conference on Alzheimer's Disease, Vancouver, British Columbia, Canada. Title: *Lysine-specific molecular tweezers protect neurons against Aβ-induced synaptotoxicity and lower Aβ and p-tau load in a mouse model of Alzheimer's disease.* Authors: **A. Attar**, C. Ripoli, E. Riccardi, P. Maiti, T. Liu, M. R. Jones, F. Yang, C. Tseng, F.-G. Klärner, T. Schrader, S. A. Frautschy, C. Grassi, G. Bitan. Presentation.
5. November 2011, 41st Annual Meeting of the Society for Neuroscience, Washington, DC. Title: *Assessment of spatial memory in 4- and 15-month old 3×Tg Alzheimer's mice by Barnes maze using short versus long training.* Authors: **A. Attar,** T. Liu, K. Lei, M. Nejad, J. Hayes, G. Bitan.
6. November 2011, 41st Annual Meeting of the Society for Neuroscience, Washington, DC. Title: *UCLA Brain Awareness Week 2011: Keys to success.* Authors: **A. Attar**, S. K. Madsen, M. S. Levine, C. E. Evans, J. B. Watson.
7. November 2011, 41st Annual Meeting of the Society for Neuroscience, Washington, DC. Title: *Neuroscience outreach at UCLA: Project Brainstorm undergraduate course in 2011.* Authors: S. K. Madsen, C. A. Ghiani, **A. Attar**, N. A. Suthana, R. Romero-Calderon, M. S. Levine, C. E. Evans, J. B. Watson.
8. March 2011, 42nd Annual Meeting of the American Society for Neurochemistry, St. Louis, MO. Title: *Molecular Tweezers – potential therapeutics for amyloid-related diseases.* Authors: G. Bitan, **A. Attar**, J.M. Bronstein, M.-F. Chesselet, Z. Du, M. Ehrmann, S.A. Frautschy, M.R. Jones, F.-G. Klärner, T. Liu, J.A. Loo, D.H.J. Lopes, P. Maiti, E.S. Pang, S. Prabhudesai, F. Richter, T. Schrader, S. Sinha, P. Talbiersky, M. Tan, A. Tennstädt, C. Wang, C.-W. Xie, and F. Yang.
9. November 2010, 40th Annual Meeting of the Society for Neuroscience, San Diego, CA. Title: *Molecular tweezers reduce amyloid β-protein burden in transgenic mice by inhibiting Aβ assembly.* Authors: **A. Attar**, S. Sinha, P. Maiti, M. Tan, R. Bakshi, P. Y. Kuo, F. Yang, M. R. Jones, C. W. Xie, F.-G. Klarner, T. Schrader, S. A. Frautschy, G. Bitan. Presentation.
10. November 2010, 40th Annual Meeting of the Society for Neuroscience, San Diego, CA. Title: *Molecular tweezers are broad-spectrum protein aggregation inhibitors showing promise for Parkinson's disease therapy.* Authors: G. Bitan, S. Sinha, D. H. Lopes, **A. Attar**, K. McDaniel, R. Bakshi, S. Prabhudesai, J. Bronstein, F. Richter, C. Zhu, M.-F. Chesselet, T. Schrader, F.-G. Klarner.
11. November 2010, 40th Annual Meeting of the Society for Neuroscience, San Diego, CA. Title: *Neuroscience outreach at UCLA: Project Brainstorm undergraduate*

course. Authors: **A. Attar**, C. A. Ghiani, A. M. Rizk-Jackson, N. A. Suthana, R. Romero-Calderon, M. S. Levine, C. E. Evans, J. B. Watson.

12. November 2010, 40th Annual Meeting of the Society for Neuroscience, San Diego, CA. Title: *UCLA brain awareness week 2010:, promoting public engagement in neuroscience.* J. B. Watson, W. Fujioka, **A. Attar**, A. M. Rizk-Jackson, M. Ziehn, M. Bonitati, C. A. Ghiani, C. E. Evans.
13. July 2010, 13th Meeting of the Alzheimer's Association International Conference on Alzheimer's Disease. Title: *Small molecule inhibitor of amyloid β-protein oligomerization reduces brain Aβ load in an Alzheimer's disease mouse model.* Authors: **A. Attar**, S. Sinha, P. Maiti, F. Yang, D. Gant, M. Jones, P. Talbiersky, T. Schrader, F.-G. Klärner, S. Frautschy, G. Bitan.
14. July 2010, 10th Annual Meeting of the Alzheimer's Association International Conference on Alzheimer's Disease. Title: *Novel, small molecule inhibitors of protein aggregation for treatment of amyloid-related diseases.* Authors: G. Bitan, S. Sinha, **A. Attar**, P. Maiti, D. Lopes, Z. Du, M. Tan, S. Prabhudesai, P. Talbiersky, R. Bakshi, P. Kuo, F. Yang, D. Gant, M. R. Jones, C. Xie, J. M. Bronstein, C. Wang, S. A. Frautschy, F. Klärner, T. Schrader
15. October 2009, 39th Annual Meeting of the Society for Neuroscience, Chicago, IL. Title: *Small molecule inhibitors of amyloid β-protein oligomerization reverse deficits in spatial working memory in an Alzheimer's disease mouse model.* Authors:, **A. Attar**, S. Sinha, P.-Y. Kuo, R. Bakshi, F. Yang, S. Hu, D. Gant, P. Talbiersky, F.-G. Klarner, T. Schrader, S. Frautschy, G. Bitan.
16. October 2009, 39th Annual Meeting of the Society for Neuroscience, Chicago, IL. Title: *Rational, structure-based small molecule inhibitors of protein assembly show promise for Alzheimer's and Parkinson's diseases.* Authors: G. Bitan, S. Sinha, **A. Attar**, P.-Y. Kuo, R. Bakshi, T. Schrader, F.-G. Klärner, P. Talbiersky, J. Polkowska, S. Frautschy, F. Yang, S. Hu, D. Gant, J. Bronstein, S. Prabhudesai, C.-W. Xie, M. Tan, G. B. Benedek, and A. Lomakin.,
17. July 2009, 23rd Symposium of the Protein Society, Boston, MA. Title: *Rationally identified small molecules inhibit amyloid β-protein assembly and toxicity by a novel mechanism.* Authors: S. Sinha, **A. Attar**, P.-Y. Kuo, R. Bakshi, P. Maiti, P. Talbiersky, A. Lomakin, M. Tan, E. Pang, Z. Du, F. Yang, S. Hu, D. Gant, M. Jones, C. Wang, J. Loo, S. Frautschy, C.-W. Xie, G. Benedek, T. Schrader, and G. Bitan.
18. March 2009, 9th International Conference on Alzheimer's Disease/ Parkinson's Disease. Title: *Rationally designed small molecule inhibitor of amyloid-β-protein assembly rescues spatial working memory deficits in a mouse model of Alzheimer's disease.* Authors: **A. Attar**, S. Sinha, R. Bakshi, T. Shrader, P. Talbiersky, J. Polkowska, T. Gersthagen, G. Benedek, A. Lomakin, C.W. Xie, M. Tan, S. Frautschy, F. Yang, S. Hu, D. Gant, G. Bitan.
19. March 2009, 9th International Conference on Alzheimer's Disease/ Parkinson's Disease. Title: *Rationally designed inhibitors of amyloid β-protein assembly and toxicity.* Authors: G. Bitan, H. Li, S. Sinha, **A. Attar**, R. Bakshi, T. Schrader, P. Talbiersky, J. Polkowska, T. Gersthagen, G. Benedek, A. Lomakin, C.W. Xie, M. Tan, B. Urbanc, L. Cruz, S. Frautschy, F. Yang, S. Hu, D. Gant, M. Bowers, M. Murray, J.E. Shea, C. Wu.

20. April 2007 Federation of American Societies for Experimental Biology Annual Meeting. Title: *Intracerebroventricular (ICV) benzamil attenuates the maintenance phase of DOCA-salt hypertension: Role of the paraventricular nucleus of the hypothalamus.* Authors: J. M. Abrams, K. A. Krawczewski, **A. Attar**, W. C. Engeland, J. W. Osborn.

HONORS AND AWARDS:

2013	Alzheimer's Association Young Investigator Award, Southern California
2013	Department of Neurology/Mazz Prize 1st Place Poster Presentation Award
2010−2013	NIH Ruth L. Kirschstein National Research Service Award for Predoctoral Fellows
2009−2013	UCLA Neuroscience Interdepartmental Ph.D. Program Travel Award
2012	Alzheimer's Association International Conference 2012 Travel Fellowship
2010−2012	BRI/Semel Graduate Student Travel Award, UCLA
2010	NIH-funded Training Program in Neural Repair at UCLA
2007	Outstanding Alumni Award, Department of Neuroscience, University of Minnesota
2007	B.Sc. awarded with Latin Honors: *Summa cum laude,* University of Minnesota
2007	B.Sc. awarded with Distinction, University of Minnesota
2006	College of Biological Sciences Scholarship, University of Minnesota
2004−2006	Dean's List, College of Biological Sciences, University of Minnesota
2005	Freshman-Sophomore Honors, College of Biological Sciences, University of Minnesota

Chapter 1

Alzheimer's Disease and Therapies

1.1 Alzheimer's Disease

1.1.1 Significance and Risk Factors

Alzheimer's Disease (AD) International estimates that today, over 35 million people are living with dementia worldwide [4]. The average annual increase in incidence between 2010 and 2050 is expected to be 16.15 million, largely due to longer life expectancies and the aging baby boomers, meaning that 682 million people will live with dementia in the next 40 years [6]. Dementia is an umbrella term that describes a variety of conditions categorized by impairments in memory, behavior, and ability to think clearly. In 2013, the Diagnostic and Statistical Manual of Mental Disorders Edition 5, released by the American Psychiatric Association, redefined dementia (Latin for "mad" or "insane") as a neurocognitive disorder with the intent to reduce the stigma associated with it. To meet criteria for dementia, one must have symptoms severe enough to interfere with daily life, including a decline in memory and at least one of the following four categories: 1) the ability to speak coherently or understand language; 2) the ability to recognize and identify objects; 3) the ability to perform motor activities; or 4) the ability to think abstractly, plan and execute complex tasks, and make sound judgments; but assuming intact motor and sensory functions [9]. The most prevalent type of dementia is AD.

In the United States, AD is estimated to affect 5.2 million people in 2013, of which 200,000 are under age 65 [9]. Of these people, 3.2 million are women and 1.8 million are men, though this is not reflective of increased incidence [10,11] and is attributed to the longer life expectancy of women. The greatest risk factor for AD is age with an estimated prevalence of 4% under age 65, 13% from age 65−74, 44% from age 75−84, and 38% at age ≥ 85 [9]. The number of afflicted family members correlates with increased risk [12], however less than 1% of cases are dominantly inherited due to known genetic mutations [13]. The genetics of AD are discussed in Section 1.1.4. Additional risk factors include a gene for cholesterol transport − *APOE*, positive correlation with moderate traumatic brain injury [14,15], cardiovascular disease and its associated risk factors, such as smoking [16], obesity [17,18], diabetes [19], high cholesterol [18,20], and hypertension [18,21], and a negative correlation with education level [22,23], and social and cognitive engagement [24,25].

AD is the sixth leading cause of death in the United States [9]. The top five most common reasons, from highest to lowest incidence, for hospitalization of people with AD are 1) fainting, falling, or trauma, 2) ischemic heart disease, 3) gastrointestinal disease, 4) pneumonia, and 5) delirium or mental status change. Pneumonia often is a contributing factor to the death of people with AD [26]. In addition to the emotional and physical costs associated with AD, it is also a massive economic burden. In 2012, 15.4 million unpaid caregivers, typically relatives, provided an estimated 17.5 billion hours of care, which included assistance with activities of daily living and was valued at $216.4 billion [9]. Furthermore, total estimated 2013 healthcare costs in the US, of which 70% is paid

by Medicare/Medicaid, are $203 billion. These costs are projected to increase to $1.2 trillion by 2050 [9].

1.1.2 Pathophysiology and Biomarkers

There are three clinical disease stages of AD: presymptomatic, prodromal or amnestic or non-amnestic mild cognitive impairment (MCI), and AD dementia. The presymptomatic stage consists of cognitively normal individuals that have begun to develop the pathological features of AD, amyloid plaques and neurofibrillary tangles (NFTs) described in the next paragraph. The next stage, MCI, represents the onset of cognitive symptoms — often deficits in episodic memory with amnestic MCI and attention or language with non-amnestic MCI, and can encompass some progression in cognitive dysfunction. This stage also may be associated with irritability, anxiety, and depression. The last stage of dementia, as defined above, consists of impairments in multiple cognitive domains, such as executive functions, language, and visuospatial functions. At this stage, behavioral changes may present in the form of aggression, agitation, emotional distress, restlessness, and sleep disturbance. Patients often are diagnosed during the MCI stage as their concerns about their changes in cognition increase. The disease course lasts on average 3−8 years depending on age of diagnosis [27], out of which ~40% of the time is spent in the most severe stage of the disease [28].

It is widely believed that AD pathogenesis begins with the accumulation of amyloid β-protein (Aβ), either due to enhanced production [29] or decreased clearance [30]. Homo-assemblies of Aβ appear toxic, though the structures and mechanisms are unknown. Toxicity is manifested as synaptic and cellular dysfunction, neurotransmitter

disturbances, deposition of amyloid plaques (Figure 1.1), tau modification and aggregation into NFTs (Figure 1.1), gliosis, oxidative damage, and progressive neurodegeneration, including the loss of neurons of the hippocampus and of cholinergic neurons in the nucleus basalis of Meynert. Amyloid plaques and NFTs are the two main hallmarks of AD. Amyloid deposits can be generally grouped into three categories: 1) senile plaques, which manifest as areas of damaged neuropil containing fibrillar deposits of Aβ (described below in section 1.1.5.3 *Different Assembly Structures*), often with dense plaque cores, reactive glia and surrounded by dystrophic neurites; 2) diffuse plaques, which also manifest in the neuropil but have a "cotton candy-like" appearance with little or no fibrillar Aβ and little neuropil damage; and 3) vascular deposits found in the walls of cerebral blood vessels containing fibrillar Aβ. NFTs are aggregates of post-transcriptionally modified tau protein, described further in section 1.1.6.3 below. Functional deficits correlate more closely with NFTs than with plaque levels [31]. The loss of synapses is thought to be the most highly correlated with the level of cognitive dysfunction [32], however, synaptic sprouting has also been

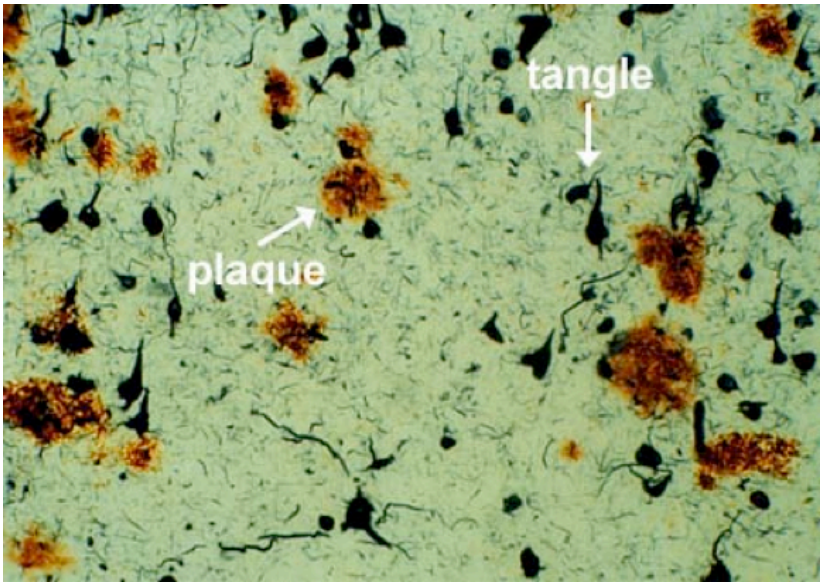

Figure 1.1: Extracellular amyloid plaques and intracellular neurofibrillary tangles
Adapted from[1]

reported as a response to synaptic amyloid accumulation [33] and so has an increase in synaptic size that accompanies synaptic loss [34,35].

Assessment of the ordered appearance of these disease features, or biomarkers, can be used to facilitate diagnosis and to predict conversion from MCI to AD. Current biomarkers can be grouped into identifiers of amyloid plaque deposition and of neurodegeneration. The five most explored biomarkers are 1) decreased cerebrospinal fluid (CSF) Aβ, specifically the 42-residue isoform – Aβ42, 2) increased brain amyloid levels as measured by positron emission tomography (PET) imaging, 3) increased CSF tau levels, 4) decreased fluorodeoxyglucose, a glucose analogue, uptake as measured by PET (FDG-PET), and 5) brain atrophy as measured by structural magnetic resonance imaging (MRI).

Both decreased CSF-Aβ42 levels and increased brain amyloid measured by PET imaging are biomarkers of AD representing Aβ plaque deposition. Low concentrations of CSF Aβ42 correlate with both the clinical diagnosis of AD and Aβ deposition at autopsy [36] and nearly all patients with a clinical diagnosis of AD have brain amyloid that can be detected using PET with different amyloid-binding tracers [37]. Pittsburgh compound B, a PET tracer that binds to fibrillar Aβ described below in section 1.5.3, *Different Assembly Structures*, but not to soluble Aβ or diffuse plaques, also correlates well with post-mortem analysis of brain Aβ deposition [38] (Figure 1.2).

Increased CSF tau levels, decreased brain metabolism measured by FDG-PET, and cerebral atrophy are biomarkers of AD representing neurodegeneration. Increase in CSF tau indicates neuronal damage and is used as a marker also in ischemic and traumatic brain injury [39,40]. Thus on its own, increased CSF tau is not indicative of AD.

However, it is correlated highly positively with NFTs load at autopsy [41], disease severity, and rate of progression through the three clinical stages [42]. Interestingly, increased CSF tau is not observed in pure tauopathies, such as supranuclear palsy and corticobasal degeneration, although larger brain NFTs load is observed in these diseases upon autopsy than in AD [43]. It is believed that as tau accumulates within neurons and axons as a result of a pathological signaling cascade, the accumulation results in cellular damage and tau is released into the extracellular space and thus the CSF, as the extracellular fluid and brain CSF are in dynamic equilibrium [44]. FDG-PET is used to measure net brain glucose metabolism and largely indicates synaptic activity [45]. FDG-PET correlates well with levels of the synaptic protein synaptophysin, a presynaptic

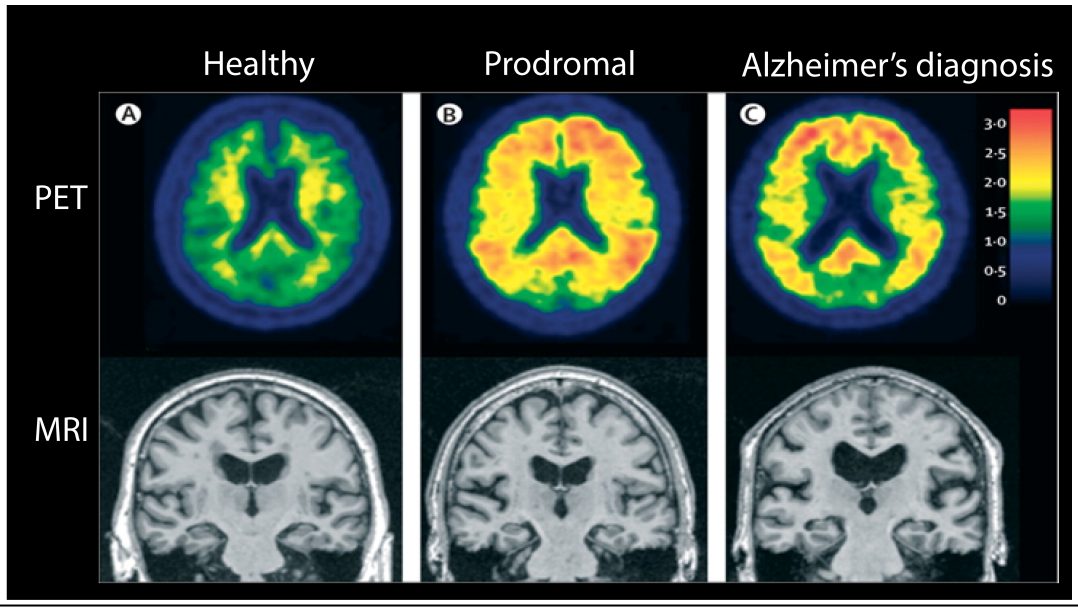

Figure 1.2: Imaging of Amyloid deposition by PET and brain atrophy by MRI (A) A cognitively normal individual with no evidence of Aβ on PET amyloid imaging with Pittsburgh compound B and no evidence of atrophy on MRI. (B) A cognitively normal individual who has no evidence of neurodegenerative atrophy on MRI, but has significant Aβ deposition on PET amyloid imaging. (C) An individual who has dementia and a clinical diagnosis of AD, positive PET amyloid imaging, and neurodegenerative atrophy on MRI. Adapted from [2]

protein used to assess synaptic density [46]. Decreasing levels of FDG uptake also correlate well with cognitive impairment [47], low CSF Aβ, specifically Aβ42, and high CSF total tau and tau phosphorylated at residue 181, a marker for NFTs [48]. Lastly, volumetric measures of brain atrophy and ventricular enlargement by structural MRI show a strong correlation with the severity of cognitive impairment [49,50] (Figure 1.2). By the last clinical stage of AD, brain atrophy can be seen as a result of the death of up to 80% of the neurons of the hippocampus [51].

In 2010, Jack et. al [2] proposed a model of dynamic biomarkers of the Alzheimer's pathological cascade (Figure 1.3), which related the ordered, temporal, and often spatial appearance of the different pathological and clinical events to disease stage. Considering that Aβ-related biomarkers present early in AD and may plateau before the

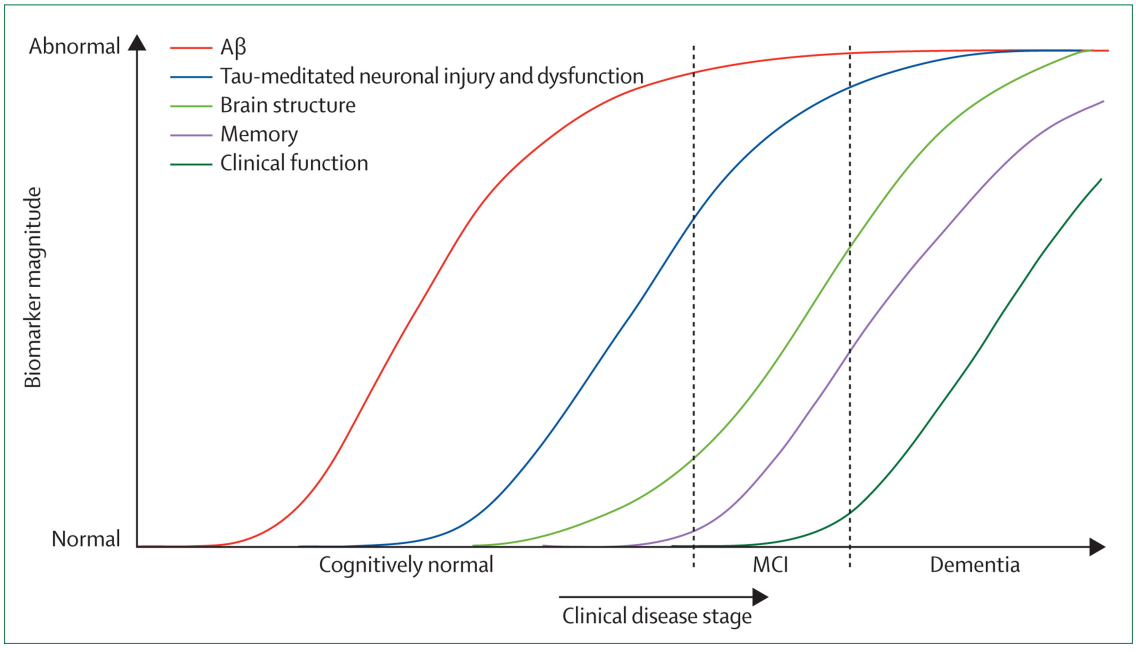

Figure 1.3: Dynamic biomarker theory of Alzheimer's disease pathological cascade
Aβ is identified by CSF Aβ42 or PET amyloid imaging. Tau-mediated neuronal injury and dysfunction is identified by CSF tau or FDG-PET. Brain structure is measured by structural MRI. Adapted from [2]

onset of clinical symptoms, and that biomarkers of neuronal injury, such as increased CSF tau, lowered brain metabolism, and cerebral atrophy, present later in the disease and correlate well with clinical symptom severity, comprehensive biomarker-based disease staging can be possible by simultaneous analysis of several biomarkers. This tactic may be utilized for reduced stage variability in clinical trials and better targeting of drug to stage [33].

1.1.3 Production of Aβ By Enzymatic Cleavage

To better understand the genetics and putative mechanisms of AD, one must first understand the proteins involved. Thus, in this section I describe the physiological processes leading to the production of different Aβ isoforms. Aβ is a product of sequential cleavage of amyloid β-protein precursor (APP), first outside the membrane by β-secretase to release the N-terminal ectodomain of APP called soluble APPβ from the C-terminal, membrane-anchored domain called C99, and then within the membrane by γ-secretase to release Aβ and the APP intracellular cytoplasmic domain (Figure 1.4). Another enzyme, α-secretase, cleaves APP within the Aβ region, after Aβ residue 16, leading to formation of a shorter peptide, p3, which is not associated with disease. β-Secretase consistently produces Aβ starting at D1 (APP672). In contrast, γ-secretase is an imprecise enzyme, which cleaves APP in several locations leading to peptides ending at various C-terminal positions, most commonly from 38 to 43 (though never 41). Historically, the most studied forms of Aβ have been the most abundant ones, the 40- and 42-residue forms, but studies of the 38- and 43-residue forms are on the rise. Changes in the length of Aβ have a major effect on the aggregation kinetics, toxicity, and role in AD,

as described in the next paragraph and in section 1.5.3, *Different Assembly Structures*. Regardless of the exact length, Aβ isoforms form oligomers, which are believed to be the major neurotoxic assembly state of Aβ [52], and then go on to make fibrils that are found deposited in the brain.

In the AD brain, Aβ deposits in both the brain parenchyma and vasculature. Classic, dense-core amyloid plaques and diffuse plaques are parenchymal deposits composed primarily of Aβ42 and Aβ43 [53-55], whereas vascular amyloid

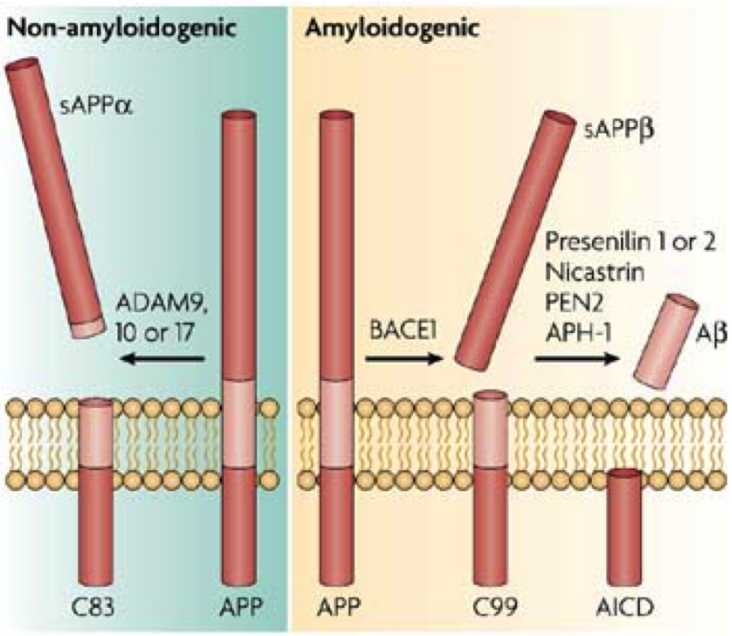

Figure 1.4: Enzymatic Cleavage of Aβ From APP
Aβ is derived via proteolysis from a larger precursor molecule called amyloid β-protein precursor (APP), a type 1 transmembrane protein consisting of 695–770 amino acids. APP can undergo proteolytic processing by one of two pathways. Most is processed through the non-amyloidogenic pathway. The first enzymatic cleavage in this pathway is mediated by α-secretase, of which three putative candidates belonging to the family of a disintegrin and metalloprotease (ADAM) have been identified: ADAM9, ADAM10 and ADAM17. Cleavage by α-secretase occurs within the Aβ domain, thereby preventing the generation and release of Aβ. Two fragments are released by α-secretase cleavage, a large, amino-terminal ectodomain (sAPPα) and a smaller carboxy-terminal fragment, C83. C83 then undergoes cleavage mediated by γ-secretase to generate p3 (not shown). APP molecules that are not cleaved by the non-amyloidogenic pathway become a substrate for β-secretase (β-site APP-cleaving enzyme 1; BACE1), releasing an ectodomain (sAPPβ), and retaining the last 99 amino acids of APP (C99) within the membrane. The first amino acid of C99 is the first amino acid of Aβ. C99 is cleaved subsequently 38–43 amino acids from the amino terminus to release Aβ and APP intracellular domain (AICD), by the γ-secretase complex, which is made up of presenilin 1 or 2, nicastrin, anterior pharynx defective 1 (APH-1) and presenilin enhancer 2 (PEN2). This cleavage predominantly produces Aβ40, and the more amyloidogenic Aβ42 at a ratio of 10:1. Adapted from [3]

consists mainly of Aβ40 [56,57]. Levels of Aβ in the CSF, which are used as a biomarker for AD, differ between the Aβ isoforms. In non-demented persons, levels of CSF Aβ were found to be 40>38>42>39>37 [58]. In patients with AD, levels of Aβ42 and Aβ37 decreased and levels of Aβ38 and Aβ40 increased [58] or remained unchanged [59,60]. Aβ39 concentration levels were unchanged [58]. In plasma, different groups have shown no change [61] or different directions of change for levels of Aβ38, Aβ40, and Aβ42 between patients with AD and age-matched normal individuals [62,63]. Clinically, Aβ42 has been most closely associated with AD because familial AD-linked mutations in the *PSEN1* and *PSEN2* genes, which encode the catalytic unit of γ-secretase, presenilin-1 and presenilin-2, respectively, result in increased Aβ42 levels [64,65], and Aβ42 is more prone to aggregation [53,66,67] and is more neurotoxic than Aβ40 [68-71].

1.1.4 Alzheimer's Disease Genetics

The genetic contribution to AD is estimated to be about 80% based on twin and family studies [72]. However, less than 1% of AD cases are characterized by a Mendelian inheritance pattern. These patients present with early-onset (< 60 years old) familial AD [13]. The other 99% is considered to be sporadic, can be early or late-onset (≥ 60 years old), and thought to be influenced by environmental interactions with the mostly unknown genetic variants.

Most early-onset AD is sporadic, but ~5% is caused by rare, fully penetrant mutations in three different genes: *APP, PSEN1,* and *PSEN2* [73]. Other causes of early onset dementia may be head injury and alcohol abuse [74] and mutations near the PAX transcription activation domain interaction protein gene [75] or in the gene encoding

PEN2, a component of the γ-secretase complex [76]. Mutations discovered in the *APP, PSEN1*, and *PSEN2* genes, which invariably lead to familial AD suggested a causative role for Aβ in AD. *APP* was the first gene to be identified as linked to AD. It was mapped to chromosome 21 in 1987 by several groups [77-79]. In 1990, the first pathogenic mutation in *APP*, called the Dutch mutation, was reported. This mutation leads to a substitution of glutamate to glutamine at Aβ residue 22 and causes a disease called hereditary cerebral hemorrhage with amyloidosis, Dutch type [80]. In 1995, several early-onset mutations were identified in *PSEN1* [81] and *PSEN2* [82], which shifted APP processing towards increased production of the more amyloidogenic form, Aβ42 [83]. To date, 24 mutations have been reported in *APP*, 185 in *PSEN1*, and 12 in *PSEN2* [84]. These mutations are inherited in an autosomal dominant and fully penetrant manner and all in *PSEN1* and *PSEN2* and some in *APP* lead to a common phenotype of an increase in the Aβ42/Aβ40 ratio [65]. For a detailed discussion regarding *APP* mutations causing intra-Aβ amino acid changes, the corresponding disease phenotypes, and protein aggregation characteristics, please see Chapter 38 in Bio-Nanoimaging: Protein Misfolding & Aggregation [85]. These mutations provide particular insight into important regions, interactions, and structures involved in the way Aβ self-assembles and affects susceptible brain regions.

Additional genes have been identified for late-onset AD, but the only gene variant that is widely accepted to be an established risk factor for AD is the ε4 allele of the *APOE* gene [86]. In contrast, carrying one or two copies of the ε2 allele is associated with reduced risk for AD [87]. Two amino acids distinguish the ε2, ε3, and ε4 isoforms of ApoE – ε2:C112/C158, ε3:C112/R158, ε4:R112/R158. The ε4 allele increases the risk for

AD by ~400% in persons carrying a single copy and 800−1500% in carriers of two copies as compared to the ε3 carriers [84]. Functionally, APOE is a plasma protein and transports cholesterol and lipoproteins in the blood. It is thought also to be involved in Aβ aggregation and reduced clearance of Aβ from the brain in AD by mechanisms that are not well understood [88]. Other genes, such as *ATXN1* (Ataxin 1) and *ABCA7* (ATP-binding cassette subfamily A member 7), identified by genome wide association studies may increase risk for AD by 10−20% [84].

1.1.5 Protein Aggregation

As Alzheimer's is a disease of aberrant protein aggregation, it is important to understand the structures and interactions involved at the protein level in AD.

1.1.5.1 Amyloid

The genome of a living organism may encode >30,000 proteins, all of which must adopt particular three-dimensional structures, which are encoded by their amino acid sequences and sometimes require particular environments, as in the case of naturally unfolded proteins [89,90], to carry out their biological function [91]. β-Sheet is the second most common secondary structure in proteins, following the α-helix. It is made up of stretches of amino acids, called β-strands that form backbone hydrogen bonds with other β-strands to stabilize the β-sheet (Figure 1.5). In fibrils, the β-sheet structure has the β-strands perpendicular to the long axis of the fibril and is hydrogen bonded along the long axis of the fibril. Filament elongation occurs by the stacking of multiple β-sheets to extend the long axis of the fibril. Fibrils are composed of two or more filaments (Figure

1.5). Aggregation of soluble polypeptides or proteins into insoluble amyloid fibrils containing the cross-β structural motif is the hallmark of amyloidoses [92].

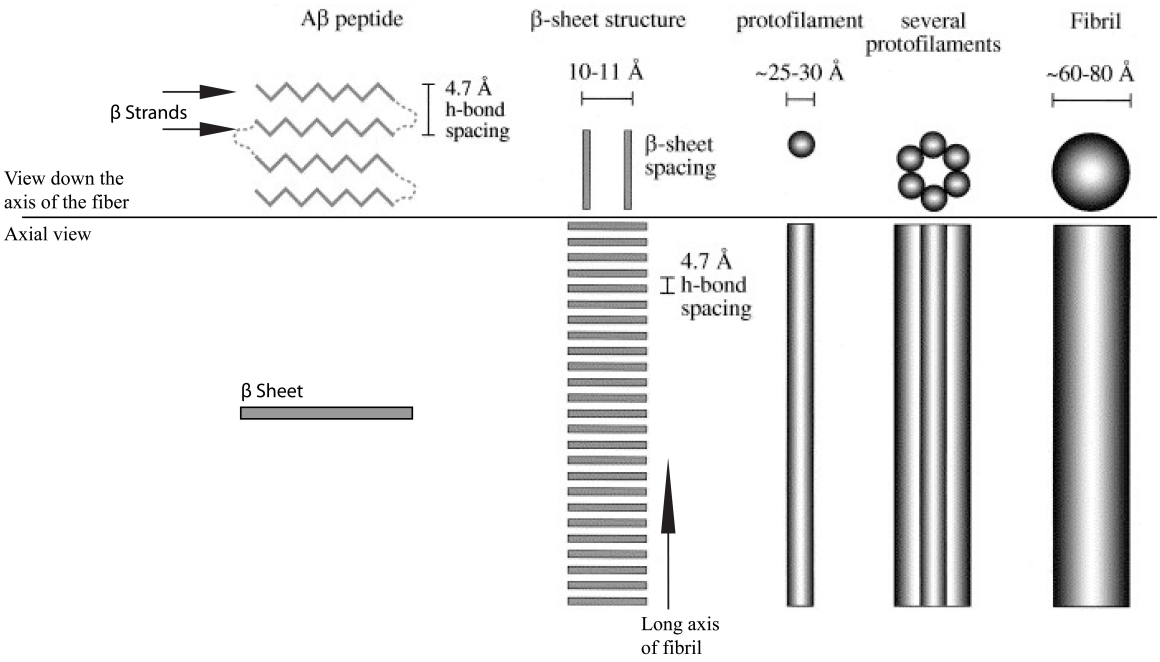

Figure 1.5: The hierarchy of structures from the Aβ peptide folded into a β-pleated sheet structure through protofilaments to amyloid fibrils.
Adapted from [5]

Given that self-association of polypeptides can be induced in many unrelated proteins, the β-sheet secondary structure of amyloids has been hypothesized to be a primordial, default structure of polypeptides [91]. Dobson went as far as proposing that potentially any protein might form amyloid given the appropriate conditions, typically denaturing conditions [93]. This view has been debated in light of evidence that particular sequences may be required for amyloid formation [94]. Nonetheless, in view of the high abundance of such sequences in biologically active proteins, it might be surprising that only a few dozen diseases of protein aggregation are known [95].

Remarkably, the shared, common structural characteristics of amyloid deposits found in all amyloidoses, β-sheet secondary structure and staining with metachromatic dyes or thioflavins, are independent of the amino acid sequence of the proteins that comprise them [96-98]. The proteins involved in amyloidoses can be divided into natively structured and natively unfolded proteins. For the first group, which includes proteins such as prion, transthyretin, Cu/Zn-superoxide dismutase 1, and β_2-microglobulin, amyloid formation requires partial unfolding, leading to formation of metastable, toxic oligomers and subsequently, β-sheet rich fibrils. Proteins in the second group, including Aβ, tau, α-synuclein, and islet amyloid polypeptide, are thought to undergo partial folding to create similar metastable structures leading to self-assembly and toxicity [99].

Aberrant protein self-assembly involves formation of multiple oligomeric structures, ranging from dimers to protofibrillar structures, most of which have been reported to be toxic [100]. Most likely, different mechanisms of oligomerization and fibrillization act in concert, and the contribution of each depends largely on the experimental and environmental conditions, as well as on the particular protein under study. These topics are expanded in sections 1.5.3 and 1.5.4 below.

The molecular interactions that mediate the aberrant self-assembly process include backbone and side-chain hydrogen bonds complemented by hydrophobic and electrostatic interactions involving side chains of particular amino acids. The role of hydrophobic interactions is well known. For example, a major driving force of aggregation in the case of naturally folded proteins is exposure of hydrophobic regions that are buried in the native structure, due to partial unfolding of the protein, followed by

abnormal sequestering of the exposed side chains through uncontrolled intermolecular interactions leading to aggregation. In comparison, the contribution of electrostatic interactions is less well recognized, though multiple studies have indicated their importance in amyloid assembly, specifically in fibril morphology [101], the size of oligomers [102], and the relative amount of α-helix or β-sheet secondary structures involved in amyloid formation [103]. For example, many familial AD-linked mutations within the Aβ-encoding region of the *APP* gene lead to an increase in the positive charge of Aβ sequence and to enhanced aggregation kinetics [104,105].

1.1.5.2 The Amyloid Cascade Hypothesis of Alzheimer's Disease

In 1992, the "amyloid cascade hypothesis" proposed that aggregation and precipitation of Aβ were the cause of all the other pathological processes, including NFTs, cell loss, and dementia in AD [106]. Since then, many observations have changed the focus from insoluble amyloid plaques to soluble Aβ oligomers as the primary cause of toxicity. In human studies, oligomers have been detected in brain [107] and in CSF [108] of patients with AD at concentrations significantly higher than in age-matched healthy individuals. In wild-type (WT) rodents, administration of extracted soluble Aβ oligomers from human AD brains or cell culture medium inhibited long-term potentiation (LTP), reduced hippocampal dendritic spine density, and disrupted learned behavior [109,110]. Additional evidence supporting a central role of Aβ oligomers in AD came from experiments in transgenic animals [111,112] and *in vitro* systems [68,113].

Many of the familial AD-linked mutations that affect regions of APP outside of the Aβ sequence increase Aβ levels. In contrast, the Dutch [E22Q], Arctic [E22G], Italian

[E22K], and Osaka (ΔE22) modifications cause a decrease in secreted Aβ (See Table 1.1 for amino acid abbreviations). Because both a decrease in Aβ levels, resulting from intra-Aβ substitutions, and an increase in Aβ levels, resulting from other familial AD-linked mutations, cause disease, the concentration of Aβ may be only part of the problem. This conclusion is supported by the existence of non-demented individuals with extensive Aβ plaque pathology.

Table 1.1 One letter abbreviations of amino acids				
Alanine = A	Cysteine = C	Aspartic acid = D	Glutamic acid = E	Phenylalanine = F
Glycine = G	Histidine = H	Isoleucine = I	Lysine = K	Leucine = L
Methionine = M	Asparagine = N	Proline = P	Glutamine = Q	Arginine = R
Serine = S	Threonine = T	Valine = V	Tryptophan = W	Tyrosine = Y

1.1.5.3 Different Assembly Structures

In Aβ fibrils, Aβ molecules are organized in in-register, parallel β-sheets in which the β-strands comprise residues 12−24 and 30−40 in Aβ40, and residues 18−26 and 31−42 in Aβ42 [114,115]. The two β-strands are connected by a turn in the region 21−30 and are stabilized by a salt bridge between K28 and E22 or D23 [116] and by hydrophobic interactions between K28 and V24 (See Table 1.1 for amino acid abbreviations) [117]. A common view of fibril formation is as a nucleation-dependent polymerization reaction. The nucleation step has a high-energy barrier and therefore is the rate-limiting step. Following nucleation, a relatively rapid fibril elongation process takes place [118]. The precursor structure to the fibril, the protofibril, was described as curvilinear, up to 200-nm long fibril-like structure that has a high β-sheet content, similar to mature fibrils. Early-stage protofibrils have a “beaded” appearance with a periodicity of 3−6 nm [119], which at later time points becomes smooth [120]. The “beads” that join

together to form early protofibrils are spherical aggregates [121], which were hypothesized to be the same as "paranuclei" — pentamer/hexamer assemblies of Aβ42 that have spherical structures similar to the protofibrils "beads" [122,123]. In support of the idea that Aβ42 hexamers in particular are building blocks for larger assemblies, several other oligomer structures have been described that are composed of small multiples of the hexamer, including dodecamers and octadecamers observed in the same experiments where paranuclei were identified [123], Aβ-derived diffusible ligands, which can be dodecamers of Aβ42 produced *in vitro* [124], and Aβ*56, an oligomer extracted from brains of Tg2576 mice and named after its apparent molecular weight – 56 kDa, which correlates with an Aβ42 dodecamer [112]. As Aβ oligomers are believed to initiate the pathogenic mechanisms in AD, an intense search for "the toxic structures" responsible for AD has led to the nominal, functional, and structural descriptions of many Aβ assemblies. In addition to the four assemblies mentioned above — protofibrils, paranuclei, Aβ-derived diffusible ligands, Aβ*56 — others include secreted cell-derived and brain-derived low-order oligomers, amylospheroids, annular assemblies, amyloid pores, and more. For a detailed description of each, see Rahimi et al. 2008, especially Table 1 [100].

1.1.5.4 Factors Controlling Aβ Assembly

Multiple lines of evidence demonstrate that difference in peptide length is a key factor controlling early oligomerization. As mentioned above in section 1.1.3, *Production of Aβ by Enzymatic Cleavage*, the two-amino-acids difference between Aβ40 and Aβ42 can have a major effect on the aggregation kinetics, toxicity, and role in AD. The two C-

terminal amino acids of Aβ42, I41 and A42 (See Table 1.1 for amino acid abbreviations) induce distinct biophysical properties from those of Aβ40. Jarrett et al. found that under similar condition, Aβ39 or Aβ40 remained soluble for days whereas Aβ42 and Aβ43 aggregated within hours [67]. As mentioned above, Aβ42 forms different oligomers than Aβ40. For example, pentamer and hexamer "paranuclei" are predominant Aβ42 oligomers whereas dimer, trimer, and tetramer are more abundantly represented in the Aβ40 oligomer population [123]. Modeling studies suggest that in Aβ40, because the C-terminus is shorter and less hydrophobic than in Aβ42, the N-terminus competes with the C-terminus for interaction with the central hydrophobic cluster (CHC, residues 17−21) [102,125,126]. Thus, the C-terminus–CHC interactions are a higher component in early Aβ42 folding versus Aβ40 folding [126].

Another factor that may facilitate Aβ self-assembly is the loss of electrostatic repulsion among monomers [127]. The larger the net charge of each of two molecules, either both positive or both negative, the more repulsion would occur between them. This theory is supported by the increase in aggregation properties of the Dutch [E22Q], Arctic [E22G], Tottori [D7N], and Iowa [D23N] mutations [85], where a negatively charged amino acid is substituted by a neutral one, changing the net charge of the Aβ peptide from -3 to -2. Similarly, the E22 deletion mutation causes the loss of a negative charge. This suggests that local electrostatic repulsion and global changes in peptide net charge may be linked to the familial AD caused by the corresponding mutations. Mutations affecting the Aβ sequence also highlight the paramount impact one amino acid change can have on multiple characteristics from protein function and folding to brain pathology and age of disease onset.

Perturbation of "native" metastable structures could also affect Aβ assembly. As mentioned in the previous section, in the Aβ monomer, a turn region has been identified within the decapeptide Aβ(21–30), which may be one of the earliest conformations formed [116]. This turn, which was hypothesized to nucleate Aβ folding and assembly, is stabilized by hydrophobic interactions between V24 and K28 and by long-range electrostatic interactions between K28 and either E22 or D23. Supporting the role of the turn in nucleation, Sciaretta et al. [128] have shown that an Aβ40 analogue containing a lactam cross-link between D23 and K28 formed amyloid fibrils substantially faster than WT Aβ40, with no detectable lag phase in the fibrillization process. In agreement with the hypothesis of the prominent role of this turn region in Aβ assembly, the turn also has been found in the fibril structure of Aβ40 and Aβ42 [129-132]. The destabilization of the turn by substitutions (or deletion) at positions 22 or 23, but not 21, and the positive correlation observed between such destabilization and higher oligomerization propensity of the Dutch, Arctic, Italian, and Iowa Aβ variants have been implicated in the causation of the resulting familial AD [133].

1.1.6 Modes of Aβ Toxicity

Much of AD literature dealing with Aβ aggregation and therapeutics directed at Aβ aggregation suggests that Aβ is toxic. However, often a gap is left regarding how and why. Here, I provide a brief overview of some of the most studied links between Aβ and the observed toxicity.

Epidemiological, functional neuroimaging, and neuropathological data point to disruptions in brain metabolism and energetics as playing a role in the pathogenesis of

cognitive impairments and AD. Population studies have implicated metabolic disorders, such as obesity and diabetes mellitus type 2, as risk factors for AD [134]. Excessive energy intake through the diet has been shown to induce cognitive dysfunction by promoting inflammatory responses [135], and to exacerbate Aβ deposition and memory impairment in a mouse model of AD [136]. The interactions of Aβ with the mitochondria and its dysfunction have been implicated in the neuronal metabolic deficits that occur in AD. The effects of Aβ on mitochondria are described further below in section 1.1.6.1. Much of the energy used by the brain and neurons is for neurotransmission [137]. Thus, the decrease in brain metabolism as seen by FDG-PET in AD, indicates reduced cellular function and correlates with disease severity [47]. Imbalance in excitatory neurotransmission in AD, potentially caused by Aβ, result in Ca^{2+} dysregulation (Figure 1.6) and excessive glutamate receptor activation. These mechanisms, which are described further below in section 1.1.6.2, can result in seizures [138] and degeneration of synapses

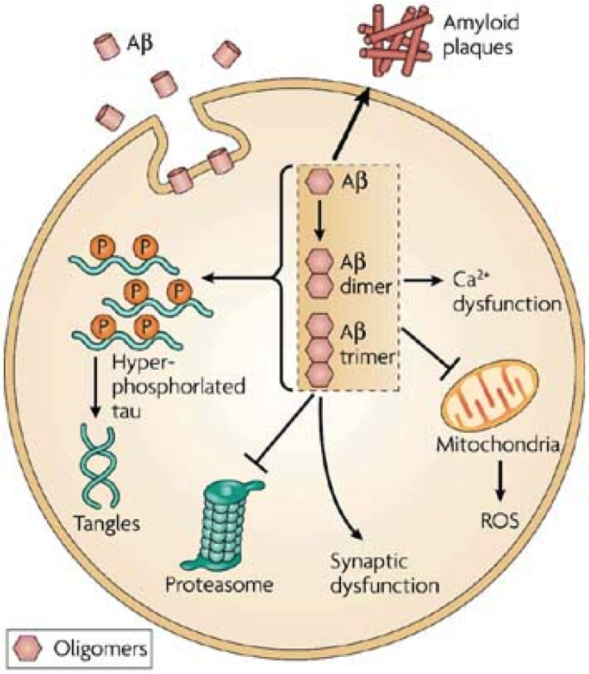

Figure 1.6: Modes of Aβ toxicity
Aβ produced intracellularly or taken up from extracellular sources, has various pathological effects on cell and organelle function. Intracellular Aβ can exist as a monomer that aggregates into oligomers, and any of these species may mediate pathological events *in vivo*, particularly within dysfunctional neurons. Evidence suggests that intracellular Aβ may contribute to pathology by facilitating tau hyperphosphorylation, disrupting proteasome and mitochondria function, and triggering calcium and synaptic dysfunction. Adapted from [3]

and neurons [139].

Another suggested mechanism by which amyloidogenic protein assemblies cause toxicity is disruption of membrane integrity. This could result from direct distortion of physical properties of membranes [140,141], such as formation of non-specific channels or pores [142], which may result in apoptosis [143] or increased membrane permeabilization and conductivity [142,144]. To explain the cause of the range of toxic effects observed for different Aβ fibril preparations, Yoshiike et al. [145] suggested that the surface composition of different morphologies of amyloid fibrils, specifically clusters of positive charge, were the relevant component. Through chemical modification or amino acid substitution in Aβ, they showed that changes in the surface structures of Aβ fibrils led to changes in properties responsible for electrostatic and/or hydrophobic interactions and could be manipulated to suppress Aβ toxicity [145].

Positively charged K residues (See Table 1.1 for amino acid abbreviations) have been shown to play a prominent role in membrane interactions and toxicity of the proteins involved in AD and likely in other amyloid-related diseases. Recently, the binding sites of five toxicity inhibitors, Congo red, Myricetin, melatonin, nicotine, and curcumin, on Aβ were explored computationally and then tested *in vitro* to gain insight into the surface components of aggregates that contribute to their toxic effects [146]. All five molecules were found to dock at or near K28, supporting the importance of this charged residue in Aβ assembly and toxicity. The other K residue in Aβ, K16, resides next to the CHC, which is known to be important in regulating Aβ fibrillogenesis [147-149]. K16 itself has been reported to be solvent-exposed and thus not participate directly in Aβ self-assembly but rather to be available for interaction with cell membranes or

potential inhibitors [150-152]. The triple substitution R5A, K16A, and K28A in Aβ resulted in significant loss of Aβ40 fibril toxicity in human embryonic kidney cells [145], presumably due to removal of the positively charged residues that could interact with and disrupt the cell membrane. Thus, in both oligomers and fibrils, electrostatic attraction between positively charged K residues and negatively charged membrane phospholipid head groups, together with hydrophobic interactions between the K butylene and lipid hydrocarbon chains, presumably contribute to the toxic effect of Aβ and other amyloidogenic protein assemblies [145,153-155].

The "cholinergic hypothesis" of memory dysfunction [156] proposed in 1982 that degeneration of cholinergic neurons in the nucleus basalis of Meynert [157] and the reduction in the synthesis [158], uptake [159], and release [160] of acetylcholine contributed to the deficits in cognitive function seen in AD. Aβ binds to α7-nicotinic acetylcholine receptors in cortical and hippocampal synaptic membrane preparations, and this interaction leads to the inhibition of acetylcholine release and Ca^{2+} flux leading to neuronal death [161]. Activation of α7-nicotinic acetylcholine receptors by nicotine was neuroprotective against Aβ42-induced neurotoxicity *in vitro* [162].

Studies also have suggested a role for metal ions, specifically Zn^{2+}, Cu^{2+}, Fe^{3+}, and Al^{3+}, in accelerating Aβ aggregation and enhancing Aβ toxicity [163]. Many other mechanisms of Aβ toxicity also have been suggested, from intracellular signaling by interaction with cell surface receptors, such as cellular prion protein [164], low-density lipoprotein receptor related protein, receptor for advanced glycation end products, α-7-nicotinic acetylcholine receptor, and N-methyl-D-aspartate (NMDA) receptors [3], to

induction of the inflammatory system [165], but these topics are beyond the scope of this thesis.

1.1.6.1 Aβ-induced Mitochondrial Dysfunction

Mitochondria generate cellular energy in the form of adenosine triphosphate (ATP) and regulate levels of Ca^{2+} and reactive oxygen species (ROS) [166]. Neuronal activity has a high energy cost and neurons are particularly sensitive to changes in mitochondrial function [137], especially at the synapse where Ca^{2+} homeostasis is critical for function [167]. In cells expressing the *APP* Swedish mutation, Aβ levels in the culture medium correlate with the percentage of cells with abnormal mitochondrial morphologies, distribution, and fragmented mitochondria. Inhibition of β-secretase, and thus reduction of Aβ levels, prevents these abnormalities [168]. Aβ can induce mitochondrial membrane permeabilization by interacting with the membrane permeability transition pore [169], cause the collapse of the mitochondrial membrane potential, generate excessive ROS by disrupting cellular Ca^{2+} homeostasis [170], and induce ATP depletion by interacting with ATP synthase [171]. In Tg2576 mice, a mouse model of AD, Aβ progressively accumulates in synaptic mitochondria, before accumulation is seen in mitochondria found in the cell body, and this accumulation results in functional alterations, such as decreased mitochondrial respiration and respiratory enzyme activity, elevated ROS production, and compromised Ca^{2+} handling capacity [172], though refuting evidence also has been reported that did not find differences in presynaptic mitochondrial function in several mouse models of AD [173]. The interaction of Aβ with the mitochondria has been demonstrated to induce apoptosis

pathways [169,174]. Interestingly, as mitochondria have their own DNA, studies of the nine haplotypes found in Caucasian populations show that in patients with AD, but not in healthy controls, there is an association between the *APOE* ε4 allele and certain mitochondrial polymorphisms that increase AD susceptibility, whereas other haplotypes may neutralize the harmful effects of the *APOE* ε4 allele [175].

1.1.6.2 Aβ-induced Excitotoxicity

Consistent with the involvement of the glutamatergic system and the NMDA receptor in learning and memory, disruption of the homeostasis of this system has been linked with the pathophysiological processes underlying AD [176,177]. The NMDA receptor is both voltage-dependent, a result of the Mg^{2+} block of the ion pore at resting state, and ligand-gated. This means that co-activation by two agonists is required for activation of the receptor. Because of this requirement, the NMDA receptor is considered a coincidence detector and thus plays a role in learning and memory. Excitotoxicity, or chronic, mild activation of NMDA receptors that leads to synaptotoxicity and neurodegeneration, correlates with cognitive dysfunction in AD [139,178,179]. Numerous AD-related pathologies, such as Aβ deposition, Aβ oligomers, hyperphosphorylated tau in NFTs, oxidative stress, mitochondrial dysfunction, tonically elevated levels of glutamate, and inflammation have been associated with increased sensitivity and/or activity of the glutamatergic system in AD [139,180-183]. Specifically, Aβ has been shown to stimulate Ca^{2+} influx into neurons through a mechanism that can be blocked using NMDA antagonists [181,184]. Aβ also has been found to influence intracellular Ca^{2+} concentrations, buffering, release from intracellular stores, and

sequestration [185,186]. Sustained increases in cytoplasmic Ca^{2+} concentrations promote depletion of presynaptic glutamate stores, resulting in impaired synaptic transmission. Aβ may increase residence of glutamate in the synaptic cleft through inhibition, and even reversal, of uptake mechanisms [187]. Non-glutamate agonists of NMDA receptors, such as homocysteic acid, also have been shown to be elevated in AD [188]. Aβ42 has been shown to inhibit the sodium-potassium ATPase pump, and therefore could induce neuron depolarization and relief of the Mg^{2+} block of NMDA receptors [189]. Thus, both direct and indirect effects of Aβ are likely to keep the NMDA receptor chronically open in AD. This pathological tonic activation would be expected to cause a constant low level influx of Ca^{2+}, even under resting conditions, depolarizing the postsynaptic terminal (Figure 1.7). As a result, incoming physiological signals may not be recognized against this raised background noise and, consequently, synaptic plasticity and LTP are impaired. Ultimately, the excessive influx of Ca^{2+} ions could cause death of the postsynaptic neuron via associated effects, such as the formation of free radicals, changes in nuclear chromatin, and DNA breakage [8,181,190]. Ca^{2+} influx can also trigger seizure activity, activation of programmed cell death mechanisms, and damage to structural proteins [191].

1.1.6.3 Tau Toxicity

NFTs are another pathological hallmark of AD and are thought to be a significant contributor to the disease progression. Tau, the main component of NFT, is a microtubule-associated protein that promotes, stabilizes, and organizes microtubule assembly. It is localized predominantly in axons where it plays a role in axonal growth

and transport. In the adult human brain, alternative splicing during expression can result in six different isoforms of tau that differ by the presence or absence of acidic regions in the N-terminus and three versus four repeat regions of a conserved tubulin-binding motif in the C-terminus. These structural differences confer different affinity of the tau isoforms for microtubules [192]. Phosphorylation of five residues inside the repeat regions is used to modulate interactions between tau and microtubules [193] and degradation of tau [194]. Tau mutations, though not genetically linked to AD, have been shown to alter the relative proportion of the various tau isoforms [195], impair the ability

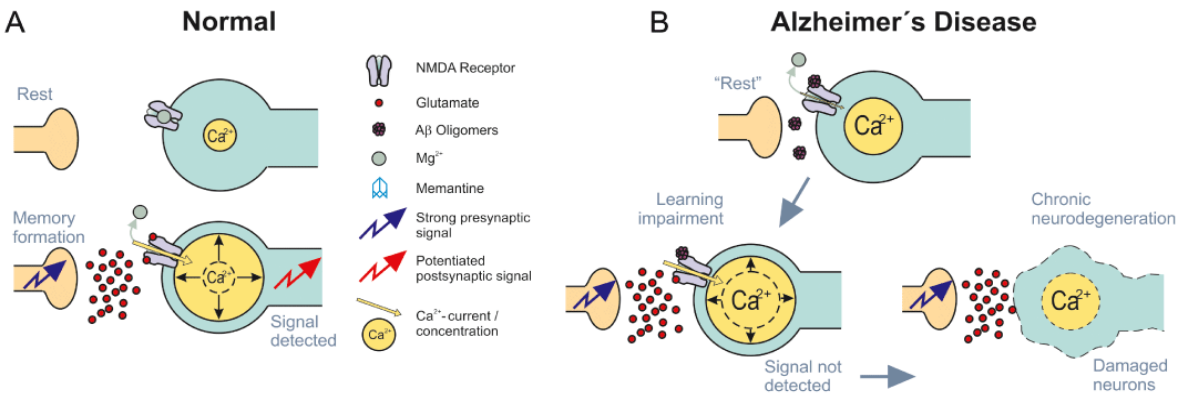

Figure 1.7: Aβ's interaction with NMDA receptors causes excitotoxicity
(A) Under normal physiological conditions, synaptic plasticity/learning depends on the detection of a relevant (sufficiently strong) synaptic signal over the background noise (here referring to transient, high- vs. prolonged, moderate intracellular Ca^{2+} levels), resulting in a sufficient signal-to-noise ratio. Intracellular Ca^{2+} concentrations at any single time point are represented by different sizes of the yellow Ca^{2+} containing circles. For simplification, the roles of other receptors (e.g. AMPA) and feedback inhibition have been omitted from this cartoon. (B) The signal-to-noise ratio hypothesis assumes that in AD, due to a tonic overactivation of NMDA receptors by, for example, soluble Aβ oligomers, Mg^{2+} no longer is effective enough to play its 'filtering' function. In turn, synaptic noise rises, impairing detection of the relevant synaptic signal required for learning/plasticity. The light blue straight arrows indicate the proposed course of events, i.e., first symptomatic disturbance of synaptic plasticity, followed by synaptotoxicity and ultimately neuronal death. Soluble Aβ oligomers represented as aggregates of small mauve circles – here binding directly to NMDA receptors for simplification, but probably interacting more directly with anchoring protein complexes and thereby affecting the function of their associated proteins such as NMDA receptors. Adapted from[8]

of tau to bind and promote the assembly of microtubules [196], and/or enhance the aggregation of tau into filaments [197], which are a common pathological finding in the AD brain.

As described previously, the abundance and location of NFTs correlate with the severity of cognitive decline in AD [31,198]. NFTs can confer toxicity by displacing and reducing the number of cytoplasmic organelles [199], inhibiting the proteasome [200], and/or inhibiting axonal transport [201,202]. Tau oligomers also may play a role in AD as reflected by their ability to inhibit microtubule assembly [203], disassemble microtubules [204], and cause synaptic loss in tau transgenic mice before NFTs formation [205,206]. Tau hyperphosphorylation at up to 21 epitopes, largely by glycogen synthase kinase 3β and cell division protein kinase 5 [207], is an early pathogenic event that precedes NFTs formation [208]. Hyperphosphorylation of tau by both increased phosphorylation and decreased dephosphorylation, limits its degradation, resulting in accumulation of tau inside the cell. Hyperphosphorylated tau then dimerizes into paired helical filaments – similar to two threads of tau wound around eachother − that further aggregate to form NFTs [209].

Hyperphosphorylation has been shown to limit tau's ability to promote microtubule assembly and to cause cell death [209]. Other post-transcriptional modifications of tau, such as glycosylation [210] and truncation [211,212] in addition to aberrant tau-mediated intracellular signaling play a role in tau-mediated neurotoxicity [213,214]. Disruption of the normal function of tau and even just the presence of truncated tau or the overexpression of tau can enhance the vulnerability of neurons. Tau-mediated disruption of intracellular transport, specifically transport of mitochondria,

results in fewer mitochondria in neural processes [202,215,216] and decreased ATP levels [202], and may increase the susceptibility of neurons to excitotoxicity [217,218]. Thus, tau-mediated toxicity is thought to occur by both loss of normal function and gain of toxic function.

It is believed that tau is a downstream mediator of Aβ toxicity in AD (Figure 1.6; for review, see [219]) as reduction in tau levels provides protection against Aβ toxicity in primary neurons [220]. Tau-null mice are protected, compared to WT mice, against behavioral deficits caused by overexpression of mutant human APP [221]. In addition, injection of Aβ42 fibrils into the brain of P301L tau transgenic mice, but not WT mice, significantly increases tau phosphorylation, the number of NFTs, and degenerating neurites [222].

1.1.6.4 Defective Cellular Protein Degradation

Another pathological hallmark of AD is dystrophic neurites, or gross focal swellings of neuronal processes and protein accumulation. Defective autophagic lysosomal proteolysis and proteasomal proteolysis also likely contribute to the pathology in AD. Autophagy is a clearance mechanism for large, long-lived proteins and aggregates, as well as organelles such as mitochondria. The proteasome is a complex for clearing soluble cytosolic proteins. Although each system preferentially degrades specific substrates, some substrates, such as tau, can be degraded by both mechanisms, depending on conformation, size, and post-translational modifications [223]. Soluble, monomeric tau is an ideal substrate for the proteasome, whereas low-order tau oligomers may be preferentially degraded by autophagy. Both systems are inhibited in AD [200,224,225].

Dystrophic neurites containing autophagic vacuoles are abundant in the AD brain, suggesting autophagy disruption [225,226]. In fact, the levels of undigested protein in AD brain parallels certain lysosomal storage disorders [227]. Similar to AD, the ε4 allele of *APOE* also promotes disease development in one lysosomal storage disorder, Niemann-Pick disease type C, suggesting an underlying relationship in disease etiology [228]. Mouse models of AD have severe autophagy neuropathology as well. TgCRND8 mice, which have two human mutations in *APP*, display extensive autophagic-lysosomal pathology [229,230]. Deletion of an endogenous inhibitor of lysosomal proteases, cystatin B, rescues lysosomal pathology, decreases extracellular amyloid deposition, and ameliorates learning and memory deficits in these mice [230]. An early disease-specific pathologic change in sporadic AD is the enlargement of specific endosomes, which reflects pathologic acceleration of endocytosis [231,232] and this is exacerbated by the ε4 allele of *APOE* [231]. Proteasomal activity also is decreased in AD-sensitive brain regions, compared to uninvolved regions [200,233] and aggregated paired helical filaments of tau and Aβ oligomers have been shown to inhibit the proteasome *in vitro* [200,224].

There have been a number of single-factor theories proposed to explain the etiology of AD: channel hypothesis, metal hypothesis, axonal transport dysfunction hypothesis, mitochondrial cascade hypothesis, and the amyloid cascade hypothesis [234]. However, to date, no one theory can explain all aspects of the disease. It is, thus, likely that sporadic AD, similarly to cancer, is a result of multiple insults, including a combination of "deficient" alleles of numerous genes, stress, stroke, accelerated "aging"

through lifestyle choices, and environmental factors such as levels of metals in consumables.

1.1.7 Animal Models of Alzheimer's Disease

Many animal models of AD exist, falling in categories of "spontaneous" or "induced" models, with "induced" being further subdivided into "transgenic" and "nontransgenic." Some species such as dogs, cats, sheep, and nonhuman primates spontaneously develop plaque or tau pathology along with neurobehavioral impairment and thus can be used as spontaneous models. Induced models may include animals with Aβ injected directly into the brain [110] or introduced by viral vectors [235], animals treated with drugs that result in increased Aβ, such as Thiorphan which inhibits the Aβ degrading enzyme – neprilysin [236], and systemic lipopolysaccharide which increases activities of Aβ producing enzymes β- and γ-secretase [237]. Transgenic animal models of AD, from *drosophila melanogaster* to *caenorhabditis elegans* to rodents, are the most popular and have been developed for the study of AD on the basis of the amyloid cascade hypothesis by taking advantage of the mutations in *APP, PSEN1* and *PSEN2* that cause familial forms of AD. Upon the discovery of familial AD mutations in *APP*, Games et al. [238] reported the first successful application of overexpression of transgenes containing familial AD mutations, in the PDAPP mouse model, so named for the use of the platelet derived growth factor-β promoter to drive the *APP* gene. This model showed about 10-fold increase in human APP and Aβ compared with mouse APP levels [238], developed minimal plaque deposition by 6-m of age, which became substantial by 9-m of age [239] along with synapse loss [240] and learning deficits [241]. Subsequently, many other AD

mouse models were developed with a similar approach of using familial AD-causing mutations (see review [29]). Common features of the models include elevated levels of Aβ, plaque deposition, dystrophic neurites, gliosis, and behavioral changes, such as hyperactivity or anxiety and age-related learning and memory deficits [29,242]. Mouse models with multiple transgenes have been developed that provide a distinct time-to-phenotype advantage over single-transgene models [243-246].

Transgenic mouse models of AD are not perfect proxies of disease, though, and do not produce the full spectrum of AD pathology. First, the models are based on expression of mutant genes implicated in a small subset of the AD patient population and thus an underlying assumption is that sporadic and familial AD are highly similar. Second, the lines are designed to express much higher than physiological levels of the disease-relevant proteins to obtain pathology in a timely manner [238,243,247]. Third, the temporal sequence of plaque pathology and cognitive deficits does not mimic human disease. Some mouse models present cognitive deficits before significant plaque pathology [242], whereas in humans, plaque pathology often is present for substantial periods of time before cognitive symptoms appear [2,248]. Additionally, the spatial appearance of Aβ and tau pathology may not match the human disease [249]. Fourth, many of the mouse models do not display significant, if any, neurodegeneration [250,251]. This major difference between mouse models and human AD may be partly overcome by the presence of multiple mutations or transgenes. For example, the 5×FAD mouse [252], which harbors three *APP* and two *PSEN1* mutations, does show obvious neuronal loss [252]. Lastly, many of the models do not display cytoskeletal pathology, i.e., NFTs [253]. This has been overcome by the inclusion of tau mutations, typically

associated with frontotemporal dementia, in the model [249,254]. However, the utilization of multiple mutations mentioned in points four and five, further distances the models from sporadic AD.

The following chapters describe experiments using a triple transgenic (3×Tg) mouse model of AD that overexpresses two familial AD mutations in humanized genes: the Swedish *APP* form (APP_{Swe}: K595N, M596L; See Table 1.1 for amino acid abbreviations) and *PSEN1*(M146V). In addition, this model carries the tau gene mutation (P301L), which causes frontotemporal dementia [249]. Inclusion of the tau component makes this model unique and more physiologically relevant because even though Aβ assembly is believed to be the key causative event in AD, tau hyperphosphorylation and aggregation may be equally important [255].

The first neuropathological manifestation in the brains of the 3×Tg mice develops at 3-m of age as intracellular Aβ deposition in the hippocampus [249]. The high levels of intracellular Aβ deposition correlate with impairment of synaptic plasticity, including deficits in LTP. Thus, intracellular Aβ is hypothesized to exacerbate synaptic dysfunction [249]. However, it is important to consider that many Aβ antibodies used in immunohistochemistry may also bind APP and thus a clear distinction between the effects of intracellular Aβ and APP is difficult [256]. Next, the 3×Tg mice develop Aβ plaques followed by NFTs in AD-relevant brain regions (hippocampus, cortex, and amygdala) [249], and reactive astrogliosis can be found co-localized with Aβ deposits [249]. Though memory deficits can be observed by 4-m of age [257-259], observation of Aβ deposition, NFTs, and long-term memory deficits require a minimum age of 9−12 m and become robust by 18–20 m. This mouse model, similar to most mouse models of

AD, does not exhibit significant neuron death at ages where other AD symptoms are prevalent [249]. Nevertheless, this AD model exhibits not only the two neuropathological hallmarks of AD, amyloid plaques and NFTs, but also neurofunctional symptoms, all of which are vital for proper assessment of potential drugs for AD.

1.2 Alzheimer's Disease Therapies

1.2.1 Current Therapies

Five drugs currently are approved by the Food and Drug Administration for use in AD and fall into two categories: acetylcholinesterase inhibitors (AChEIs) and glutamate modulators. All five drugs were approved between 1993 and 2003, none address the underlying etiology of AD, and their efficacy varies greatly between individuals. During the first year, patients' performance in measures of cognition, activities of daily living, behavioral symptoms, and Clinical Global Impression of change may improve significantly for 10–20% of patients, plateau for 30–50% of patients, or continue to deteriorate for 20–40% of patients [260]. Meta-analysis of long-term, open-label, follow-up or observational studies show that continued use of AChEIs provides cognitive benefits for 2–5 years and delays nursing-home placement, especially with the combination therapy that is now typical for AD management [260]. In addition to multiple pharmacologic methods, combination therapy can include non-pharmacologic interventions, such as task simplification, environment modification, and caregiver education on communication, which are used to address behavioral disturbances. Optimistically, combination therapy can be expected to improve symptoms, delay and

reduce emerging problematic behaviors, decrease the rate of overall decline, and lower the impact of AD on patients and caregivers [260].

The AChEIs were the first pharmacologic strategy for AD and were based on the "cholinergic hypothesis" of memory dysfunction, described above in section 1.1.6 [156]. They include tacrine (brand name: Cognex), donepezil hydrochloride (Aricept), rivastigmine tartrate (Exelon), and galantamine hydrochloride (Razadyne). Tacrine hydrochloride was approved in 1993 and was a first generation AChEI that is now largely discontinued due to high levels of liver toxicity [261]. Galantamine also acts as an allosteric nicotinic receptor modulator and has been shown to stimulate the presynaptic release of acetylcholine and other neurotransmitters *in vitro* [262].

As described above in the *Aβ-Induced Excitotoxicity* section 1.1.6.2, Aβ can induce toxicity by affecting glutamate homeostasis, directly impacting NMDA receptor function, and thus driving synaptic dysfunction. The most recent Food and Drug Administration-approved drug for AD is memantine (2003; brand name: Namenda). It is a noncompetitive NMDA receptor antagonist with strong voltage dependency and rapid channel unblocking kinetics [263]. These characteristics allow memantine to prevent the perpetual and pathological influx of Ca^{2+} into postsynaptic neurons and the resulting excitotoxicity. Memantine, in a way, replaces the Mg^{2+} block that is displaced in AD by low baseline depolarization and is more effective than Mg^{2+} as a filter of signal-to-noise at the glutamatergic synapse because it has a higher threshold for displacement by depolarization, thus preserving the physiologic actions of glutamate required for learning and memory (Figure 1.8) [8]. Importantly, memantine has a narrow therapeutic window which is attributed to its mechanism of action — high concentrations of memantine

prevent the normal function of NMDA receptors [8]. By preventing excitotoxicity, memantine can reduce neurodegeneration, as found in animal models [264] and even upregulate central nervous system genes involved in neurogenesis, neural differentiation, memory, and neurotransmission [265]. In humans, retrospective analyses show a trend for a disease-slowing tendency of memantine due to its neuroprotective effects [8].

Other pharmacologic approaches to AD therapy with yet inconclusive results include nicotine, selegiline, vitamin E, ginkgo biloba, piracetam, hormone replacement therapy, anti-inflammatory drugs, statins, and folic acid [266,267].

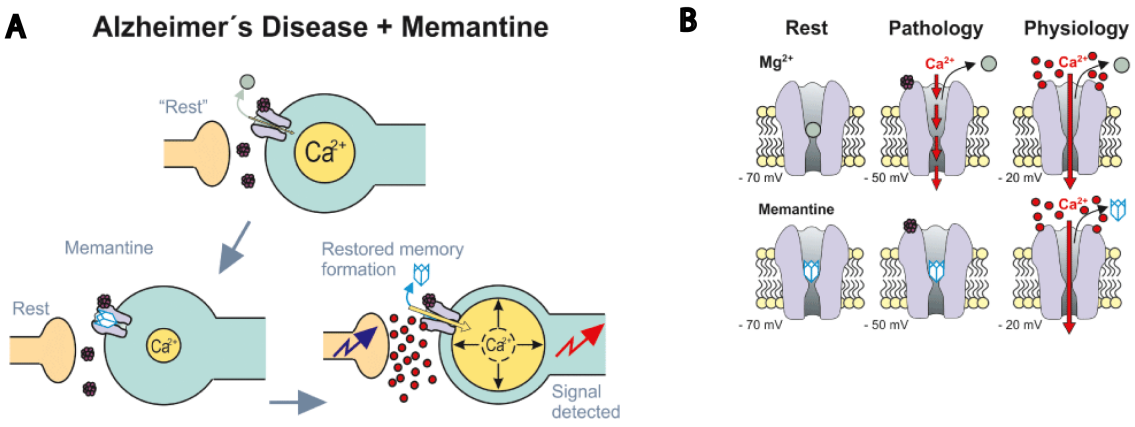

Figure 1.8: The interaction of Aβ with NMDA receptors causes excitotoxicity
A) A schematic illustrating memantine's proposed mechanism of action in AD based on the signal-to-noise hypothesis. Memantine serves as a more effective filter than Mg^{2+}, blocking pathological 'noise' at glutamatergic synapses and thereby allowing detection of the relevant synaptic signal. Synaptic plasticity is restored and synaptotoxicity/ultimate neuronal death is prevented by the same mechanism of action. B) Schematic illustrating the hypothesis explaining how the fast unblocking kinetics of memantine allows this voltage-dependent compound to differentiate between the physiological and pathological activation of NMDA receptors. Under resting therapeutic conditions [i.e., in their continuing presence at −70 mV (left), Mg^{2+} (top) or memantine (bottom)] occupy the NMDA receptor channel. Both Mg^{2+} and memantine leave the NMDA receptor channel upon strong synaptic depolarization (−20 mV, right) due to their pronounced voltage dependency and rapid unblocking kinetics. However, memantine – in contrast to Mg^{2+} – does not leave the channel easily upon moderate prolonged depolarization during chronic excitotoxic insults caused by Aβ oligomers, which tonically activates NMDA receptors (−50 mV, center). Transient, strong, and prolonged moderate Ca^{2+} influx are illustrated by the full and dashed red arrows respectively. Adapted from [8]

1.2.2 Therapy Research

As AD is a multifactorial disease, numerous avenues have been taken in the search for efficacious therapeutics. In addition to the AChEIs and NMDA receptor antagonists, other drug categories include: 1) Aβ-targeting molecules, discussed in the next few paragraphs; 2) tau kinase inhibitors; 3) antioxidants, especially mitochondria-targeted; 4) anti-inflammatory agents, such as non-steroidal anti-inflammatory drugs; 5) neuroprotective agents, such as brain-derived neurotrophic factor and resveratrol that is currently in phase III clinical trials; 6) histone deacetylases; 7) anti-diabetics; 8) and APOE related therapies targeting both its loss of function and gain of toxic function. For an extensive review of 140 substances studied in mice between 2001−2011, see Li et al. [268,269].

Aβ-targeting treatment strategies include: inhibition of Aβ production, promotion of Aβ clearance, and modulation of Aβ aggregation. The most common approaches to inhibition of Aβ production are inhibition of β-secretase or γ-secretase. Though these approaches have been successful *in vitro* and in pre-clinical studies, none have succeeded in clinical trials. The most advanced drug candidate to fail in clinical trials was Semagacestat, a γ-secretase inhibitor sponsored by Eli Lilly, which failed in 2010. One major challenge with secretase inhibitors is that they have multiple substrates. Thus, although inhibition may reduce Aβ production, it also inhibits cleavage of other important substrates leading to unwanted side effects. A particularly pertinent example is Notch protein cleavage by γ-secretase. Notch is a transmembrane receptor involved in

regulating cell-fate decisions and its correct processing by γ-secretase is essential for proper cellular function.

The most common approaches to promotion of Aβ clearance have been passive and active immunotherapy. Immunotherapeutic Aβ degradation has been suggested to work through phagocytic clearance of Aβ by microglia [270] and/or through binding of antibodies to Aβ, resulting in prevention of its assembly and neurotoxicity [271]. Similar to inhibition of Aβ production, promotion of Aβ clearance has been successful in pre-clinical studies, however, clinical trials of Solanezumab, Bapineuzumab, and Gammagard, sponsored by Eli Lilly, Pfizer/Johnson & Johnson, and Baxter, respectively, have all failed. The reasons for failure of these clinical trials of course may be related to the efficacy of the drug. However, additional reasons for failure have been suggested that relate to the poor sensitivity in tests for early diagnosis. For example, inclusion of MCI patient populations that may be too far along in disease progression but are the earliest that AD can be identified, could result in clinical trial failure regardless of the drug. Treatment of this population may stop disease progression but will likely not lead to functional improvement due to the irreversible loss of neurons. Since clinical trials are prohibitively expensive it is possible that their duration is not long enough to see small functional differences. Further, since the underlying cause of AD has not been identified, it is possible that seemingly similar patient populations could have different dominating disease components, which would dilute out possible drug effects seen in one group by the whole population.

The last Aβ-targeting treatment strategy is modulating the self-assembly of Aβ in an effort to reconfigure Aβ assembly into nontoxic structures, prevent aggregation, or

promote disaggregation. This approach may be advantageous relative to the others because it directly targets the deleterious form of Aβ rather than just its presence. Further, general strategies for inhibition of aberrant protein aggregation may be applicable to the many other amyloidoses with similar elements. In the last decade, numerous inhibitors targeting Aβ oligomerization and toxicity have been developed, including: curcumin [272], *scyllo*-inositol [273,274], amyloid-binding dyes [275], polyphenols [276], catechols [277], and flavonoids [278,279]. Interestingly, some amyloid-binding dyes and polyphenols have been shown to reduce toxicity by accelerating Aβ fibrillogenesis [275,276,280], a strategy followed in view of the observation that fibrils are less toxic than oligomers. Whereas other compounds, including *scyllo*-inositol [273,281,282], the polyphenols epigallocatechin-3-gallate [283,284], resveratrol [285], Aβ42 C-terminal fragments [286,287], and molecular tweezers, which are the focus of this thesis [288], were found to stabilize non-toxic oligomers. Three inhibitors of Aβ assembly/toxicity currently are in phase-2 clinical trials: PBT2 [289], *scyllo*-inositol (ELN005), and epigallocatechin-3-gallate (Sunphenon). Methylene blue (Rember and LTMX formulations) is being explored in a phase-2 clinical trial as an inhibitor of tau aggregation. However, because of the lack of understanding of the mechanisms of actions of these molecules, there is reason for caution. For example, PBT2 was developed as a Cu^{2+}/Zn^{2+} chelator but may actually work by inhibiting the phosphatase calcineurin [290]. In a recent clinical trial, PBT2 lowered CSF Aβ42 significantly relative to placebo but the study did not find correlations between changes in CSF Aβ40, Aβ42, total tau, or hyperphosphorylated tau and cognitive performance [291]. S*cyllo*-inositol was reported to cause nine deaths in the high-dose groups in a recent phase 2A trial [292] and

epigallocatechin-3-gallate was reported to promote formation of toxic tau oligomers [293]. For a full discussion of the *in vivo* research of epigallocatechin-3-gallate and its comparison to molecular tweezers, see [294].

The failure of AD clinical trials in the last decade [295,296] might be partially attributed to the common methods of drug discovery, namely large-scale compound screens or empirically identified leads. Though high-throughput screens generally are efficient and leads discovered empirically, particularly from food sources, tend to be safe, lack of understanding of the mechanism of action of the compounds selected by either strategy may result in pursuing nonviable leads and unpredictable complications. The necessity for better mechanistic understanding has been underscored in recent years by studies showing that many inhibitors of protein aggregation are promiscuous in their inhibition, a behavior attributable to the inhibitors forming colloids around protein fibrils and thereby sequestering them rather than actually disrupting the assembly process [297,298]. Complicating matters further, inhibition of fibril formation or dissociation of existing fibrils may yield both toxic [299,300], and non-toxic oligomers, depending on the particular proteins and inhibitors studied [99].

Large-scale, high-throughput screens based on identifying binding interactions are best suited for compounds that fit tightly in a small, deep pocket and bind to the target with affinity similar to, or higher than, the natural ligand or substrate. However, in the case of amyloid, stable structure in the fibrils is achieved as a sum of numerous weak interactions spread across large, flat areas, where it would be difficult for a small molecule to compete effectively [301]. In addition, because of the high flexibility of amyloids, even molecules that bind with relatively high affinity can be accommodated

without sufficiently disrupting the amyloid lattice [302]. Inhibiting oligomer formation and toxicity is even more difficult because the structures of oligomers not only are unknown, but also are constantly changing. These challenges in drug discovery and development specifically for protein aggregation may be circumvented by using rational approaches to the problem, considering the weakest links of the target(s) and the fundamental interactions within and among the individual building blocks necessary for abnormal self-assembly and toxicity.

Because the structures of the most toxic assemblies, the metastable oligomers of amyloidogenic proteins, are poorly understood [100,303,304], continued research towards better characterization of these structures is vital. At the same time, the tremendous magnitude of the financial and psychological burden AD and other amyloidoses create for individuals and societies make the search for disease-modifying intervention highly urgent. Therefore, scientists and physicians do not have the luxury of waiting for complete structural details to be deciphered and must act now to create the best possible solutions to the problem using currently available information.

The focus of this dissertation is *in vivo* characterization of a small molecule that was rationally identified as an aggregation inhibitor/modulator, based on mechanistic understanding of its interaction with proteins. Importantly, the compound binds to its targets regardless of their aggregation state, including prior to formation of oligomers, thereby circumventing the problem of the unknown structures of the oligomers.

1.2.3 Molecular Tweezers: Artificial Lysine (K) Receptors

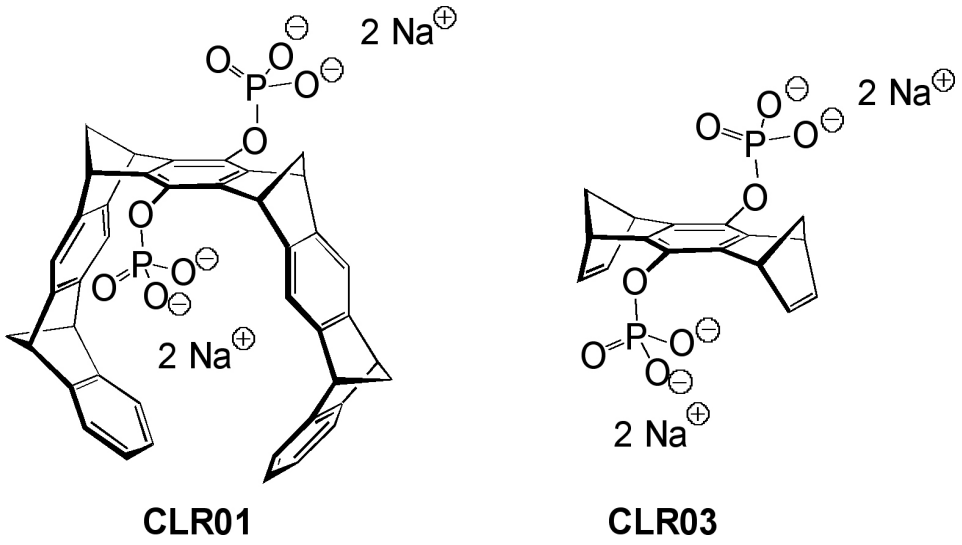

Fig. 1.9. Structure of the molecular tweezers CLR01 and CLR03
Adapted from [7]

Molecular tweezers (MTs) developed by Drs. Klärner and Schrader at University of Duisburg-Essen, Germany, are small molecules that act as selective, artificial K receptors (See Table 1.1 for amino acid abbreviations). MTs bind with dissociation constant, K_d = 10–20 μM to K residues and with ~10-times lower affinity to R residues in peptides and proteins [288,305,306]. They have a horseshoe-shaped structure composed of two hydrocarbon arms capable of hydrophobic interactions with the alkyl side chains of K residues, which gets threaded through the central cavity of the MT [305,307]. At their bridgehead, MTs have negatively charged groups, e.g. phosphates, which form ionic interactions with the positively charged ammonium or guanidinium groups of K and R, respectively. Binding of the MT derivative termed CLR01 (Figure 1.9) [288]) to K16 and K28, and to a lower extent to R5, in Aβ was confirmed by solution-state, 2D-nuclear magnetic resonance and electron-capture dissociation mass spectrometry [288].

MTs utilize the same types of interactions, hydrophobic and electrostatic, found in early Aβ assembly and presumably K-mediated interaction of Aβ with cell membranes.

Understanding this, Dr. Gal Bitan hypothesized that competition by MTs for these interactions could inhibit Aβ assembly, decrease Aβ-induced toxicity, and also be applicable to other amyloidogenic proteins [288]. The *in vitro* studies of CLR01 with Aβ and other amyloidogenic proteins and subsequent studies with a zebrafish model of α-synuclein toxicity, performed by collaborators, will be summarized in Chapter 2. *In vivo* analysis of CLR01 in a transgenic AD mouse model and toxicity analysis of CLR01 are discussed in Chapter 3 and 4, respectively, and are original work for this dissertation. The influence of CLR01 on normal protein assembly also has been assessed and is discussed in Chapter 4.

The data presented in the following chapters has been obtained using the MT derivatives CLR01 and CLR03 (Figure 1.9). CLR03 differs from CLR01 in that it has a truncated hydrocarbon skeleton. Consequently, it can form electrostatic, but not hydrophobic interactions, it is not expected to bind specifically to K residues, and has been used as a negative control. In multiple experiments CLR03 was found to have minimal or no effect on the assembly or toxicity of the proteins under study, highlighting the functional importance of the hydrophobic side arms of MTs for interacting with K residues.

1.3 References

1. Rasool S, Martinez-Coria H, Wu JW, LaFerla F, Glabe CG (2013) Systemic vaccination with anti-oligomeric monoclonal antibodies improves cognitive function by reducing Aβ deposition and tau pathology in 3xTg-AD mice. Journal of Neurochemistry 126: 473-482.

2. Jack CR, Jr., Knopman DS, Jagust WJ, Shaw LM, Aisen PS, et al. (2010) Hypothetical model of dynamic biomarkers of the Alzheimer's pathological cascade. Lancet Neurology 9: 119-128.

3. LaFerla FM, Green KN, Oddo S (2007) Intracellular amyloid-β in Alzheimer's disease. Nat Rev Neurosci 8: 499-509.

4. Prince M, Prina M, Guerchet M (2013) World Alzheimer Report 2013. London: Alzheimer's Disease International.

5. Serpell LC (2000) Alzheimer's amyloid fibrils: structure and assembly. Biochimica et Biophysica Acta 1502: 16-30.

6. (2012) Dementia: A Public Health Priority. United Kingdom: World Health Organization

7. Prabhudesai S, Sinha S, Attar A, Kotagiri A, Fitzmaurice AG, et al. (2012) A novel "molecular tweezer" inhibitor of α-synuclein neurotoxicity in vitro and in vivo. Neurotherapeutics 9: 464-476.

8. Danysz W, Parsons CG (2012) Alzheimer's disease, β-amyloid, glutamate, NMDA receptors and memantine--searching for the connections. Br J Pharmacol 167: 324-352.

9. Thies W, Bleiler L (2013) 2013 Alzheimer's disease facts and figures. Alzheimer's & Dementia : the Journal of the Alzheimer's Association 9: 208-245.

10. Hebert LE, Scherr PA, McCann JJ, Beckett LA, Evans DA (2001) Is the risk of developing Alzheimer's disease greater for women than for men? American Journal of Epidemiology 153: 132-136.

11. Bachman DL, Wolf PA, Linn RT, Knoefel JE, Cobb JL, et al. (1993) Incidence of dementia and probable Alzheimer's disease in a general population: the Framingham Study. Neurology 43: 515-519.

12. Lautenschlager NT, Cupples LA, Rao VS, Auerbach SA, Becker R, et al. (1996) Risk Of Dementia Among Relatives Of Alzheimers Disease Patients In the Mirage Study - What Is In Store For the Oldest Old. Neurology 46: 641-650.

13. Statistics about Alzheimers disease. The Alzheimer's Association.

14. Plassman BL, Havlik RJ, Steffens DC, Helms MJ, Newman TN, et al. (2000) Documented head injury in early adulthood and risk of Alzheimer's disease and other dementias. Neurology 55: 1158-1166.

15. Lye TC, Shores EA (2000) Traumatic brain injury as a risk factor for Alzheimer's disease: a review. Neuropsychology Review 10: 115-129.

16. Anstey KJ, von Sanden C, Salim A, O'Kearney R (2007) Smoking as a risk factor for dementia and cognitive decline: a meta-analysis of prospective studies. American Journal of Epidemiology 166: 367-378.

17. Whitmer RA, Gustafson DR, Barrett-Connor E, Haan MN, Gunderson EP, et al. (2008) Central obesity and increased risk of dementia more than three decades later. Neurology 71: 1057-1064.

18. Kivipelto M, Ngandu T, Fratiglioni L, Viitanen M, Kareholt I, et al. (2005) Obesity and vascular risk factors at midlife and the risk of dementia and Alzheimer disease. Archives of Neurology 62: 1556-1560.

19. Ahtiluoto S, Polvikoski T, Peltonen M, Solomon A, Tuomilehto J, et al. (2010) Diabetes, Alzheimer disease, and vascular dementia: a population-based neuropathologic study. Neurology 75: 1195-1202.

20. Solomon A, Kivipelto M, Wolozin B, Zhou J, Whitmer RA (2009) Midlife serum cholesterol and increased risk of Alzheimer's and vascular dementia three decades later. Dementia and Geriatric Cognitive Disorders 28: 75-80.

21. Ninomiya T, Ohara T, Hirakawa Y, Yoshida D, Doi Y, et al. (2011) Midlife and late-life blood pressure and dementia in Japanese elderly: the Hisayama study. Hypertension 58: 22-28.

22. Fitzpatrick AL, Kuller LH, Ives DG, Lopez OL, Jagust W, et al. (2004) Incidence and prevalence of dementia in the Cardiovascular Health Study. Journal of the American Geriatrics Society 52: 195-204.

23. Stern Y, Gurland B, Tatemichi TK, Tang MX, Wilder D, et al. (1994) Influence of education and occupation on the incidence of Alzheimer's disease. JAMA : the Journal of the American Medical Association 271: 1004-1010.

24. Fratiglioni L, Paillard-Borg S, Winblad B (2004) An active and socially integrated lifestyle in late life might protect against dementia. Lancet Neurology 3: 343-353.

25. Hall CB, Lipton RB, Sliwinski M, Katz MJ, Derby CA, et al. (2009) Cognitive activities delay onset of memory decline in persons who develop dementia. Neurology 73: 356-361.

26. Rudolph JL, Zanin NM, Jones RN, Marcantonio ER, Fong TG, et al. (2010) Hospitalization in community-dwelling persons with Alzheimer's disease: frequency and causes. Journal of the American Geriatrics Society 58: 1542-1548.

27. Brookmeyer R, Corrada MM, Curriero FC, Kawas C (2002) Survival following a diagnosis of Alzheimer disease. Archives of Neurology 59: 1764-1767.

28. Arrighi HM, Neumann PJ, Lieberburg IM, Townsend RJ (2010) Lethality of Alzheimer disease and its impact on nursing home placement. Alzheimer Disease and Associated Disorders 24: 90-95.

29. Elder GA, Gama Sosa MA, De Gasperi R (2010) Transgenic mouse models of Alzheimer's disease. Mt Sinai J Med 77: 69-81.

30. Mawuenyega KG, Sigurdson W, Ovod V, Munsell L, Kasten T, et al. (2010) Decreased clearance of CNS β-amyloid in Alzheimer's disease. Science 330: 1774.

31. Bennett DA, Schneider JA, Wilson RS, Bienias JL, Arnold SE (2004) Neurofibrillary tangles mediate the association of amyloid load with clinical Alzheimer disease and level of cognitive function. Archives of Neurology 61: 378-384.

32. Terry RD, Masliah E, Salmon DP, Butters N, DeTeresa R, et al. (1991) Physical basis of cognitive alterations in Alzheimer's disease: synapse loss is the major correlate of cognitive impairment. Annals of Neurology 30: 572-580.

33. Gylys KH, Fein JA, Yang F, Miller CA, Cole GM (2007) Increased cholesterol in Aβ-positive nerve terminals from Alzheimer's disease cortex. Neurobiology of Aging 28: 8-17.

34. Bertoni-Freddari C, Fattoretti P, Casoli T, Meier-Ruge W, Ulrich J (1990) Morphological adaptive response of the synaptic junctional zones in the human dentate gyrus during aging and Alzheimer's disease. Brain Research 517: 69-75.

35. Arendt T (2009) Synaptic degeneration in Alzheimer's disease. Acta Neuropathol 118: 167-179.

36. Strozyk D, Blennow K, White LR, Launer LJ (2003) CSF Aβ42 levels correlate with amyloid-neuropathology in a population-based autopsy study. Neurology 60: 652-656.

37. Rowe CC, Ng S, Ackermann U, Gong SJ, Pike K, et al. (2007) Imaging β-amyloid burden in aging and dementia. Neurology 68: 1718-1725.

38. Ikonomovic MD, Klunk WE, Abrahamson EE, Mathis CA, Price JC, et al. (2008) Post-mortem correlates of in vivo PiB-PET amyloid imaging in a typical case of Alzheimer's disease. Brain 131: 1630-1645.

39. Hesse C, Rosengren L, Andreasen N, Davidsson P, Vanderstichele H, et al. (2001) Transient increase in total tau but not phospho-tau in human cerebrospinal fluid after acute stroke. Neuroscience Letters 297: 187-190.

40. Ost M, Nylen K, Csajbok L, Ohrfelt AO, Tullberg M, et al. (2006) Initial CSF total tau correlates with 1-year outcome in patients with traumatic brain injury. Neurology 67: 1600-1604.

41. Tapiola T, Overmyer M, Lehtovirta M, Helisalmi S, Ramberg J, et al. (1997) The level of cerebrospinal fluid tau correlates with neurofibrillary tangles in alzheimers-disease. Neuroreport 8: 3961-3963.

42. Shaw LM, Vanderstichele H, Knapik-Czajka M, Clark CM, Aisen PS, et al. (2009) Cerebrospinal fluid biomarker signature in Alzheimer's disease neuroimaging initiative subjects. Annals of Neurology 65: 403-413.

43. Grossman M, Farmer J, Leight S, Work M, Moore P, et al. (2005) Cerebrospinal fluid profile in frontotemporal dementia and Alzheimer's disease. Annals of Neurology 57: 721-729.

44. Arai H, Terajima M, Miura M, Higuchi S, Muramatsu T, et al. (1995) Tau in cerebrospinal fluid: a potential diagnostic marker in Alzheimer's disease. Annals of Neurology 38: 649-652.

45. Attwell D, Laughlin SB (2001) An energy budget for signaling in the grey matter of the brain. Journal of Cerebral Blood Flow and Metabolism 21: 1133-1145.

46. Rocher AB, Chapon F, Blaizot X, Baron JC, Chavoix C (2003) Resting-state brain glucose utilization as measured by PET is directly related to regional synaptophysin levels: a study in baboons. NeuroImage 20: 1894-1898.

47. Minoshima S, Giordani B, Berent S, Frey KA, Foster NL, et al. (1997) Metabolic reduction in the posterior cingulate cortex in very early Alzheimer's disease. Annals of Neurology 42: 85-94.

48. Petrie EC, Cross DJ, Galasko D, Schellenberg GD, Raskind MA, et al. (2009) Preclinical evidence of Alzheimer changes: convergent cerebrospinal fluid biomarker and fluorodeoxyglucose positron emission tomography findings. Archives of Neurology 66: 632-637.

49. Jack CR, Jr., Petersen RC, O'Brien PC, Tangalos EG (1992) MR-based hippocampal volumetry in the diagnosis of Alzheimer's disease. Neurology 42: 183-188.

50. Ott BR, Cohen RA, Gongvatana A, Okonkwo OC, Johanson CE, et al. (2010) Brain ventricular volume and cerebrospinal fluid biomarkers of Alzheimer's disease. Journal of Alzheimer's Disease 20: 647-657.

51. Morris RG, Kopelman MD (1986) The memory deficits in Alzheimer-type dementia: a review. The Quarterly journal of experimental psychology A: Human experimental psychology 38: 575-602.

52. Kirkitadze MD, Bitan G, Teplow DB (2002) Paradigm shifts in Alzheimer's disease and other neurodegenerative disorders: The emerging role of oligomeric assemblies. J Neurosci Res 69: 567-577.

53. Barrow CJ, Zagorski MG (1991) Solution structures of β peptide and its constituent fragments: relation to amyloid deposition. Science 253: 179-182.

54. Guntert A, Dobeli H, Bohrmann B (2006) High sensitivity analysis of amyloid-β peptide composition in amyloid deposits from human and PS2APP mouse brain. Neuroscience 143: 461-475.

55. Tamaoka A, Sawamura N, Odaka A, Suzuki N, Mizusawa H, et al. (1995) Amyloid β Protein 1-42/43 (Aβ 1-42/43) In Cerebellar Diffuse Plaques - Enzyme-Linked Immunosorbent Assay and Immunocytochemical Study. Brain Research 679: 151-156.

56. Miller DL, Papayannopoulos IA, Styles J, Bobin SA (1993) Peptide compositions of the cerebrovascular and senile plaque core amyloid deposits of Alzheimer's disease. Archives of Biochemistry and Biophysics 301: 41-52.

57. Iwatsubo T, Odaka A, Suzuki N, Mizusawa H, Nukina N, et al. (1994) Visualization of Aβ42(43) and Aβ40 in senile plaques with end-specific Aβ monoclonals: Evidence that an initially deposited species is Aβ42(43). Neuron 13: 45-53.

58. Wiltfang J, Esselmann H, Bibl M, Smirnov A, Otto M, et al. (2002) Highly conserved and disease-specific patterns of carboxyterminally truncated Aβ peptides 1-37/38/39 in addition to 1-40/42 in Alzheimer's disease and in patients with chronic neuroinflammation. Journal of Neurochemistry 81: 481-496.

59. Lewczuk P, Esselmann H, Otto M, Maler JM, Henkel AW, et al. (2004) Neurochemical diagnosis of Alzheimer's dementia by CSF Aβ42, Aβ42/Aβ40 ratio and total tau. Neurobiology of Aging 25: 273-281.

60. Schoonenboom NS, Mulder C, Van Kamp GJ, Mehta SP, Scheltens P, et al. (2005) Amyloid β 38, 40, and 42 species in cerebrospinal fluid: more of the same? Annals of Neurology 58: 139-142.

61. Mehta PD, Pirttila T (2005) Increased cerebrospinal fluid Aβ38/Aβ42 ratio in Alzheimer disease. Neuro-degenerative Diseases 2: 242-245.

62. Wang T, Xiao S, Liu Y, Lin Z, Su N, et al. (2013) The efficacy of plasma biomarkers in early diagnosis of Alzheimer's disease. Int J Geriatr Psychiatry.

63. Rembach A, Faux NG, Watt AD, Pertile KK, Rumble RL, et al. (2013) Changes in plasma amyloid β in a longitudinal study of aging and Alzheimer's disease. Alzheimers Dement.

64. Suzuki N, Cheung TT, Cai XD, Odaka A, Otvos L, Jr., et al. (1994) An increased percentage of long amyloid β protein secreted by familial amyloid β protein precursor (β APP717) mutants. Science 264: 1336-1340.

65. Scheuner D, Eckman C, Jensen M, Song X, Citron M, et al. (1996) Secreted amyloid β-protein similar to that in the senile plaques of Alzheimer's disease is increased in vivo by the presenilin 1 and 2 and APP mutations linked to familial Alzheimer's disease. Nature Medicine 2: 864-870.

66. Hilbich C, Kisters-Woike B, Reed J, Masters CL, Beyreuther K (1991) Aggregation and secondary structure of synthetic amyloid β A4 peptides of Alzheimer's disease. Journal of Molecular Biology 218: 149-163.

67. Jarrett JT, Berger EP, Lansbury PT, Jr. (1993) The C-terminus of the β protein is critical in amyloidogenesis. Annals of the New York Academy of Sciences: 144-148.

68. Dahlgren KN, Manelli AM, Stine WB, Jr., Baker LK, Krafft GA, et al. (2002) Oligomeric and fibrillar species of amyloid-β peptides differentially affect neuronal viability. Journal of Biological Chemistry 277: 32046-32053.

69. Hoshi M, Sato M, Matsumoto S, Noguchi A, Yasutake K, et al. (2003) Spherical aggregates of β-amyloid (amylospheroid) show high neurotoxicity and activate tau protein kinase I/glycogen synthase kinase-3β. Proc Natl Acad Sci U S A 100: 6370-6375.

70. Iijima K, Liu HP, Chiang AS, Hearn SA, Konsolaki M, et al. (2004) Dissecting the pathological effects of human Aβ40 and Aβ42 in Drosophila: a potential model for Alzheimer's disease. Proc Natl Acad Sci U S A 101: 6623-6628.

71. McGowan E, Pickford F, Kim J, Onstead L, Eriksen J, et al. (2005) Aβ42 is essential for parenchymal and vascular amyloid deposition in mice. Neuron 47: 191-199.

72. Gatz M, Reynolds CA, Fratiglioni L, Johansson B, Mortimer JA, et al. (2006) Role of genes and environments for explaining Alzheimer disease. Archives of General Psychiatry 63: 168-174.

73. Mendez MF (2012) Early-onset Alzheimer's disease: nonamnestic subtypes and type 2 AD. Arch Med Res 43: 677-685.

74. McMurtray A, Clark DG, Christine D, Mendez MF (2006) Early-onset dementia: frequency and causes compared to late-onset dementia. Dement Geriatr Cogn Disord 21: 59-64.

75. Rademakers R, Cruts M, Sleegers K, Dermaut B, Theuns J, et al. (2005) Linkage and association studies identify a novel locus for Alzheimer disease at 7q36 in a Dutch population-based sample. Am J Human Genetics 77: 643-652.

76. Sala Frigerio C, Piscopo P, Calabrese E, Crestini A, Malvezzi Campeggi L, et al. (2005) PEN-2 gene mutation in a familial Alzheimer's disease case. J Neurol 252: 1033-1036.

77. Goldgaber D, Lerman MI, McBridge OW, V S, Gajdusek DC (1987) Characterization and chromosomal localization of a cDNA encoding brain amyloid of Alzheimer's disease. Science 235: 877-880.

78. Kang J, Lemaire H-G, Unterbeck A, Salbaum JM, Masters CL, et al. (1987) The precursor of Alzheimer's disease amyloid A4 protein resembles a cell-surface receptor. Nature 325: 733-736.

79. Tanzi RE, Gusella JF, Watkins PC, Bruns GAB, St. George-Hyslop PH, et al. (1987) Amyloid b-protein gene: cDNA, mRNA distribution, and genetic linkage near the Alzheimer locus. Science 235: 880-884.

80. Levy E, Carman MD, Fernandez-Madrid IJ, Power MD, Lieberburg I, et al. (1990) Mutation of the Alzheimer's disease amyloid gene in hereditary cerebral hemorrhage, Dutch-type. Science 248: 1124-1126.

81. Sherrington R, Rogaev EI, Liang Y, Rogaeva EA, Levesque G, et al. (1995) Cloning of a gene bearing missense mutations in early-onset familial Alzheimer's disease. Nature 375: 754-760.

82. Levy-Lahad E, Wasco W, Poorkaj P, Romano DM, Oshima J, et al. (1995) Candidate gene for the chromosome 1 familial Alzheimer's disease locus. Science 269: 973-977.

83. Vetrivel KS, Zhang YW, Xu H, Thinakaran G (2006) Pathological and physiological functions of presenilins. Molecular Neurodegeneration 1: 4.

84. Tanzi RE (2012) The genetics of Alzheimer disease. Cold Spring Harbor perspectives in medicine 2.

85. Attar A, Meral D, Urbanc B, Bitan G (2013) Assembly of amyloid β-protein variants containing familial Alzheimer's disease-linked amino acid substitutions. In: Uversky VN, Lyubchenko V, editors. Bionanoimaging: Protein Misfolding & Aggregation: Elsevier. pp. In press.

86. Strittmatter WJ, Saunders AM, Schmechel D, Pericak-Vance M, Enghild J, et al. (1993) Apolipoprotein E: high-avidity binding to β-amyloid and increased frequency of type 4 allele in late-onset familial Alzheimer disease. Proc Natl Acad Sci USA 90: 1977-1981.

87. Corder EH, Saunders AM, Risch NJ, Strittmatter WJ, Schmechel DE, et al. (1994) Protective effect of apolipoprotein E type 2 allele for late onset Alzheimer disease. Nature Genetics 7: 180-184.

88. Potter H, Wisniewski T (2012) Apolipoprotein e: essential catalyst of the Alzheimer amyloid cascade. Int Journal of Alzheimer's Disease 2012: 489428.

89. Das S, Mukhopadhyay D (2011) Intrinsically unstructured proteins and neurodegenerative diseases: conformational promiscuity at its best. IUBMB Life 63: 478-488.

90. Dyson HJ, Wright PE (2005) Intrinsically unstructured proteins and their functions. Nat Rev Mol Cell Biol 6: 197-208.

91. Dobson CM (2001) The structural basis of protein folding and its links with human disease. Philos Trans R Soc Lond B Biol Sci 356: 133-145.

92. Stroud JC, Liu C, Teng PK, Eisenberg D (2012) Toxic fibrillar oligomers of amyloid-β have cross-β structure. Proc Natl Acad Sci U S A 109: 7717-7722.

93. Dobson CM (2003) Protein folding and misfolding. Nature 426: 884-890.

94. Goldschmidt L, Teng PK, Riek R, Eisenberg D (2010) Identifying the amylome, proteins capable of forming amyloid-like fibrils. Proc Natl Acad Sci U S A 107: 3487-3492.

95. Buxbaum J (1996) The amyloidoses. Mt Sinai J Med 63: 16-23.

96. Makin OS, Serpell LC (2005) Structures for amyloid fibrils. FEBS J 272: 5950-5961.

97. Dobson CM (2004) Principles of protein folding, misfolding and aggregation. Semin Cell Dev Biol 15: 3-16.

98. Pastor MT, Kummerer N, Schubert V, Esteras-Chopo A, Dotti CG, et al. (2008) Amyloid toxicity is independent of polypeptide sequence, length and chirality. Journal of Molecular Biology 375: 695-707.

99. Liu T, Bitan G (2012) Modulating self-assembly of amyloidogenic proteins as a therapeutic approach for neurodegenerative diseases: strategies and mechanisms. ChemMedChem 7: 359-374.

100. Rahimi F, Shanmugam A, Bitan G (2008) Structure–function relationships of pre-fibrillar protein assemblies in Alzheimer's disease and related disorders. Curr Alzheimer Res 5: 319-341.

101. Marshall KE, Morris KL, Charlton D, O'Reilly N, Lewis L, et al. (2011) Hydrophobic, aromatic, and electrostatic interactions play a central role in amyloid fibril formation and stability. Biochemistry 50: 2061-2071.

102. Yun S, Urbanc B, Cruz L, Bitan G, Teplow DB, et al. (2007) Role of electrostatic interactions in amyloid β-protein (A β) oligomer formation: a discrete molecular dynamics study. Biophys J 92: 4064-4077.

103. Yanagi K, Ashizaki M, Yagi H, Sakurai K, Lee YH, et al. (2011) Hexafluoroisopropanol induces amyloid fibrils of islet amyloid polypeptide by enhancing both hydrophobic and electrostatic interactions. Journal of Biological Chemistry 286: 23959-23966.

104. Li H, Monien BH, Fradinger EA, Urbanc B, Bitan G (2010) Biophysical characterization of Aβ42 C-terminal fragments: inhibitors of Aβ42 neurotoxicity. Biochemistry 49: 1259-1267.

105. Betts V, Leissring MA, Dolios G, Wang R, Selkoe DJ, et al. (2008) Aggregation and catabolism of disease-associated intra-Aβ mutations: reduced proteolysis of AβA21G by neprilysin. Neurobiology of Disease 31: 442-450.

106. Hardy JA, Higgins GA (1992) Alzheimer's disease: the amyloid cascade hypothesis. Science 256: 184-185.

107. Gong Y, Chang L, Viola KL, Lacor PN, Lambert MP, et al. (2003) Alzheimer's disease-affected brain: presence of oligomeric Aβ ligands (ADDLs) suggests a molecular basis for reversible memory loss. Proc Natl Acad Sci U S A 100: 10417-10422.

108. Pitschke M, Prior R, Haupt M, Riesner D (1998) Detection of single amyloid β-protein aggregates in the cerebrospinal fluid of Alzheimer's patients by fluorescence correlation spectroscopy. Nat Med 4: 832-834.

109. Shankar GM, Bloodgood BL, Townsend M, Walsh DM, Selkoe DJ, et al. (2007) Natural oligomers of the Alzheimer amyloid-β protein induce reversible synapse loss by modulating an NMDA-type glutamate receptor-dependent signaling pathway. Journal of Neuroscience 27: 2866-2875.

110. Cleary JP, Walsh DM, Hofmeister JJ, Shankar GM, Kuskowski MA, et al. (2005) Natural oligomers of the amyloid-β protein specifically disrupt cognitive function. Nature Neuroscience 8: 79-84.

111. Hsia AY, Masliah E, McConlogue L, Yu GQ, Tatsuno G, et al. (1999) Plaque-independent disruption of neural circuits in Alzheimer's disease mouse models. Proc Natl Acad Sci USA 96: 3228-3233.

112. Lesné S, Koh MT, Kotilinek L, Kayed R, Glabe CG, et al. (2006) A specific amyloid-β protein assembly in the brain impairs memory. Nature 440: 352-357.

113. Lambert MP, Barlow AK, Chromy BA, Edwards C, Freed R, et al. (1998) Diffusible, nonfibrillar ligands derived from $A\beta_{1-42}$ are potent central nervous system neurotoxins. Proc Natl Acad Sci USA 95: 6448-6453.

114. Tycko R (2006) Characterization of amyloid structures at the molecular level by solid state nuclear magnetic resonance spectroscopy. Methods Enzymol 413: 103-122.

115. Lührs T, Ritter C, Adrian M, Riek-Loher D, Bohrmann B, et al. (2005) 3D structure of Alzheimer's amyloid-β(1–42) fibrils. Proc Natl Acad Sci USA 102: 17342-17347.

116. Lazo ND, Grant MA, Condron MC, Rigby AC, Teplow DB (2005) On the nucleation of amyloid β-protein monomer folding. Protein Science 14: 1581-1596.

117. Borreguero JM, Urbanc B, Lazo ND, Buldyrev SV, Teplow DB, et al. (2005) Folding events in the 21-30 region of amyloid β-protein (Aβ) studied *in silico*. Proc Natl Acad Sci USA 102: 6015-6020.

118. Jarrett JT, Lansbury PT, Jr (1993) Seeding "one-dimensional crystallization" of amyloid: A pathogenic mechanism in Alzheimer's disease and scrapie? Cell 73: 1055-1058.

119. Walsh DM, Hartley DM, Kusumoto Y, Fezoui Y, Condron MM, et al. (1999) Amyloid β-protein fibrillogenesis. Structure and biological activity of protofibrillar intermediates. Journal of Biological Chemistry 274: 25945-25952.

120. Seilheimer B, Bohrmann B, Bondolfi L, Muller F, Stuber D, et al. (1997) The toxicity of the Alzheimer's β-amyloid peptide correlates with a distinct fiber morphology. J Struct Biol 119: 59-71.

121. Blackley HK, Sanders GH, Davies MC, Roberts CJ, Tendler SJ, et al. (2000) In-situ atomic force microscopy study of β-amyloid fibrillization. Journal of Molecular Biology 298: 833-840.

122. Bitan G, Teplow DB (2004) Rapid photochemical cross-linking—a new tool for studies of metastable, amyloidogenic protein assemblies. Acc Chem Res 37: 357-364.

123. Bitan G, Kirkitadze MD, Lomakin A, Vollers SS, Benedek GB, et al. (2003) Amyloid β-protein (Aβ) assembly: Aβ40 and Aβ42 oligomerize through distinct pathways. Proc Natl Acad Sci USA 100: 330-335.

124. Lambert MP, Barlow AK, Chromy BA, Edwards C, Freed R, et al. (1998) Diffusible, nonfibrillar ligands derived from $A\beta_{1-42}$ are potent central nervous system neurotoxins. Proc Natl Acad Sci U S A 95: 6448-6453.

125. Urbanc B, Cruz L, Yun S, Buldyrev SV, Bitan G, et al. (2004) *In silico* study of amyloid β-protein folding and oligomerization. Proc Natl Acad Sci USA 101: 17345-17350.

126. Yang M, Teplow DB (2008) Amyloid β-protein monomer folding: free-energy surfaces reveal alloform-specific differences. Journal of Molecular Biology 384: 450-464.

127. Guo M, Gorman PM, Rico M, Chakrabartty A, Laurents DV (2005) Charge substitution shows that repulsive electrostatic interactions impede the oligomerization of Alzheimer amyloid peptides. FEBS letters 579: 3574-3578.

128. Sciarretta KL, Gordon DJ, Petkova AT, Tycko R, Meredith SC (2005) Aβ40-Lactam(D23/K28) models a conformation highly favorable for nucleation of amyloid. Biochemistry 44: 6003-6014.

129. Petkova AT, Ishii Y, Balbach JJ, Antzutkin ON, Leapman RD, et al. (2002) A structural model for Alzheimer's β-amyloid fibrils based on experimental constraints from solid state NMR. Proc Natl Acad Sci USA 99: 16742-16747.

130. Petkova AT, Yau WM, Tycko R (2006) Experimental constraints on quaternary structure in Alzheimer's β-amyloid fibrils. Biochemistry 45: 498-512.

131. Petkova AT, Leapman RD, Guo Z, Yau WM, Mattson MP, et al. (2005) Self-propagating, molecular-level polymorphism in Alzheimer's β-amyloid fibrils. Science 307: 262-265.

132. Lührs T, Ritter C, Adrian M, Riek-Loher D, Bohrmann B, et al. (2005) 3D structure of Alzheimer's amyloid-β(1-42) fibrils. Proc Natl Acad Sci U S A 102: 17342-17347.

133. Grant MA, Lazo ND, Lomakin A, Condron MM, Arai H, et al. (2007) Familial Alzheimer's disease mutations alter the stability of the amyloid β-protein monomer folding nucleus. Proc Natl Acad Sci U S A 104: 16522-16527.

134. Kapogiannis D, Mattson MP (2011) Disrupted energy metabolism and neuronal circuit dysfunction in cognitive impairment and Alzheimer's disease. Lancet Neurology 10: 187-198.

135. Pistell PJ, Morrison CD, Gupta S, Knight AG, Keller JN, et al. (2010) Cognitive impairment following high fat diet consumption is associated with brain inflammation. J Neuroimmunol 219: 25-32.

136. Cao D, Lu H, Lewis TL, Li L (2007) Intake of sucrose-sweetened water induces insulin resistance and exacerbates memory deficits and amyloidosis in a transgenic mouse model of Alzheimer disease. Journal of Biological Chemistry 282: 36275-36282.

137. Kann O, Kovacs R (2007) Mitochondria and neuronal activity. American Journal of Physiology - Cell Physiology 292: C641-657.

138. Larner AJ (2010) Epileptic seizures in AD patients. Neuromolecular Med 12: 71-77.

139. Wenk GL, Parsons CG, Danysz W (2006) Potential role of N-methyl-D-aspartate receptors as executors of neurodegeneration resulting from diverse insults: focus on memantine. Behavioural Pharmacology 17: 411-424.

140. McLaurin J, Chakrabartty A (1997) Characterization of the interactions of Alzheimer β-amyloid peptides with phospholipid membranes. European Journal of Biochemistry 245: 355-363.

141. Waschuk SA, Elton EA, Darabie AA, Fraser PE, McLaurin J (2001) Cellular membrane composition defines Aβ-lipid interactions. Journal of Biological Chemistry 276: 33561-33568.

142. Kagan BL, Azimov R, Azimova R (2004) Amyloid peptide channels. J Membr Biol 202: 1-10.

143. Demeester N, Baier G, Enzinger C, Goethals M, Vandekerckhove J, et al. (2000) Apoptosis induced in neuronal cells by C-terminal amyloid β-fragments is correlated with their aggregation properties in phospholipid membranes. Molecular Membrane Biology 17: 219-228.

144. Kayed R, Sokolov Y, Edmonds B, McIntire TM, Milton SC, et al. (2004) Permeabilization of lipid bilayers is a common conformation-dependent activity of soluble amyloid oligomers in protein misfolding diseases. Journal of Biological Chemistry 279: 46363-46366.

145. Yoshiike Y, Akagi T, Takashima A (2007) Surface structure of amyloid-β fibrils contributes to cytotoxicity. Biochemistry 46: 9805-9812.

146. Keshet B, Gray JJ, Good TA (2010) Structurally distinct toxicity inhibitors bind at common loci on β-amyloid fibril. Protein Science 19: 2291-2304.

147. de Groot NS, Aviles FX, Vendrell J, Ventura S (2006) Mutagenesis of the central hydrophobic cluster in Aβ42 Alzheimer's peptide. Side-chain properties correlate with aggregation propensities. FEBS J 273: 658-668.

148. Esler WP, Stimson ER, Ghilardi JR, Lu YA, Felix AM, et al. (1996) Point substitution in the central hydrophobic cluster of a human β-amyloid congener disrupts peptide folding and abolishes plaque competence. Biochemistry 35: 13914-13921.

149. Yan Y, Liu J, McCallum SA, Yang D, Wang C (2007) Methyl dynamics of the amyloid-β peptides Aβ40 and Aβ42. Biochem Biophys Res Commun 362: 410-414.

150. Zhang SS, Casey N, Lee JP (1998) Residual structure in the Alzheimer‘s disease peptide - Probing the origin of a central hydrophobic cluster. Folding & Design 3: 413-422.

151. Zhang S, Iwata K, Lachenmann MJ, Peng JW, Li S, et al. (2000) The Alzheimer's peptide Aβ adopts a collapsed coil structure in water. J Struct Biol 130: 130-141.

152. Chen Z, Krause G, Reif B (2005) Structure and orientation of peptide inhibitors bound to β-amyloid fibrils. Journal of Molecular Biology 354: 760-776.

153. Bokvist M, Lindstrom F, Watts A, Grobner G (2004) Two types of Alzheimer's β-amyloid (1-40) peptide membrane interactions: aggregation preventing transmembrane anchoring versus accelerated surface fibril formation. Journal of Molecular Biology 335: 1039-1049.

154. Chauhan A, Ray I, Chauhan VP (2000) Interaction of amyloid β-protein with anionic phospholipids: possible involvement of Lys28 and C-terminus aliphatic amino acids. Neurochem Res 25: 423-429.

155. Hertel C, Terzi E, Hauser N, Jakob-Rotne R, Seelig J, et al. (1997) Inhibition of the electrostatic interaction between β-amyloid peptide and membranes prevents β-amyloid-induced toxicity. Proc Natl Acad Sci U S A 94: 9412-9416.

156. Bartus RT, Dean RL, 3rd, Beer B, Lippa AS (1982) The cholinergic hypothesis of geriatric memory dysfunction. Science 217: 408-414.

157. Whitehouse PJ, Price DL, Struble RG, Clark AW, Coyle JT, et al. (1982) Alzheimer's disease and senile dementia: loss of neurons in the basal forebrain. Science 215: 1237-1239.

158. Craig LA, Hong NS, McDonald RJ (2011) Revisiting the cholinergic hypothesis in the development of Alzheimer's disease. Neurosci Biobehav Rev 35: 1397-1409.

159. Rylett RJ, Ball MJ, Colhoun EH (1983) Evidence for high affinity choline transport in synaptosomes prepared from hippocampus and neocortex of patients with Alzheimer's disease. Brain Research 289: 169-175.

160. Nilsson L, Nordberg A, Hardy J, Wester P, Winblad B (1986) Physostigmine restores 3H-acetylcholine efflux from Alzheimer brain slices to normal level. J Neural Transm 67: 275-285.

161. Wang HY, Lee DHS, D'Andrea MR, Peterson PA, Shank RP, et al. (2000) β-amyloid(1-42) binds to α 7 nicotinic acetylcholine receptor with high affinity - Implications for Alzheimer's disease pathology. Journal of Biological Chemistry 275: 5626-5632.

162. Kihara T, Shimohama S, Sawada H, Kimura J, Kume T, et al. (1997) Nicotinic Receptor Stimulation Protects Neurons Against β-Amyloid Toxicity. Annals of Neurology 42: 159-163.

163. Bush AI (2003) The metallobiology of Alzheimer's disease. Trends in Neurosciences 26: 207-214.

164. Lauren J, Gimbel DA, Nygaard HB, Gilbert JW, Strittmatter SM (2009) Cellular prion protein mediates impairment of synaptic plasticity by amyloid-β oligomers. Nature 457: 1128-1132.

165. Akiyama H, Barger S, Barnum S, Bradt B, Bauer J, et al. (2000) Inflammation and Alzheimer's disease. Neurobiology of Aging 21: 383-421.

166. Benard G, Bellance N, James D, Parrone P, Fernandez H, et al. (2007) Mitochondrial bioenergetics and structural network organization. Journal of Cell Science 120: 838-848.

167. Rusakov DA (2006) Ca2+-dependent mechanisms of presynaptic control at central synapses. The Neuroscientist : A Review Journal Bringing Neurobiology, Neurology and Psychiatry 12: 317-326.

168. Wang X, Su B, Siedlak SL, Moreira PI, Fujioka H, et al. (2008) Amyloid-β overproduction causes abnormal mitochondrial dynamics via differential modulation of mitochondrial fission/fusion proteins. Proc Natl Acad Sci USA 105: 19318-19323.

169. Tillement L, Lecanu L, Papadopoulos V (2011) Alzheimer's disease: effects of β-amyloid on mitochondria. Mitochondrion 11: 13-21.

170. Ferreiro E, Oliveira CR, Pereira CM (2008) The release of calcium from the endoplasmic reticulum induced by amyloid-β and prion peptides activates the mitochondrial apoptotic pathway. Neurobiology of Disease 30: 331-342.

171. Schmidt C, Lepsverdize E, Chi SL, Das AM, Pizzo SV, et al. (2008) Amyloid precursor protein and amyloid β-peptide bind to ATP synthase and regulate its activity at the surface of neural cells. Molecular Psychiatry 13: 953-969.

172. Du H, Guo L, Yan S, Sosunov AA, McKhann GM, et al. (2010) Early deficits in synaptic mitochondria in an Alzheimer's disease mouse model. Proc Natl Acad Sci USA 107: 18670-18675.

173. Choi SW, Gerencser AA, Ng R, Flynn JM, Melov S, et al. (2012) No consistent bioenergetic defects in presynaptic nerve terminals isolated from mouse models of Alzheimer's disease. Journal of Neuroscience 32: 16775-16784.

174. Estus S, Tucker HM, Vanrooyen C, Wright S, Brigham EF, et al. (1997) Aggregated Amyloid-β Protein Induces Cortical Neuronal Apoptosis and Concomitant Apoptotic Pattern Of Gene Induction. Journal of Neuroscience 17: 7736-7745.

175. Carrieri G, Bonafe M, De Luca M, Rose G, Varcasia O, et al. (2001) Mitochondrial DNA haplogroups and APOE4 allele are non-independent variables in sporadic Alzheimer's disease. Human Genetics 108: 194-198.

176. Hardy J, Cowburn R (1987) Glutamate neurotoxicity and Alzheimer's disease. Trends in Neurosciences 10: 406.

177. Francis PT (2003) Glutamatergic systems in Alzheimer's disease. International Journal of Geriatric Psychiatry 18: S15-21.

178. Greenamyre JT, Young AB (1989) Excitatory amino acids and Alzheimer's disease. Neurobiology of Aging 10: 593-602.

179. Butterfield DA, Pocernich CB (2003) The glutamatergic system and Alzheimer's disease - Therapeutic implications. CNS Drugs 17: 641-652.

180. Wenk GL (2006) Neuropathologic changes in Alzheimer's disease: potential targets for treatment. Journal of Clinical Psychiatry 67 Suppl 3: 3-7; quiz 23.

181. De Felice FG, Velasco PT, Lambert MP, Viola K, Fernandez SJ, et al. (2007) Aβ oligomers induce neuronal oxidative stress through an N-methyl-D-aspartate receptor-dependent mechanism that is blocked by the Alzheimer drug memantine. Journal of Biological Chemistry 282: 11590-11601.

182. Parihar MS, Brewer GJ (2007) Mitoenergetic failure in Alzheimer disease. American Journal of Physiology - Cell Physiology 292: C8-23.

183. Parameshwaran K, Dhanasekaran M, Suppiramaniam V (2008) Amyloid β peptides and glutamatergic synaptic dysregulation. Experimental Neurology 210: 7-13.

184. Alberdi E, Sanchez-Gomez MV, Cavaliere F, Perez-Samartin A, Zugaza JL, et al. (2010) Amyloid β oligomers induce Ca2+ dysregulation and neuronal death through activation of ionotropic glutamate receptors. Cell Calcium 47: 264-272.

185. Mattson MP, Barger SW, Cheng B, Lieberburg I, Smith-Swintosky VL, et al. (1993) β-Amyloid precursor protein metabolites and loss of neuronal Ca2+ homeostasis in Alzheimer's disease. Trends in Neurosciences 16: 409-414.

186. Brzyska M, Elbaum D (2003) Dysregulation of calcium in Alzheimer's disease. Acta Neurobiologiae Experimentalis 63: 171-183.

187. Gegelashvili G, Schousboe A (1997) High affinity glutamate transporters: regulation of expression and activity. Molecular Pharmacology 52: 6-15.

188. Clarke R, Smith AD, Jobst KA, Refsum H, Sutton L, et al. (1998) Folate, vitamin B12, and serum total homocysteine levels in confirmed Alzheimer disease. Archives of Neurology 55: 1449-1455.

189. Gu QB, Zhao JX, Fei J, Schwarz W (2004) Modulation of Na(+),K(+) pumping and neurotransmitter uptake by β-amyloid. Neuroscience 126: 61-67.

190. Danysz W, Parsons CG, Mobius HJ, Stoffler A, Quack G (2000) Neuroprotective and symptomatological action of memantine relevant for Alzheimer's disease--a unified glutamatergic hypothesis on the mechanism of action. Neurotoxicity Research 2: 85-97.

191. Fujikawa DG (2005) Prolonged seizures and cellular injury: understanding the connection. Epilepsy Behav 7 Suppl 3: S3-11.

192. Lu M, Kosik KS (2001) Competition for microtubule-binding with dual expression of tau missense and splice isoforms. Molecular Biology of the Cell 12: 171-184.

193. Drewes G, Trinczek B, Illenberger S, Biernat J, Schmitt-Ulms G, et al. (1995) Microtubule-associated protein/microtubule affinity-regulating kinase (p110mark). A novel protein kinase that regulates tau-microtubule interactions and dynamic instability by phosphorylation at the Alzheimer-specific site serine 262. Journal of Biological Chemistry 270: 7679-7688.

194. Dickey CA, Kamal A, Lundgren K, Klosak N, Bailey RM, et al. (2007) The high-affinity HSP90-CHIP complex recognizes and selectively degrades phosphorylated tau client proteins. Journal of Clinical Investigation 117: 648-658.

195. Hutton M, Lendon CL, Rizzu P, Baker M, Froelich S, et al. (1998) Association of missense and 5'-splice-site mutations in tau with the inherited dementia ftdp-17. Nature 393: 702-705.

196. Hong M, Zhukareva V, Vogelsberg-Ragaglia V, Wszolek Z, Reed L, et al. (1998) Mutation-specific functional impairments in distinct Tau isoforms of hereditary FTDP-17. Science 282: 1914-1917.

197. Nacharaju P, Lewis J, Easson C, Yen S, Hackett J, et al. (1999) Accelerated filament formation from tau protein with specific FTDP-17 missense mutations. FEBS Letters 447: 195-199.

198. Arriagada PV, Growdon JH, Hedley-Whyte ET, Hyman BT (1992) Neurofibrillary tangles but not senile plaques parallel duration and severity of Alzheimer's disease. Neurology 42: 631-639.

199. Lin WL, Lewis J, Yen SH, Hutton M, Dickson DW (2003) Ultrastructural neuronal pathology in transgenic mice expressing mutant (P301L) human tau. J Neurocytol 32: 1091-1105.

200. Keck S, Nitsch R, Grune T, Ullrich O (2003) Proteasome inhibition by paired helical filament-tau in brains of patients with Alzheimer's disease. Journal of Neurochemistry 85: 115-122.

201. Stamer K, Vogel R, Thies E, Mandelkow E, Mandelkow EM (2002) Tau blocks traffic of organelles, neurofilaments, and APP vesicles in neurons and enhances oxidative stress. Journal of Cell Biology 156: 1051-1063.

202. Thies E, Mandelkow EM (2007) Missorting of tau in neurons causes degeneration of synapses that can be rescued by the kinase MARK2/Par-1. Journal of Neuroscience 27: 2896-2907.

203. Alonso AD, Grundkeiqbal I, Iqbal K, Koudinov AR, Koudinova NV, et al. (1996) Alzheimers Disease Hyperphosphorylated Tau Sequesters Normal Tau Into Tangles Of Filaments and Disassembles Microtubules Biochemical Characterization Of Alzheimers Soluble Amyloid β Protein In Human Cerebrospinal Fluid - Association With High Density Lipoproteins. Nature Medicine 2: 783-787.

204. Alonso AD, Grundke-Iqbal I, Barra HS, Iqbal K (1997) Abnormal phosphorylation of tau and the mechanism of Alzheimer neurofibrillary degeneration: sequestration of microtubule-associated proteins 1 and 2 and the disassembly of microtubules by the abnormal tau. Proc Natl Acad Sci USA 94: 298-303.

205. Yoshiyama Y, Higuchi M, Zhang B, Huang SM, Iwata N, et al. (2007) Synapse loss and microglial activation precede tangles in a P301S tauopathy mouse model. Neuron 53: 337-351.

206. Eckermann K, Mocanu MM, Khlistunova I, Biernat J, Nissen A, et al. (2007) The β-propensity of Tau determines aggregation and synaptic loss in inducible mouse models of tauopathy. Journal of Biological Chemistry 282: 31755-31765.

207. Gong CX, Iqbal K (2008) Hyperphosphorylation of microtubule-associated protein tau: a promising therapeutic target for Alzheimer disease. Current Medicinal Chemistry 15: 2321-2328.

208. Braak H, Braak E (1995) Staging of Alzheimer's disease-related neurofibrillary changes. Neurobiology of Aging 16: 271-278; discussion 278-284.

209. Gendron TF, Petrucelli L (2009) The role of tau in neurodegeneration. Mol Neurodegener 4: 13.

210. Wang JZ, Grundkeiqbal I, Iqbal K (1996) Glycosylation Of Microtubule-Associated Protein Tau - an Abnormal Posttranslational Modification In Alzheimers Disease. Nature Medicine 2: 871-875.

211. Zilka N, Filipcik P, Koson P, Fialova L, Skrabana R, et al. (2006) Truncated tau from sporadic Alzheimer's disease suffices to drive neurofibrillary degeneration in vivo. FEBS Lett 580: 3582-3588.

212. Fasulo L, Ugolini G, Visintin M, Bradbury A, Brancolini C, et al. (2000) The neuronal microtubule-associated protein tau is a substrate for caspase-3 and an effector of apoptosis. Journal of Neurochemistry 75: 624-633.

213. Sharma VM, Litersky JM, Bhaskar K, Lee G (2007) Tau impacts on growth-factor-stimulated actin remodeling. Journal of Cell Science 120: 748-757.

214. Hwang SC, Jhon DY, Bae YS, Kim JH, Rhee SG (1996) Activation of phospholipase C-γ by the concerted action of tau proteins and arachidonic acid. Journal of Biological Chemistry 271: 18342-18349.

215. Cente M, Filipcik P, Pevalova M, Novak M (2006) Expression of a truncated tau protein induces oxidative stress in a rodent model of tauopathy. The European Journal of Neuroscience 24: 1085-1090.

216. Chee F, Mudher A, Newman TA, Cuttle M, Lovestone S, et al. (2006) Overexpression of tau results in defective synaptic transmission in Drosophila neuromuscular junctions. Biochemical Society Transactions 34: 88-90.

217. Kanki R, Nakamizo T, Yamashita H, Kihara T, Sawada H, et al. (2004) Effects of mitochondrial dysfunction on glutamate receptor-mediated neurotoxicity in cultured rat spinal motor neurons. Brain Research 1015: 73-81.

218. Van Westerlaak MG, Joosten EA, Gribnau AA, Cools AR, Bar PR (2001) Chronic mitochondrial inhibition induces glutamate-mediated corticomotoneuron death in an organotypic culture model. Experimental Neurology 167: 393-400.

219. Bloom GS, Ren K, Glabe CG (2005) Cultured cell and transgenic mouse models for tau pathology linked to β-amyloid. Biochim Biophys Acta 1739: 116-124.

220. Rapoport M, Dawson HN, Binder LI, Vitek MP, Ferreira A (2002) Tau is essential to β-amyloid-induced neurotoxicity. Proc Natl Acad Sci USA 99: 6364-6369.

221. Roberson ED, Scearce-Levie K, Palop JJ, Yan F, Cheng IH, et al. (2007) Reducing endogenous tau ameliorates amyloid β-induced deficits in an Alzheimer's disease mouse model. Science 316: 750-754.

222. Gotz J, Chen F, van Dorpe J, Nitsch RM (2001) Formation of neurofibrillary tangles in P301L tau transgenic mice induced by Ab42 fibrils. Science 293: 1491-1495.

223. Lee MJ, Lee JH, Rubinsztein DC (2013) Tau degradation: the ubiquitin-proteasome system versus the autophagy-lysosome system. Progress in Neurobiology 105: 49-59.

224. Tseng BP, Green KN, Chan JL, Blurton-Jones M, LaFerla FM (2008) Aβ inhibits the proteasome and enhances amyloid and tau accumulation. Neurobiology of Aging 29: 1607-1618.

225. Nixon RA, Cataldo AM (2006) Lysosomal system pathways: genes to neurodegeneration in Alzheimer's disease. Journal of Alzheimer's disease : JAD 9: 277-289.

226. Masliah E, Mallory M, Deerinck T, DeTeresa R, Lamont S, et al. (1993) Re-evaluation of the structural organization of neuritic plaques in Alzheimer's disease. Journal of Neuropathology and Experimental Neurology 52: 619-632.

227. Nixon RA, Yang DS, Lee JH (2008) Neurodegenerative lysosomal disorders: a continuum from development to late age. Autophagy 4: 590-599.

228. Nixon RA (2004) Niemann-Pick Type C disease and Alzheimer's disease: the APP-endosome connection fattens up. The American Journal of Pathology 164: 757-761.

229. Chishti MA, Yang DS, Janus C, Phinney AL, Horne P, et al. (2001) Early-onset amyloid deposition and cognitive deficits in transgenic mice expressing a double mutant form of amyloid precursor protein 695. Journal of Biological Chemistry 276: 21562-21570.

230. Yang DS, Stavrides P, Mohan PS, Kaushik S, Kumar A, et al. (2011) Reversal of autophagy dysfunction in the TgCRND8 mouse model of Alzheimer's disease ameliorates amyloid pathologies and memory deficits. Brain 134: 258-277.

231. Cataldo AM, Peterhoff CM, Troncosco JC, Gomez-Isla T, Hyman BT, et al. (2000) Endocytic pathway abnormalities precede amyloid β deposition in sporadic Alzheimer's disease and Down syndrome - Differential effects of APOE genotype and presenilin mutations. American Journal of Pathology 157: 277-286.

232. Jiang Y, Mullaney KA, Peterhoff CM, Che S, Schmidt SD, et al. (2010) Alzheimer's-related endosome dysfunction in Down syndrome is Aβ-independent but requires APP and is reversed by BACE-1 inhibition. Proc Natl Acad Sci USA 107: 1630-1635.

233. Keller JN, Hanni KB, Markesbery WR (2000) Impaired proteasome function in Alzheimer's disease. Journal of Neurochemistry 75: 436-439.

234. Zerovnik E (2010) Protein conformational pathology in Alzheimer's and other neurodegenerative diseases; new targets for therapy. Curr Alzheimer Res 7: 74-83.

235. Stoppelkamp S, Bell HS, Palacios-Filardo J, Shewan DA, Riedel G, et al. (2011) In vitro modelling of Alzheimer's disease: degeneration and cell death induced by viral delivery of amyloid and tau. Exp Neurol 229: 226-237.

236. Mouri A, Zou LB, Iwata N, Saido TC, Wang D, et al. (2006) Inhibition of neprilysin by thiorphan (i.c.v.) causes an accumulation of amyloid β and impairment of learning and memory. Behav Brain Res 168: 83-91.

237. Lee JW, Lee YK, Yuk DY, Choi DY, Ban SB, et al. (2008) Neuro-inflammation induced by lipopolysaccharide causes cognitive impairment through enhancement of β-amyloid generation. J Neuroinflammation 5: 37.

238. Games D, Adams D, Alessandrini R, Barbour R, Berthelette P, et al. (1995) Alzheimer-type neuropathology in transgenic mice overexpressing V717F b-amyloid precursor protein. Nature 373: 523-527.

239. Reilly JF, Games D, Rydel RE, Freedman S, Schenk D, et al. (2003) Amyloid deposition in the hippocampus and entorhinal cortex: Quantitative analysis of a transgenic mouse model. Proc Natl Acad Sci USA 100: 4837-4842.

240. Dodart JC, Mathis C, Saura J, Bales KR, Paul SM, et al. (2000) Neuroanatomical abnormalities in behaviorally characterized App(V717F) transgenic mice. Neurobiology of Disease 7: 71-85.

241. Chen GQ, Chen KS, Knox J, Inglis J, Bernard A, et al. (2000) A learning deficit related to age and β-amyloid plaques in a mouse model of Alzheimer's disease. Nature 408: 975-979.

242. Games D, Buttini M, Kobayashi D, Schenk D, Seubert P (2006) Mice as models: transgenic approaches and Alzheimer's disease. Journal of Alzheimer's Disease 9: 133-149.

243. Hsiao K, Chapman P, Nilsen S, Eckman C, Harigaya Y, et al. (1996) Correlative memory deficits, Aβ elevation, and amyloid plaques in transgenic mice. Science 274: 99-102.

244. King DL, Arendash GW (2002) Behavioral characterization of the Tg2576 transgenic model of Alzheimer's disease through 19 months. Physiol Behav 75: 627-642.

245. Siman R, Reaume AG, Savage MJ, Trusko S, Lin YG, et al. (2000) Presenilin-1 P264L knock-in mutation: Differential effects on Aβ production, amyloid deposition, and neuronal vulnerability. Journal of Neuroscience 20: 8717-8726.

246. Duff K, Eckman C, Zehr C, Yu X, Prada CM, et al. (1996) Increased Amyloid-β-42(43) In Brains Of Mice Expressing Mutant Presenilin 1. Nature 383: 710-713.

247. Games D, Adams D, Alessandrini R, Barbour R, Berthelette P, et al. (1995) Alzheimer-type neuropathology in transgenic mice overexpressing V717F β-amyloid precursor protein [see comments]. Nature 373: 523-527.

248. Price JL, Morris JC (1999) Tangles and plaques in nondemented aging and "preclinical" Alzheimer's disease. Annals of Neurology 45: 358-368.

249. Oddo S, Caccamo A, Shepherd JD, Murphy MP, Golde TE, et al. (2003) Triple-transgenic model of Alzheimer's disease with plaques and tangles: intracellular Aβ and synaptic dysfunction. Neuron 39: 409-421.

250. Irizarry MC, McNamara M, Fedorchak K, Hsiao K, Hyman BT (1997) APPSw transgenic mice develop age-related Ab deposits and neuropil abnormalities, but no neuronal loss in CA1. J Neuropathol Exp Neurol 56: 965-973.

251. Irizarry MC, Soriano F, McNamara M, Page KJ, Schenk D, et al. (1997) Ab deposition is associated with neuropil changes, but not with overt neuronal loss in

the human amyloid precursor protein V717F (PDAPP) transgenic mouse. Journal of Neuroscience 17: 7053-7059.

252. Oakley H, Cole SL, Logan S, Maus E, Shao P, et al. (2006) Intraneuronal β-amyloid aggregates, neurodegeneration, and neuron loss in transgenic mice with five familial Alzheimer's disease mutations: potential factors in amyloid plaque formation. Journal of Neuroscience 26: 10129-10140.

253. Duyckaerts C, Potier MC, Delatour B (2008) Alzheimer disease models and human neuropathology: similarities and differences. Acta neuropathologica 115: 5-38.

254. Lewis J, Dickson DW, Lin WL, Chisholm L, Corral A, et al. (2001) Enhanced neurofibrillary degeneration in transgenic mice expressing mutant tau and APP. Science 293: 1487-1491.

255. Buerger K, Ewers M, Pirttila T, Zinkowski R, Alafuzoff I, et al. (2006) CSF phosphorylated tau protein correlates with neocortical neurofibrillary pathology in Alzheimer's disease. Brain 129: 3035-3041.

256. Winton MJ, Lee EB, Sun E, Wong MM, Leight S, et al. (2011) Intraneuronal APP, not free Aβ peptides in 3xTg-AD mice: implications for tau versus Aβ-mediated Alzheimer neurodegeneration. Journal of Neuroscience 31: 7691-7699.

257. Attar A, Liu T, Chan W-TC, Hayes J, Nejad M, et al. (2013) A Shortened Barnes Maze Protocol Reveals Memory Deficits at 4-Months of Age in the Triple-Transgenic Mouse Model of Alzheimer's Disease. PLoS One.

258. Clinton LK, Blurton-Jones M, Myczek K, Trojanowski JQ, LaFerla FM (2010) Synergistic Interactions between Aβ, tau, and α-synuclein: acceleration of neuropathology and cognitive decline. Journal of Neuroscience 30: 7281-7289.

259. Billings LM, Oddo S, Green KN, McGaugh JL, LaFerla FM (2005) Intraneuronal Aβ causes the onset of early Alzheimer's disease-related cognitive deficits in transgenic mice. Neuron 45: 675-688.

260. Atri A (2011) Effective pharmacological management of Alzheimer's disease. American Journal of Managed Care 17 Suppl 13: S346-355.

261. Hansen RA, Gartlehner G, Kaufer DJ, Lohr KN, Carey T (2006) Drug Class Review on Alzhimer's Drugs: Final Report. Portland: Oregon Health and Science University.

262. Samochocki M, Zerlin M, Jostock R, Groot Kormelink PJ, Luyten WH, et al. (2000) Galantamine is an allosterically potentiating ligand of the human α4/β2 nAChR. Acta Neurologica Scandinavica Supplementum 176: 68-73.

263. Parsons CG, Gruner R, Rozental J, Millar J, Lodge D (1993) Patch clamp studies on the kinetics and selectivity of N-methyl-D-aspartate receptor antagonism by

memantine (1-amino-3,5-dimethyladamantan). Neuropharmacology 32: 1337-1350.

264. Miguel-Hidalgo JJ, Alvarez XA, Cacabelos R, Quack G (2002) Neuroprotection by memantine against neurodegeneration induced by β-amyloid(1-40). Brain Research 958: 210-221.

265. Chen TF, Huang RF, Lin SE, Lu JF, Tang MC, et al. (2010) Folic Acid potentiates the effect of memantine on spatial learning and neuronal protection in an Alzheimer's disease transgenic model. Journal of Alzheimer's Disease 20: 607-615.

266. Evans JG, Wilcock G, Birks J (2004) Evidence-based pharmacotherapy of Alzheimer's disease. International Journal of Neuropsychopharmacology 7: 351-369.

267. Doody RS, Stevens JC, Beck C, Dubinsky RM, Kaye JA, et al. (2001) Practice parameter: management of dementia (an evidence-based review). Report of the Quality Standards Subcommittee of the American Academy of Neurology. Neurology 56: 1154-1166.

268. Li C, Ebrahimi A, Schluesener H (2013) Drug pipeline in neurodegeneration based on transgenic mice models of Alzheimer's disease. Ageing Research Reviews 12: 116-140.

269. Liu CC, Kanekiyo T, Xu H, Bu G (2013) Apolipoprotein E and Alzheimer disease: risk, mechanisms and therapy. Nat Rev Neurol 9: 106-118.

270. Bard F, Cannon C, Barbour R, Burke RL, Games D, et al. (2000) Peripherally administered antibodies against amyloid β-peptide enter the central nervous system and reduce pathology in a mouse model of Alzheimer disease. Nature Medicine 6: 916-919.

271. Solomon B, Koppel R, Frankel D, Hanan-Aharon E (1997) Disaggregation of Alzheimer β-amyloid by site-directed mAb. Proc Natl Acad Sci U S A 94: 4109-4112.

272. Yang F, Lim GP, Begum AN, Ubeda OJ, Simmons MR, et al. (2005) Curcumin inhibits formation of amyloid β oligomers and fibrils, binds plaques, and reduces amyloid in vivo. Journal of Biological Chemistry 280: 5892-5901.

273. McLaurin J, Kierstead ME, Brown ME, Hawkes CA, Lambermon MH, et al. (2006) Cyclohexanehexol inhibitors of Aβ aggregation prevent and reverse Alzheimer phenotype in a mouse model. Nature Medicine 12: 801-808.

274. Townsend M, Cleary JP, Mehta T, Hofmeister J, Lesné S, et al. (2006) Orally available compound prevents deficits in memory caused by the Alzheimer amyloid-β oligomers. Annals of Neurology 60: 668-676.

275. Necula M, Kayed R, Milton S, Glabe CG (2007) Small molecule inhibitors of aggregation indicate that amyloid β oligomerization and fibrillization pathways are independent and distinct. Journal of Biological Chemistry 282: 10311-10324.

276. Ladiwala AR, Dordick JS, Tessier PM (2011) Aromatic Small Molecules Remodel Toxic Soluble Oligomers of Amyloid β through Three Independent Pathways. Journal of Biological Chemistry 286: 3209-3218.

277. Di Giovanni S, Eleuteri S, Paleologou KE, Yin G, Zweckstetter M, et al. (2010) Entacapone and tolcapone, two catechol O-methyltransferase inhibitors, block fibril formation of α-synuclein and β-amyloid and protect against amyloid-induced toxicity. Journal of Biological Chemistry 285: 14941-14954.

278. Lu JH, Ardah MT, Durairajan SS, Liu LF, Xie LX, et al. (2011) Baicalein Inhibits Formation of α-Synuclein Oligomers within Living Cells and Prevents Aβ Peptide Fibrillation and Oligomerisation. Chembiochem.

279. Thapa A, Woo ER, Chi EY, Sharoar MG, Jin HG, et al. (2011) Biflavonoids Are Superior to Monoflavonoids in Inhibiting Amyloid-β Toxicity and Fibrillogenesis via Accumulation of Nontoxic Oligomer-like Structures. Biochemistry 50: 2445-2455.

280. Necula M, Breydo L, Milton S, Kayed R, van der Veer WE, et al. (2007) Methylene blue inhibits amyloid Aβ oligomerization by promoting fibrillization. Biochemistry 46: 8850-8860.

281. McLaurin J, Golomb R, Jurewicz A, Antel JP, Fraser PE (2000) Inositol stereoisomers stabilize an oligomeric aggregate of Alzheimer amyloid β peptide and inhibit Aβ-induced toxicity. Journal of Biological Chemistry 275: 18495-18502.

282. Dasilva KA, Shaw JE, McLaurin J (2010) Amyloid-β fibrillogenesis: structural insight and therapeutic intervention. Exp Neurol 223: 311-321.

283. Rezai-Zadeh K, Shytle D, Sun N, Mori T, Hou H, et al. (2005) Green tea epigallocatechin-3-gallate (EGCG) modulates amyloid precursor protein cleavage and reduces cerebral amyloidosis in Alzheimer transgenic mice. Journal of Neuroscience 25: 8807-8814.

284. Ehrnhoefer DE, Bieschke J, Boeddrich A, Herbst M, Masino L, et al. (2008) EGCG redirects amyloidogenic polypeptides into unstructured, off-pathway oligomers. Nat Struct Mol Biol 15: 558-566.

285. Ladiwala AR, Lin JC, Bale SS, Marcelino-Cruz AM, Bhattacharya M, et al. (2010) Resveratrol selectively remodels soluble oligomers and fibrils of amyloid Aβ into off-pathway conformers. Journal of Biological Chemistry 285: 24228-24237.

286. Fradinger EA, Monien BH, Urbanc B, Lomakin A, Tan M, et al. (2008) C-terminal peptides coassemble into Aβ42 oligomers and protect neurons against Aβ42-induced neurotoxicity. Proc Natl Acad Sci USA 105: 14175-14180.

287. Li H, Monien BH, Lomakin A, Zemel R, Fradinger EA, et al. (2010) Mechanistic investigation of the inhibition of Aβ42 assembly and neurotoxicity by Aβ42 C-terminal fragments. Biochemistry 49: 6358-6364.

288. Sinha S, Lopes DH, Du Z, Pang ES, Shanmugam A, et al. (2011) Lysine-specific molecular tweezers are broad-spectrum inhibitors of assembly and toxicity of amyloid proteins. Journal of the American Chemical Society 133: 16958-16969.

289. Lannfelt L, Blennow K, Zetterberg H, Batsman S, Ames D, et al. (2008) Safety, efficacy, and biomarker findings of PBT2 in targeting Aβ as a modifying therapy for Alzheimer's disease: a phase IIa, double-blind, randomised, placebo-controlled trial. Lancet Neurology 7: 779-786.

290. Crouch PJ, Savva MS, Hung LW, Donnelly PS, Mot AI, et al. (2011) The Alzheimer's therapeutic PBT2 promotes amyloid-β degradation and GSK3 phosphorylation via a metal chaperone activity. Journal of Neurochemistry 119: 220-230.

291. Faux NG, Ritchie CW, Gunn A, Rembach A, Tsatsanis A, et al. (2010) PBT2 rapidly improves cognition in Alzheimer's Disease: additional phase II analyses. Journal of Alzheimer's Disease 20: 509-516.

292. (2009) Elan and Transition Therapeutics Announce Modifications to ELND005 Phase II Clinical Trials in Alzheimer's Disease.

293. Takashima A (2010) The Mechanism of tau aggregation and its relation to neuronal dysfunction. Alzheimer's Association Interantional Conference on Alzheimer's disease. Honolulu, HI: Alzheimer Dement. pp. S144, Abstract No. PL-104-103.

294. Attar A, Rahimi F, Bitan G (2013) Modulators of Amyloid Protein Aggregation and Toxicity: EGCG and CLR01. Translational Neuroscience: In Press.

295. Grill JD, Cummings JL (2010) Current therapeutic targets for the treatment of Alzheimer's disease. Expert Rev Neurother 10: 711-728.

296. Mullard A (2012) Sting of Alzheimer's failures offset by upcoming prevention trials. Nature Reviews Drug Discovery 11: 657-660.

297. Feng BY, Toyama BH, Wille H, Colby DW, Collins SR, et al. (2008) Small-molecule aggregates inhibit amyloid polymerization. Nat Chem Biol 4: 197-199.

298. McGovern SL, Caselli E, Grigorieff N, Shoichet BK (2002) A common mechanism underlying promiscuous inhibitors from virtual and high-throughput screening. Journal of Medicinal Chemistry 45: 1712-1722.

299. Martins IC, Kuperstein I, Wilkinson H, Maes E, Vanbrabant M, et al. (2008) Lipids revert inert Aβ amyloid fibrils to neurotoxic protofibrils that affect learning in mice. EMBO J 27: 224-233.

300. Sharma AK, Pavlova ST, Kim J, Finkelstein D, Hawco NJ, et al. (2012) Bifunctional compounds for controlling metal-mediated aggregation of the Aβ42 peptide. Journal of the American Chemical Society 134: 6625-6636.

301. Roberts BE, Shorter J (2008) Escaping amyloid fate. Nat Struct Mol Biol 15: 544-546.

302. Landau M, Sawaya MR, Faull KF, Laganowsky A, Jiang L, et al. (2011) Towards a pharmacophore for amyloid. PLoS Biol 9: e1001080.

303. Haass C, Selkoe DJ (2007) Soluble protein oligomers in neurodegeneration: lessons from the Alzheimer's amyloid β-peptide. Nat Rev Mol Cell Biol 8: 101-112.

304. Fändrich M (2012) Oligomeric intermediates in amyloid formation: structure determination and mechanisms of toxicity. Journal of Molecular Biology 421: 427-440.

305. Fokkens M, Schrader T, Klärner FG (2005) A molecular tweezer for lysine and arginine. Journal of the American Chemical Society 127: 14415-14421.

306. Lopes DH, Sinha S, Rosensweig C, Bitan G (2012) Application of photochemical cross-linking to the study of oligomerization of amyloidogenic proteins. Methods in Molecular Biology 849: 11-21.

307. Talbiersky P, Bastkowski F, Klärner FG, Schrader T (2008) Molecular clip and tweezer introduce new mechanisms of enzyme inhibition. Journal of the American Chemical Society 130: 9824-9828.

Chapter 2

Disrupting Self-Assembly and Toxicity of Amyloidogenic Protein Oligomers by "Molecular Tweezers" – from the Test Tube to Animal Model

2.1 Introduction

Common molecular interactions mediate the aberrant self-assembly process seen with amyloid β-protein (Aβ), including backbone and side-chain hydrogen bonds complemented by hydrophobic and electrostatic interactions involving side chains of particular amino acids. Unique in their ability to participate in both hydrophobic and electrostatic interactions among the twenty proteinogenic amino acids are K residues. Due to this unique feature, K residues play a prominent role in protein folding and biological processes [2]. For example, ubiquitination at K residues marks proteins for proteasomal degradation and acetylation of histones at K residues regulates transcription. In the 40-residue isoform of amyloid β-protein, Aβ40, site-specific modification at the only two K residues in the sequence of the protein, K16 and K28, by cholesterol oxidation products, resulted in enhanced aggregation kinetics relative to the unmodified protein [3]. As the mechanism of action of molecular tweezers and their potential functionality in treatment of amyloidoses is dependent on binding to K residues in amyloid β-protein (Aβ) and other proteins involved in aberrant aggregation, assembly,

and toxicity, it is important to understand better the role of K residues in Aβ, which is described in section 2. Then, sections 3 and 4 will describe the *in vitro* studies done so far with CLR01 and section 5 will compare CLR01 to molecules currently in clinical trials. This chapter will end with the description of CLR01's efficacy in a zebrafish model of α-synuclein (α-syn) toxicity in section 6.

2.2 K Residues are Important Determinants of Aβ Structure, Assembly Kinetics, and Toxicity

To gain insight into the role of K residues in Aβ assembly and toxicity, each of the two K residues was individually substituted by A and the effect of the substitution on secondary structure, morphology, and toxicity in cell culture of both Aβ40 and Aβ42 was studied [4]. Circular dichroism (CD) spectroscopy was used to monitor the initial secondary structure and the temporal change of secondary structure in six Aβ alloforms: wild-type (WT) Aβ40, [K16A]Aβ40, [K28A]Aβ40, WT Aβ42, [K16A]Aβ42, and [K28A]Aβ42. The spectra subsequently were deconvoluted to allow for quantitative comparison of the content of the α-helix, β-sheet, and statistical coil structures in the substituted analogues relative to the WT peptides, during their self-assembly [4].

Comparing the initial and final α-helix, β-sheet, and statistical coil content of WT Aβ40 to the two Aβ40 analogues containing K→A substitutions, Sinha et. al. found that initially, the three analogues had similar content of each conformational element — predominantly statistical coil and a small contribution of β-sheet. Following incubation under conditions that promote fibril formation, the conformational transition of the A-substituted Aβ analogues were substantially slower than those of their WT counterparts.

The slowest transition was of [K16A]Aβ42, which did not reach completion at the final time point measured – 9 d, compared to the transition of WT Aβ42, which was complete in 24 h. Interestingly, following incubation, [K16A]Aβ40 showed a higher β-sheet and lower statistical coil content than WT Aβ40. In fact, the β-sheet content of [K16A]Aβ40 fibrils was as high as that of Aβ42, which is more amyloidogenic, and typically its fibrils display higher β-sheet content than Aβ40 fibrils [4].

The conformational change in the case of the K→A Aβ42 analogues was substantially more variable compared to the Aβ40 analogues. The initial α-helix content of the Aβ42 analogues was minimal and similar to each other. However, over time, in WT Aβ42 and [K28A]Aβ42 the α-helix content decreased to zero and the β-sheet content increased, whereas in [K16A]Aβ42, the α-helix content increased and became the predominant secondary structure element with concomitant decrease of β-sheet content to zero. This is a highly unusual behavior and I am unaware of any other substitution that promotes such a high increase in α-helix content in an Aβ42 analogue.

Though [K28A]Aβ42 followed a conformational transition similar to that of WT Aβ42, it had substantially lower final β-sheet content, lower than all the Aβ40 analogues, and a corresponding high final statistical coil content, the highest of all the six Aβ alloforms. Thus, both K16 and K28 were found to be important determinants in Aβ42 assembly into β-sheet-rich fibrils, supporting the central role K residues play in this process.

Using the same samples characterized by CD spectroscopy, the effect of the K→A substitutions on Aβ morphology was analyzed by electron microscopy (EM). All six alloforms displayed quasi-globular or amorphous morphology immediately following

dissolution and progressed to form fibrillar structures [4]. Aβ40, Aβ42 and their K16A analogues all showed long, unbranched fibrils. However, corresponding to its unusual behavior measured by CD spectroscopy, [K16A]Aβ42 also was characterized by abundant globular structures that appeared to "decorate" the fibrils. Presumably, within these structures [K16A]Aβ42 was in the predominantly α-helical conformation observed by CD spectroscopy. Interestingly, both [K28A]Aβ40 and [K28A]Aβ42 produced thicker, shorter, branched fibrils and a wider distribution of fibril diameters compared to the WT and K16A analogues, suggesting that the K28A substitution induced a higher nucleation rate relative to the analogues containing the native K28 residue. As the overall conformational transition kinetics in both [K28A]Aβ40 and [K28A]Aβ42 was slower than in their WT counterparts, the data indicate a large decrease in the elongation rates of the K28A analogues. These observations are in agreement with the important role of the electrostatic and hydrophobic interactions involving K28, which stabilize a turn in the Aβ(21–30) region [16].

The stark contrast between the structural transitions of [K16A]Aβ40 and [K16A]Aβ42, namely the high final β-sheet content of [K16A]Aβ40 versus the very low β-sheet content of [K16A]Aβ42, suggests an important interplay between the C-terminus and the central hydrophobic cluster (CHC) region, which is affected differently in Aβ40 and Aβ42 by the adjacent, charged K16. In Aβ40, this residue appears to inhibit early folding, whereas in Aβ42, K16 seems to facilitate β-sheet formation. It is interesting to compare and contrast these results with the study by Usui et al., in which K16 in Aβ40 was modified by the addition of cholesterol oxidation products leading to increased aggregation kinetics and toxicity [3]. The increase in β-sheet content correlates with the

removal of the positive charge of K16, and/or a general increase in hydrophobicity in this region, though the different modifications of K16 by Sinha et al. and Usui et al. led to opposite effects on the assembly kinetics and toxicity of the resulting peptides.

Modeling studies indicate that in Aβ40, because the C-terminus is shorter and less hydrophobic than in Aβ42, which has I41 and A42, the N-terminus competes with the C-terminus for interaction with the CHC [17-19]. Thus, the C-terminus–CHC interactions are a higher relative component in early Aβ42 folding versus Aβ40 [19] and consequently, perturbation of K16 would be predicted to affect Aβ42 more than Aβ40. Possibly, in Aβ40 K16 promotes electrostatic N-terminus–CHC interactions (e.g., with D1, E3, D7), and thus the substitution of K16 by A shifts the scales towards increased C-terminus–CHC leading to increased β-sheet content. In the case of Aβ42, where the C-terminus–CHC interaction is predominant, conceivably K16 facilitates formation of an intermediate state necessary for the transition into β-sheet and the absence of such stabilization explains the substantial decrease in β-sheet content and slow conformational transition in [K16A]Aβ42. Alternatively, the obligatory α-helical intermediate in the conformational transition of Aβ [20] may be stabilized by the K16A substitution in Aβ42.

To assess the impact of the A substitutions on Aβ-induced toxicity, the six alloforms were incubated with differentiated rat pheochromocytoma (PC-12) cells and the lactate-dehydrogenase release (LDH) assay was used to measure cell viability [4]. Unexpectedly, despite the relatively minor influence of the K16A substitution on Aβ40 assembly, [K16A]Aβ40 was not toxic to the cells even at a concentration as high as 100 μM (Figure 1). Previously, Ono et al. found that the level of toxicity of small Aβ40 oligomers correlated with β-sheet content [21]. Thus, it was highly surprising that even

though the β-sheet content in [K16A]Aβ40 was higher than that of WT Aβ40 and similar to the WT Aβ42 levels, no toxicity was observed with this isoform. These data strongly suggest direct involvement of K16 in Aβ-mediated toxicity, presumably through interaction with the cell membrane. In support of this interpretation of the data, [K16A]Aβ42 also showed substantially reduced toxicity relative to WT Aβ42 (Figure 2.1) despite the distinct effects of the K16A substitution on Aβ40 and Aβ42 conformation.

The K28A substitution also led to reduced toxicity of the resulting Aβ42 analogue relative to the WT counterpart, but the reduction in toxicity was substantially smaller than for the K16A analogues. In the case of the [K28A]Aβ analogues, the decreased toxicity correlated with major perturbation of the conformational transition and assembly process. Therefore, a conservative interpretation of the data is that substitution of K28 by A

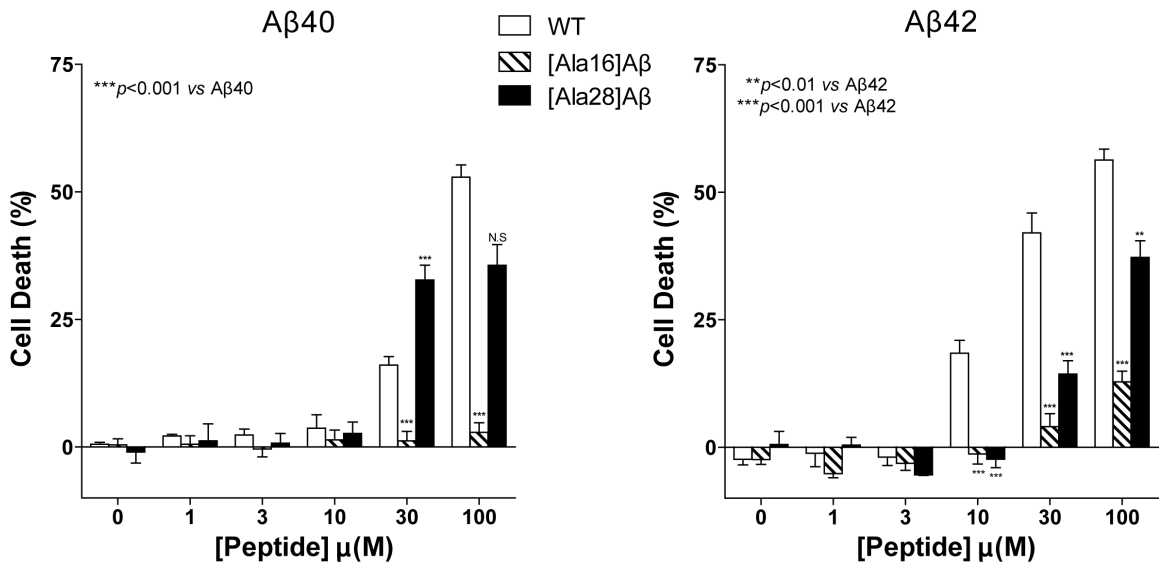

Figure 2.1 Toxicity of Aβ40, Aβ42, and their A-substituted analogues
Aβ40, Aβ42, and their respective K→A analogues were incubated with differentiated PC-12 cells for 48 h, and cell death was measured using the LDH release assay. The results are an average of four to six experiments and are presented as mean ± SEM. Statistical significance was calculated by one-way analysis of variance. Adapted from [4]

disrupts the turn in Aβ(21–30) leading to formation of oligomers and fibrils with different structures from those formed by the WT peptides. These structures are still toxic, but to a lesser extent than those of WT Aβ40 and Aβ42.

Based on the surprising findings that substitution of K16 by A led to a dramatic loss of toxicity in both Aβ40 and Aβ42, it is possible to predict that mutations in *APP* leading to this or similar substitutions may be found to be protective from Alzheimer's Disease (AD), similar to the recently discovered protective mutation that causes an A2T substitution in Aβ [22]. Interestingly, a new kindred has been discovered recently in which a heterozygous *APP* mutation leading to a K16N substitution causes familial AD [23] with the pure K16N, without WT, oligomers showing little toxicity *in vitro*. Ostensibly, this might be perceived as contradicting our hypothesis that K16 is directly involved in mediating Aβ toxicity. However, in support of our interpretation, [K16N]Aβ42 was found to have reduced toxicity compared to WT Aβ42. Apparently, the early onset familial AD associated with this mutation correlates with formation of highly toxic mixed oligomers of WT and K16N Aβ and possibly by increased total Aβ concentration due to perturbation of the α-secretase cleavage site and/or reduced Aβ clearance [23].

Recently, our group discovered that deletion of K1 in islet amyloid polypeptide (IAPP), a highly amyloidogenic peptide hormone whose self-assembly is closely associated with pancreatic β-cell death in type-2 diabetes, causes substantial decrease in the peptide's toxicity [24]. These findings provide additional support for an important role of K residues in mediating toxicity of amyloidogenic proteins.

The data discussed above suggest that disruption of molecular interactions involving K residues may lead to modulation of Aβ assembly and inhibition of Aβ toxicity. Moreover, because K residues are common to almost all proteins, this strategy may be applied to inhibition of the toxicity of amyloidogenic proteins in general, not just Aβ. At the same time, this very argument raises the question whether the strategy can be applied specifically to inhibition of toxic amyloidogenic proteins without interfering with normal protein folding and function. The following sections will describe the application of "molecular tweezers" (MTs), which bind non-covalently with moderate affinity to K residues and achieve this very goal, inhibiting the assembly and toxicity of amyloidogenic proteins without interfering with normal physiology.

2.3 Molecular Tweezers are Broad-spectrum Assembly and Toxicity Inhibitors *In Vitro*

To test the hypothesis that perturbation of molecular interactions involving K residues would disrupt amyloidogenic assembly, the effect of CLR01 on formation of β-sheet-rich fibrils was analyzed in nine different proteins that were either naturally unstructured (Aβ, tau, α-syn, IAPP, calcitonin, and prion protein (PrP; residues 106–126)) or structured (insulin, β_2-microglobulin, and transthyretin). The percentage of K residues in these proteins ranges from 2.7–10.7% (Table 2.1). Each protein was incubated under aggregation-promoting conditions in the absence or presence of CLR01 or CLR03. The aggregation reaction was followed by thioflavin T (ThT) fluorescence [25] and EM, except in the cases of transthyretin and PrP(106–126), which did not show sufficient ThT

binding upon fibril formation and therefore their aggregation was monitored by the increase in turbidity at $\lambda = 360$ nm [26,27].

Table 2.1: Amyloidogenic proteins studied

Protein	Length (aa)	Lys	% Lys	Arg	% Arg	Associated Disease	Reference
Aβ40, Aβ42	40, 42	2	5.0, 4.8	1	2.5, 2.4	AD	[5]
Tau (embryonic)	352	37	10.5	14	4.0	AD, tauopathies	[5]
α-Syn	140	15	10.7	0	0.0	PD, synucleinopathies	[8]
IAPP	37	1	2.7	1	2.7	Type-2 diabetes	[9]
Calcitonin	32	1	3.1	0	0.0	Medullary Carcinoma of the Thyroid	[10]
Insulin	51	2	3.9	1	2.0	Injection-related nodular amyloidosis	[11]
β_2-Microglobulin	99	8	8.1	5	5.1	Dialysis-related amyloidosis	[12]
Transthyretin	147	8	5.4	5	3.4	Senile systemic amyloidosis, Familial amyloid polyneuropathy	[13,14]
PrP(106–126)	21	2	9.5	0	0.0		[15]

Adapted from [1]

The protein concentration in each case was selected to enable aggregation within a reasonable time frame, ranging from < 2 h for the most amyloidogenic peptide, IAPP, to over a week for the slowest protein, α-syn. In most cases, CLR01 was found to inhibit the aggregation completely at a 1:1 concentration ratio and in some cases at sub-stoichiometric concentrations (less CLR01 than protein), suggesting inhibition of both the nucleation and elongation steps [1]. Interestingly, substoichiometric inhibition was found in the cases of calcitonin and IAPP, both of which are hormones sharing some structural similarity, such as a disulfide-bridge constrained 6/7-residue region in their N-terminus.

In agreement with the ThT fluorescence/turbidity measurements, morphological examination of all proteins studied showed formation of amorphous aggregates in the

presence of CLR01, as opposed to the typical amyloid fibrils formed in the absence of MTs or in the presence of CLR03 [1]. The only exception to the rule was PrP(106–126), whose aggregation was not inhibited by CLR01, presumably because the two K residues in this peptide are located away from the amyloidogenic sequence that mediates its aggregation.

In follow-up experiments, the capability of CLR01 to inhibit the toxicity induced by amyloidogenic proteins was tested. The proteins were incubated first under conditions that promote oligomerization and then added exogenously to cultured cells. Differentiated PC-12 cells were used to study Aβ, α-syn, calcitonin, β_2-microglobulin, and transthyretin, whereas rat insulinoma (RIN5fm) cells were used in IAPP and insulin experiments. The 3-(4,5-dimethylthiazol-2-yl)-2,5-diphenyltetrazolium bromide (MTT) reduction assay was used for measurement of cell viability in all cases [1]. In addition, because α-syn is predominantly an intracellular protein, CLR01 inhibition of endogenous α-syn expressed in HEK 293 cells also was tested [6].

Because MTs potentially can bind to any exposed Lys and at sufficiently high concentration likely would disrupt cellular processes, it was important to determine first whether a sufficient window existed between CLR01 concentrations that reduced cell viability and those needed for inhibition of toxicity caused by amyloidogenic proteins. CLR01 was found to increase cell viability by 5–15% relative to control cells at concentrations up to 200 μM, whereas at 400 μM, it caused a 10–20% decrease in cell viability [1]. Therefore, CLR01 concentration was kept below 400 μM in all subsequent experiments. The results are summarized in Table 2.2 [1]. Because the proteins were added exogenously in these assays, the CLR01 concentration at half-maximal inhibition

(IC_{50}) depended on the concentration of the respective protein. The CLR01:protein stoichiometry, estimated as the ratio between the concentration of the protein used and

Table 2.2: CLR01 inhibits toxicity of amyloidogenic proteins

Protein	Concentration in toxicity assay (μM)	Cells	IC_{50} (μM)	IC_{50}:Conc.
Aβ40	20	PC-12	14±11	0.7
Aβ42	10	PC-12	52±18	5.2
α-Syn	20	PC-12	3±1	0.15
IAPP	0.01	RIN5fm	6±3	600
Calcitonin	15	PC-12	28±4	1.9
Insulin	5	RIN5fm	13±2	2.8
β_2-Microglobulin	10	PC-12	28±6	2.8
Transthyretin	1	PC-12	54±19	54

Adapted from [1]

the IC_{50}, varied, though in most cases it was in the same order of magnitude. Because the endogenous concentrations of most of the proteins used are in the nM range, the data suggested that nM concentrations of CLR01, several orders of magnitude below toxic concentrations, might inhibit aggregation of these proteins *in vivo*. In support of this view, though the IC_{50} of CLR01 for inhibition of 20 μM exogenously added α-syn was 3–4 μM, 1 μM of CLR01 was sufficient for complete inhibition of cell death induced by expression of endogenous α-syn in HEK 293 cells [6].

2.4 CLR01 Remodels Aβ and α-Syn Oligomers into Non-toxic Structures and Dissociates Pre-formed Fibrils

Due to the increasing evidence that soluble oligomers of Aβ and other amyloidogenic proteins are the most toxic structural species involved in amyloidoses [28-30], Sinha et al. [1] explored how CLR01 affected Aβ42 oligomerization using dot blots

with the oligomer-specific antibody, A11 [31]. In the absence of MTs, A11 immunoreactivity was observed immediately and continued to increase over several days. In contrast, Aβ42 samples incubated in the presence of CLR01 never showed A11 reactivity suggesting that the reaction of CLR01 with Aβ was fast and induced structural changes precluding formation of the toxic oligomers recognized by A11. Interestingly, dynamic light scattering (DLS) experiments showed that oligomers formed by 10 μM Aβ42 in the absence or presence of equimolar CLR01 had essentially the same sizes, though their abundance increased relative to Aβ42 alone [1]. Sodium dodecyl sulphate-polyacrylamide gel electrophoresis (SDS-PAGE) and native-PAGE/Western blot analyses of 200 nM Aβ42 prepared in neurobasal cell culture medium or artificial cerebrospinal fluid for electrophysiologic experiments did not show a difference in assembly size between preparations in the absence or presence of CLR01 [32]. Thus, the structural changes CLR01 induces in Aβ42 oligomers are relatively small and cannot be discerned by low-resolution methods, such as DLS, EM, or PAGE/Western blot. Possibly, dot blot experiments but not Western blot experiments saw differences in Aβ assemblies in the absence or presence of CLR01 because the oligomer specific antibody, A11, recognizes a type of structure that is disrupted by CLR01. However, the size of this structure is not changed and thus no difference is seen by Western blot. Nonetheless, these structural changes have two important outcomes — the oligomers formed in the presence of CLR01 are non-toxic, and binding of CLR01 prevents fibril formation.

The effect of CLR01 also was assessed on oligomerization of α-syn. Samples of 20 μM α-syn were incubated for 12 d and aliquots were analyzed daily using SDS-PAGE and native-PAGE [6]. α-Syn migrated in several bands likely corresponding to monomer,

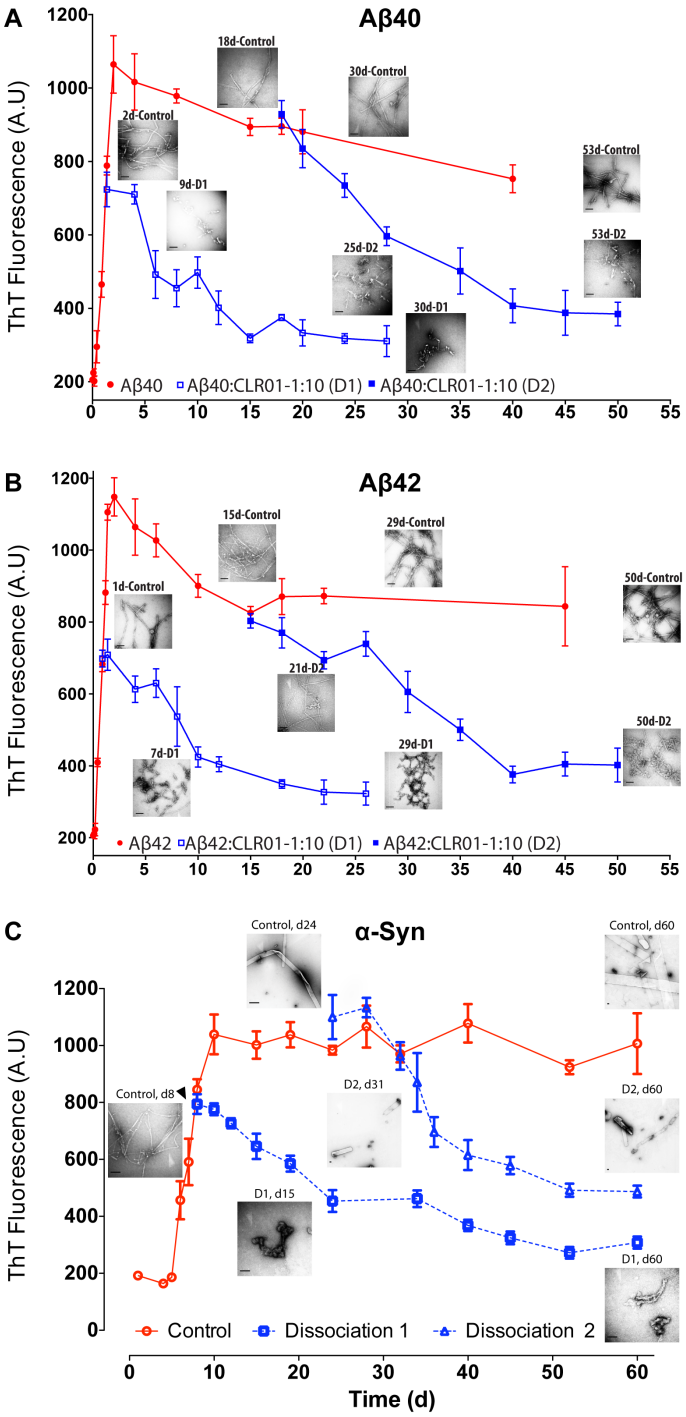

Figure 2.2 CLR01 disaggregates Aβ and α-syn fibrils *in vitro*
Disaggregation of A) Aβ40, B) Aβ42, or C) α-syn fibrils by CLR01 was initiated in each case at two time points, the first when immature fibrils formed and the second when fibrils had a chance to mature and consolidate for at least 2 weeks. The reactions were monitored using ThT fluorescence. Electron micrographs were obtained periodically and show the morphology of each protein at the indicated time points. A, B adapted from [1], C adapted from [6]

low molecular weight oligomers, and a smear of higher molecular weight assemblies. Similarly to the data observed with Aβ42, in the presence of CLR01 there was no difference in the size of the α-syn oligomers prepared in the absence or presence of CLR01 detected by SDS-PAGE or native-PAGE yet the abundance of high-molecular weight species increased in the presence of CLR01 [6]. The data observed for Aβ42 and α-syn suggest that upon interaction with CLR01, amyloidogenic proteins self-assemble into oligomers of similar size to those formed in the absence of the MT, but are not toxic. The increase in abundance of such oligomers in the presence of CLR01 is

attributed to stabilization of these structures and prevention of further aggregation and fibril formation.

If MTs are to be developed as therapeutic drugs, it is important to examine whether they can not only prevent protein aggregation but also disassemble pre-formed fibrils, as those are expected to exist in the affected tissues of patients. Therefore, the capability of CLR01 to dissociate fibrils of Aβ (Figure 2.2A, B), α-syn (Figure 2.2C), or IAPP [24] was examined. Each protein was allowed to aggregate and form immature or mature fibrils and then incubated further with 10-fold excess CLR01. In all cases, ThT fluorescence measurements showed that CLR01 caused steady dissociation of the present fibrils. EM images revealed remodeling of the assembly state first from long and unbranched, to shorter, branched fibrils and then to amorphous aggregates. The putative mechanism by which the excess CLR01 effected fibril dissociation is by shifting the equilibrium between the fibrillar and soluble states of the proteins and preventing re-association of monomers with the fibrils. *In vivo*, this is predicted to allow clearance of the offending proteins by various mechanisms, such as the proteasome, lysosome, and/or specific and non-specific proteolytic enzymes, which fail to clear these proteins in their aggregated, fibrillar forms.

2.5 Comparison of CLR01 with Assembly Inhibitors Currently in Clinical Trials

Approximately fifty treatments are in phase-2 or 3 clinical trials for AD, of which 10–20% target Aβ assembly directly or indirectly [33,34]. Examples of drug candidates in this category include ELND-005, Sunphenon, Tramiprosate/Alzhemed, and PBT2, of

which the first three compounds originated from natural sources. Tramiprosate is a glycosaminoglycan mimetic that binds to soluble Aβ and prevents fibrillization [35]. Though it was found to be effective in preclinical animal studies, Tramiprosate failed in clinical trials, potentially due to methodological issues, and has been now rebranded as a natural memory-protecting agent called Vivimind (Ovos Natural Health, Canada). PBT2 is a 2nd-generation clioquinol derivative and similar to clioquinol, it is a chelating agent for Zn^{2+} and Cu^{2+}, which are thought to induce brain Aβ aggregation. PBT2 has shown positive results in phase-2 clinical trials and has yet to progress to phase-3 trials.

ELND-005 is a natural sugar derivative, *scyllo*-inositol (SI), which has good oral bioavailability and crosses the blood-brain barrier via inositol transporters. Though the mechanism by which SI interacts with Aβ is not understood, the compound has been reported to promote both dissociation of Aβ aggregates and modulation of the aggregation process into formation of relatively large, presumably non-toxic assemblies [36-38]. Studies of SI in transgenic mouse models of AD showed reduction in soluble and insoluble Aβ, plaque burden, and synaptic loss, and improved spatial memory [36]. Phase-2 clinical trials for ELND-005 have been completed with mixed results, of which 9 deaths in the high-dose groups caused significant safety concern and cognitive and functional co-primary endpoints did not achieve statistical significance [39].

Sunphenon is the commercial name of (–)-epigallocatechin-3-gallate (EGCG), a polyphenol from green tea thought to function by many modalities, including anti-aggregation, scavenging of reactive oxygen species and other antioxidant activities, activation of cell signaling cascades, such as the protein kinase C pathway, and Fe^{3+} chelation [34,40]. Though EGCG has relatively poor bioavailability, it has been reported

to inhibit Aβ and α-syn assembly and toxicity, presumably by binding to the unfolded proteins and preventing conversion to toxic oligomers [41]. Peripheral administration of EGCG decreased Aβ plaque load in mice [42]. A phase-2/3 clinical trial pursued by Charite University, Berlin, Germany currently is recruiting patients.

In contrast to SI and EGCG, for which the mechanistic basis of the interaction with Aβ or other amyloidogenic proteins is not known, the binding of CLR01 to these proteins occurs at K residues and to a lower extent at R residues and the basis for the binding has been well-characterized. Therefore, it was of interest to compare the capability of these three compounds to inhibit the aggregation, oligomerization, and toxicity of Aβ.

Three-fold excess of either EGCG or CLR01 were found to inhibit completely the formation of β-sheet-rich fibrils in Aβ42 [7]. In contrast, surprisingly, 10-fold excess of SI showed only weak inhibition. ThT fluorescence in samples of Aβ42 incubated in the presence of 10-fold excess SI increased steadily with no apparent lag phase, though the rate of increase was slower than that of Aβ42 alone, suggesting that SI might facilitate nucleation, and attenuate elongation of Aβ42 fibrils, similarly to the effect of the K28A substitution discussed above.

The effect of the three inhibitors on Aβ42 oligomerization was assessed using the oligomer-specific antibody A11 [31], as described above. Aβ42 incubated in the presence of CLR01 or EGCG did not show A11 immunoreactivity, whereas in agreement with the weak inhibition observed in ThT fluorescence experiments, Aβ42 incubated in the presence of SI showed similar A11 immunoreactivity to control samples of Aβ42 alone.

The data suggest a similar, quick remodeling of Aβ42 assemblies by both EGCG and CLR01, but not SI, to a conformation that is not recognized by A11.

The effect of the three compounds on Aβ-induced toxicity was compared in differentiated PC-12 cells, primary hippocampal neurons, and mixed primary hippocampal neuronal/microglial cultures using the LDH-release assay (Figure 2.3). Again, in agreement with the inhibition of aggregation and oligomerization, both CLR01 and EGCG were potent inhibitors of cell death [7], whereas SI showed weak or no inhibition in the different cell cultures at the 10-fold excess concentration tested. Of note,

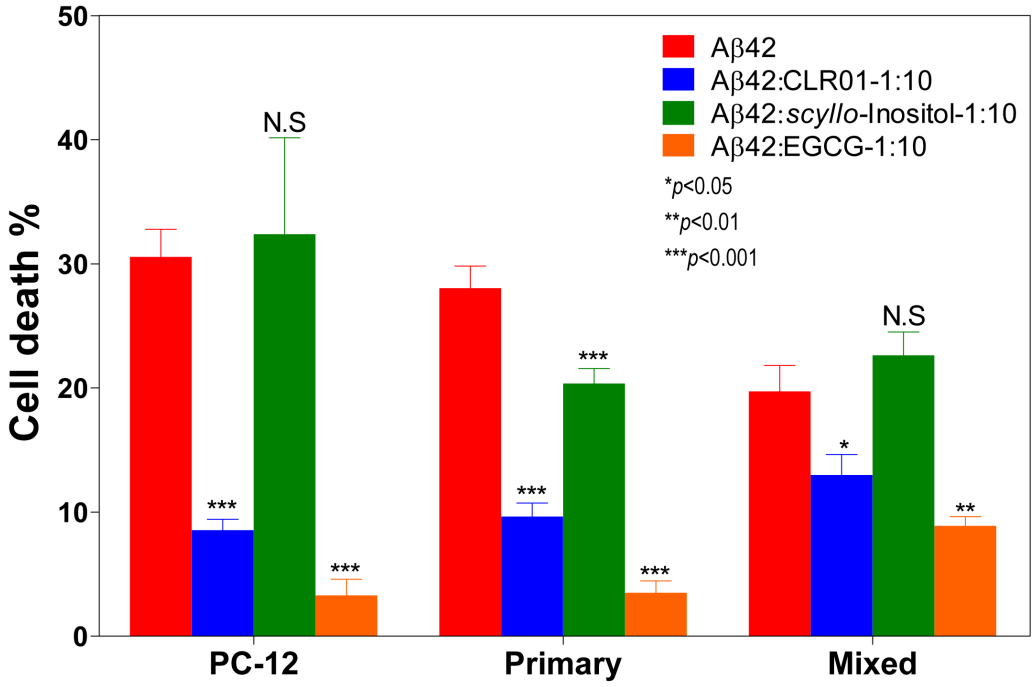

Figure 2.3. Comparison of inhibition of Aβ42-induced cell death by SI, EGCG, and CLR01
Ten μM Aβ42 was added to differentiated PC-12 cells, primary rat hippocampal neurons, or primary rat hippocampal neurons mixed with glial cells in the absence or presence of 10-fold excess of each inhibitor. Cells were incubated with the peptide:inhibitor mixtures for 48 h and cell death was measured using the LDH release assay. The data are presented as mean ± SEM for 3 independent experiments. *p<0.05, **p<0.01, ***p<0.001 compared to the Aβ42 in each group (one-way analysis of variance). Adapted from [7]

the amount of SI used in these studies is less than the amounts used in the original studies [36-38], though the same as the other inhibitors, thus resulting in the difference in effectiveness compared to the literature.

Interestingly, solution-state nuclear magnetic resonance investigation of the interaction of EGCG with Aβ40 revealed only weak contacts between the polyphenol and Aβ monomers, and could not identify a binding site, in contrast to the clear binding sites identified for CLR01 in similar experiments [7]. These findings suggest that EGCG binds to Aβ at later assembly stages than CLR01. A recent solid-state nuclear magnetic resonance study has suggested that EGCG binding interferes particularly with aromatic interactions in the CHC region of Aβ [43], yet how this interaction relates to the inhibition of Aβ oligomer-induced toxicity remains to be elucidated.

2.6 CLR01 Protects Zebrafish from α-Syn Toxicity

Zebrafish (ZF) embryos have been emerging as efficient models for investigating amyloid disease mechanisms, and for screening and evaluating drug candidates [44-46]. For example, a recent study has examined methylene blue as an inhibitor of tau- and polyglutamine-induced toxicity in ZF, and unfortunately, did not find beneficial effects of the drug in this model [47].

CLR01's ability to inhibit α-syn-induced toxicity *in vivo* was tested in a novel ZF model that expresses human wild type α-syn as a fusion protein with red fluorescent protein (DsRed) under a neuronal promoter starting ~12 h post fertilization (hpf). Following expression of the fusion protein, α-syn and DsRed are cleaved apart rapidly intracellularly to release native α-syn. This results in robust α-syn expression and DsRed

fluorescence in surviving embryos, but the survival rate of embryos expressing these proteins is about half that of embryos expressing DsRed alone, illustrating the toxic effect of the α-syn expression. Moreover, ~80% of surviving embryos expressing α-syn show various degrees of deformation resulting from extensive neuronal apoptosis and nearly 100% of the embryos are paralyzed. Consequently, all deformed and most non-deformed embryos die within 10 d post fertilization.

Addition of CLR01 to the water environment of the ZF embryos at 8 hpf caused a dramatic increase in ZF survival (Figure 2.4) and improved the phenotype in a dose-dependent manner [6]. At 10 d post fertilization, nearly half of the higher-dosed group,

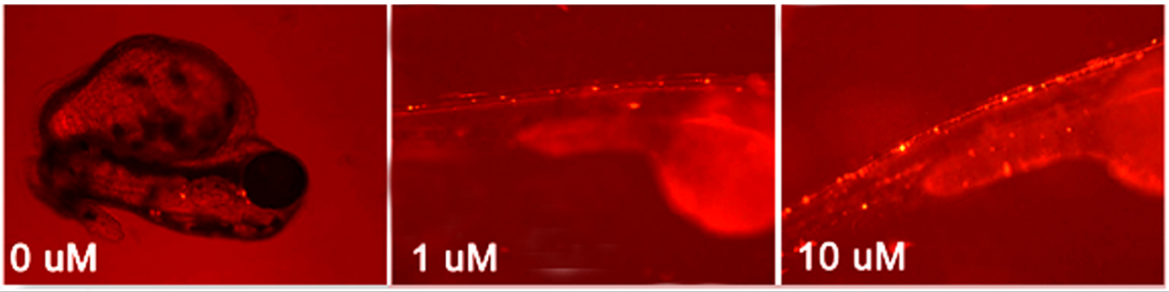

Figure 2.4 CLR01 ameliorates α-syn neurotoxicity in zebrafish
ZF embryos were treated with CLR01 at 8 hpf and were monitored for abnormal appearance and survival. Bright-field and fluorescent overlay images were taken at 72 hpf. Adapted from [6]

10 μM, remained alive and overall, CLR01 increased survival 10 d post fertilization by 13-fold. CLR01 also reduced apoptosis levels to control conditions, i.e., apoptosis levels in CLR01-treated ZF expressing α-syn and DsRed were the same as those in ZF expressing DsRed alone.

Immunohistochemistry revealed abundant α-syn-immunoreactive small clumps in DsRed-positive neurons of untreated ZF (Figure 2.5A, B). In contrast, ZF treated with CLR01 also showed α-syn immunoreactivity but the protein was soluble and dispersed homogeneously together with DsRed in the cytoplasm (Figure 2.5C–E). The

concentration level of α-syn measured by Western blot decreased by ~80% in treated ZF (Figure 2.5F), without changes in levels of DsRed or α-syn expression, as assessed by reverse-transcriptase polymerase chain reaction [6].

Many proteins that aggregate in neurodegenerative disorders have been shown to inhibit protein degradation [48]. To assess whether this was the case here and whether it

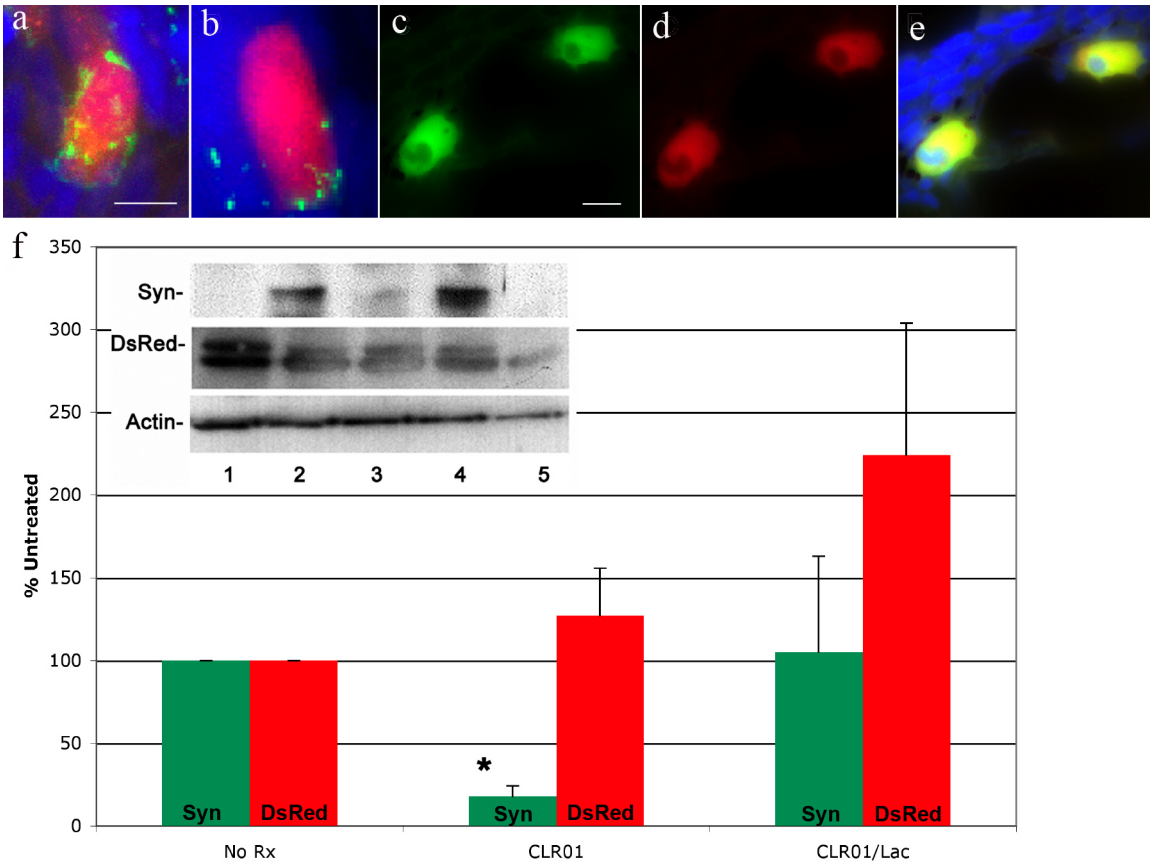

Figure 2.5 CLR01 prevents α-syn aggregation and proteasome inhibition
(a–e) ZF embryos expressing α-syn-DsRed (72 hpf) were subjected to immunohistochemistry. Green represents anti-α-syn antibody binding, red is DsRed, and blue is 4',6-diamidino-2-phenylindole-stained nuclei. (a, b) Representative neurons in untreated ZF. (c, d) CLR01-treated embryos. (e) Merged image of panels (c and d). (f) α-Syn expression inhibits the 26S ubiquitin-proteasome system (UPS) in ZF embryos. Embryos were lysed and proteins subjected to WB analysis (10 embryos per condition, N = 4). Lane 1, DsRed control; lane 2, untreated ZF expressing α-syn-DsRed; lane 3, α-syn-DsRed expressing ZF treated with CLR01; lane 4, α-syn-DsRed expressing ZF treated with CLR01 and lactacystin (Lac); lane 5, untreated wild-type embryos. Optical densities for α-syn (green bars) and DsRed (red bars) were normalized to actin and expressed as the percentage of untreated controls (*$p < 0.0002$ using Student's *t*-test). Adapted from [6]

was related to the decrease in α-syn concentration levels upon CLR01 treatment, the ubiquitin-proteasome system (UPS) was inhibited in treated ZF using lactacystin. Upon treatment with both CLR01 and Lac, α-syn was still soluble, rather than clumped, in the neurons of the treated ZF, yet α-syn concentration remained at the same level as in untreated ZF (Figure 2.5F), demonstrating that the UPS was largely responsible for the 80% decrease in α-syn concentration levels observed in CLR01-treated ZF in the absence of Lac [6]. The data suggest that α-syn assemblies inhibit the UPS and that by remodeling α-syn into a soluble, non-toxic form, CLR01 allows rapid clearance of the protein by the UPS. The data not only are encouraging and supporting further exploration of the use of CLR01 for Parkinson's disease therapy, but also suggest a plausible mechanism by which CLR01 works *in vivo* — keeping the offending protein in a soluble, non-toxic form and thereby facilitating its rapid clearance. Importantly, the data support the putative process-specific mechanism of MTs because the putative labile binding of CLR01 to the K residues in α-syn efficiently inhibited the protein's aggregation but not its ubiquitination, which occurs at K residues and is required for UPS-mediated degradation.

2.7 Conclusions

CLR01 is a novel solution for the problem of aberrant protein folding and self-assembly into toxic oligomers and aggregates, which underlies over 30 cureless human diseases. The CLR01 approach is based on targeting K residues as key elements participating in the combination of hydrophobic and electrostatic interactions that are central in the aberrant assembly process. The findings listed above demonstrate that K residues are highly important mediators of both assembly and toxicity of Aβ, α-syn, and

IAPP, supporting the rationale behind this strategy and suggesting that K residues likely play similar roles in the aggregation and toxicity of other amyloidogenic proteins.

Rather than screening molecules for their ability to break the amyloid cross-β structure, or exploring empirically found neutraceuticals, the application of MTs as broad-spectrum inhibitors of amyloid proteins' toxicity is based on targeting the fundamental molecular interactions involved in nascent oligomer formation.

The micromolar affinity of MTs for K residues may seem at first to be a shortcoming for a drug candidate. However, this actually appears to be the key feature of the ability of MTs to affect the abnormal folding and assembly of amyloidogenic proteins without disrupting normal physiology. Because of their moderate affinity and labile binding, MTs disrupt only the weak interactions involved in aberrant self-assembly but not the stable structures or high-affinity interactions of normal proteins, which are tightly controlled and have been shaped by millions of years of evolution. Thus, MTs are *process-specific*, rather than protein-specific because they disrupt the abnormal folding and assembly of multiple amyloidogenic proteins, but not the normal folding and function of stable proteins. To our knowledge, CLR01 is the first example of an inhibitor selected using a rational approach that uses a process-specific, rather than a protein-specific, mode of action. Using process-specific inhibitors is highly attractive for developing disease-modifying therapy for amyloidoses because the inhibitors act only on the pathologic aggregation, sparing normal physiological processes (e.g., production of the offending proteins described in the next chapter).

To date, K-specific MTs have been shown to inhibit the assembly and toxicity of thirteen different disease related amyloidogenic proteins ([1] and unpublished results).

CLR01, the lead MT, has the ability to disassemble fibrils and prevent formation of toxic oligomers of both Aβ and α-syn. In cell culture, CLR01 prevents cell death at levels comparable to EGCG, a compound currently in clinical trials. *In vivo*, CLR01 inhibits deformation and early death in a ZF model of α-syn toxicity by keeping α-syn soluble and restoring α-syn degradation by the proteasome. Thus far, multiple experiments in various systems have produced data supporting further development of MTs in general, and CLR01 in particular, as therapeutic agents for AD, Parkinson's disease, and other amyloid-related diseases. These are exciting and somewhat surprising results for small molecules that act using a heretofore-unexplored, process-specific mechanism, binding to virtually any exposed K residue with micromolar affinity. Additional study of these molecules *in vivo* is necessary for moving forward from pre-clinical to clinical trials for AD and related diseases and Chapter 3 will illustrate one such set of experiments.

2.8 References

1. Sinha S, Lopes DH, Du Z, Pang ES, Shanmugam A, et al. (2011) Lysine-specific molecular tweezers are broad-spectrum inhibitors of assembly and toxicity of amyloid proteins. Journal of the American Chemical Society 133: 16958-16969.

2. Freiman RN, Tjian R (2003) Regulating the regulators: lysine modifications make their mark. Cell 112: 11-17.

3. Usui K, Hulleman JD, Paulsson JF, Siegel SJ, Powers ET, et al. (2009) Site-specific modification of Alzheimer's peptides by cholesterol oxidation products enhances aggregation energetics and neurotoxicity. Proc Natl Acad Sci USA 106: 18563-18568.

4. Sinha S, Lopes DH, Bitan G (2012) A Key Role for Lysine Residues in Amyloid β-Protein Folding, Assembly, and Toxicity. ACS Chem Neurosci 3: 473-481.

5. Goedert M, Spillantini MG (2006) A century of Alzheimer's disease. Science 314: 777-781.

6. Prabhudesai S, Sinha S, Attar A, Kotagiri A, Fitzmaurice AG, et al. (2012) A novel "molecular tweezer" inhibitor of α-synuclein neurotoxicity in vitro and in vivo. Neurotherapeutics 9: 464-476.

7. Sinha S, Du Z, Maiti P, Klärner FG, Schrader T, et al. (2012) Comparison of three amyloid assembly inhibitors: the sugar scyllo-inositol, the polyphenol epigallocatechin gallate, and the molecular tweezer CLR01. ACS Chem Neurosci 3: 451-458.

8. Venda LL, Cragg SJ, Buchman VL, Wade-Martins R (2010) α-Synuclein and dopamine at the crossroads of Parkinson's disease. Trends in Neurosciences 33: 559-568.

9. Clark A, Charge SB, Badman MK, MacArthur DA, de Koning EJ (1996) Islet amyloid polypeptide: actions and role in the pathogenesis of diabetes. Biochemical Society Transactions 24: 594-599.

10. Melvin KE, Miller HH, Tashjian AH, Jr. (1971) Early diagnosis of medullary carcinoma of the thyroid gland by means of calcitonin assay. New England Journal of Medicine 285: 1115-1120.

11. Endo JO, Rocken C, Lamb S, Harris RM, Bowen AR (2010) Nodular amyloidosis in a diabetic patient with frequent hypoglycemia: sequelae of repeatedly injecting insulin without site rotation. Journal of the American Academy of Dermatology 63: e113-114.

12. Floege J, Ehlerding G (1996) β-2-microglobulin-associated amyloidosis. Nephron 72: 9-26.

13. Joao Saraiva M, Mendes Sousa M, Cardoso I, Fernandes R (2004) Familial amyloidotic polyneuropathy: protein aggregation in the peripheral nervous system. J Mol Neurosci 23: 35-40.

14. Plante-Bordeneuve V, Said G (2000) Transthyretin related familial amyloid polyneuropathy. Current Opinion in Neurology 13: 569-573.

15. Vassallo N (2009) Properties and pathogenicity of prion-derived peptides. Protein & Peptide Letters 16: 230-238.

16. Lazo ND, Grant MA, Condron MC, Rigby AC, Teplow DB (2005) On the nucleation of amyloid β-protein monomer folding. Protein Science 14: 1581-1596.

17. Urbanc B, Cruz L, Yun S, Buldyrev SV, Bitan G, et al. (2004) *In silico* study of amyloid β-protein folding and oligomerization. Proc Natl Acad Sci USA 101: 17345-17350.

18. Yun S, Urbanc B, Cruz L, Bitan G, Teplow DB, et al. (2007) Role of electrostatic interactions in amyloid β-protein (Aβ) oligomer formation: a discrete molecular dynamics study. Biophys J 92: 4064-4077.

19. Yang M, Teplow DB (2008) Amyloid β-protein monomer folding: free-energy surfaces reveal alloform-specific differences. Journal of Molecular Biology 384: 450-464.

20. Kirkitadze MD, Condron MM, Teplow DB (2001) Identification and characterization of key kinetic intermediates in amyloid β-protein fibrillogenesis. Journal of Molecular Biology 312: 1103-1119.

21. Ono K, Condron MM, Teplow DB (2009) Structure-neurotoxicity relationships of amyloid β-protein oligomers. Proc Natl Acad Sci U S A 106: 14745-14750.

22. Jonsson T, Atwal JK, Steinberg S, Snaedal J, Jonsson PV, et al. (2012) A mutation in APP protects against Alzheimer's disease and age-related cognitive decline. Nature 488: 96-99.

23. Kaden D, Harmeier A, Weise C, Munter LM, Althoff V, et al. (2012) Novel APP/Aβ mutation K16N produces highly toxic heteromeric Aβ oligomers. EMBO Mol Med 4: 647-659.

24. Lopes DHJ, Attar A, Du Z, McDaniel K, Dutt S, et al. (2013) The molecular tweezer CLR01 inhibits islet amyloid polypeptide assembly and toxicity via an unexpected mechanism. Submitted for publication.

25. LeVine H, 3rd (1999) Quantification of β-sheet amyloid fibril structures with thioflavin T. Methods in Enzymology 309: 274-284.

26. Kanapathipillai M, Ku SH, Girigoswami K, Park CB (2008) Small stress molecules inhibit aggregation and neurotoxicity of prion peptide 106-126. Biochemical and Biophysical Research Communications 365: 808-813.

27. Wang SS, Wen WS (2010) Examining the influence of ultraviolet C irradiation on recombinant human γ D-crystallin. Molecular Vision 16: 2777-2790.

28. Rahimi F, Shanmugam A, Bitan G (2008) Structure–function relationships of pre-fibrillar protein assemblies in Alzheimer's disease and related disorders. Curr Alzheimer Res 5: 319-341.

29. Fändrich M (2012) Oligomeric intermediates in amyloid formation: structure determination and mechanisms of toxicity. Journal of Molecular Biology 421: 427-440.

30. Straub JE, Thirumalai D (2010) Principles governing oligomer formation in amyloidogenic peptides. Curr Opin Struct Biol 20: 187-195.

31. Kayed R, Head E, Thompson JL, McIntire TM, Milton SC, et al. (2003) Common structure of soluble amyloid oligomers implies common mechanism of pathogenesis. Science 300: 486-489.

32. Attar A, Ripoli C, Riccardi E, Maiti P, Li Puma DD, et al. (2012) Protection of primary neurons and mouse brain from Alzheimer's pathology by molecular tweezers. Brain 135: 3735-3748.

33. Mangialasche F, Solomon A, Winblad B, Mecocci P, Kivipelto M (2010) Alzheimer's disease: clinical trials and drug development. Lancet Neurology 9: 702-716.

34. Amijee H, Scopes DI (2009) The quest for small molecules as amyloid inhibiting therapies for Alzheimer's disease. Journal of Alzheimer's disease : JAD 17: 33-47.

35. Gervais F, Paquette J, Morissette C, Krzywkowski P, Yu M, et al. (2007) Targeting soluble Aβ peptide with Tramiprosate for the treatment of brain amyloidosis. Neurobiology of Aging 28: 537-547.

36. McLaurin J, Kierstead ME, Brown ME, Hawkes CA, Lambermon MH, et al. (2006) Cyclohexanehexol inhibitors of Aβ aggregation prevent and reverse Alzheimer phenotype in a mouse model. Nature Medicine 12: 801-808.

37. Fenili D, Brown M, Rappaport R, McLaurin J (2007) Properties of scyllo-inositol as a therapeutic treatment of AD-like pathology. Journal of Molecular Medicine 85: 603-611.

38. Shaw JE, Chio J, Dasgupta S, Lai AY, Mo GC, et al. (2012) A β (1-42) assembly in the presence of scyllo-inositol derivatives: identification of an oxime linkage as important for the development of assembly inhibitors. ACS Chem Neurosci 3: 167-177.

39. Salloway S, Sperling R, Keren R, Porsteinsson AP, van Dyck CH, et al. (2011) A phase 2 randomized trial of ELND005, scyllo-inositol, in mild to moderate Alzheimer disease. Neurology 77: 1253-1262.

40. Mandel SA, Amit T, Kalfon L, Reznichenko L, Weinreb O, et al. (2008) Cell signaling pathways and iron chelation in the neurorestorative activity of green tea polyphenols: special reference to epigallocatechin gallate (EGCG). Journal of Alzheimer's disease : JAD 15: 211-222.

41. Ehrnhoefer DE, Bieschke J, Boeddrich A, Herbst M, Masino L, et al. (2008) EGCG redirects amyloidogenic polypeptides into unstructured, off-pathway oligomers. Nat Struct Mol Biol 15: 558-566.

42. Rezai-Zadeh K, Shytle D, Sun N, Mori T, Hou H, et al. (2005) Green tea epigallocatechin-3-gallate (EGCG) modulates amyloid precursor protein cleavage and reduces cerebral amyloidosis in Alzheimer transgenic mice. Journal of Neuroscience 25: 8807-8814.

43. Lopez del Amo JM, Fink U, Dasari M, Grelle G, Wanker EE, et al. (2012) Structural properties of EGCG-induced, nontoxic Alzheimer's disease A β oligomers. Journal of Molecular Biology 421: 517-524.

44. Gama Sosa MA, De Gasperi R, Elder GA (2012) Modeling human neurodegenerative diseases in transgenic systems. Human Genetics 131: 535-563.

45. Xia W (2010) Exploring Alzheimer's disease in zebrafish. Journal of Alzheimer's Disease 20: 981-990.

46. Paquet D, Schmid B, Haass C (2010) Transgenic zebrafish as a novel animal model to study tauopathies and other neurodegenerative disorders in vivo. Neurodegener Dis 7: 99-102.

47. van Bebber F, Paquet D, Hruscha A, Schmid B, Haass C (2010) Methylene blue fails to inhibit Tau and polyglutamine protein dependent toxicity in zebrafish. Neurobiology of Disease 39: 265-271.

48. Bence NF, Sampat RM, Kopito RR (2001) Impairment of the ubiquitin-proteasome system by protein aggregation. Science 292: 1552-1555.

Chapter 3

Protection of primary neurons and mouse brain from Alzheimer's pathology by molecular tweezers

3.1 Abstract

Alzheimer's disease (AD) is a devastating cureless neurodegenerative disorder affecting over 35 million people worldwide. The disease is caused by toxic oligomers and aggregates of amyloid β-protein and the microtubule-associated protein tau. Recently, the K-specific molecular tweezer CLR01 has been shown to inhibit aggregation and toxicity of multiple amyloidogenic proteins, including amyloid β-protein and tau, by disrupting key interactions involved in the assembly process. Following up on these encouraging findings, here, I asked whether CLR01 could protect primary neurons from AD-associated synaptotoxicity and reduce AD-like pathology *in vivo*. Using cell culture and brain slices, I found that CLR01 effectively inhibited synaptotoxicity induced by the 42-residue isoform of amyloid β-protein, including ~80% inhibition of changes in dendritic spines density and long-term potentiation and complete inhibition of changes in basal synaptic activity. Using a radiolabeled version of the compound I found that CLR01 crossed the mouse blood-brain barrier at ~2% of blood levels. One-m treatment of 15-m old triple-transgenic mice with CLR01 resulted in a decrease in brain amyloid β-protein aggregates, hyperphosphorylated tau, and microglia load as observed by

immunohistochemistry. Importantly, no signs of toxicity were observed in the treated mice and CLR01 treatment did not affect the amyloidogenic processing of amyloid β-protein precursor. Examining induction or inhibition of the cytochrome P450 metabolism system by CLR01 revealed minimal interaction. Together, these data suggest that CLR01 is safe for use at concentrations well above those showing efficacy in mice. The efficacy and toxicity results support a process-specific mechanism of action of molecular tweezers and suggest that these are promising compounds for developing disease-modifying therapy for AD and related disorders.

3.2 Introduction

Alzheimer's Disease (AD) is the leading cause of dementia, affecting over 35 million people worldwide [1]. Neuropathologically, AD is characterized by accumulation of neuritic plaques, comprising mainly fibrillar amyloid β-protein (Aβ), and neurofibrillary tangles made of filamentous hyperphosphorylated tau (p-tau). The inceptive assault on susceptible neurons is believed to be mediated by Aβ- and possibly tau-oligomers that disrupt synaptic communication [2,3] before cognitive symptoms can be detected. Thus, if formation of these toxic assemblies can be prevented before overt neurodegeneration occurs, the brain may be able to mount a defense and possibly recover.

Dr. Bitan sought compounds that would modulate the assembly of Aβ and tau and inhibit their toxicity at the earliest possible step. Dr. Bitan identified K residues as attractive targets where interference would disrupt assembly because these residues have a unique ability to participate in both hydrophobic and electrostatic interactions involved

in the assembly process of amyloidogenic proteins, including Aβ and tau [4-11]. Therefore, he conjectured that compounds that bind specifically to K residues might inhibit formation of toxic Aβ and tau assemblies.

K-specific "molecular tweezers" (MTs), originally reported in 2005 [12], bind to K residues with a dissociation constant of ~20 μM. Their specificity for K results from the K butylene moiety threading through the MT cavity and facilitating hydrophobic interactions with the MT sidewalls, and the ε-ammonium group's electrostatic attraction to the negatively charged bridgehead groups of the MTs. Thus, MTs utilize the same types of interactions involved in early Aβ assembly [4] allowing them to compete with these interactions and disrupt Aβ assembly and toxicity. A similar mechanism is expected to inhibit tau toxicity.

Recently, Dr. Bitan and colleagues have shown that a MT derivative called CLR01 was a potent inhibitor of assembly and toxicity of multiple disease-related amyloidogenic proteins, including Aβ and tau [13]. CLR01 was found to inhibit Aβ oligomerization, dissociate pre-formed Aβ fibrils, and stabilize non-toxic amorphous assemblies. Mass-spectrometry and nuclear magnetic resonance experiments confirmed binding of CLR01 to K in Aβ at the earliest stages of assembly [13]. CLR01 was found to inhibit Aβ-induced toxicity in differentiated rat pheochromocytoma cells and in primary rat hippocampal cultures or mixed neuronal/glial cultures [14] at micromolar concentrations. In addition, CLR01 was found to rescue zebrafish expressing human wild-type (WT) α-synuclein from severe deformation and early death by keeping the intracellular α-synuclein soluble and allowing its proteasomal clearance [15].

In light of these encouraging results, colleagues and I evaluated the effect of CLR01 on synaptic dysfunction *in vitro* and on AD-related brain pathology in transgenic mice. Colleagues and I also studied several aspects of CLR01's drug-like characteristics and possible toxicity to evaluate the potential of MTs as mechanism-based drugs for AD and related diseases. The initial assessment described here suggests that CLR01 is an efficacious and safe drug lead.

3.3 Materials and Methods

Molecular Tweezers:

CLR01 and CLR03 were prepared and purified as described previously [16].

Protein and sample preparation:

The 42-residue isoform of Aβ (Aβ42) was obtained from the University of California-Los Angeles Biopolymers Laboratory or from AnaSpec (Fremont, CA). Sample preparation was performed as described previously [17]. Briefly, Aβ42 was disaggregated by treatment with 1,1,1,3,3,3-hexafluoroisopropanol (Sigma, St. Louis, MO) as described previously [18]. Dried peptide films were stored at –20°C until use. For dendritic spine experiments, 27 μg films were dissolved in 20 μl of 60 mM sodium hydroxide, sonicated for 1 min, and then diluted to 30 μM with 180 μl of neurobasal media. For electrophysiological experiments, 50 μg films were dissolved in 11 μl of dimethyl sulfoxide to reach a concentration of 1 mM and sonicated for 10 min. For basal synaptic transmission experiments, 2 μl of the solution was then diluted to 5 ml with culture media to reach a final concentration of 400 nM. For long-term potentiation (LTP)

experiments, 40 µl of Aβ42 from 100 µM stock solution was incubated for 12 h at 4 °C to promote protein oligomerization. This preparation was further diluted with artificial cerebrospinal fluid (CSF) in the absence or presence of CLR01 to reach the final Aβ42 concentration of 200 nM immediately prior to experiments.

Selection of Aβ42 concentrations for synaptotoxicity experiments:

For dendritic-spine experiments, Dr. Bitan and colleagues looked for relatively harsh conditions, which would induce robust spine retraction. Preliminary experiments using 10 µM Aβ42 led to substantial cell death that did not allow reliable quantitation of dendritic spine density, whereas 3 µM Aβ42 produced spine retraction and abundant varicosities without overt cell death enabling evaluation of the protective effect of CLR01.

Similarly, for electrophysiologic experiments, Dr. Bitan and colleagues tested Aβ concentrations in the nanomolar range based on data from our and other groups demonstrating that 200 nM Aβ42 produced inhibition of synaptic transmission and plasticity of sufficient magnitude for measuring a potential rescuing action of CLR01. In our experience, concentrations slightly lower than 200 nM produce impairment of the synaptic function that is too small and does not allow detecting statistically significant changes following CLR01 treatments. Moreover, several papers by Arancio and co-workers have shown that picomolar Aβ concentrations actually enhance LTP rather than inhibiting it [19-21].

Animals:

Surgical and all other procedures performed at University of California-Los Angeles were compliant with the National Research Council Guide for the Care and Use

of Laboratory Animals, approved by the University of California-Los Angeles Institutional Animal Care Use Committee, and performed with strict adherence to the guidelines set out in the National Institutes of Health *Guide for the Care and Use of Laboratory Animals* at the Greater Los Angeles Veterans Affairs Healthcare System. Experiments performed in the Catholic University of Rome complied with Italian Ministry of Health guidelines, with national laws (Legislative decree 116/1992) and with European Union guidelines on animal research (No. 86/609/EEC). At University of California-Los Angeles, pregnant embryonic day 18 Sprague–Dawley rats for primary neuronal culture experiments were purchased from Charles River Laboratory (Wilmington, MA) and triple-transgenic (3×Tg) mice were bred in-house. In the Catholic University of Rome, Wistar rats and C57Bl/6 mice were bred in-house. Animals were kept on a standard diet and 12 h light/dark cycle with food and water provided *ad libitum*.

Primary neuronal culture for dendritic spine morphology:

Hippocampal neurons were prepared as described previously [17] and plated on poly-D-K-coated (0.1 mg/ml) 13-mm round glass cover slips in 24-well culture plates at a density of 300,000 cells/well. Experiments were performed as described previously [17]. Briefly, rat primary hippocampal neurons were grown for 3 weeks. Half of the growth medium (1 ml) was removed and new media (600 µl), media containing 30 µM of freshly prepared Aβ42 (200 µl), and media containing 300 µM CLR01 or CLR03 (200 µl), were immediately added resulting in a final concentration of 3 µM Aβ42 and 30 µM CLR01 or CLR03. Following 72 h of incubation, neurons were fixed with 4% paraformaldehyde and stained with 1,1'-dioctadecyl-3,3,3',3'-tetramethylindocarbocyanine perchlorate (Invitrogen). The neurons were visualized using a confocal laser-scanning microscope

(Leica, Bannockburn, IL) at 2,000× magnification. The total number of spines/100 μm were counted using ImageJ [22]. At least 100 dendritic branches from 10-15 individual neurons were selected per experimental condition. All data for all experiments are shown as means ± standard error of the mean and the level of significance was set at $P < 0.05$. Statistical analysis was performed in Prism 5.0c (GraphPad, La Jolla, CA) using 1-way analysis of variance (ANOVA) with Tukey's *post hoc* multiple-comparison test.

Autaptic neuron culture preparation and synaptic transmission studies:

Basal synaptic transmission was studied in autaptic microcultures of hippocampal neurons using the patch-clamp technique in the whole-cell configuration, as described previously [23]. Rat cortical astrocytes were plated onto glass coverslips (coated with agarose and sprayed with a mixture of poly-D-K and collagen 3 days before plating) in Dulbecco's Modified Eagle Medium supplemented with 10% fetal bovine serum and antibiotics. After 4–6 days, half the medium volume was replaced with neurobasal medium consisting of 2% B27, 0.5% L-Q, and 1% penicillin-streptomycin-neomycin antibiotic mixture. One day later, hippocampal neurons from postnatal d 0–2 Wistar rat brains were suspended in neuronal medium and plated at 25,000 per cm^2 onto the glial microislands. Two weeks later, autapses had formed and were ready to be studied. Every 4 days, half the neuronal medium volume was replaced with fresh neuronal medium supplemented with 2 μM cytosine arabinoside. Patch-clamp currents were recorded using an Axopatch 200B amplifier (Molecular Devices), and the pCLAMP system (version 10, Molecular Devices) was used for data acquisition and analysis. Patch pipettes resistances were 3–4 MΩ when filled with intracellular solution consisting of (in mM): 136 KCl, 17.8 4-(2-hydroxyethyl)-1-piperazineethanesulfonic acid, 1 ethyleneglycol tetraacetic

acid, 0.6 $MgCl_2$, 4 ATP, 0.3 GTP, 12 creatine phosphate, and 50 U/ml phosphocreatine kinase. The extracellular solution contained (in mM): 140 NaCl; 2 KCl; 10 4-(2-hydroxyethyl)-1-piperazineethanesulfonic acid; 10 glucose; 4 $MgCl_2$; and 4 $CaCl_2$, pH 7.4. All experiments were performed at room temperature (23–25°C).

Briefly, neurons were voltage-clamped at a membrane potential (V_m) of -70 mV, and stimuli mimicking action potentials (2 ms at 0 mV) were delivered every 6 s to evoke excitatory postsynaptic currents (EPSCs). The amplitudes and frequency of miniature EPSCs (mEPSCs) were evaluated in 60-s recordings (V_m = -70 mV). The detection threshold of mEPSCs was set to 3.5-times the baseline standard deviation. These parameters were measured in cells exposed for 24 h to freshly prepared 200 nM Aβ42, 200 nM Aβ42 + 2 μM CLR01, or vehicle. Two μl of Aβ42 (from 1 mM stock solution in dimethyl sulfoxide) were mixed with 20 μl of CLR01 (from 1 mM stock solution in H_2O) and diluted up to 5 ml to the final concentrations of Aβ42 and CLR01 — 400 nM and 4 μM, respectively. Five ml of the media was removed and replaced with 5 ml of fresh media containing dimethyl sulfoxide vehicle, Aβ42 alone, or Aβ42 and CLR01.

Long-term potentiation recordings:

To study synaptic transmission, Dr. Bitan and colleagues measured the peak amplitudes of field excitatory postsynaptic potentials (fEPSPs) elicited by stimuli of increasing amplitudes, before and after slice exposure to artificial CSF containing either 200 nM freshly prepared Aβ42 or the same amount of dimethyl sulfoxide contained in the Aβ42 solutions (vehicle) in the absence or presence of 10-fold excess MTs, and plotted input/output curves. Coronal hippocampal slices (400-μm thick) were obtained from 8-weeks old male C57BL/6 mice according to standard procedures [23]. Brain

slices were cut using a vibratome (VT1000S, Leica Microsystems) and incubated in the cutting solution containing (in mM): 124 NaCl, 3.2 KCl, 1 NaH_2PO_4, 26 $NaHCO_3$, 2 $MgCl_2$, 1 $CaCl_2$, 10 glucose, 2 Na-pyruvate, and 0.6 ascorbic acid (pH 7.4, 95% O_2/5% CO_2) for at least 60 min at 30–32°C, and then stored in the same solution at room temperature until use.

Briefly, fEPSP evoked by Schaffer collateral stimulation were recorded from the *cornu ammonis* (CA)1 subfield of the hippocampus. During the electrophysiological recordings, slices were perfused with artificial CSF (in mM): 124 NaCl, 3.2 KCl, 1 NaH_2PO_4, 1 $MgCl_2$, 2 $CaCl_2$, 26 $NaHCO_3$, and 10 glucose (pH 7.4, 95% O_2/5% CO_2) maintained at 30–32°C by an in-line solution heater and temperature controller (TC-344B, Warner Instruments) in a submerged recording chamber. Data acquisition and stimulation protocols were performed with the Digidata 1440 Series interface and pClamp 10 software (Molecular Devices). The stimulation intensity that produced one-third of the maximal response was used for the test pulses, and the LTP-induction protocol consisted of four trains of 50 stimuli at 100 Hz repeated every 20 s hereto called the high frequency stimulation (HFS) paradigm. After 20–30 min of stable baseline responses to test stimulations delivered once every 20 s, LTP was induced with the HFS paradigm. Responses to test pulses then were recorded every 20 s for 60 min to measure LTP. The magnitude of LTP was measured 60 min after tetanus and expressed as a percentage of baseline fEPSP peak amplitude. Reported fEPSP amplitudes at 60 min are averages from recordings obtained during the last 5 min of post-tetanus recordings. The mean values observed during the last 10 min of pre-tetanus recordings were considered to represent the baseline at 100%. For experiments, 40 μl of Aβ42 from 100 μM stock

solution and 40 µl of CLR01 from 1 mM stock solution were mixed and either immediately diluted to a final volume of 20 ml, corresponding to final Aβ42 concentration 200 nM and final CLR01 concentration 2 µM, or were incubated for 1 h and then diluted. The diluted mixture then was immediately added to slices and incubated for 20 min followed by LTP induction with a standard HFS paradigm. Statistical analysis in all electrophysiologic experiments (Student's unpaired *t*-test) was performed with SYSTAT 10.2 (Statcom, Inc., Richmond, CA, USA).

Western blot analysis of Aβ42 species used in electrophysiologic experiments:

The assembly size of the Aβ42 species was analyzed in both denaturing and native conditions using Aβ42 preparations that were identical to those in the electrophysiologic experiments above.

The Aβ42 solutions for sodium dodecyl sulphate-polyacrylamide gel electrophoresis (SDS-PAGE) analysis were mixed with NuPAGE® LDS sample buffer 4× (at the final Aβ concentration of 200 nM) and separated on 10–20% gradient *Novex*® *Tricine* precast gels (Invitrogen) according to the manufacturer's protocol. Native PAGE was performed using 10–20% gradient Tris–glycine precast gels (Invitrogen). Native sample buffer 2× (Invitrogen) was added to the samples (at the final Aβ concentration of 200 nM) and samples then were electrophoresed in native buffer (Invitrogen) at 125 V. After electrophoresis under denaturing or non-denaturing conditions, the proteins were transferred to 0.2-µm nitrocellulose membranes (Amersham Biosciences, Buckinghamshire, UK). Membranes were blocked for 1 h, at room temperature, in a suspension of 5% non-fat milk in Tris-buffered saline containing 0.1% Tween-20 prior to incubation overnight at 4 °C with monoclonal antibody (mAb) 6E10 (Signet, Dedham,

MA, USA; 1:1000). Membranes were washed 3 times with Tris-buffered saline containing 0.1% Tween-20 and then incubated with horseradish peroxidase-conjugated anti-mouse secondary antibody (Cell Signaling; 1:2000) at room temperature for 1 h. Development was done after 5 min of incubation with enhanced chemiluminescence reagents (SuperSignal west Femto Pierce) and exposed to Hyperfilm (Amersham Biosciences). Molecular sizes for immunoblot analysis were determined using a ColorBurst^{TM} Electrophoresis Marker (Sigma-Aldrich) and Rainbow molecular weight markers (Amersham Biosciences). The bovine serum albumin was stained with Coomassie Blue (Sigma-Aldrich) to approximate the molecular weight in native conditions.

Blood-brain barrier experiments:

Three WT and three transgenic mice were anesthetized by intraperitoneal injection of ketamine and xylazine. Two μCi/g of ^{3}H-CLR01 as a 11.8 μg/g of ^{3}H-CLR01 + CLR01 mixture, where the ^{3}H-CLR01 made up 10% of the total CLR01, was injected into the jugular vein. Mice remained anesthetized for 1 h following injection at which point blood was collected via cardiac puncture, the mouse perfused thoroughly through the heart with phosphate buffered saline, and the brain collected. One hemisphere of the brain or 100-350 μl of blood were digested with 1 ml Solvable (Perkin Elmer, Waltham, MA), added to Ultima Gold Liquid Scintillation Cocktail (Perkin Elmer) and read in a Triathler Liquid Scintillation Counter (model 425-034; Hidex, Turku, Finland). Brain penetration percentage was calculated as activity per g of brain relative to activity per ml of blood. Statistical analysis (Student's unpaired *t*-test) was performed using Prism 5.0d (GraphPad).

Treatment of triple-transgenic mice with CLR01:

Fourteen to fifteen-m old, 3×Tg mice (n = 6–7) and WT control mice (n = 11–12) were anesthetized with 3% isoflurane gas (oxygen 2 L/min) and miniosmotic pumps (model 1004, Alzet, Cupertino, CA) were subcutaneously implanted on the dorsal back. The pumps contained CLR01 in sterile saline (40 μg/kg/day) or saline as vehicle. The 40 μg/kg/day dose was chosen based on limited knowledge, at the time this experiment was initiated, of the solubility and safety of CLR01. On day 28, mice were anesthetized with pentobarbital (100 mg/kg) and blood was collected by cardiac puncture. Mice were perfused with cold, non-fixative saline buffer containing protease and phosphatase inhibitors (Roche, Indianapolis, IN) as described previously [24].

Immunohistochemistry:

Analysis was performed according to previously published protocols [24,25]. Paraffin-embedded mouse brain regions from -2.97 to -3.08 bregma were deparaffinized and endogenous peroxidase activity was quenched with 0.3% hydrogen peroxide in methanol. The tissue was steamed for 60 min in 2% citrate-buffered antigen-unmasking solution (Vector Labs, Burlingame, CA). Sections were blocked with Tris-buffered saline containing 5% normal horse serum (Vector Labs), 3% bovine serum albumin, and 0.1% Tween-20 and antibodies were diluted in the same solution. Sections were incubated with mAb 6E10 (Covance, Princeton, NJ) diluted 1:1,000, anti-p-tau mAb AT8 (Thermo Scientific) for phosphorylated paired helical filaments diluted 1:45, anti-tau mAb HT7 (Thermo Scientific) for total tau diluted 1:1,000, anti-Iba1 polyclonal antibody for microglia (Wako, Richmond, VA) diluted 1:1,000, or anti-GFAP mAb for astrocytes (Sigma) diluted 1:5,000 at 37 ºC for 1 h and then overnight at 4 ºC. This was followed by

incubation with a secondary, biotinylated anti-mouse immunoglobulin-G (Vector Labs) diluted 1:1,200 for 6E10, AT8, HT7, and 1:3,000 for GFAP, or biotinylated anti-rabbit immunoglobulin-G diluted 1:1,000 for Iba1 in 1.5% normal horse serum with 3% bovine serum albumin in Tris-buffered saline with 0.1% Tween-20 for 1 h at 37 ºC. Slides then were incubated with an avidin:biotinylated enzyme complex (ABC Elite Vectastain kit, Vector Labs) using a peroxidase detection system for 80 min at 37 ºC as described previously [25]. Antigen was visualized using metal-enhanced 3,3′-diaminobenzidine tetrahydrochloride (Thermo Scientific). Immunohistochemistry for all treatment groups was performed simultaneously and analysis of slides was randomized. Adjacent slides treated similarly except in the absence of a primary antibody were evaluated as negative controls. Microscopic quantification utilized images analyzed with in-house-written macros for NIH-Image (http://rsb.info.nih.gov/nih-image) or ImageJ (http://rsbweb.nih.gov/ij/) to assess deposit size and number.

Linear mixed effects models were used to evaluate the treatment effect on the outcome of Aβ, and p-tau load. Specifically, treatment groups, litters, and brain areas were included as the fixed effects and the random intercept was included as the random effect to account for the correlation among multiple measurements from the same mice. In the models, different areas of the brain also were allowed to have different variance in the random effects. The estimated treatment effect was calculated for the total brain and each brain area. For analysis of total tau, microglia, and astrocytes, statistical analysis (Student's unpaired *t*-test) were performed using Prism 5.0d (GraphPad).

Mouse behavioral analysis:

General activity and exploratory behavior were assessed during a single 7-min session and quantified using an automated tracking system (EthoVision 3.0) as described previously [26]. Multiple locomotor-based endpoints, including velocity (cm/s), mobility (% time) and meander (deg/cm), were quantified. Habituation rates for each endpoint were quantified by calculating the percent change between the observed mean during the initial 90 sec interval and the final 90 sec interval. Statistical analysis for all endpoints was performed using 2-way (treatment, genotype) ANOVA.

Brain extraction and Western blot for amyloid β-protein precursor cleavage products:

Relevant brain regions (hippocampus, entorhinal and piriform cortices) were dissected out of one hemisphere of CLR01- or vehicle-treated 3×Tg mouse brains at euthanasia. Brain regions were sonicated in a volume of Tris-buffered saline (20 mM Tris-HCl, 150 mM NaCl, pH 7.4) 4–7 times the tissue weight, then pelleted at 157,000 *g* for 15 min at 4 °C. The supernate was saved as the soluble fraction. The pellet was homogenized in Tris-buffered saline with 1% Triton X-100 and pelleted again. That supernate was saved as the detergent-soluble fraction. Both fractions were subjected to a BCA protein assay (Thermo Fisher Scientific, Rockford, IL) following the manufacturer's protocol. The soluble fraction was fractionated on 10% Tris-Tricine SDS-PAGE gels and subjected to Western blot using mAb 22C11 (Millipore, Billerica, MA), which recognizes the N-terminal region of amyloid β-protein precursor (APP), at 1:1000 dilution. The detergent-soluble fraction was fractionated on 10–20% gradient Tris-Tricine gels (Invitrogen) and subjected to Western blot analysis probed with polyclonal antibody APP369 [27], specific for the C-terminal region of APP at 1:1000 dilution. All blots were

stripped and re-probed with an anti-β-actin polyclonal antibody (AbFrontier, South Korea) at 1:2,000 dilution as a loading control. Blots were visualized using enhanced chemiluminescence (GE Healthcare, Pittsburgh, PA) and bands quantified densitometrically using ImageJ. Statistical analysis (2-way ANOVA for treatment and genotype) was performed using Prism 5.0d (GraphPad).

CLR01 stability and cytochrome P450 inhibition:

In vitro evaluation of CLR01's stability in plasma and liver microsomes, and inhibition of cytochrome P450 (CYP450) was performed by Wolfe Laboratories, Inc. (Watertown, MA). The experimental details are proprietary and therefore only a brief description of each experiment is given. For stability measurements, CLR01 was incubated with mouse or human plasma or liver microsomes and a nicotinamide adenine dinucleotide phosphate-regenerating system. Testing was conducted at 15 min intervals up to 60 min. Following protein precipitation by an organic solvent, samples were analyzed by high-performance liquid chromatography-mass spectrometry to determine overall stability and half-life of clearance. Testosterone was used as a positive control. For CYP450 inhibition, CLR01 was prepared at eight concentrations ranging from 0–25 μM with each of the following individual human recombinant CYP450 isoforms (1A2, 2C9, 2C19, 2D6, and 3A4) and the appropriate CYP450 substrate. Aliquots of the test samples were extracted using an organic solvent and analyzed by high-performance liquid chromatography-mass spectrometry to determine the CYP450 half-maximal inhibition concentration values.

Cytochrome P450 induction by pregnane X receptor reporter gene assay:

African green monkey kidney cells were plated in 96-well plates at a density of 7,000 cells per well in Dulbecco's modified Eagle's medium (Invitrogen) with 10% fetal bovine serum (Fisher Scientific) containing penicillin and streptomycin. Twenty-four h post-plating, cells were transfected with the appropriate plasmids using Lipofectamine 2000 (Invitrogen) according to the manufacturer's instructions. The total DNA per well was 115 ng and contained a mixture of each of the following plasmids: pSV40-β-galactosidase (40 ng), XREM-Luc (20 ng), pSG5-hPXR (5 ng), and pBluescript (50 ng). Luciferase activity was determined using a standard luciferase assay system (Promega). The β-galactosidase activity was determined using standard methods by the *O*-nitrophenolgalactoside assay and was read at 420 nm. Cells were treated with 10 mM rifampicin (Sigma) or CLR01 for 24 h. Data are normalized to β-galactosidase activity ($n = 8$).

3.4 Results

3.4.1 CLR01 rescues neurons from amyloid β-protein-induced retraction of dendritic spines.

The strongest anatomical correlate for the degree of cognitive impairment in AD is synapse loss [28,29]. Post-mortem ultrastructural stereological analysis of the hippocampal CA1 regions of brains of patients with mild cognitive impairment showed 18% synapse loss that progressed to 55% in mild AD [30]. In primary neuronal cultures, oligomers of Aβ42 have been shown to cause substantial decrease in dendritic spine density [31]. Additionally, Aβ toxicity has been shown to lead to neuritic abnormalities and axonal varicosities in AD mouse models [32,33].

To assess the effect of MTs on Aβ42-induced synapse loss, Dr. Bitan and colleagues treated primary hippocampal neurons with 3 μM Aβ42 for 72 h in the presence or absence of 10-fold excess of CLR01 or a negative control derivative, CLR03 [13], and quantified spine density. Aβ42 induced abundant varicosities (yellow arrows, Figure 3.1A) and caused a decline in the number of dendritic spines to 20.9 ± 1.3% of baseline (Figure 3.1B). In the presence of CLR01, spine density was rescued to 79.6 ± 2.3% of baseline ($P < 0.001$ compared to Aβ42 alone) and varicosities were reduced, whereas CLR03 was inactive (22.5 ± 1.2% of baseline). In these and further experiments addressing synaptotoxicity, Dr. Bitan and colleagues adjusted the Aβ42 concentration empirically to elicit a sufficiently robust toxic response allowing measurement of inhibition by MTs.

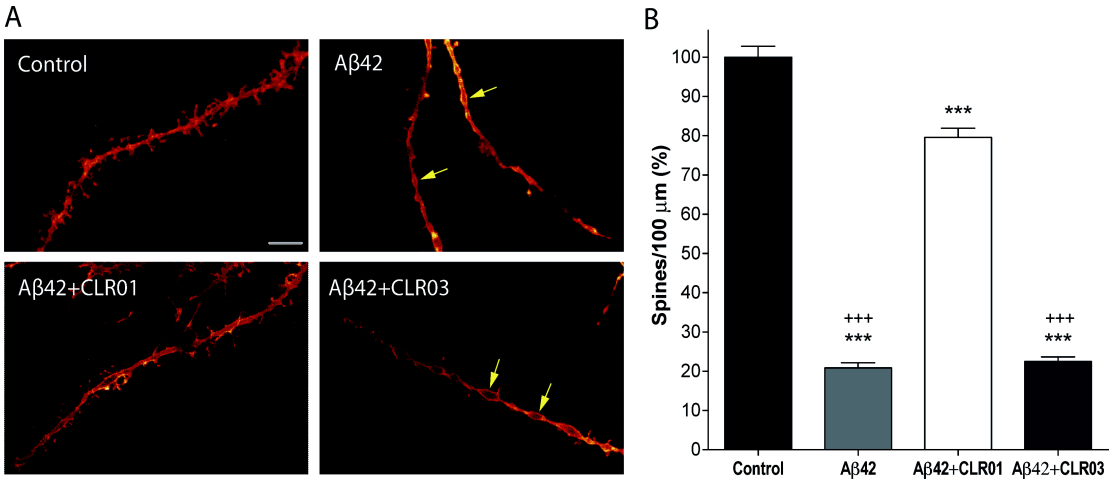

Figure 3.1 CLR01 protects neurons from Aβ-induced changes in dendritic spine number and morphology
A) Rat primary hippocampal neurons were incubated for 72 h with media alone or with Aβ42 in the absence or presence of MTs. Yellow arrows point to Aβ42-induced varicosities. The scale bar denotes 5 μm. B) The number of dendritic spines per 100 μm was quantified. ***$P < 0.001$ compared to control; $^{+++}P < 0.001$ compared to Aβ42 + CLR01.

3.4.2 CLR01 prevents disruption of basal synaptic transmission.

Changes in gene expression and synaptic vesicle trafficking in the brains of

patients with AD and transgenic mice suggest that synaptic function is compromised prior to the physical degeneration of the synapses [34,35]. Electrophysiologic experiments allow measurement of the earliest neuronal insults by Aβ. Previous reports have documented changes in basal excitatory synaptic neurotransmission due to Aβ42 deposition ([36] and references therein). In a set of experiments designed to test the capability of CLR01 to rescue Aβ42-induced inhibition of basal synaptic transmission in autaptic microcultures of hippocampal neurons, Dr. Bitan and colleagues measured the amplitudes of EPSC, evoked by stimuli mimicking action potentials, in hippocampal neurons exposed for 24 h to 200 nM Aβ42 in the absence or presence of 2 μM CLR01. Culture

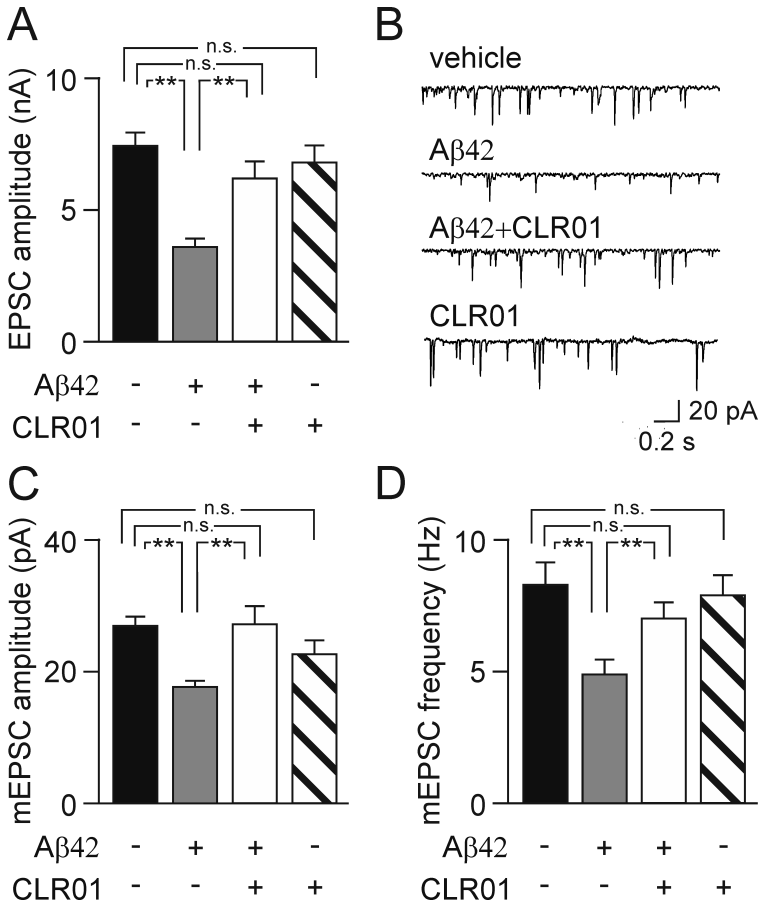

Figure 3.2 CLR01 rescues Aβ42-induced inhibition of evoked and spontaneous synaptic neurotransmission in autaptic hippocampal neurons
A) Mean EPSC amplitude measured after 24 h of treatment with vehicle, 200 nM Aβ42, 200 nM Aβ42 + 2 μM CLR01 or 2 μM CLR01. B) Representative traces showing mEPSCs recorded in neurons subjected to each treatment. C, D) Mean mEPSC amplitude (C) and frequency (D) following 24-h treatment with vehicle, 200 nM Aβ42, 200 nM Aβ42 + 2 μM CLR01 or 2 μM CLR01. **P < 0.001.

treatment with Aβ42 alone produced a 51.8% reduction of mean EPSC amplitude [3.6 ± 0.3 nA (n = 38) vs. 7.4 ± 0.5 nA in controls (n = 25), $P < 0.001$, Figure 3.2A]. In contrast, in autaptic hippocampal neurons exposed to Aβ42 in the presence of CLR01 (or with CLR01 alone), EPSC amplitudes were not significantly different from controls [6.2 ± 0.6 nA (n = 18); 6.8 ± 0.7 nA (n = 18), respectively].

Application of Aβ42 to hippocampal CA1 pyramidal neurons has been reported to reduce 2-amino-3-(5-methyl-3-oxo-1,2-oxazol-4-yl)propanoic acid (AMPA) receptor-mediated spontaneous, mEPSC amplitude and frequency by 60% and 45%, respectively [37]. mEPSC frequency is thought to be a reflection of presynaptic glutamate release, whereas the amplitude reflects the postsynaptic AMPA receptor response to glutamate [37].

Spontaneous neurotransmitter release was studied by recording mEPSC (Figure 3.2B) under the same experimental conditions as described above. Dr. Bitan and colleagues found that Aβ42 treatment reduced mEPSC amplitude by 34.5% (17.6 ± 1.0 pA [n = 38] vs. 26.9 ± 1.6 pA in controls [n = 25], $P < 0.001$, Figure 3.2C) and mEPSC frequency by 41.6% (4.9 ± 0.5 Hz, [n = 38] vs. 8.4 ± 0.8 Hz in control [n = 25], $P < 0.005$; Figure 3.2D). In neurons treated with Aβ42 in the presence of CLR01, both parameters were not significantly different from controls [mEPSC amplitude: 27.2 ± 2.7 pA; mEPSC frequency: 7.1 ± 0.6 Hz, (n = 18)]. Application of CLR01 alone did not significantly affect either the frequency (7.9 ± 0.8 Hz; n = 18) or the amplitude (22.5 ± 2.1 pA; n = 18) of mEPSC.

3.4.3 CLR01 protects synaptic plasticity against Aβ42-induced insults.

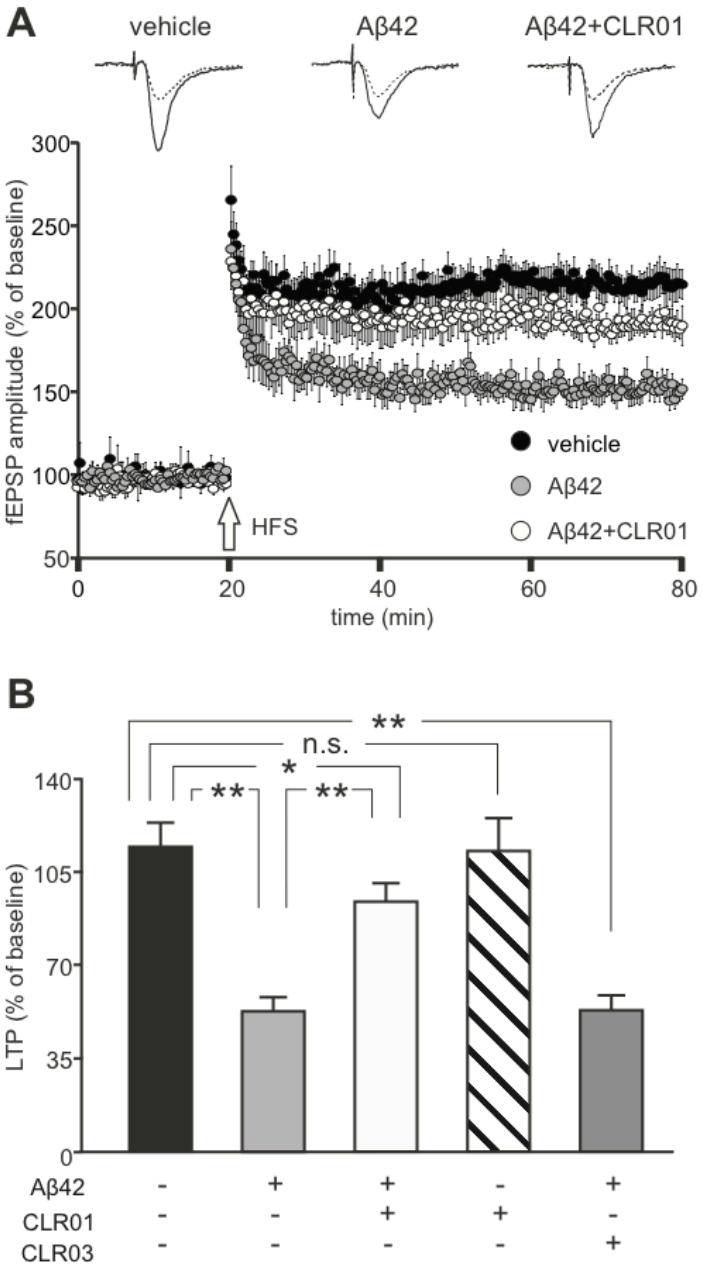

Signalling through AMPA and *N*-methyl-D aspartate receptors is critical for long-term potentiation (LTP), a cellular correlate for learning and memory that is expressed as an increase in efficiency of synaptic transmission [38]. Inhibition of LTP, manifested as a decrease in fEPSP amplitudes and slopes, has been observed upon application of different Aβ oligomers to rat hippocampal slices [19,39].

To further evaluate the protective effect of CLR01 on Aβ42-induced synaptotoxicity, Dr. Bitan and colleagues studied

Figure 3.3 CLR01 attenuates Aβ42-induced inhibition of long-term potentiation at CA3–CA1 synapses

A) Time course of fEPSP amplitudes before and after HFS (indicated by arrow) in slices treated for 20 min with vehicle (black circles), 200 nM Aβ42 (grey circles), or 200 nM Aβ42 + 2 μM CLR01 pre-incubated for 1 h prior to application (white circles). Results are expressed as percentages of baseline fEPSP amplitude (=100%). Insets show representative traces of fEPSP at baseline (dotted lines) and during the last 5 min of LTP recording (solid lines). B) Bar graph showing mean LTP changes measured during the last 5 min of recording following slice exposure to vehicle or different combinations of 200 nM Aβ42, 2 μM CLR01 and 2 μM CLR03. **P < 0.001; *P < 0.05.

LTP at the Schaffer collateral–CA1 synapses in hippocampal brain slices. The Aβ concentration selected, 200 nM, did not influence basal synaptic transmission in brain slices, thus avoiding potentially producing confounding effects on LTP, as documented by the stability of pre-tetanus fEPSP recordings and the absence of significant differences between the pre- and post-Aβ application input/output curves. Higher Aβ concentrations (e.g., 500 nM) did inhibit basal synaptic transmission in brain slices (data not shown). Under control conditions, i.e., when hippocampal slices were perfused with vehicle alone for 20 min before HFS, the fEPSP amplitude recorded 60 min post HFS displayed increases of +115.0 ± 8.8% over baseline (n = 11). In hippocampal brain slices perfused with 200 nM Aβ42 for the 20 min preceding HFS, the LTP was significantly smaller at +53.7 ± 5.1% over baseline (n = 10, $P < 0.001$, Figure 3.3A). Co-application of 200 nM Aβ42 and 2 μM CLR01 significantly ameliorated LTP inhibition relative to Aβ42 alone [fEPSP amplitude increases of +75.4% ± 7.7% (n = 8), $P < 0.05$, not shown in graph]. Though this rescuing effect was statistically significant, its magnitude was small relative to the protective effects of CLR01 in cell culture (Figures 3.1–3.2). A potential explanation is differences in diffusion to the cellular targets between Aβ42 oligomers and CLR01, which may diminish the effectiveness of CLR01 in brain slices relative to cultured neurons. To test this hypothesis, Dr. Bitan and colleagues examined whether a 1-h incubation of Aβ42 with CLR01 prior to application to hippocampal slices would produce stronger protection. Indeed, 1-h pre-incubation of Aβ42 with CLR01 provided a stronger protective effect, raising the fEPSP amplitude potentiation to +94.2% ± 7.4% over baseline (n = 12, $P < 0.001$ vs. Aβ42 alone, and $P < 0.05$ vs. controls; Figure 3.3A, B).

Control LTP experiments were performed in brain slices exposed to 2 μM CLR01 alone or 200 nM Aβ42 in the presence of 2 μM CLR03. Application of CLR01 alone did not significantly affect LTP (fEPSP amplitude potentiation of +113.2 ± 11.7% over baseline; $n = 6$) whereas Aβ42 + CLR03 caused LTP inhibitions not significantly different from those produced by Aβ42 alone (+53.6 ± 5.9%; $n = 8$; $P < 0.001$ vs. controls, Figure 3.3B).

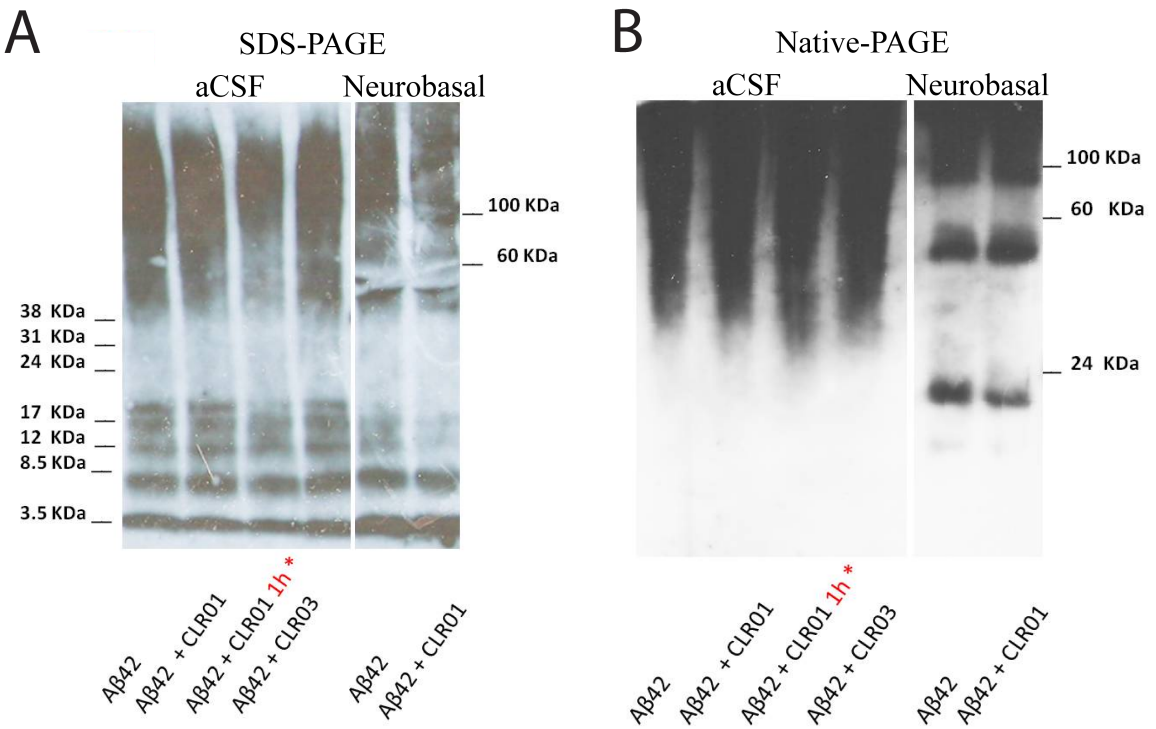

* 1 h pre-incubation of Aβ42 with CLR01

Figure 3.4 Assembly size distribution pattern of Aβ42 preparations in the absence or presence of MTs
Preparations of Aβ42 alone, Aβ42 + CLR01, Aβ42 + CLR01 incubated for 1 h or Aβ42 + CLR03 in artificial CSF or neurobasal media were fractionated using SDS-PAGE (A) or native-PAGE (B) and then analyzed by Western blot using mAb 6E10. CLR01 caused minor changes in the assembly size distributions, generally characterized by moderately decreasing the abundance of mid-size oligomers and increasing the abundance of larger assemblies.

Analysis of the Aβ42 assembly size distribution in the neurobasal media or artificial CSF preparations used in the electrophysiology experiments described above by native- or SDS-PAGE Western blots showed a mixture of species ranging from monomer to large oligomers. Little difference was observed between distributions of species in the absence or presence of MTs (Figure 3.4).

3.4.4 CLR01 is pharmacologically stable and penetrates the brain at similar levels in wild-type and transgenic mice.

Towards evaluating the potential of MTs for drug development, Dr. Bitan and colleagues studied the stability of CLR01 in plasma and liver microsomes. Biotransformation of CLR01 was measured during 60 min incubation in human or mouse plasma or liver microsome preparations, an abundant source of drug metabolizing enzymes [40,41]. In comparison with testosterone, which was used as a positive control and was degraded down to 29% in human, and 1% in mouse liver microsomes, no degradation of CLR01 was observed in these preparations. Similarly, CLR01 was found to be 100% stable in human and mouse plasma for 60 min at 37ºC. It is possible that because of the minimal degradation, lower doses may be required for treatment.

The blood-brain barrier (BBB) is suggested to be compromised in humans with AD [42,43] and in transgenic animal models of Alzheimer's [44]. Thus, I analyzed brain permeability of CLR01 both in 3×Tg [45], and in healthy, WT mice to assess how much of the penetration is due to the disruption of the BBB seen with disease and how much may be due to other mechanisms, such as transporters. Tritium-labeled CLR01 (^{3}H-CLR01) was administered intravenously to 12-m old, WT or 3×Tg mice. One-h post

injection, blood was collected, mice were perfused to remove blood from the brain vasculature, euthanized, and the brains were collected. Brain penetration percentage was calculated as activity per g of brain relative to activity per ml of blood. There was a small, non-significant difference in brain penetration of CLR01 between WT (1.74 ± 0.35%) and 3×Tg mice (1.98 ± 0.11%). There was no difference in percent of injected CLR01 found in the blood one-h post injection between WT and transgenic mice, 15.5 ± 1.3% and 15.7 ± 3.5%, respectively.

3.4.5 CLR01 reduces brain Aβ and tau burden and ameliorates microgliosis in transgenic mice without apparent toxicity.

In light of the promising *in vitro* data, I next conducted an initial *in vivo* study to assess the efficacy of peripherally administered CLR01 in transgenic mice using immunohistochemical changes of Aβ and p-tau burden, and brain inflammation as endpoints. Similarly to the BBB experiments described above, in these experiments, I used the 3×Tg mouse model of AD, which overexpresses mutant forms of the human genes encoding presenilin 1 (mutation M146V) and APP (mutation KM670/671NL), each of which causes early-onset familial AD, and tau (mutation P301L), which causes frontotemporal dementia. These mice model particularly relevant pathologic features of AD by encompassing both amyloid plaques and neurofibrillary tangles [45].

Mixed-gender, 14–15-m old mice, n = 6–7 per group, were treated for 28 days with 40 μg/kg/day CLR01 in saline as a vehicle, or with vehicle alone, administered subcutaneously using osmotic minipumps. Following treatment, the mice were sacrificed and their brains were analyzed by immunohistochemistry for the presence of plaques, tangles, and inflammatory markers. Analysis of brain sections from vehicle-treated mice

using mAb 6E10 showed amyloid plaques deposited predominantly in the subiculum and CA1 regions of the hippocampus (Figure 3.5A), as reported previously [45]. In addition, the mice showed phosphorylated paired helical filaments detected by the anti-p-tau mAb AT8, predominantly in the hippocampal regions CA1 and CA3 (Figure 3.5D). Mice

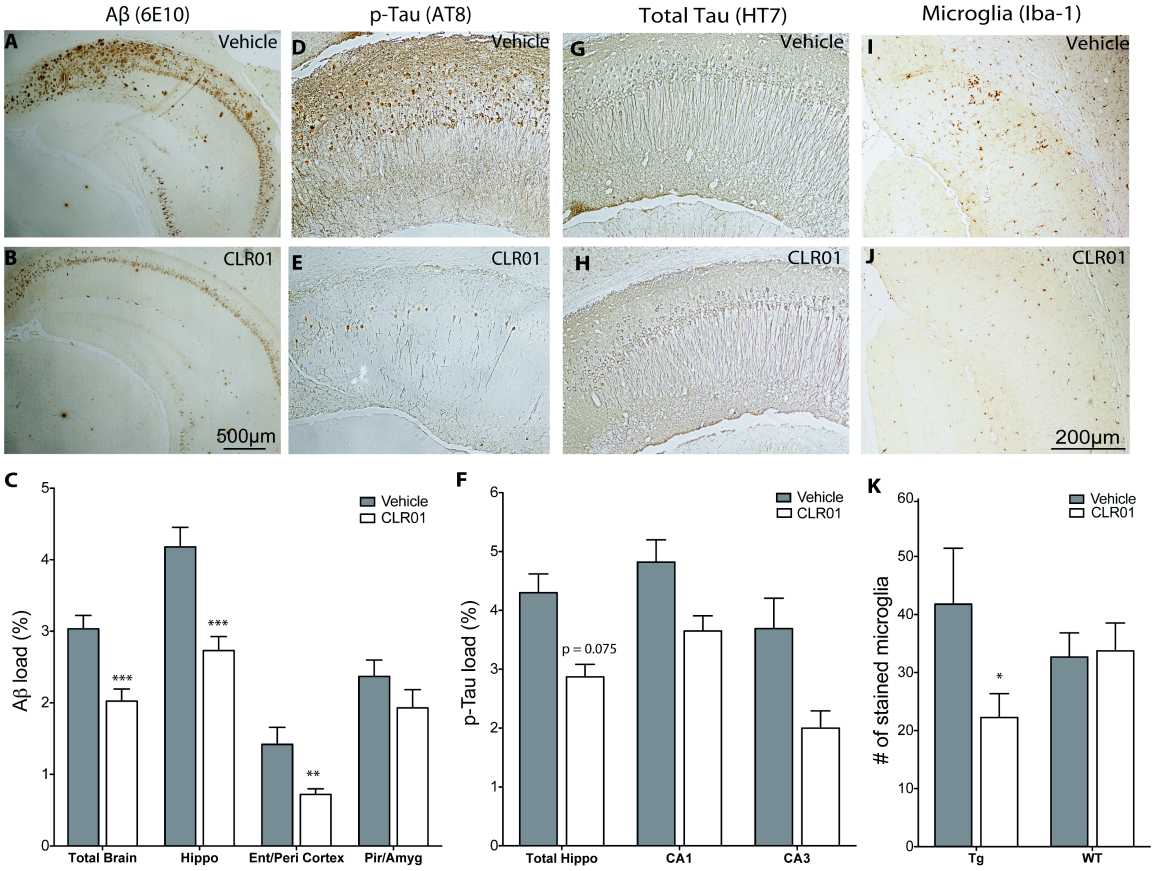

Figure 3.5 CLR01 decreases Aβ and p-tau deposition and ameliorates microgliosis in transgenic mouse brain

Triple-transgenic mice were treated with 40 μg/kg/day CLR01 or vehicle. A, D, G, I) Vehicle-treated transgenic mouse hippocampus. B, E, H, J) CLR01-treated transgenic mouse hippocampus. A, B) transgenic mouse brain stained with mAb 6E10 showing amyloid plaque deposition. C) % Aβ burden was quantified by calculating the total 6E10-stained area divided by the total area measured (Hippo – hippocampus, Ent – entorhinal, Peri – perirhinal, Pir – piriform cortices, Amyg – amygdala). D, E) transgenic mouse brain showing AT8-positive neurofibrillary tangles in the CA1 region. F) % Aggregated p-tau load was quantified by calculating the total AT8-stained area divided by the total area. G, H) transgenic mouse brain stained with mAb HT7 for total tau. I, J) transgenic mouse brain showing Iba1-positive microglia in the subiculum and CA1 region. K) Number of stained microglia in a 1.14 mm^2 area of hippocampus per treatment condition. The scale bar in panel B applies to both panels A and B. The scale bar in panel J applies to panels D–J. *$P < 0.05$, **$P < 0.01$, ***$P < 0.001$ compared to vehicle-treated mice.

treated with CLR01 showed a significant decrease in Aβ burden of 33.3% in the total brain area analyzed (% burden: vehicle-treated 3.03 ± 0.19% vs. CLR01-treated 2.02 ± 0.17%, $P < 0.01$, Figure 3.5B, C), 34.7% in the hippocampus (vehicle-treated 4.18 ± 0.27% vs. CLR01-treated 2.73 ± 0.20%, $P < 0.05$), 49.3% in the perirhinal and entorhinal cortices (vehicle-treated 1.42 ± 0.24% vs. CLR01-treated 0.72 ± 0.08%, $P < 0.05$), and 18.6% in the piriform cortex and amygdala (vehicle-treated 2.37 ± 0.23% vs. CLR01-treated 1.93 ± 0.25%). Similarly, a 33.3% reduction in AT8-positive p-tau was observed in the total brain area analyzed (% burden: vehicle-treated 4.30 ± 0.32% vs. CLR01-treated 2.87 ± 0.21%, $P = 0.075$; Figure 3.5E, F), 24.3% reduction in CA1 (vehicle-treated 4.82 ± 0.38% vs. CLR01-treated 3.65 ± 0.26%), and a 45.8% reduction in CA3 (vehicle-treated 3.69 ± 0.52% vs. CLR01-treated 2.00 ± 0.29%) regions in mice treated with CLR01. These data were not statistically significant but a major trend was observed. In contrast, immunohistochemistry with the anti-tau mAb HT7 showed no effect on total tau (Figure 3.5G, H).

Compared to vehicle-treated 3×Tg mice (Figure 3.5I), the CLR01-treated 3×Tg mice showed a 46.2% reduction in the number of microglia per hippocampal area (vehicle-treated 41.79 ± 9.64 vs. CLR01-treated 22.5 ± 4.12, $P < 0.05$; Figure 3.5J, K) and in the microglial stained area (data not shown). Similarly, a 43.9% reduction in microglial stained area was found in the cortex of CLR01-treated mice relative to vehicle-treated mice (data not shown). In comparison, there was essentially no difference between vehicle- and CLR01-treated WT mice in the level of microgliosis (vehicle-treated 32.67 ± 4.16 vs. CLR01-treated 33.73 ± 4.81, Figure 3.5K). In contrast to the effect on microglia, CLR01 treatment had little or no impact on the number or staining

level of astrocytes in transgenic or WT mice in either the hippocampus or cortex (data not shown).

As has been described previously [46], I found that the 3×Tg females in our study had more Aβ pathology than the males. The vehicle-treated females (n = 3) had 204% the Aβ load of the males (n = 3) in the hippocampus, 394% in the entorhinal/perirhinal cortices, and 205% in the piriform cortex/amygdala region. A similar trend was observed with the CLR01-treated mice (n = 4 females, 3 males): 138% in the hippocampus, 164% in the entorhinal/perirhinal cortices, and 308% in the piriform cortex/amygdala region. Correspondingly the effect of CLR01 treatment was substantially more pronounced in females than in males. Female mice showed a decrease of 45% in Aβ load in the hippocampus whereas males had a decrease of 19%. A similar trend was observed in the entorhinal/perirhinal cortices, 64% decrease in females and 15% decrease in males, whereas in the piriform cortex/amygdala region, the trend was reversed — 17% decrease in females and a 45% decrease in males. Consistent with the previous study [46], the p-tau load did not differ significantly between male and female 3×Tg vehicle-treated mice and CLR01 treatment affected p-tau load to the same extent in both genders.

Table 3.1 No toxic effect of CLR01 on weight change (% of pre-surgery baseline)

Genotype	Treatment	Day 0	Day 8	Day 23	Day 28
Wild-type	Vehicle	100.0 ± 0.0	96.7 ± .01	97.8 ± .01	96.2 ± .01
	CLR01	100.0 ± 0.0	95.6 ± .05	96.2 ± .01	95.8 ± .01
3×Tg	Vehicle	100.0 ± 0.0	95.6 ± .02	97.4 ± .01	97.6 ± .02
	CLR01	100.0 ± 0.0	95.9 ± .02	100.4 ± .02	97.8 ± .03

Because CLR01 may bind to K residues in proteins other than Aβ and tau and

affect their activity, I used several criteria, including appetite loss, weight loss (Table 3.1), lethargy, and mortality, to explore whether CLR01 treatment had adverse effects on the 3×Tg mice. I did not observe any adverse effects, though the number of mice and indices measured were limited and thus may influence the sensitivity of this analysis. To assess potential interactions between CLR01 treatment and general behavioral measures, mouse activity was analyzed during a single 7-min monitoring period. I did not observe any significant changes in velocity, path shape, or mobility between the CLR01-treated and the vehicle-treated transgenic or WT mice (Table 3.2). Similarly, no effects were observed on habituation rates in any of these measures (Table 3.2). As hyperactivity and other perturbations of locomotor activity, as well as disruptions of habituation, commonly have been observed following central nervous system toxicity [47,48], the lack of such

Table 3.2 No toxicity of CLR01 by behavioral end points

Geno type	**Treat-ment**	**Velocity (cm/s)**	**Velocity Habitu-ation (% change)**	**Mobility (% time)**	**Mobility Habitu-ation (% change)**	**Meander (deg/cm)**	**Meander Habitu-ation (% change)**
Wild-type	Vehicle	4.6 ± 0.6	-24 ± 7	63 ± 6	-33 ± 13	425 ± 39	40 ± 10
	CLR01	5 ± 1	-15 ± 16	65 ± 5	-50 ± 31	418 ± 34	48 ± 20
3×Tg	Vehicle	5.5 ± 0.7	-24 ± 8	71 ± 4	-25 ± 11	377 ± 32	49 ± 15
	CLR01	5.6 ± 0.7	-9 ± 7	75 ± 4	-8 ± 6	358 ± 30	21 ± 8
P-value (2-way ANOVA)	Treat-ment effect	0.62	0.23	0.58	0.99	0.71	0.49
	Geno-type effect	0.43	0.77	0.083	0.19	0.12	0.52
	Inter-action effect	0.78	0.80	0.82	0.35	0.85	0.21

behavioral effects suggests that the 28-day CLR01 regimen did not adversely impact the neural systems subserving these traits.

To address further potential concerns regarding toxicity due to the unique mechanism of CLR01, I studied the effect of CLR01 in several *in vitro* and *in vivo* systems. Previously, CLR01 showed no toxicity below 400 μM in cell lines and in primary neurons [13,14], a concentration that is 1–3 orders of magnitude higher than needed for inhibition of toxicity in cell culture. Zebrafish treated with CLR01 up to 10 μM dissolved in the water in which the fish developed showed no signs of toxicity [15]. In mouse brain slices treated with 2 μM CLR01 alone, no changes were seen in levels of LTP (Fig. 3.3B). I also did not find adverse effects by weight, activity, or mortality in mice treated subcutaneously with CLR01 doses from 40 μg/kg/day (Tables 3.1, 3.2) up to 1,200 μg/kg/day (data not shown) or in mice treated intracerebroventricularly with 10 μM CLR01 (data not shown), suggesting the existence of sufficient therapeutic window for CLR01. I assessed the effect of CLR01 on APP processing. In the APP sequence, K residues exist directly N-terminal to the α-secretase cleavage site and two residues N-terminal to the β-secretase cleavage site (in the 3×Tg mice used here, the K-M dipeptide as positions 670 and 671 is replaced by N-L). Additionally, several K residues are a few amino acids C-terminal to the γ-secretase cleavage site. Brain extracts from WT and transgenic mice treated with either vehicle or CLR01 were analyzed by Western blots using antibodies specific for the soluble N-terminal portion of APP (sAPP), or for the C-terminal fragments (CTFs) of APP. I found no differences in concentration levels of sAPP, CTF-α, or CTF-β between vehicle- and CLR01-treated mice (Figure 3.6), supporting CLR01's putative process-specific mechanism of action.

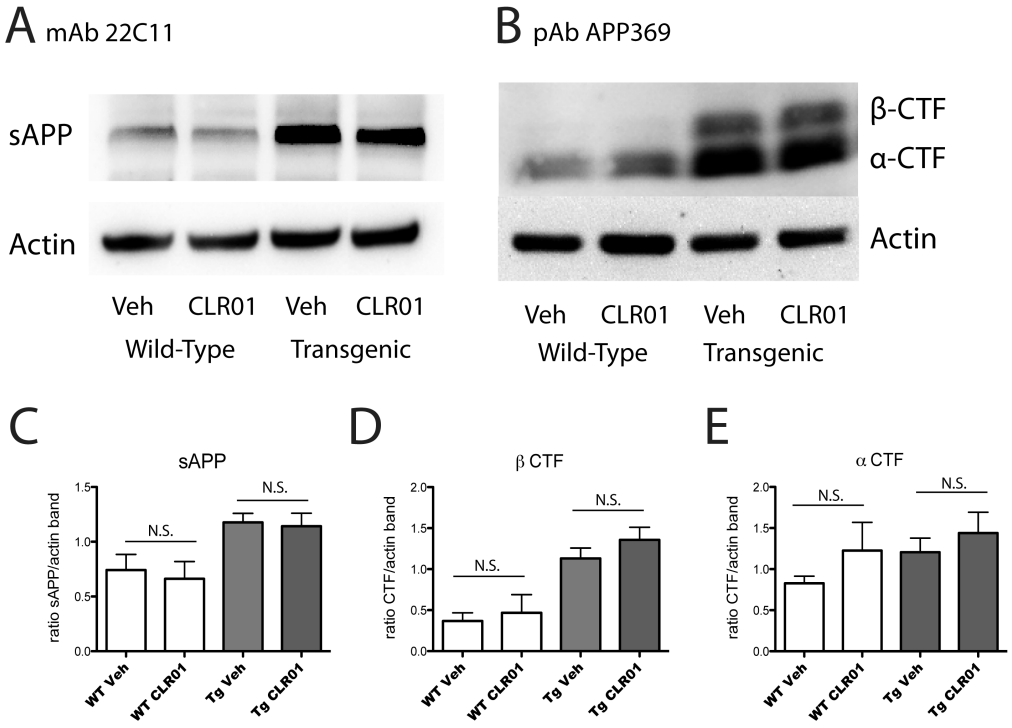

Figure 3.6 No difference in levels of sAPP, CTF-α, or CTF-β with CLR01 treatment
Soluble and detergent-soluble fractions of brain extracts from vehicle- or CLR01-treated WT or transgenic mice were subjected to Western blot analysis. A) N-terminal APP antibody 22C11 used to assess levels of sAPP. B) C-terminal APP antibody APP369 used to assess levels of CTF-α and CTF-β. Densitometric analysis of Western blots for C) sAPP; D) CTF-β; and E) CTF-α was calculated after normalizing to the actin loading control. WT Veh n = 4, WT CLR01 n = 4, Tg Veh n = 12, Tg CLR01 n = 10.

3.4.6 CLR01 interacts weakly with major cytochrome P450 isoforms.

The CYP450 family of enzymes catalyzes the oxidation of a vast array of endobiotic and xenobiotic molecules to increase their hydrophilicity during phase-I metabolism, accounting for ~75% of the total number of metabolic reactions in the body [49,50]. Thus, inhibition or activation of CYP450 enzymes may cause metabolic toxicity. In addition, drug–drug interactions are an important consideration in development of new therapeutics and are highly related to the CYP450 system. Induction or inhibition of

particular CYP450 isozymes by one drug or food product may affect the rate of metabolism of other substrates (i.e., drugs) of these isozymes. Thus, it is important to evaluate the interaction of MTs with CYP450 if they are to become drug candidates.

Measurement of the inhibitory potency of CLR01 on five major CYP450 isoforms responsible for 95% of drug metabolism [50] yielded the following half-maximal inhibition concentration values, listed in order from the most potently inhibited enzyme to the least: 2C19 (1.5 μM) > 3A4 (1.7 μM) > 2C9 (2.2 μM) > 2D6 (3.6 μM) > 1A2 (>20 μM). Inhibitory potency values less than 1 μM are expected to cause drug interactions of at least 2-fold, based on comparison of *in vivo* drug interaction data and primary experimental *in vitro* results for 44 drugs [40]. The half-maximal inhibition concentration values for the interaction of CLR01 with the CYP450 were above the 1-μM threshold for all the isoforms tested. The *in vitro* inhibition order is generally expected to line up with the *in vivo* magnitude of drug–drug interactions involving the substrates for the specific CYP450 isoforms [40].

Dr. Bitan and colleagues also evaluated induction of the CYP450 system using the pregnane X receptor (PXR) reporter gene assay [51]. PXR is a nuclear receptor and transcription factor for genes that are highly involved in xenobiotic and endobiotic uptake, metabolism and elimination. It is a key activator of the xenobiotic-inducible CYP3A, CYP2B, CYP2C, and glutathione S-transferase gene expression. Importantly, the PXR ligand-binding domain is uniquely large allowing the receptor to bind promiscuously to a large variety of structurally diverse molecules in different orientations [52], making it a robust target whose activation can be used to predict CYP450 induction and potential toxicity of new experimental drugs [53].

To evaluate PXR activation and potential toxicity of CLR01, African green monkey kidney fibroblasts were transfected with plasmids containing luciferase and β-galactosidase reporter genes under control of a PXR response element. Forty-eight h post-transfection, the cells were treated for 24 h with 10 μM rifampicin, an antibiotic and known PXR ligand, as a positive control, or with different concentrations of CLR01. At concentrations up to 1 μM, CLR01 exhibited luciferase activity similar to that of vehicle alone. At 10 and 50 μM, CLR01 induced a luciferase activity 56.4% and 39.5% the magnitude of rifampicin, respectively (Figure 3.7). Fifty μM of CLR01 reduced the β-galactosidase induction by 39.6%. These data demonstrate minimal PXR activation by low μM concentrations of CLR01 compared to a known ligand of PXR and a commonly used drug, rifampicin.

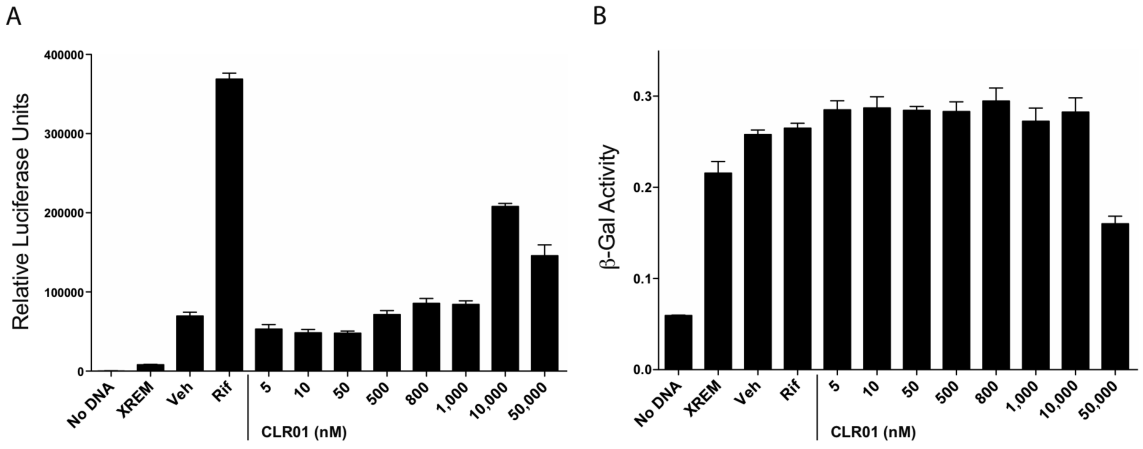

Figure 3.7 Weak induction of the CYP450 system by CLR01
Cells were treated with 10 μM rifampicin (rif; positive control) or CLR01 for 24 h. Cells transfected with luciferase but not PXR (XREM) were used as a negative control. A) Luciferase activity was determined using a standard luciferase assay system (Promega). B) β-galactosidase activity was determined using standard methods by the ONPG assay.

The highest plasma concentration found in pharmacokinetic experiments in which CLR01 was administered intravenously at 1 mg/kg (25-times the dose used for the

experiments shown in Figure 3.5), was under 11 μM at time zero [54], suggesting that toxicity is not anticipated at doses needed for the *in vivo* effects observed on aggregated Aβ, p-tau, and microgliosis.

3.5 Discussion

Recently, Dr. Bitan and colleagues have reported that CLR01 is a process-specific inhibitor of aberrant assembly and toxicity of amyloidogenic proteins [13]. The putative mechanism of action of MTs and the reason I refer to them as process-specific is their labile, moderate-affinity binding to solvent-exposed K residues, thereby disrupting a combination of hydrophobic and electrostatic interactions that are key to the aberrant self-assembly process. Dr. Bitan and colleagues previously showed that CLR01 inhibited the assembly and toxicity of multiple disease-associated proteins, disaggregated pre-formed Aβ fibrils and stabilized non-toxic assemblies [13]. Additionally, by a similar effect on α-synuclein, CLR01 prevented developmental deformities and death, and facilitated proteasomal clearance of α-synuclein, in a novel zebrafish model [15]. Following up on these promising efficacy data and minimal toxicity found for CLR01 in cell culture or in zebrafish, here I report its capability to protect synaptic structure, function, and plasticity against Aβ insults and to ameliorate brain pathology in AD transgenic mice.

Based on *in vitro* experiments using electron microscopy, dot blots with an oligomer-specific antibody, dynamic light scattering, and solution-state nuclear magnetic resonance [13], Dr. Bitan and colleagues expected that incubation of Aβ42 with CLR01 would lead to a rapid modulation of Aβ42 to a non-toxic state. Using electrophysiologic

readouts as functional correlates of the toxicity state, Dr. Bitan and colleagues found that CLR01 provided significant relief from Aβ42-induced toxic effects on basal synaptic activity and LTP, supporting our prediction. Additionally, comparison of co-application with pre-incubation of Aβ and CLR01 before addition to brain slices in LTP experiments showed that pre-incubation increased the protective effect without changing the distribution of Aβ species as analyzed by native- and SDS-PAGE Western blots (Figure 3.4). The lack of difference seen by the Western blot analysis compared to the positive difference seen in cell viability [13,14], dendritic spine (Figure 3.1), and electrophysiologic assays (Figures 3.2, 3.3) suggest that the changes in Aβ assembly induced by CLR01 are subtle or that CLR01 binding prevents contacts with the cellular targets of the toxic Aβ species. The increased protective effect following pre-incubation supports our previous findings of rapid disruption of Aβ42 self-association and its remodeling into non-toxic structures by CLR01 [13], which is common to a number of inhibitors [55]. One such inhibitor, *scyllo*-inositol was shown to inhibit LTP deficits caused by cell-secreted Aβ oligomers when pre-incubated with conditioned media containing these oligomers prior to application to slices [56], similar to CLR01, whereas, post-application of *scyllo*-inositol after incubation of cells with the conditioned media provided no protection against Aβ toxicity.

As a first step in characterizing CLR01 *in vivo*, I quantified the BBB permeability of CLR01 in both WT and transgenic mice. Though BBB disruption has been reported in AD and transgenic mouse models, I found genotype-independent, ~2% BBB permeability, 1 h post-injection, in both 12-m old WT and 3×Tg mice, consistent with a

previous study of the 3×Tg mice at 11-m of age [57]. At this age range, the mice display a moderate disease phenotype, which apparently does not affect BBB integrity.

Next, I assessed brain Aβ and p-tau load in a small group of transgenic mice treated continuously for 28 days and found a significant decrease in Aβ levels (Figure 3.5). Similar effects were observed on p-tau and microglia, though due to the small sample size, statistical significance was not reached in all cases. Based on CLR01's ability to disaggregate pre-formed fibrils *in vitro* [13], it is possible that a similar action disaggregated amyloid plaques in the brains of the treated mice into soluble, non-toxic structures amenable to clearance and/or degradation. Though additional experiments are needed to establish the mechanism by which CLR01 exerted its beneficial effects in the mice, the clearance hypothesis is supported by our recent *in vivo* study in zebrafish expressing human α-synuclein that were treated with CLR01 and showed recovery of proteasomal activity and increased α-synuclein clearance [15].

Consistent with Aβ-induced neuroinflammation [58], the reduction in Aβ load correlated with a decrease in microgliosis (Figure 3.5). Though activation of microglia plays a dual role in the brain — phagocytosing deposited Aβ [59,60] and releasing cytotoxic compounds, such as reactive oxygen and nitrogen species [61,62], reducing brain microgliosis typically is considered a beneficial treatment outcome in AD [58].

Though mechanisms of tau toxicity in AD are still under discussion, oligomerization and hyperphosphorylation, likely downstream of Aβ insults, are believed to be involved [63,64]. I found reduction in levels of p-tau (Figure 3.5), which could result from either direct disaggregation by CLR01, as was shown *in vitro* [13] and eventual clearance, be downstream of the significant decrease in Aβ aggregates, or reflect

both mechanisms. Answering the question will require additional exploration, yet the data suggest that MTs' process-specific mode of action is uniquely suitable to affect both the Aβ and tau components of AD pathology and therefore using these compounds is a promising intervention strategy.

Labile binding to K residues with micromolar affinity is a unique mode of action that potentially could disrupt normal protein function and cause side effects. However, the aberrant self-assembly process that leads to the formation of toxic Aβ and tau oligomers involves many weak intra- and intermolecular interactions [65]. Thus, the labile binding of MTs is predicted to be effective in preventing these weak interactions without substantially disrupting structurally stable proteins. In practice, solvent-exposed K residues are commonly used for covalent attachment of biotin, fluorescent dyes, or other tags without interfering with biological activity of stably folded proteins. It is therefore plausible that non-covalent binding of CLR01 to these proteins with high on-off rate does not affect their bioactivity. Supporting this proposed process-specific mechanism, I found no interference with APP processing (Figure 3.6) despite the proximity of K residues to both the α- and β-secretase cleavage sites in WT APP (α secretase only in the 3×Tg mice). Similarly, Dr. Bitan and colleagues showed previously that the labile binding of CLR01 to K residues prevented α-synuclein aggregation but not the ubiquitination required for proteasomal clearance [15].

Because synaptic deterioration prior to neuronal loss correlates with onset of amnestic mild cognitive impairment [66], it can be considered a prominent pathological feature of AD. Thus, treatments that can prevent the loss of functional synapses during prodromal or early stages of the disease may complement the brain's innate

compensatory defense mechanisms and significantly forestall additional AD-related cognitive symptoms. Furthermore, structural and functional synaptic alterations have been shown to be pharmacologically reversible in old, transgenic AD mice [67], suggesting that treatment after minor synaptic loss, but before overt neuronal loss, might delay or even reverse cognitive dysfunction. The prevention of spine retraction, rescue of Aβ-induced reduction in basal synaptic activity, and improvement of LTP by CLR01 demonstrate its ability to ameliorate AD-associated phenotypes of synaptic dysfunction.

Process-specific modulation of amyloid protein self-assembly is a novel approach towards treatment of amyloidoses. Much work still lies ahead for developing MTs as therapeutic tools for amyloid-related disease, including addressing additional questions about potential toxicity in more stringent systems and therapeutic effects on disease-associated behavioral deficits. As multiple proteins of unrelated sequences cause amyloidoses, a treatment paradigm that is process-specific is a promising approach to the problem. With brain penetration of ~2% of blood levels, robust stability in plasma and liver microsomes, and weak interaction with major CYP450 isoforms, CLR01 shows a favorable drug profile and is expected to be stable inside the brain. The next chapter will further explore the safety profile of CLR01 *in vivo*, the stability of the parent CLR01 compound, the effect of CLR01 on normal protein assembly, and will begin to characterize the brain levels of CLR01 over time.

3.6 References

1. (2011) 2011 Alzheimer's disease facts and figures. Alzheimers Dement 7: 208-244.

2. Kirkitadze MD, Bitan G, Teplow DB (2002) Paradigm shifts in Alzheimer's disease and other neurodegenerative disorders: The emerging role of oligomeric assemblies. J Neurosci Res 69: 567-577.

3. Kayed R (2010) Anti-tau oligomers passive vaccination for the treatment of Alzheimer's disease. Hum Vaccin 6: 47-51.

4. Lazo ND, Grant MA, Condron MC, Rigby AC, Teplow DB (2005) On the nucleation of amyloid β-protein monomer folding. Protein Science 14: 1581-1596.

5. Petkova AT, Ishii Y, Balbach JJ, Antzutkin ON, Leapman RD, et al. (2002) A structural model for Alzheimer's β-amyloid fibrils based on experimental constraints from solid state NMR. Proc Natl Acad Sci USA 99: 16742-16747.

6. Usui K, Hulleman JD, Paulsson JF, Siegel SJ, Powers ET, et al. (2009) Site-specific modification of Alzheimer's peptides by cholesterol oxidation products enhances aggregation energetics and neurotoxicity. Proc Natl Acad Sci USA 106: 18563-18568.

7. Li W, Sperry JB, Crowe A, Trojanowski JQ, Smith AB, 3rd, et al. (2009) Inhibition of tau fibrillization by oleocanthal via reaction with the amino groups of tau. Journal of Neurochemistry 110: 1339-1351.

8. Vana L, Kanaan NM, Hakala K, Weintraub ST, Binder LI (2011) Peroxynitrite-induced nitrative and oxidative modifications alter tau filament formation. Biochemistry 50: 1203-1212.

9. Cohen TJ, Guo JL, Hurtado DE, Kwong LK, Mills IP, et al. (2011) The acetylation of tau inhibits its function and promotes pathological tau aggregation. Nat Commun 2: 252.

10. Huang A, Stultz CM (2008) The effect of a ΔK280 mutation on the unfolded state of a microtubule-binding repeat in Tau. PLoS Comput Biol 4: e1000155.

11. Sinha S, Lopes DHJ, Bitan G (2012) A key role for lysine residues in amyloid β-protein folding, assembly, and toxicity. ACS Chem Neurosci 3: 473-481.

12. Fokkens M, Schrader T, Klärner FG (2005) A molecular tweezer for lysine and arginine. Journal of the American Chemical Society 127: 14415-14421.

13. Sinha S, Lopes DH, Du Z, Pang ES, Shanmugam A, et al. (2011) Lysine-specific molecular tweezers are broad-spectrum inhibitors of assembly and toxicity of amyloid proteins. Journal of the American Chemical Society 133: 16958-16969.

14. Sinha S, Du Z, Maiti P, Klärner F-G, Schrader T, et al. (2012) Comparison of three amyloid assembly inhibitors – the sugar scyllo-inositol, the polyphenol epigallocatechin gallate, and the molecular tweezer CLR01. ACS Chem Neurosci 3: 451-458.

15. Prabhudesai S, Sinha S, Attar A, Kotagiri A, Fitzmaurice AG, et al. (2012) A novel "molecular tweezer" inhibitor of α-synuclein neurotoxicity in vitro and in vivo. Neurotherapeutics 9: 464-476.

16. Talbiersky P, Bastkowski F, Klärner FG, Schrader T (2008) Molecular clip and tweezer introduce new mechanisms of enzyme inhibition. Journal of the American Chemical Society 130: 9824-9828.

17. Maiti P, Piacentini R, Ripoli C, Grassi C, Bitan G (2010) Surprising toxicity and assembly behaviour of amyloid β-protein oxidized to sulfone. Biochem J 433: 323-332.

18. Rahimi F, Maiti P, Bitan G (2009) Photo-induced cross-linking of unmodified proteins (PICUP) applied to amyloidogenic peptides. Journal of Visualized Experiments: http://www.jove.com/index/details.stp?id=1071.

19. Puzzo D, Privitera L, Leznik E, Fa M, Staniszewski A, et al. (2008) Picomolar amyloid-β positively modulates synaptic plasticity and memory in hippocampus. Journal of Neuroscience 28: 14537-14545.

20. Puzzo D, Privitera L, Fa M, Staniszewski A, Hashimoto G, et al. (2011) Endogenous amyloid-β is necessary for hippocampal synaptic plasticity and memory. Annals of Neurology 69: 819-830.

21. Puzzo D, Arancio O (2012) Amyloid-β Peptide: Dr. Jekyll or Mr. Hyde? Journal of Alzheimer's Disease.

22. Abramoff MD, Magelhaes PJ, Ram SJ (2004) Image Processing with ImageJ. Biophotonics International 11: 36-42.

23. Ripoli C, Piacentini R, Riccardi E, Leone L, Li Puma DD, et al. (2012) Effects of different amyloid β-protein analogues on synaptic function. Neurobiology of Aging: In press.

24. Lim GP, Yang F, Chu T, Chen P, Beech W, et al. (2000) Ibuprofen suppresses plaque pathology and inflammation in a mouse model for Alzheimer's disease. Journal of Neuroscience 20: 5709-5714.

25. Frautschy SA, Hu W, Kim P, Miller SA, Chu T, et al. (2001) Phenolic anti-inflammatory antioxidant reversal of Aβ-induced cognitive deficits and neuropathology. Neurobiology of Aging 22: 993-1005.

26. Gale GD, Yazdi RD, Khan AH, Lusis AJ, Davis RC, et al. (2009) A genome-wide panel of congenic mice reveals widespread epistasis of behavior quantitative trait loci. Molecular Psychiatry 14: 631-645.

27. Buxbaum JD, Gandy SE, Cicchetti P, Ehrlich ME, Czernik AJ, et al. (1990) Processing of Alzheimer β/A4 amyloid precursor protein: modulation by agents that regulate protein phosphorylation. Proc Natl Acad Sci USA 87: 6003-6006.

28. Terry RD, Masliah E, Salmon DP, Butters N, DeTeresa R, et al. (1991) Physical basis of cognitive alterations in Alzheimer's disease: synapse loss is the major correlate of cognitive impairment. Annals of Neurology 30: 572-580.

29. DeKosky ST, Scheff SW (1990) Synapse loss in frontal cortex biopsies in Alzheimer's disease: correlation with cognitive severity. Annals of Neurology 27: 457-464.

30. Scheff SW, Price DA, Schmitt FA, DeKosky ST, Mufson EJ (2007) Synaptic alterations in CA1 in mild Alzheimer disease and mild cognitive impairment. Neurology 68: 1501-1508.

31. Shankar GM, Li S, Mehta TH, Garcia-Munoz A, Shepardson NE, et al. (2008) Amyloid-β protein dimers isolated directly from Alzheimer's brains impair synaptic plasticity and memory. Nature Medicine 14: 837-842.

32. Stokin GB, Lillo C, Falzone TL, Brusch RG, Rockenstein E, et al. (2005) Axonopathy and transport deficits early in the pathogenesis of Alzheimer's disease. Science 307: 1282-1288.

33. Tsai J, Grutzendler J, Duff K, Gan WB (2004) Fibrillar amyloid deposition leads to local synaptic abnormalities and breakage of neuronal branches. Nature Neuroscience 7: 1181-1183.

34. Westphalen RI, Scott HL, Dodd PR (2003) Synaptic vesicle transport and synaptic membrane transporter sites in excitatory amino acid nerve terminals in Alzheimer disease. J Neural Transm 110: 1013-1027.

35. Yao PJ, Zhu M, Pyun EI, Brooks AI, Therianos S, et al. (2003) Defects in expression of genes related to synaptic vesicle trafficking in frontal cortex of Alzheimer's disease. Neurobiology of Disease 12: 97-109.

36. Malinow R, Hsieh H, Wei. W (2008) Impact of β amyloid on excitatory synaptic transmission and plasticity. Synaptic Plasticity and the Mechanism of Alzheimer's Disease. Berlin Heidelberg: Springer-Verlag. pp. 63-68.

37. Parameshwaran K, Sims C, Kanju P, Vaithianathan T, Shonesy BC, et al. (2007) Amyloid β-peptide Aβ(1-42) but not Aβ(1-40) attenuates synaptic AMPA receptor function. Synapse 61: 367-374.

38. Bliss TV, Collingridge GL (1993) A synaptic model of memory: long-term potentiation in the hippocampus. Nature 361: 31-39.

39. Lambert MP, Barlow AK, Chromy BA, Edwards C, Freed R, et al. (1998) Diffusible, nonfibrillar ligands derived from $A\beta_{1-42}$ are potent central nervous system neurotoxins. Proc Natl Acad Sci USA 95: 6448-6453.

40. Obach RS, Walsky RL, Venkatakrishnan K, Gaman EA, Houston JB, et al. (2006) The utility of in vitro cytochrome P450 inhibition data in the prediction of drug-drug interactions. J Pharmacol Exp Ther 316: 336-348.

41. Paine MF, Hart HL, Ludington SS, Haining RL, Rettie AE, et al. (2006) The human intestinal cytochrome P450 "pie". Drug Metab Dispos 34: 880-886.

42. Matsumoto Y, Yanase D, Noguchi-Shinohara M, Ono K, Yoshita M, et al. (2007) Blood-brain barrier permeability correlates with medial temporal lobe atrophy but not with amyloid-β protein transport across the blood-brain barrier in Alzheimer's disease. Dement Geriatr Cogn Disord 23: 241-245.

43. Zipser BD, Johanson CE, Gonzalez L, Berzin TM, Tavares R, et al. (2007) Microvascular injury and blood-brain barrier leakage in Alzheimer's disease. Neurobiology of Aging 28: 977-986.

44. Ujiie M, Dickstein DL, Carlow DA, Jefferies WA (2003) Blood-brain barrier permeability precedes senile plaque formation in an Alzheimer disease model. Microcirculation 10: 463-470.

45. Oddo S, Caccamo A, Shepherd JD, Murphy MP, Golde TE, et al. (2003) Triple-transgenic model of Alzheimer's disease with plaques and tangles: intracellular Aβ and synaptic dysfunction. Neuron 39: 409-421.

46. Hirata-Fukae C, Li HF, Hoe HS, Gray AJ, Minami SS, et al. (2008) Females exhibit more extensive amyloid, but not tau, pathology in an Alzheimer transgenic model. Brain Research 1216: 92-103.

47. Hess EJ, Albers LJ, Le H, Creese I (1986) Effects of chronic SCH23390 treatment on the biochemical and behavioral properties of D1 and D2 dopamine receptors: potentiated behavioral responses to a D2 dopamine agonist after selective D1 dopamine receptor upregulation. J Pharmacol Exp Ther 238: 846-854.

48. Platel A, Porsolt RD (1982) Habituation of exploratory activity in mice: a screening test for memory enhancing drugs. Psychopharmacology (Berl) 78: 346-352.

49. Guengerich FP (2008) Cytochrome p450 and chemical toxicology. Chem Res Toxicol 21: 70-83.

50. Williams JA, Hyland R, Jones BC, Smith DA, Hurst S, et al. (2004) Drug-drug interactions for UDP-glucuronosyltransferase substrates: a pharmacokinetic explanation for typically observed low exposure (AUCi/AUC) ratios. Drug Metab Dispos 32: 1201-1208.

51. Jones SA, Moore LB, Wisely GB, Kliewer SA (2002) Use of in vitro pregnane X receptor assays to assess CYP3A4 induction potential of drug candidates. Methods Enzymol 357: 161-170.

52. Staudinger JL, Ding X, Lichti K (2006) Pregnane X receptor and natural products: beyond drug-drug interactions. Expert Opin Drug Metab Toxicol 2: 847-857.

53. Staudinger JL, Lichti K (2008) Cell signaling and nuclear receptors: new opportunities for molecular pharmaceuticals in liver disease. Mol Pharm 5: 17-34.

54. Attar A, Chan W-TC, Klärner F-G, Schrader T, Bitan G Safety and pharmacokinetic characterization of the molecular tweezer CLR01 *in vivo*. Manuscript in preparation.

55. Liu T, Bitan G (2012) Modulating self-assembly of amyloidogenic proteins as a therapeutic approach for neurodegenerative diseases: strategies and mechanisms. ChemMedChem 7: 359-374.

56. Townsend M, Cleary JP, Mehta T, Hofmeister J, Lesné S, et al. (2006) Orally available compound prevents deficits in memory caused by the Alzheimer amyloid-β oligomers. Annals of Neurology 60: 668-676.

57. Bourasset F, Ouellet M, Tremblay C, Julien C, Do TM, et al. (2009) Reduction of the cerebrovascular volume in a transgenic mouse model of Alzheimer's disease. Neuropharmacology 56: 808-813.

58. Akiyama H, Barger S, Barnum S, Bradt B, Bauer J, et al. (2000) Inflammation and Alzheimer's disease. Neurobiology of Aging 21: 383-421.

59. Ard MD, Cole GM, Wei J, Mehrle AP, Fratkin JD (1996) Scavenging Of Alzheimers Amyloid β-Protein By Microglia In Culture. Journal of Neuroscience Research 43: 190-202.

60. Frautschy SA, Cole GM, Baird A (1992) Phagocytosis and deposition of vascular beta-amyloid in rat brains injected with Alzheimer beta-amyloid. Am J Pathol 140: 1389-1399.

61. Colton CA, Gilbert DL (1987) Production of superoxide anions by a CNS macrophage, the microglia. FEBS Lett 223: 284-288.

62. Chao CC, Hu S, Molitor TW, Shaskan EG, Peterson PK (1992) Activated microglia mediate neuronal cell injury via a nitric oxide mechanism. J Immunol 149: 2736-2741.

63. Gendron TF, Petrucelli L (2009) The role of tau in neurodegeneration. Mol Neurodegener 4: 13.

64. Bloom GS, Ren K, Glabe CG (2005) Cultured cell and transgenic mouse models for tau pathology linked to β-amyloid. Biochim Biophys Acta 1739: 116-124.

65. Roberts BE, Shorter J (2008) Escaping amyloid fate. Nat Struct Mol Biol 15: 544-546.

66. Arendt T (2009) Synaptic degeneration in Alzheimer's disease. Acta Neuropathol 118: 167-179.

67. Smith DL, Pozueta J, Gong B, Arancio O, Shelanski M (2009) Reversal of long-term dendritic spine alterations in Alzheimer disease models. Proc Natl Acad Sci U S A 106: 16877-16882.

Chapter 4

Safety and pharmacological characterization of the molecular tweezer CLR01 in mice

4.1 Abstract

The "molecular tweezer" CLR01 is a broad-spectrum inhibitor of abnormal protein self-assembly, which acts by binding K residues with low micromolar affinity. In a triple-transgenic mouse model of Alzheimer's disease (AD), CLR01 was found to reduce amyloid plaque burden and hyperphosphorylated tau levels following subcutaneous administration for 1 m. CLR01 also has been tested in several additional *in vitro* and *in vivo* models of amyloidoses all without signs of toxicity. With the eventual goal of developing CLR01 as a therapeutic drug for AD and other amyloidoses, here I had several goals related to the safety and pharmacokinetics of CLR01: 1) to explore the process-specific mechanism of action allowing CLR01 to disrupt aberrant protein assembly safely; 2) to determine the safety margin of CLR01 in mice; 3) to characterize CLR01's blood–brain barrier (BBB) permeability in young (2-m old), middle-aged (12-m old), or old (22-m old) AD transgenic and wild-type mice; and 4) to begin to parse out potential modes of metabolism of CLR01.

Studies of CLR01's effect on tubulin polymerization did not show disruption of the process until 55-fold excess CLR01 was used, supporting its process-specific

mechanism of action. In an acute, 24-h toxicity study of a single intraperitoneal injection, only a high dose of 100 mg/kg CLR01, which is 2500-fold higher than the dose used for efficacy studies in the triple-transgenic model, induced behavioral signs of distress and liver toxicity observed histopathology and serologically. In a chronic, 30-d toxicity study, daily injection of up to 10 mg/kg did not show any signs of behavioral or histopathological toxicity. Surprisingly, lower cholesterol levels were found in CLR01-treated relative to vehicle-treated mice.

In healthy humans, increased age is associated with elevated BBB permeability, which increases further with vascular- or AD-related dementia. BBB breakdown also has been shown in transgenic mouse models of AD. To characterize BBB penetration of CLR01, radiolabeled CLR01 containing ^{3}H in the hydrocarbon backbone was injected intravenously into triple-transgenic or WT mice at three different ages. The plasma half-life of CLR01 was found to be 40−120 min and the brain penetration of CLR01 was 1−3% of blood levels. Though CLR01 was almost completely removed from the blood by 8 h, unexpectedly, levels of brain CLR01 remained steady over 72 h. Multiple or larger doses resulted in a larger concentration of CLR01 in the brain. Thus, with the sustained brain levels following one administration and increased levels with different dosing regimens, it is possible that sufficiently large amounts of CLR01 are available in the brain, for protein aggregation disruption at low dosing regimens. Lastly, the molecular structure of CLR01 suggests that dephosphorylation may be a likely mode of catabolism. However, measurement of CLR01 metabolism *in vitro* did not find evidence of dephosphorylation.

The favorable safety profile and BBB permeability levels found for CLR01, together with efficacy shown in animal models of AD and other protein-aggregation diseases, support development of CLR01 as a valuable lead towards disease-modifying therapy for multiple amyloidoses.

4.2 Introduction

Alzheimer's disease (AD) and Parkinson's disease, along with over 30 other diseases, are amyloidoses, in which aberrant protein folding and aggregation is a central pathologic process. Amyloidoses are characterized by self-assembly of one or more proteins into toxic oligomers and insoluble amyloid. Currently, amyloidoses have no cure. Inhibition of the aberrant aggregation process is highly challenging because unlike traditional drug targets that have defined structures and in many cases, specific binding sites or active sites, toxic oligomers of amyloidogenic proteins are metastable structures that sample numerous conformations and amyloid fibrils are characterized by flat surfaces. These structures are largely devoid of specific binding pockets [1,2]. One possible solution to these challenges is to aim for one step prior to the unknown and unfavorable structures, specifically targeting the amino acid interactions.

Recently, Dr. Bitan and colleagues reported that the molecular tweezer, CLR01, is a novel, broad-spectrum inhibitor of abnormal protein self-assembly, which acts by a "process-specific" mechanism and inhibits the aggregation and toxicity of multiple amyloidogenic proteins [3-5]. CLR01 is a small molecule, originally developed as an artificial K receptor [6,7] that binds K residues with low micromolar affinity [3,6,8]. The binding is highly labile [9], yet it is selective to K and involves inclusion of the K side-

chain within the tweezer cavity (Figure 4.1). CLR01 also binds to R, yet with ~10-fold lower affinity [7,10]. Selective binding to K is achieved by a combination of hydrophobic and electrostatic interactions. K is the only proteinaceous amino acid that effectively forms both types of interactions – hydrophobic interactions involving the butylene chain, and Coulombic attraction/repulsion of its ε-NH_3^+ group. Both types of interactions are important in aberrant protein self-assembly. Thus, CLR01 competes for the same interactions that are key to nucleation and aggregation by most amyloidogenic proteins [11,12].

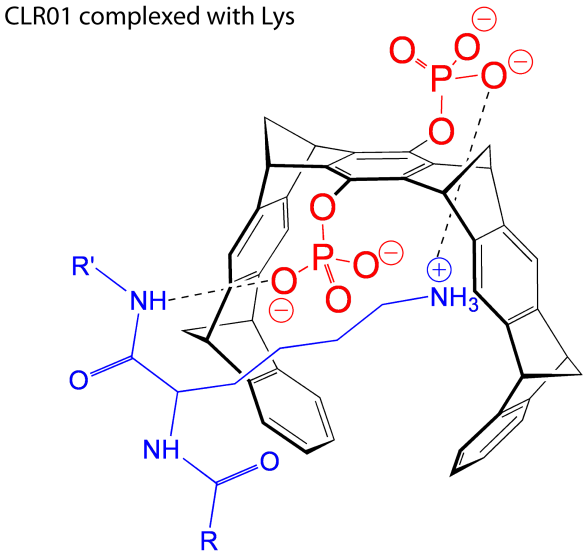

Figure 4.1 Schematic representation of the interaction between CLR01 and K

The moderate-affinity binding of CLR01 to K is key to its process-specific mechanism. The forces that mediate normal protein assembly are thought to be optimized by evolution and thus tend to be strong. The forces that mediate abnormal protein assembly have not had the opportunity to participate in this evolutionary process. Consequently, the binding energies involved are substantially weaker than those controlling normal protein structure and function. Therefore, although CLR01 may bind to exposed K residues in virtually any protein, Dr. Bitan and I reasoned that at sufficiently low concentrations, labile binding with micromolar affinity would only affect

relatively weak interactions, such as those that mediate aberrant protein oligomerization and nucleation.

The data generated to date have supported our conjecture. CLR01 prevented deformation and mortality in a zebrafish model of α-synuclein (α-syn) toxicity by keeping α-syn soluble, preventing its neurotoxic effects, and promoting disinhibition of the 26S ubiquitin-proteasome system, thus allowing it to degrade the excess α-syn [4]. Peripheral, subcutaneous (SC) CLR01 administration in a triple-transgenic (3×Tg) mouse model of AD resulted in a significant decrease in amyloid plaque burden and hyperphosphorylated tau, with an accompanying decrease in levels of microglia [5]. Similarly, peripheral administration of CLR01 to familial amyloidotic polyneuropathy mice expressing mutant transthyretin led to a significant decrease in transthyretin deposition and associated endoplasmic reticulum-stress, apoptosis, and protein oxidation markers [13]. In support of the putative process-specific mechanism of CLR01, no signs of toxicity were observed in any of these studies. CLR01 was used at up to the 10 μM in the zebrafish model (in the water environment [4]), at 40 μg/kg/day in the AD mouse model [5], and at 1.2 mg/kg/day in the transthyretin model [13].

In vitro studies of metabolic toxicity and drug–drug interaction involving the cytochrome P450 system showed minimal inhibition of five major isoforms with half-maximal inhibition concentration values above levels expected to cause drug–drug interactions [5]. Minimal activation of the cytochrome P450 system by CLR01 was detected up to 10-μM concentrations in a cell-culture system compared to the antibiotic rifampicin, which was used as a positive control [5]. In nerve growth factor-differentiated rat pheochromocytoma cells treated with CLR01, no toxicity was detected up to 200 μM,

whereas a mild decrease in cell viability was observed at 400 μM—1−3 orders of magnitude higher than concentrations needed for inhibition of the toxicity of different amyloidogenic proteins in cell culture [3,14].

Further support of the process-specific mechanism came from the observation that CLR01 did not affect processing of amyloid β-protein precursor (APP) in the treated AD mice. In APP, K residues are located N-terminally to the α- and β-secretase cleavage sites. Ostensibly, CLR01 binding to these residues could have affected APP processing. However, no differences were found in levels of APP cleavage products between brain extracts of vehicle- or CLR01-treated mice [5]. To further examine the putative process-specific mechanism and toxicity profile of CLR01, here Dr. Bitan evaluated the effect of the compound *in vitro* on a physiologic (as opposed to aberrant) protein self-assembly process—tubulin polymerization— and *in vivo* using wild-type (WT) mice to which CLR01 was administered at high doses either as a one-time bolus or daily for 1 m.

A large number of amyloidoses affect the central nervous system (CNS). If molecular tweezers are to be developed as drugs for these diseases, they likely will need to cross the blood–brain barrier (BBB). In the AD-mouse-treatment study, SC administration of CLR01 resulted in clear CNS effects [5], suggesting that the compound penetrated through the BBB into the brain of the mice. However, that study did not address the brain penetration levels or possible mechanisms. The BBB becomes compromised with aging [15] and this compromise is thought to be exacerbated in patients with certain neurodegenerative diseases, including AD [16-18]. Previously, I reported that using ^{3}H-CLR01 injected intravenously, I found radioactivity levels in the brain to be ~2% of blood levels in 12-m old WT and 3×Tg AD mice [5]. I present here a

characterization of the BBB's permeability to CLR01 and the effects of age and neurodegenerative disease. I also assessed a likely route of metabolism of CLR01 in mouse brain.

4.3 Materials and Methods

Mice

All procedures were compliant with the National Research Council Guide for the Care and Use of Laboratory Animals, and approved by the University of California at Los Angeles (UCLA) Institutional Animal Care Use Committee. Two-m old WT C57BL/6J mice for toxicity studies were purchased from Jackson Laboratory (Bar Harbor, Maine, Stock 000664). 3×Tg and WT mice with the same genetic background [19] for BBB studies were bred at UCLA. Mice were housed 2–4 per cage under standard conditions, maintained on a 12-h dark and 12-h light cycle with *ad libitum* access to rodent chow and water.

CLR01

CLR01 was produced and purified as described previously [7]. ^{3}H-CLR01 was prepared by Moravek Biochemicals (Brea, CA) using a method that provides ^{3}H incorporation into the hydrocarbon skeleton (i.e., non-labile protons) [20] and yielded pure ^{3}H-CLR01 with specific activity 1.3 Ci/mmol.

Inhibition of tubulin polymerization

The effect of CLR01 on tubulin polymerization [21,22] was analyzed using a commercial kit (Cytoskeleton, Inc., Denver, Colorado). Three mg/ml porcine brain tubulin (~18 μM) were allowed to polymerize at 37 ºC in the absence or presence of

CLR01 concentrations ranging from 10–1,000 μM. The turbidity of the solution was measured as absorbance at λ = 340 nm using a Synergy HT microplate reader (BioTek, Winooski, VT). The data are an average of three independent experiments with two wells per condition.

Toxicity evaluation

For acute toxicity studies, 2-m old C57BL/6J mice were administered saline-vehicle, 10 mg/kg, or 100 mg/kg CLR01 by a single intraperitoneal (IP) injection. The mice were sacrificed 24-h after the injection. For chronic toxicity studies, 2-m old C57BL/6J mice were administered saline-vehicle, 3 mg/kg, or 10 mg/kg CLR01 by daily IP injection for 30 days. Acute-study mice were visually monitored for 1 h after injection and then every 50 min for 10 min over the first 6 h of the experiment for changes in activity and behavior. The mice also were monitored every 110 min for 10 min during the last 6 h of the experiment until they were sacrificed. Chronic-study mice were monitored for 1 h after injection and then 3 times throughout the day for 10 min each day of the first week. During that week there were no appreciable changes in the behavior, appearance, or weight of the mice. Therefore, monitoring was reduced to twice a day during the remainder of the experiment. On all occasions, the mice were monitored for any signs of severe toxicity, including bruising or bleeding, pale mucous membranes or extremities, diarrhea, dehydration, neurological signs, such as difficulty ambulating or paralysis, tachypnea or dyspnea, or abdominal distension.

Following the treatment, mice were anesthetized with pentobarbital and blood was collected by cardiac puncture and placed in tubes containing a clot activator for serum separation (Capiject T-MG tubes, Terumo Medical Products, Somerset, NJ). Next,

the lungs were filled through the trachea with 4% paraformaldehyde to prevent collapse and tissues (brain, heart-lung, liver, kidney, and spleen) were collected and fixed for 72 h in 4% paraformaldehyde at a ratio of ~1:10 tissue:fixative (v/v). Tissues then were transferred into a 70%-ethanol solution and transferred to the UCLA Mouse Pathology Core for paraffin embedding, sectioning, and tissue histopathology analysis. Serum was analyzed by the UCLA Division of Laboratory Animal Medicine (DLAM) Animal Serology & Molecular Diagnostic Laboratory for an 11-panel serum chemical analysis using the ACE Alera Clinical Chemistry system (Alfa Wassermann Diagnostic Technologies, West Caldwell, NJ). The panel included: alanine aminotransferase, aspartate aminotransferase, albumin, alkaline phosphatase, creatinine, total bilirubin, lactate dehydrogenase, blood urea nitrogen, cholesterol, total protein, and glucose.

Plasma concentration and blood–brain barrier permeability

For studies of plasma concentration, CLR01 was administered by either SC or intravenous (IV) injection at 1 mg/kg or by oral gavage at 10 mg/kg and plasma was collected at time points between 0.33−24 h. Three mice were used per time point. The concentration of CLR01 in plasma was determined using liquid chromatography-mass spectrometry (LC-MS) by interpolation of sample peak area data into the calibration curve.

The following groups of mice were used for CLR01 BBB penetration studies: 3×Tg and the corresponding WT mice at 2-m, 12-m, and 22−24-m (hereafter called 22-m) of age. The groups were as follows: 2-m WT, 2-m Tg, 12-m WT, 12-m Tg, 22-m WT, 22-m Tg. Mice were administered ^{3}H-CLR01 intravenously. Two μCi per gram of mouse

body weight, which are equal to 11.86 μg/g of CLR01 in which ^{3}H-CLR01 made up 10% of the total CLR01, were injected into the jugular vein. Blood and brain were collected at 0.5, 1, 3, 8, 24, or 72 h (not all time points were collected for all groups). For times ≤ 3 h, mice were anesthetized by IP injection of ketamine and xylazine. Anesthesia and the use of the jugular vein was due to initial difficulties with tail vein injections. The mice remained anesthetized following the injection until the specified time point, at which point they were given a lethal dose of pentobarbital. Then, blood was collected via a cardiac puncture, and the brain harvested with or without a perfusion step (see section 4.4.3 below). For time points 8–72 h, mice were not anesthetized and ^{3}H-CLR01 was injected into the tail vein. This change was due to the difficulty of keeping mice anesthetized for longer than 3 h and difficulties with tail vein injections were overcome by utilizing the help of UCLA veterinarians. No differences were observed between mice given anesthesia and jugular vein injections versus tail vein injections. Euthanasia procedures were the same as described above. For all mice, one hemisphere of the brain and 100–350 μl of blood were separately digested following instructions from Perkin-Elmer (document: Scintillation Cocktails and Consumables) with 1 ml Solvable (Perkin-Elmer, Waltham, MA), added to Ultima Gold Liquid Scintillation Cocktail (Perkin-Elmer) and read in a Triathler Liquid Scintillation Counter model 425-034, (Hidex, Turku, Finland). Brain permeability percentage was calculated as counts per minute (CPM) per g of brain relative to CPM per ml of blood. The data are an average of values from three mice per genotype/age/time combination.

For CLR01 transport-saturation studies using 5× the CLR01 dose, ^{3}H-CLR01 was kept at 10% of the total CLR01 mixture and a total of 59.3 μg of CLR01 (10 μCi) per g of

mouse body weight was injected IV (22-m WT 5× dose). For CLR01 brain-accumulation studies, two 11.86-μg/g injections were administered at equal time intervals (22-m WT 2× inj). In these experiments, mice were injected at time = 0 and at t = ½ of euthanasia time. For example, in the original, single-injection experiments, a mouse would receive an injection at t = 0 and then be euthanized at t = 1 h. In this experiment, a mouse received one injection at t = 0, a second injection at t = 0.5 h, and then was euthanized at t = 1 h.

In experiments using ^{3}H-CLR01, urine was collected when possible over the period between injection and euthanasia. In all cases, I found that the urine was radioactive. Unfortunately, comparison among mice proved to be difficult. I could not normalize the radioactivity because the amount of urine in the bladder prior to injection and the volume produced during the experiment could not be calculated. Thus, I can simply conclude qualitatively that CLR01 is excreted through the urine, but cannot provide quantitative measures of what percentage of the compound is excreted this way.

In vitro metabolism

Potential dephosphorylation of CLR01 was analyzed by incubating 100 nmol CLR01 with 0.08 units of alkaline phosphatase (ALP; calf intestinal alkaline phosphatase, Promega, Madison, Wisconsin) for 60 min at 60 ºC. One enzymatic unit is defined as the amount of enzyme required to catalyze the hydrolysis of 1 μmol of p-nitrophenylphosphate per minute. Five to 50 nmol of p-nitrophenylphosphate disodium salt (Fisher, Waltham, Massachusetts) were used as a positive control and for generation of a standard curve. The amount of inorganic phosphate generated was measured

spectrophotometrically using an EnzChek Phosphate Assay kit (Life Technologies, Carlsbad, California) according to the manufacturer's instructions on a Beckman Coulter (Brea, California), model DU-640 spectrophotometer at $\lambda = 360$ nm. Baseline values were subtracted from readings and compared to the standard curve resulting from serial ALP reactions to calculate the amount of inorganic phosphate. Similarly, potential dephosphorylation of CLR01 by brain homogenates was measured. For these experiments, one brain hemisphere was homogenized by sonication in the presence of cOmplete protease-inhibitor cocktail (Roche, Penzberg, Germany). Protein concentration was measured using a BCA Protein Assay Kit (Pierce, Rockford, Illinois). A "phosphate-mop" system was used according to the EnzChek Phosphate Assay kit instructions to sequester inorganic phosphates naturally present in 1.5 mg of brain, and then 50-nmol CLR01 or different concentrations of p-nitrophenylphosphate disodium salt were added and incubated for 60 min at 60 ºC.

Statistics

Data are shown as means ± standard error of the mean (SEM). Statistical analysis was performed using Prism 6.0c (GraphPad, La Jolla, CA). For all experiments, 2-way analysis of variance followed by Sidak's multiple comparisons test *post-hoc* analysis were used. The level of significance was set at $p < 0.05$.

4.4 Results

4.4.1 *In vitro* examination of the process-specific mechanism of CLR01.

As stated above, the mechanism by which CLR01 remodels the assembly of amyloidogenic proteins into non-toxic assemblies that can be degraded by normal clearance mechanisms is by its specific binding to K and R residues. The mechanism is "process-specific" because it is postulated to affect only the aberrant assembly of proteins that leads to toxic oligomers and aggregates, but not normal protein assembly as happens, e.g., in tubulin polymerization. To test whether this indeed is the case, Dr. Bitan examined the effect of CLR01 on tubulin polymerization [21,22]. Three mg/ml (~18 μM) porcine brain tubulin, which contains 3.8% K and 4.8% R, was allowed to polymerize in the absence or presence of CLR01 concentrations ranging from 10–1,000 μM.

In the absence of CLR01 or in the presence of up to 300 μM of the compound, the change in turbidity followed a typical sigmoidal curve, starting at 0.05-0.09 absorbance units (Figure 4.2). The absorbance remained unchanged for the first 10–15 minutes, which is a typical lag phase in this reaction, and then increased gradually up to ~60 min, at which point the rate of increase began to decline, and the reaction was followed for another

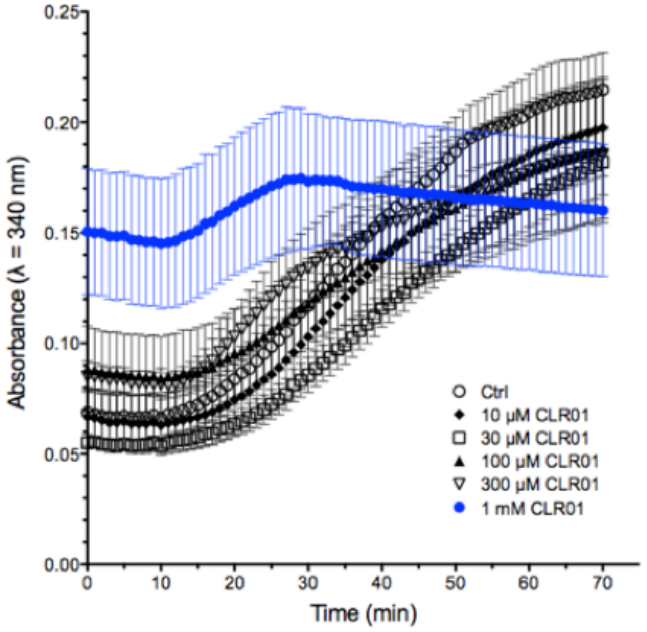

Figure 4.2 CLR01 is a "process-specific" modulator of aberrant protein assembly
Tubulin was allowed to polymerize in the absence or presence of increasing concentrations of CLR01. Perturbation of the polymerization was observed only at 1 mM CLR01. The data are an average of three independent experiments and are shown as mean ± SEM.

10 min. The only concentration at which significant modulation of the polymerization was observed was 1,000 μM (Figure 4.2, blue curve), i.e., at a tubulin:CLR01 concentration ratio ~1:55. At this high ratio, a high absorbance, 0.15, was observed immediately, followed by a slight gradual decline during the lag phase. Then, the absorbance began to increase for 30 min, followed by a slow decline for the rest of the experiment. One interpretation of these data is that at the high concentration used, 1,000 μM, binding of CLR01 to tubulin induced immediate self-assembly into an irregular aggregates. Similar immediate induction of self-assembly was observed with 4 of the 9 amyloidogenic proteins tested by Sinha et al. [3], suggesting that this reaction occurs with some, but not all proteins. In all the cases studied by Sinha et al., these aggregates were non-amyloidogenic and non-toxic.

Presumably, following the immediate aggregation in the presence of 1,000 μM CLR01, the tubulin aggregates observed at t = 0 partially disassembled as the polymerization reaction progressed, then polymerized between 10–30 min. At that point, the high CLR01 concentration appeared to interfere with the polymerization reaction and the tubulin polymers gradually disassembled again. Validation of this interpretation will require further investigation, yet it was not the focus of the current study.

The motivation for this experiment was to test whether the concentration of CLR01 needed to interfere with a controlled self-assembly process was substantially higher than that required for modulation of aberrant self-assembly, which was found indeed to be the case. Most of the protein:CLR01 concentration ratios needed for inhibition of amyloidogenic protein aggregation were in the range 1:1–1:3 [3], compared to the 1:55 tubulin:CLR01 concentration ratio at which disruption of tubulin

polymerization was observed. These results support the specificity of CLR01 for inhibition of aberrant aggregation as opposed to controlled polymerization.

4.4.2 CLR01 safety

If CLR01 indeed operated by a process-specific mechanism, remodeling the abnormal aggregation of amyloidogenic proteins at substantially lower concentrations than concentrations that would perturb normal physiological processes, one would expect the compound to have a high therapeutic index. To calculate the therapeutic index, a lethal dose must be reached. The *in vitro* data described above suggested that disruption of tubulin polymerization occurs at concentration ratios 20–50 times higher than those needed for inhibition of aggregation of amyloidogenic proteins. In addition, cell culture experiments indicated that CLR01 began to show toxicity at concentrations 1–3 orders of magnitude higher than those required for inhibition of toxicity by different amyloidogenic proteins [3,4]. The next rational step was to test the safety margin of CLR01 *in vivo*. Based on the *in vitro* and cell culture data, I expected that 100 mg/kg would be lethal to mice and therefore used it as the highest dose in out safety evaluation experiments. I evaluated the safety of CLR01 in 2-m old, male, WT mice either 24 h following a single IP injection of 10 or 100 mg/kg (acute administration) or after daily IP injection of 3 or 10 mg/kg for 30 day (chronic administration). Following euthanasia, serum was collected for chemical analysis and tissues were harvested for histopathology evaluation.

All CLR01-treated groups, except for the 100-mg/kg acute-administration group, behaved indistinguishably from control mice in terms of levels and type of activity and

grooming. The administration of 100-mg/kg CLR01 caused obvious signs of distress immediately, which lasted for ~30 min following the injection. For most mice, activity level decreased and eyelids became droopy. Some of the mice exhibited arching of the back, sporadic gasping, lying down, dragging one leg, and twitching. These signs of distress diminished after the first 30 min, at which point the mice resumed grooming and sitting on hind legs. Some mice showed decreased activity and droopy eyelids for up to 2 h following the injection. No symptoms of severe toxicity, as defined by the UCLA DLAM veterinarians, were observed for any mice, including bruising, bleeding, pale mucous membranes or extremities, diarrhea, paralysis, tachypnea or dyspnea, or abdominal distension.

Liver, kidney, spleen, heart, lung, and brain were collected for histopathology analysis. Tissue samples from heart, lung, spleen, and brain of all acutely CLR01-administered mice were indistinguishable from those of control mice. In all 100-mg/kg-dosed mice and one of eight 10-mg/kg-dosed mice of the acute-administration groups, liver degeneration and necrosis was detected in centrilobular and midlobular regions. Zonal nature of liver toxicity is common in drug-toxicity and was expected in the high-dose group.

The fact that all the mice in the high-dose group survived meant that the actual therapeutic index could not be calculated because contrary to our expectation, 100 mg/kg was under the lethal dose. However, I considered the observation of obvious liver toxicity at this high dose as sufficient for determining the maximal dose in future efficacy experiments and therefore did not treat mice with higher doses. Rather, I conducted next a 30-day, chronic-toxicity experiment in which mice were administered IP either saline-

vehicle, or 3 or 10 mg/kg/day of CLR01. Because one mouse of the eight used in the 10-mg/kg acute-administration group showed signs of liver toxicity, 10 mg/kg/day was chosen to be the high dose in this experiment.

Heart, lung, spleen, and brain from both chronically CLR01-treated groups of mice were indistinguishable from vehicle-treated mice and were free of signs of malformation, degeneration, necrosis, or inflammation within normal variability among mice. A few mice in the 3-mg/kg group showed signs of mild-to-moderate multifocal extramedullary hematopoiesis in the liver. The consulting veterinary pathologist concluded that this was possibly immune-stimulated but not pathogenic. Mild pancreatitis also was observed in one of the mice showing liver hematopoiesis and one additional mouse in the 3-mg/kg group. No signs of tissue pathology or liver necrosis, as seen in the acute study, were detected in the 10-mg/kg dosed group of mice and thus, it is highly unlikely that the hematopoiesis or inflammation found in the low-dose group were related to CLR01 treatment.

		ACUTE: 24 hr, 1 dose			CHRONIC: 30 day, daily dosing		
		Control	10 mg/kg	100 mg/kg	Control	3 mg/kg	10 mg/kg
		n=3	n=8	n=8	n=9	n=10	n=9
	Normal Range	Mean	Mean	Mean	Mean	Mean	Mean
Alanine aminotransferase U/L	22-133	30.7	36.1	**1282.88** ***	52.1	43.1	38.4
Aspartate Aminotransferase U/L	46-221	63.3	89.5	**565.25** **	367.0	150.9	236.2
Albumin g/dl	2.6-5.4	2.2	2.3	1.9	2.8	2.8	2.7
Alkaline Phosphatase U/L	16-200	107.7	126.1	101.5	98.1	104.4	106.1
Creatinine mg/dl	0.1-1.8	0.2	0.2	0.4	0.2	0.3	0.2
Total Bilirubin mg/dl	0.3-0.7	0.2	0.2	0.3	0.3	0.2	0.2
Lactate Dehydrogenase U/L	109-647	235.0	325.2	**2439.8** ***	486.6	507.0	483.0
Blood Urea Nitrogen mg/dl	2-71	22.3	19.8	22.0	21.8	22.3	24.1
Cholesterol mg/dl	34-173	93.0	91.5	**20.8** **	92.3	80.9	**56.78** **
Total Protein g/dl	4.6-7.3	4.0	3.7	3.6	4.8	4.7	4.6
Glucose mg/dl	60-133	286.0	297.8	**104.33** ***	250.6	256.7	233.9

Table 4.1: Serum chemical analysis
*** $p < 0.001$, ** $p < 0.01$

Serum chemical analysis mainly consisted of tests of renal and liver function (Table 4.1). No significant differences were observed between the control and low-dose groups in either the acute-administration or chronic-administration experiments. The

acute-administration, 100-mg/kg group showed significant increase in alanine aminotransferase, aspartate aminotransferase, and lactate dehydrogenase, and a significant decrease in cholesterol compared to both the control group and what is considered a normal range (UCLA DLAM, modified [23]). All of these changes are consistent with acute liver injury. Glucose levels were significantly lower in the 100-mg/kg acute-administration group than in the control group, but were within the normal range. Production of glucose is often the last function to be lost in liver failure, however, other changes indicating liver damage were not observed, including changes in albumin, alkaline phosphatase, or total bilirubin. In the chronic-administration experiment, the only significant serum-chemistry difference observed was ~40% lower cholesterol in the 10-mg/kg group compared to the control group. The cholesterol level was within the normal range.

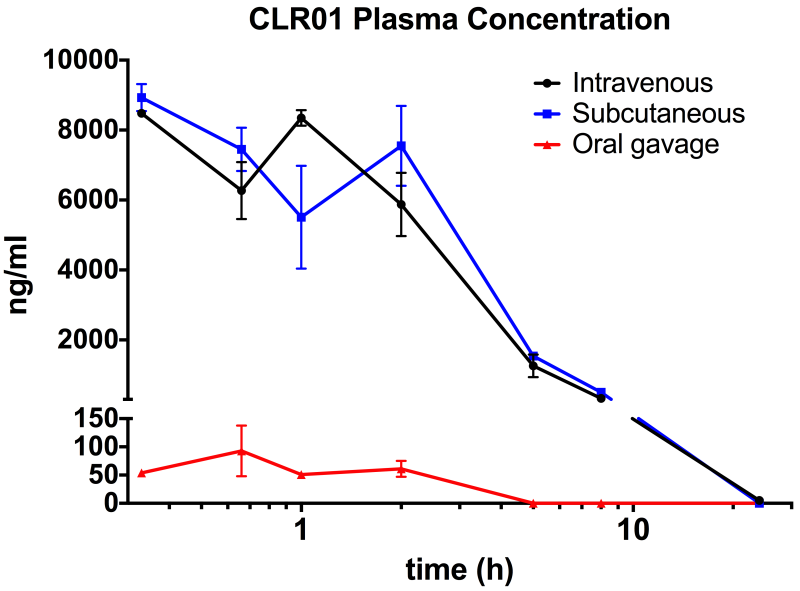

Figure 4.3 CLR01 plasma concentration by different routes of administration
Levels of CLR01 in plasma by administration of CLR01 by intravenous (black line) or subcutaneous (blue line) injection at 1 mg/kg, or by oral gavage (red line) at 10 mg/kg over 24 h. Data are given as mean ± SEM.

4.4.3 Pharmacokinetics of CLR01 *in vivo*

The plasma half-life of CLR01 was measured by LC-MS in 2-m old WT mice following administration by a SC or IV injection or by oral gavage. The SC bioavailability was found to be identical, within experimental error, to the IV administration, which was considered as 100% bioavailable (Figure 4.3). Both routes resulted in ~30% of the administered dose detected in the blood at the earliest time point measured – 20 min. In both routes, the plasma half-life was found to be ~2.5 h. Approximately 5% of the initial CLR01 levels were found in the plasma 8 h following either SC or IV administration. Oral bioavailability was negligible, suggesting that CLR01 either gets metabolized in the gastrointestinal tract and/or does not pass from the gut to the blood.

Next, I asked what percentage of the administered CLR01 penetrates through the BBB and gets into the CNS. Our first attempt was to measure CLR01 in brain extracts using LC-MS. However, this proved to be difficult. Due to the multiple negative charges of CLR01, its partial protonation at physiologic pH, and the presence of various counter-ions in biological fluids, the MS signal splits into multiple peaks resulting in low signal-to-noise ratio. The difficulty to observe the CLR01 signal in brain extracts using LC-MS suggested that the concentration was low and detection would necessitate considerable optimization of the extraction and LC-MS methods, which would require considerable effort and high costs. Therefore, I decided to test first whether CLR01 could be found in the CNS by using a radiolabeled derivative of the compound.

As the permeability of the BBB has been shown to be dependent on age and morbidity, and especially increased in AD [16] and in mouse models of AD [24,25], I assessed how age and disease progression affected the brain penetration of CLR01 by using WT and 3×Tg mice at three different ages. The 3×Tg model was chosen because it was used in a previous study, in which CLR01 was found to reduce AD-like pathology in the brain [5]. Mouse ages were chosen to correspond with: 1) a stage before Aβ burden and cognitive deficits are found at 2-m of age [19,26]; 2) a stage with minimal plaque and tangle pathology but with observable memory deficits at 12-m of age [19,27]; and 3) a stage of abundant plaque and tangle pathology with consistent behavioral deficits at 22-m of age [28]. Mice were administered ^{3}H-CLR01 IV, blood and brain were collected at time points between 0.5−72 h following CLR01 administration, and radioactivity levels were measured subsequently by liquid scintillation counting. Radioactivity is presented as CPM/g of brain or CPM/ml of blood.

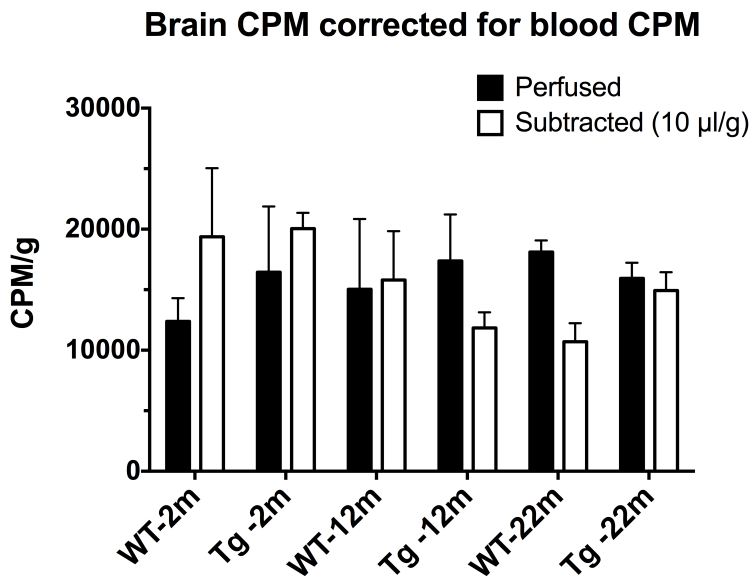

Figure 4.5 Correction for radioactivity from residual blood in the brain
Comparison of brain perfusion to remove residual blood with subtraction of calculated levels of blood radioactivity at 10 µl of blood per g of brain tissue. Data are given as mean ± SEM. The methods are not significantly different.

At 0.5 h following injection, blood

radioactivity levels in 12-m old mice were 39 ± 13% and 40 ± 6% of the injected levels, for WT and 3×Tg mice, respectively. These values were in agreement with the CLR01 concentration levels detected in plasma by LC-MS. The half-life was calculated to be ~40 min following the injection, and ~5−10% of the radioactivity observed at time 0.5 h remained in the blood after 8 h (Figure 4.4).

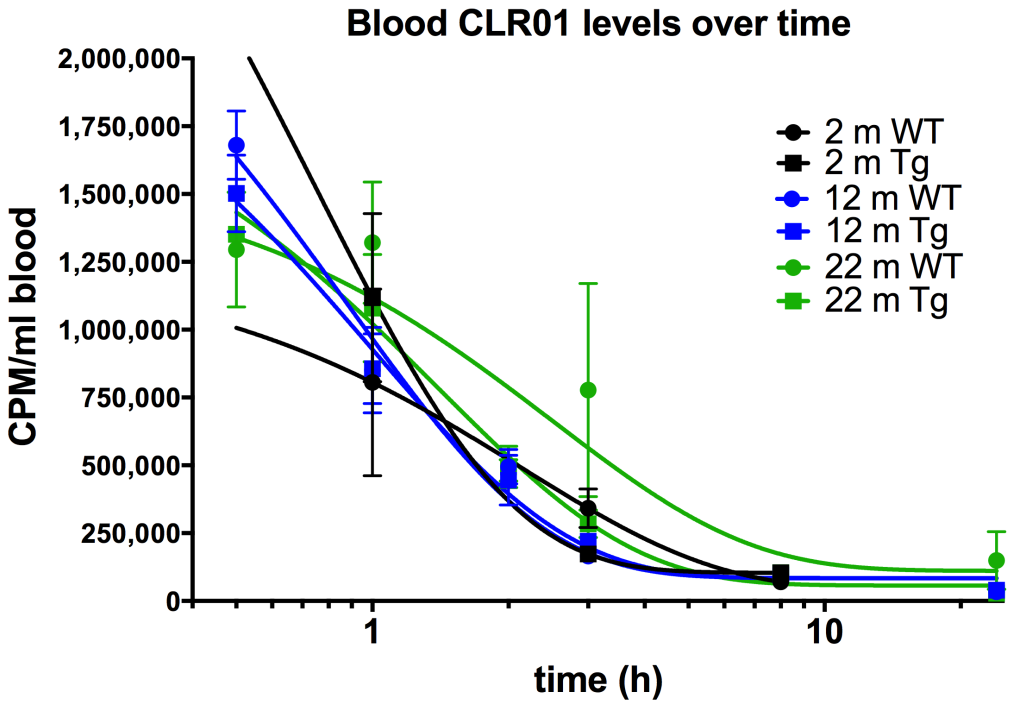

Figure 4.4 Blood CLR01 levels across groups and over time
CLR01 radioactivity levels are given per ml of blood for six groups and for times between 0.5−24 h. At 8 h post administration CLR01 levels drop to ~5−10% of values observed at 0.5 h. Data are given as mean ± SEM.

To correct for the radioactivity associated with blood ^{3}H-CLR01 in the brain vasculature, I performed both perfusion and subtraction analyses. In perfusion experiments, WT and 3×Tg mice at each of the three ages analyzed (n = 3 per group) were perfused with phosphate buffered saline following euthanasia. Perfusion lasted for either 5 min or until the liver changed color from a red to yellow, whichever was longer. In other experiments, mice were not perfused, but radioactivity associated with 10 µl of

blood per g of brain [29,30] was calculated based on brain weight and blood radioactivity levels and subtracted from brain radioactivity levels. At 1 h post injection, perfusion-corrected brain values were statistically similar to subtraction-corrected brain values (Figure 4.5). Due to difficulties associated with the perfusion analysis, specifically liver color being used as an indirect readout of brain perfusion level, and because including a perfusion step could increase variability among experiments, the rest of the experiments utilized the subtraction method, which is a common practice in BBB-permeability studies [29,30].

Brain-radioactivity levels, calculated as a percentage of blood-radioactivity levels (CPM/g)/(CPM/ml) at 1 h following the injection ranged from 0.86–3.09% depending on age and genotype (WT or 3×Tg, Figure 4.6). Analysis of brain penetration levels at 1 h by absence or presence of AD transgenes and by age showed an effect of age but not of genotype. Interestingly, 2-m old 3×Tg mice significantly differed from 12-m and 24-m old 3×Tg mice (2-m: 3.09 ± 0.55%; 12-m: 1.43 ± 0.17%; 24-m: 1.45 ± 0.28%; $p <$ 0.05), whereas in the WT group, the only significant difference was between the 2-

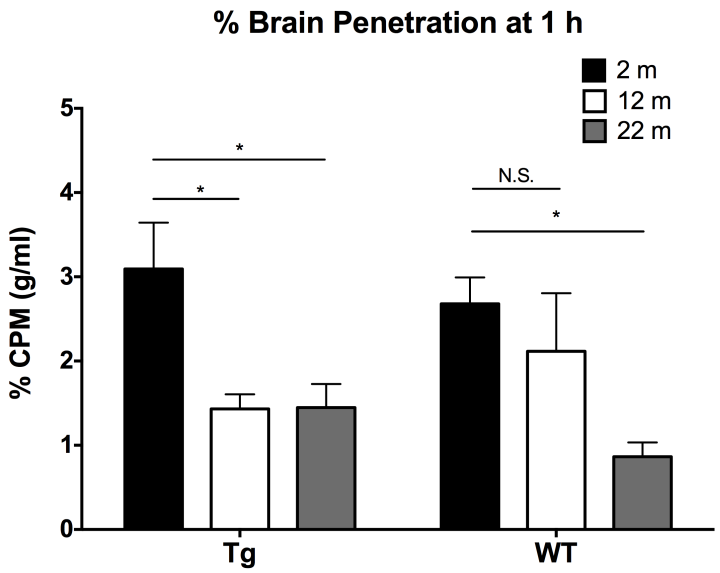

Figure 4.6 Percent brain penetration of CLR01 at 1 h
Percent of brain radioactivity per g was calculated as a function of blood radioactivity levels per ml at 1 h following IV administration of CLR01. Data are given as mean ± SEM. * $p < 0.05$.

m and 24-m old mice (2-m: 2.68 ± 0.31%; 12-m: 2.11 ± 0.69%; 24-m: 0.86 ± 0.17%; $p < 0.05$). This suggests that changes in BBB permeability occur earlier and more sharply in 3×Tg mice compared to WT mice.

A surprising finding was that although blood radioactivity levels declined rapidly (Figure 4.4), the radioactivity levels measured in the brain did not change significantly over 24 h (Figure 4.7). Brain radioactivity levels were insensitive to genotype or time after injection and thus the 24-h time point was assessed only in the 22-m old mice (both 3×Tg and WT) and the and 72-h time point was assessed only in the 22-m old WT mice. Differences were insignificant and likely represented experimental error. Furthermore,

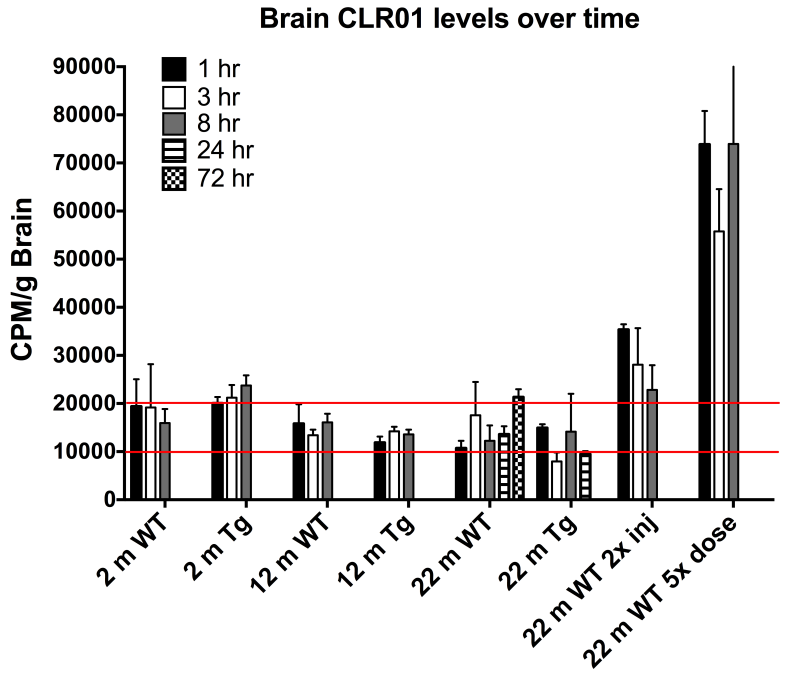

Figure 4.7 Brain CLR01 levels across groups and over time
CLR01 radioactivity levels are given per g of brain for eight groups and for times between 1−72 h. Most group×time combinations fall between 10,000−20,000 CPM/g. Double injection studies in aged WT mice show on average double the radioactivity levels of single injection group, 22 m WT. Aged WT mice dosed with 5× the amount of CLR01, show on average 5× the radioactivity levels of the 1× group, 22 m WT. Data are given as mean ± SEM.

brain radioactivity levels in 22-m old WT mice at 72-h post injection showed a similar value to the other time points, suggesting that brain CLR01 levels decline surprisingly slowly over 72 h.

To explore further the mechanics of CLR01 transport across the BBB, I asked whether the transport system was saturated. To answer this question, I injected 5-times the amount of total CLR01, keeping the ratio of ^{3}H-CLR01:CLR01 at 1:9, into 22-m old WT mice. This experiment resulted on average for all time points measured, in 5-times the absolute amount of radioactivity detected in the brain, including the correction for blood levels (Figure 4.7). The percentage of brain penetration at 1 h following the injection did not change (1× CLR01 brain penetration: 0.86 ± 0.30% of blood; 5× CLR01 brain penetration: 0.97 ± 0.28% of blood). This result suggests that the transport mechanism, whether active or passive, is concentration-dependent because there was an increase in the absolute value but not the relative value of CLR01 entering the brain.

To begin to explore whether additional dosing would increase the effective CLR01 concentration in the brain, I injected 22-m old WT mice twice over two equal time intervals and compared brain levels to mice that received one injection. On average, over the 1-, 3-, and 8-h time points measured, the amount of radioactivity found in the brain following the double-injection was twice the amount measured following the single-injection protocol (1 h: 3.3× compared to one injection, 3 h: 1.6×, 8 h: 1.9×; Figure 4.7). These data suggest that upon continuous dosing, as with the SC osmotic mini-pumps used in the efficacy study [5], CLR01 could reach sufficiently high brain concentration levels to inhibit Aβ aggregation even though the dose was relatively low — 40 μg/kg/day – when brain penetration levels are taken into account [5].

4.4.4 *In vitro* catabolism of CLR01

Previously, I reported that CLR01 was not degraded or metabolized for 1 h upon incubation at 37 ºC with human or mouse plasma or liver microsomes preparations [5]. The BBB permeability experiments described above used radioactivity as an indirect readout of CLR01 concentration levels, which could have reflected the parent compound, CLR01 itself, or metabolites. The question of the source of radioactivity seemed particularly important in view of the surprising persistence of radioactivity attributed to CLR01 in the brain. The most likely metabolism of CLR01 is cleavage of one or both phosphate groups resulting in monophosphate and hydroquinone derivatives, respectively (Figure 4.8). Each such dephosphorylation would decrease the polarity of the compound and increase its potential partition into the lipophilic brain parenchyma environment relative to the blood. In particular, the hydroquinone product is insoluble in aqueous solutions, in contrast to CLR01 and its monophosphate metabolite, which are soluble at millimolar concentrations. Thus, double dephosphorylation could result in precipitation

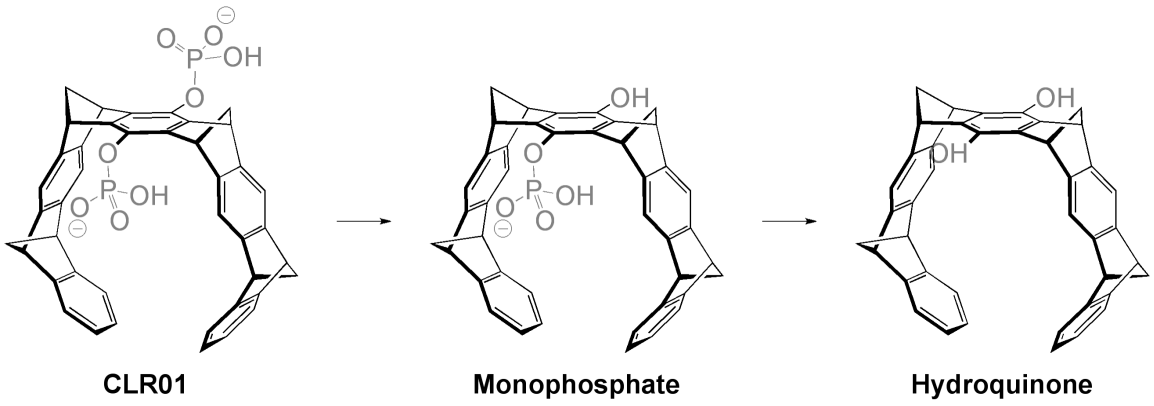

Figure 4.8 CLR01 dephosphorylation.
Molecular structure of successive CLR01 dephosphorylations at the bridgehead to monophosphate and then to hydroquinone.

and accumulation of the hydroquinone in the brain, potentially leading to misinterpretation of the BBB permeability data. Complete analysis of CLR01 metabolism in the brain was beyond the scope of the study described here. However, to evaluate the potential for dephosphorylation, I incubated CLR01 *in vitro* with ALP or brain extracts and measured the release of inorganic phosphate.

ALP is a widely distributed plasma membrane enzyme found in many tissues, which also can be released into body fluids [31]. The enzyme received its name because it shows optimal activity at pH ~9. There are four isoforms of ALP: intestinal, placental, germ cell, and tissue non-specific. All four isoforms are non-specific enzymes that catalyze the hydrolysis of a wide range of phosphate esters [32]. Tissue non-specific ALP concentration levels increase in both brain and plasma of patients with familial or sporadic AD relative to age-matched healthy individuals [33], possibly as a compensatory mechanism because the enzyme catalyzes tau dephosphorylation [34].

Because of its promiscuous hydrolysis activity, I tested whether calf intestinal ALP catalyzed CLR01 dephosphorylation by incubating the molecular tweezer with ALP and comparing the amount of inorganic phosphate released to a standard curve obtained by incubating ALP with increasing concentrations of a common substrate, p-nitrophenylphosphate. This standard curve had a detection sensitivity limit of 5 nmol. Incubation of 100 nmol CLR01 with ALP resulted in undetectable levels of inorganic phosphate.

To test whether CLR01 dephosphorylation might be catalyzed by brain phosphatases other than ALP, I incubated 50 nmol CLR01 with 1.5 mg of mouse-brain homogenate. The brain homogenate dephosphorylated the positive control substrate, p-

nitrophenylphosphate, at 99−130% of the activity of 0.8 enzymatic units of ALP. Similarly to the reaction with purified ALP, no release of inorganic phosphate was detected when the brain homogenates were incubated with CLR01 under the same conditions. Based on these results, dephosphorylation of CLR01 likely did not happen in our BBB permeability experiments and the radioactivity measured in mouse brains plausibly reflected CLR01 itself.

4.5 Discussion

Recently, I have reported that CLR01, an inhibitor of aberrant assembly and toxicity of amyloidogenic proteins [3], protected primary neurons from Aβ-induced decrease in synaptic spine density, basal synaptic activity, and long-term potentiation [5]. In addition, CLR01 treatment of 15-m old 3×Tg mice with 40 μg/kg/day CLR01 for 28 days resulted in decreased AD-related brain pathology, including amyloid plaques, neurofibrillary tangles, and microglia levels [5]. Following up on these promising efficacy data, here, I explored the putative process-specific mechanism of CLR01, its safety margin in mice, its BBB permeability and how it might be affected by age and disease, and the most likely route of CLR01 metabolism.

As stated above, no signs of toxicity have been observed in *in vivo* efficacy studies. To determine optimal dosing for subsequent studies, I sought to find out the median lethal dose, which would provide an upper limit for future dosing decisions. Effectively, I found that our highest acute dose of 100 mg/kg was not lethal but did elicit obvious behavioral signs of distress and liver damage (Table 4.1). Thus, chronic dosing at this concentration could lead to mortality. Importantly, I found that high doses of CLR01 had

no effect on brain, heart, lung, spleen, or kidney. Liver damage, found by both histology and serum analysis, was the main indicator of acute toxicity. These data will be used to direct monitoring for potential toxicity in future studies using higher doses than those used previously and potentially using species other than mouse.

In the chronic-administration experiment, the only meaningful finding was a decrease in cholesterol levels, which were still within the normal range, in the 10-mg/kg/day group (Table 4.1). This was an unexpected effect of CLR01 treatment, and may be of interest for further exploration especially for dual prevention or treatment of AD and high cholesterol, which may be prevalent in the elderly and is of significance since high cholesterol in middle age is associated with increased risk for AD [35,36]. Importantly, the chronically administered dose of 10 mg/kg/day is 250 times higher than the efficacious dose of 40 μg/kg/day [5] and thus provides a large safety margin. Additionally, concentrations up to 300 μM did not significantly affect the polymerization of tubulin *in vitro* (Figure 4.2), suggesting that CLR01 does not inhibit physiologic protein assembly unless the concentrations used are substantially higher than those needed for therapeutic effects. These findings support development of MTs in general and CLR01 in particular towards initiation of clinical trials.

It is important to note that animal dose should not be extrapolated to a human equivalent dose by conversion of body weight, but rather should be done by normalization to body surface area [37]. This method correlates well with several parameters of biology, including oxygen utilization, caloric expenditure, basal metabolism, blood volume, circulating plasma proteins, and renal function [38]. Thus, an

extrapolation using the body surface area suggests a dosing window between 0.04 – 10 mg/kg/day in mice corresponds to 0.003 − 0.81 mg/kg/day in humans.

Many of the properties of the BBB that determine the extent to which drugs are taken up by the brain are known to be altered in AD, such as disruption of tight junctions, decreased CSF reabsorption, decreased cerebral blood flow, and decreased efflux pump activity [16]. Similar BBB compromise has been reported in animal models of AD [24] [25], thus I set out to explore the differences in CLR01 brain penetration in both WT and the 3×Tg mouse model of AD. Because many of these properties, such as CSF reabsorption and BBB disruption, are not simply binary, I chose animals at three different ages, from 2−22-m, which correlate with different stages of disease progression to evaluate the effect of age and disease on drug uptake. Using ^{3}H-labeled CLR01, I found brain penetration levels between 1−3% in the different ages, whereas the absence or presence of AD transgenes had little effect on CLR01 uptake into the brain (Figure 4.6). There was no statistically significant interaction between age and presence of AD transgenes. However, I did find that 2-m old 3×Tg mice differed significantly from 12-m and 22-m old 3×Tg mice. In comparison, in the WT group, the only significant difference was between the 2-m and 22-m old mice. These data suggest that the presence of the AD-related transgenes expedites the disintegration of the BBB and thus increases the brain penetration of CLR01 by a small, but potentially meaningful, amount. Unexpectedly, I found higher penetration of CLR01 in the brains of the younger, rather than the older mice. One possible explanation of these findings, assuming the CLR01 enters the brain by a passive transport mechanism, is that the increased BBB permeability observed at old age results in faster leakage of CLR01 out of the brain than in the young mice.

Alternatively, CLR01 may be taken up by a serendipitous active transport system that is more efficient in the young mice than in older mice.

The observation that brain radioactivity did not decline with time (Figure 4.7) was peculiar. Linear regression analysis of the values between 1 − 72 h for the 22-m old WT mice resulted in a slope that was not significantly different from zero. This unexpected behavior raised a concern for a systematic error producing these data. However, both the double-injection-, and the 5×-dose experiments showed a linear increase in brain radioactivity, suggesting that the radioactivity measured in the brain reflected *bona fide* uptake of CLR01 through the BBB. Another concern was that the radioactivity measured in the brain actually came from residual blood that was not accounted for by either perfusion or subtraction of the expected values. However, the observations that blood radioactivity decreased to ~5% of the starting values by 8 h (Figure 4.4) without a correlating decrease in brain radioactivity, which remained steady over that same period, indicated that the radioactivity measured in the brain was not related to residual blood levels. Lastly, actual sample counts (~500 CPM and larger) were well above the minimum sensitivity of the liquid scintillation counting system (background is < 150 CPM). Thus, the radioactivity measured in the brain reflected the actual ^{3}H-CLR01 levels that penetrated the brain.

This fact that CLR01 penetration levels were consistent among groups and persistent over time suggests that CLR01 enters the brain and accumulates with parameters that are age-specific, as age was seen to be a significant variable in Figure 4.6. The indefinite accumulation of CLR01 in any tissue is not ideal and thus requires further exploration regarding whether the accumulation is of the parent compound or a metabolite, and

regarding any long-term toxic effects of this accumulation. One possible mechanism by which CLR01 passes across the BBB is by binding to K residues on receptors that span the membrane or get endocytosed. An analysis of the amino acid sequence of four major human cellular receptors involved in transferring cargo across the BBB – transferrin, low density lipoprotein receptor-related protein 1, glucose transporter 1, and large neutral amino acid transporter – revealed that K makes up about 3.3−6.6% of their sequences. If these K residues are exposed and are positioned within the receptor's channel, or get endocytosed upon ligand binding, they may allow CLR01 to "hitchhike" its way across membranes and across the BBB through its labile binding to these receptors and potentially through the transport of the natural cargo.

The studies presented here can help calculate the extent to which CLR01 enters the brain and compare the resulting expected concentrations of CLR01 with reported concentration of brain Aβ. Based on the experiments using SC pumps in which 0.7% of the administered CLR01 was detected in the blood at steady-state [39], the brain penetration of ~2% of blood levels found here, and the efficacy studies in the 15-m old 3×Tg mice using a 40-μg/kg/day dose [5], I estimate that ~200 fmol of CLR01 enters the brain per day. A literature search for brain concentration levels of Aβ40 and Aβ42 resulted in reported values from zero to a maximum of 280 fmol/mg brain [19]. The masses of the mouse brains used in our studies were ~0.5 mg. Thus, a total of 140 fmol Aβ may be found at a given point in 13-m old 3×Tg mice [19]. Upon accumulation of CLR01 in the brain, as I observed in the double-injection experiment, the concentration levels of CLR01 entering the brain at a 40-μg/kg/day dose and of Aβ are expected to be on the same order of magnitude, specifically, in the range of hundreds of fmols. This is

not to suggest that CLR01 does not interact with all K residues on any protein, it probably does. However, the high on-off rate of CLR01 for K residues is thought to disrupt the aberrant folding process in a way that can be thought of as resetting the clock. Thus, unlike other drugs that need to continuously engage their targets, CLR01 does not and thus less CLR01 than all of the K residues in the brain could still be effective. Additionally, the accumulation of CLR01 in the brain over time would also help address concerns about the comparative stoichiometry of CLR01 to the total number of K residues in the brain. Overall, this analysis suggests that the intracranial Aβ:CLR01 stoichiometry achieved in our study in which I found substantial decrease in AD-like pathology [5] was similar to the stoichiometry used in previous *in vitro* and cell culture experiments [3] providing strong support for the putative mechanism of action of CLR01.

The estimate of 200 fmol of CLR01 entering the brain per day upon administration of 40 μg/kg/day [5] is a conservative one, when considering two additional factors. First, the levels of CLR01 detected in the plasma following an IV injection, which is considered 100% bioavailable, were about 30% of amount injected. Thus, the amount detected may reflect the limitation of the detection method and the actual CLR01 concentration in the blood may be higher. Second, the cerebrovascular volume of the 3×Tg mice at 11-m of age has been shown to be 26% lower than that of non-transgenic littermates, potentially due to cerebrovascular amyloid deposition [40]. I did not take this difference into account in our correction for cerebral blood when calculating brain radioactivity and thus might have biased our data to reflect lower radioactivity in the older 3×Tg mice than actual values. Taking these potential biases into account lends additional support to the suggested mechanism of action of CLR01 *in vivo*.

An important question for development of CLR01 and/or other MT derivatives as therapeutic drugs is what the active pharmaceutical ingredient is. *In vitro* data suggest that binding of CLR01 itself to free K residues is what modulates the self-assembly of amyloidogenic proteins into non-amyloidogenic, non-toxic species. However, *in vivo*, CLR01 may be metabolized in currently unknown ways and the active pharmaceutical ingredient may be a metabolite. To examine potential CLR01 metabolism, previously, I tested the stability of the compound in mouse and human, plasma and liver microsomes and found 100% stability in all preparations. To explore the question of stability and potential metabolism further, here, Dr. Bitan hypothesized that the phosphate groups would be the most likely targets of metabolism and therefore asked whether they are substrates for dephosphorylation by ALP or other brain phosphatases. The question was of particular importance in view of the reported increase in ALP concentration in both brain and plasma of patients with AD relative to healthy individuals [33]. I tested the potential dephosphorylation of CLR01 under stringent conditions of excess ALP in buffer and did not find release of inorganic phosphate upon incubation of CLR01 with either the purified phosphatase or the brain extracts. A plausible explanation for the observed stability of CLR01's phosphate groups to enzymatic dephosphorylation is the rigid structure of the hydrocarbon backbone of the compound (Figure 4.1), which likely prevents its accommodation in the active sites of phosphatases.

Process-specific modulation of amyloid protein assembly is a useful approach that can be adopted for a multitude of amyloidoses. The beneficial therapeutic effects of CLR01 have been demonstrated in mouse models of AD and familial amyloidotic polyneuropathy, and a zebrafish model of Parkinson's Disease. Here, I found a favorable

safety profile and small yet persistent brain penetration – a formidable starting point for future formal development of CLR01 towards human therapy. Concurrently, Dr. Bitan and colleagues are investigating the effects of CLR01 in several other amyloidoses, some of which do not require brain penetration, and thus the findings of low toxicity for an artificial K-receptor are paramount for our future investigations.

In line with the drive towards full pre-clinical evaluation of CLR01 for AD therapy, the next major goal is to assess whether CLR01 results in functional improvement in learning and memory in animal models of AD. The next chapter describes the validation and optimization of testing memory deficits in the 3×Tg mouse model using the Barnes maze test.

4.6 References

1. (2008) Research Highlights. Chemical biology: Aggravating aggregating. Nature 451: 608-609.

2. Roberts BE, Shorter J (2008) Escaping amyloid fate. Nat Struct Mol Biol 15: 544-546.

3. Sinha S, Lopes DH, Du Z, Pang ES, Shanmugam A, et al. (2011) Lysine-specific molecular tweezers are broad-spectrum inhibitors of assembly and toxicity of amyloid proteins. Journal of the American Chemical Society 133: 16958-16969.

4. Prabhudesai S, Sinha S, Attar A, Kotagiri A, Fitzmaurice AG, et al. (2012) A novel "molecular tweezer" inhibitor of α-synuclein neurotoxicity in vitro and in vivo. Neurotherapeutics 9: 464-476.

5. Attar A, Ripoli C, Riccardi E, Maiti P, Li Puma DD, et al. (2012) Protection of primary neurons and mouse brain from Alzheimer's pathology by molecular tweezers. Brain 135: 3735-3748.

6. Fokkens M, Schrader T, Klärner FG (2005) A molecular tweezer for lysine and arginine. Journal of the American Chemical Society 127: 14415-14421.

7. Talbiersky P, Bastkowski F, Klärner FG, Schrader T (2008) Molecular clip and tweezer introduce new mechanisms of enzyme inhibition. Journal of the American Chemical Society 130: 9824-9828.

8. Acharya S, Safaie B, Wongkongkathep P, Ivanova MI, Attar A, et al. (2013) Molecular Basis for Preventing α-synuclein Aggregation by a Molecular Tweezer. Submitted for publication.

9. Bier D, Rose R, Bravo-Rodriguez K, Bartel M, Ramirez-Anguita JM, et al. (2013) Molecular tweezers modulate 14-3-3 protein-protein interactions. Nat Chem 5: 234-239.

10. Dutt S, Wilch C, Gersthagen T, Talbiersky P, Bravo-Rodriguez K, et al. (2013) Molecular tweezers with varying anions: a comparative study. J Org Chem 78: 6721-6734.

11. Attar A, Bitan G (2013) Disrupting Self-Assembly and Toxicity of Amyloidogenic Protein Oligomers by "Molecular Tweezers"- from the Test Tube to Animal Models. Curr Pharm Des: In press.

12. Sinha S, Lopes DH, Bitan G (2012) A Key Role for Lysine Residues in Amyloid β-Protein Folding, Assembly, and Toxicity. ACS Chem Neurosci 3: 473-481.

13. Ferreira N, Pereira-Henriques A, Attar A, Klärner F-G, Schrader T, et al. (2013) Molecular Tweezers Targeting Transthyretin Amyloidosis. Submitted for publication.

14. Sinha S, Du Z, Maiti P, Klärner FG, Schrader T, et al. (2012) Comparison of three amyloid assembly inhibitors: the sugar scyllo-inositol, the polyphenol epigallocatechin gallate, and the molecular tweezer CLR01. ACS Chem Neurosci 3: 451-458.

15. Zeevi N, Pachter J, McCullough LD, Wolfson L, Kuchel GA (2010) The blood-brain barrier: geriatric relevance of a critical brain-body interface. Journal of the American Geriatrics Society 58: 1749-1757.

16. Banks WA (2012) Drug delivery to the brain in Alzheimer's disease: consideration of the blood-brain barrier. Advanced Drug Delivery Reviews 64: 629-639.

17. Zipser BD, Johanson CE, Gonzalez L, Berzin TM, Tavares R, et al. (2007) Microvascular injury and blood-brain barrier leakage in Alzheimer's disease. Neurobiology of Aging 28: 977-986.

18. Farrall AJ, Wardlaw JM (2009) Blood-brain barrier: ageing and microvascular disease--systematic review and meta-analysis. Neurobiology of Aging 30: 337-352.

19. Oddo S, Caccamo A, Shepherd JD, Murphy MP, Golde TE, et al. (2003) Triple-transgenic model of Alzheimer's disease with plaques and tangles: intracellular Aβ and synaptic dysfunction. Neuron 39: 409-421.

20. Maegawa T, Hirota K, Tatematsu K, Mori Y, Sajiki H (2005) Facile and efficient postsynthetic tritium labeling method catalyzed by Pd/C in HTO. J Org Chem 70: 10581-10583.

21. Shelanski ML, Gaskin F, Cantor CR (1973) Microtubule assembly in the absence of added nucleotides. Proc Natl Acad Sci U S A 70: 765-768.

22. Lee JC, Timasheff SN (1977) In vitro reconstitution of calf brain microtubules: effects of solution variables. Biochemistry 16: 1754-1764.

23. Loeb W, Quimby FW, editor (1999) The Clinical Chemistry of Laboratory Animals. 2nd ed. Philadelphia, PA: Taylor and Francis.

24. Ujiie M, Dickstein DL, Carlow DA, Jefferies WA (2003) Blood-brain barrier permeability precedes senile plaque formation in an Alzheimer disease model. Microcirculation 10: 463-470.

25. Zhang X, Li G, Guo L, Nie K, Jia Y, et al. (2013) Age-related alteration in cerebral blood flow and energy failure is correlated with cognitive impairment in the senescence-accelerated prone mouse strain 8 (SAMP8). Italian Journal of Neurological Sciences.

26. Billings LM, Oddo S, Green KN, McGaugh JL, LaFerla FM (2005) Intraneuronal Aβ causes the onset of early Alzheimer's disease-related cognitive deficits in transgenic mice. Neuron 45: 675-688.

27. Clinton LK, Blurton-Jones M, Myczek K, Trojanowski JQ, LaFerla FM (2010) Synergistic Interactions between Aβ, tau, and α-synuclein: acceleration of neuropathology and cognitive decline. Journal of Neuroscience 30: 7281-7289.

28. Mastrangelo MA, Bowers WJ (2008) Detailed immunohistochemical characterization of temporal and spatial progression of Alzheimer's disease-related pathologies in male triple-transgenic mice. BMC Neurosci 9: 81.

29. Friden M, Ljungqvist H, Middleton B, Bredberg U, Hammarlund-Udenaes M (2010) Improved measurement of drug exposure in the brain using drug-specific correction for residual blood. Journal of Cerebral Blood Flow and Metabolism 30: 150-161.

30. Dagenais C, Rousselle C, Pollack GM, Scherrmann JM (2000) Development of an in situ mouse brain perfusion model and its application to mdr1a P-glycoprotein-deficient mice. Journal of Cerebral Blood Flow and Metabolism 20: 381-386.

31. Moss DW (1997) Physicochemical and pathophysiological factors in the release of membrane-bound alkaline phosphatase from cells. Clin Chim Acta 257: 133-140.

32. Millan JL, Fishman WH (1995) Biology of human alkaline phosphatases with special reference to cancer. Crit Rev Clin Lab Sci 32: 1-39.

33. Vardy ER, Kellett KA, Cocklin SL, Hooper NM (2012) Alkaline phosphatase is increased in both brain and plasma in Alzheimer's disease. Neuro-degenerative Diseases 9: 31-37.

34. Goldbaum O, Richter-Landsberg C (2002) Activation of PP2A-like phosphatase and modulation of tau phosphorylation accompany stress-induced apoptosis in cultured oligodendrocytes. Glia 40: 271-282.

35. Qiu C (2012) Preventing Alzheimer's disease by targeting vascular risk factors: hope and gap. Journal of Alzheimer's Disease 32: 721-731.

36. Strand BH, Langballe EM, Hjellvik V, Handal M, Naess O, et al. (2013) Midlife vascular risk factors and their association with dementia deaths: results from a Norwegian prospective study followed up for 35 years. J Neurol Sci 324: 124-130.

37. Center for Drug Evaluation and Research CfBEaR (2005) Estimating the safe starting dose in clinical trials for therapeutics in adult healhty volunteers. In: Administration USFaD, editor. Rockville, Maryland.

38. Reagan-Shaw S, Nihal M, Ahmad N (2008) Dose translation from animal to human studies revisited. FASEB journal : official publication of the Federation of American Societies for Experimental Biology 22: 659-661.

39. Lopes DHJ, Attar A, Du Z, McDaniel K, Dutt S, et al. (2013) The molecular tweezer CLR01 inhibits islet amyloid polypeptide assembly and toxicity via an unexpected mechanism. Submitted for publication.

40. Bourasset F, Ouellet M, Tremblay C, Julien C, Do TM, et al. (2009) Reduction of the cerebrovascular volume in a transgenic mouse model of Alzheimer's disease. Neuropharmacology 56: 808-813.

Chapter 5

A Shortened Barnes Maze Protocol Reveals Memory Deficits at 4-Months of Age in the Triple-Transgenic Mouse Model of Alzheimer's Disease

5.1 Abstract

Alzheimer's disease (AD) is a progressive neurodegenerative disease that manifests as memory loss, cognitive dysfunction, and dementia. Animal models of AD have been instrumental in understanding the underlying pathological mechanism and in evaluation of potential therapies. The triple transgenic (3×Tg) mouse model of AD is unique because it recapitulates both pathologic hallmarks of AD — amyloid plaques and neurofibrillary tangles. The earliest cognitive deficits in this model have been shown at 6-m of age by most groups, necessitating aging of the mice to this age before initiating evaluation of the cognitive effects of therapies.

To assess cognitive deficits in the 3×Tg mice, originally I employed a typical Barnes maze protocol of 15 training trials, but found no significant deficits in aged mice. Therefore, I shortened the protocol to include only 5 training trials to increase difficulty. I found cognitive deficits using this protocol using mainly measures from the probe day, rather than the training trials. This also decreased the effort involved with data analysis. I compared 3×Tg and wild-type mice at 4-m- and 15-m of age using both the original, long

training, and the short training paradigms. I found that differences in learning between 3×Tg and wild-type mice disappeared after the 4th training trial. Measures of learning and memory on the probe day showed significant differences between 3×Tg and wild-type mice following the short, 5-training trial protocol but not the long, 15-training trial protocol. Importantly, I detected cognitive dysfunction already at 4-m of age in 3×Tg mice using the short Barnes-maze protocol. The ability to test learning and memory in 4-m old 3×Tg mice using a shortened Barnes maze protocol offers considerable time and cost savings and provides support for the utilization of this model at pre-pathology stages for therapeutic studies.

5.2 Introduction

In this dissertation, Chapter 2 described the *in vitro* studies done on CLR01's interaction with amyloidogenic proteins that identified its anti-aggregation and anti-toxicity properties and described an *in vivo* study in a zebrafish model of α-synuclein toxicity. Chapter 3 detailed an extension of the *in vitro* studies that showed that CLR01 could protect primary neurons and brain slices from Alzheimer's Disease (AD) associated structural and functional synaptotoxicity. Furthermore, Chapter 3 reported an *in vivo* study of CLR01 performed with a triple transgenic (3×Tg) mouse model of AD where peripheral administration of CLR01 resulted in central alleviation of the hallmarks of AD – amyloid plaque and hyperphosphorylated tau load and microglia levels. Chapter 4 presented the systematic assessment of both the acute and chronic toxicity profile of CLR01, which failed to reach a lethal dose with both chronic dosing of 250-fold the previously utilized efficacious dose and with acute dosing of 2500-fold. Acute toxicity

manifested as liver damage. Blood-brain barrier penetration of CLR01 was found to be 1–3% in mice depending on age but sustained over 72 h, which supported the previously utilized low level dosing method. The next critical step in the development of CLR01 for AD therapy is to assess its functional efficacy in the form of an influence on cognitive function *in vivo*, more specifically on memory. As the Bitan lab has not performed studies of rodent memory in the past, the first step towards this goal was to validate the utility of the behavioral test and the deficits in the mouse model to be used within the context of the resources − equipment, setup, and personnel − of the Bitan lab.

Learning and memory deficits are relatively difficult to assess compared to other phenotypes, and although there is an abundance of papers describing cognitive deficit assessment in models of AD, replicating these studies *de novo* based on the literature often is challenging. Our comprehensive literature search resulted in Barnes maze [1] protocols with high variability of training periods, ranging from 4 d [2] to 15 d [3]. In addition, the age by which particular animal models of AD display cognitive deficits varies substantially, not only among models, but also in a particular model tested by different groups [2,4-7].

In addition to these challenges, assessing cognitive deficits in animal models is quite costly. For example, a new researcher embarking on assessment of learning and memory in a mouse model of AD using the Barnes maze at 8-m of age, who is paying animal *per diem* costs and minimum wage to a technician should expect to pay approximately $30,500 to establish the technique in their laboratory [Barnes maze – ~$2500; video hardware and behavior detection software – ~$8,000; aging animals – ~$1.25/day for 8-m for 60 mice = $18,000; minimal colony maintenance, running an 8 d

protocol and then analyzing 8 d of recorded behavior – ~250 h paid at minimum wage ($8.00 in California) = $2000], in addition to the cost of obtaining and breeding the mice and many smaller but numerous expenses required for establishing a working system. If the mice need to be aged to an older age, as in the case of the 3×Tg model [8], which according to the literature often is used at 10-m of age or older to show convincing deficits [9-11] compared to control wild-type (WT) animals, the costs increase substantially.

The Barnes maze originally was developed by Carol Barnes for use with rats [1] to overcome the stress induced by swimming in the Morris water maze (MWM) [12], and later was adapted for mice [13]. During the task, animals are placed in the middle of a circular table containing holes around the edges and receive negative reinforcement, in the form of bright lights, an exposed environment, loud buzzing, and sometimes air jets [14,15], motivating them to escape to a dark cage hidden underneath one of the holes. Similar to the MWM, the Barnes maze allows for evaluation of spatial reference memory and learning [16], but without inducing despair and anxiety that commonly are seen in the water maze in the form of floating and thigmotaxis [17-19]. At the same time, compared to the MWM, learning in the Barnes maze may be slow, and exploration high, due to the modest nature of the motivating stimuli [16]. Notwithstanding these differences between the two tests, many AD studies using mice have utilized the Barnes maze successfully to assess spatial memory [3,20-23].

Typical Barnes maze protocols consist of a habituation phase, in which the mouse is introduced to the environment and task, a training phase where the mouse is given numerous trials to learn the task, and a probe phase, typically performed following a 24-h

delay, in which the mouse is tested for remembering what had been previously learned. Acquisition in the training phase typically is assessed as a decrease in latency and in the number of erroneous holes searched (HS) before finding the target hole, though not necessarily going into the escape cage. Entering the escape cage through the target hole often is not used as an end-point because, unlike in the water maze, the environment is not aversive enough to require immediate escape and mice may continue to explore after having identified the target hole. Other measures, such as path length or speed, also may be used [16,24]. Long-term memory is evaluated in the probe phase, which occurs following training and a delay, by removing the escape cage and observing search behavior for a set amount of time. It is assumed that mice that remember the location of the escape cage will have a shorter latency to reach the previous location of the escape cage and will search fewer holes. Practically, this is measured as the time spent HS in the target quadrant. A mouse with intact memory is expected to spend more than 25% (chance level) of their time in the target quadrant.

The 3×Tg mouse model of AD was developed in 2003 by the La Ferla group [8] and is unique in manifesting both amyloid plaques and neurofibrillary tangles in the brain. Thus, this model recapitulates the hallmark lesions of AD more closely than models that have only plaques or only tangles. The 3×Tg model, which harbors two familial AD mutations, APP(Swe) and PS1(M146V), and the tau(P301L) mutation found in frontotemporal dementia, has been integral in studies of the relationship between amyloid β-protein (Aβ) and tau [25,26], and has been used to assess the role of intraneuronal Aβ [27,28] and several potential therapies for AD [29,30]. Studies by the LaFerla group on the cognitive deficits of this model have suggested that memory

acquisition and retention were convincingly impaired starting at 4-m of age using either the MWM or the Barnes maze [4,27]. However, other groups have not replicated deficits at this age. The youngest age at which groups other than LaFerla's have found deficits is 6-m of age using the MWM, WWWhich test, and/or nesting behavior [7,31,32]. Studies using the Barnes maze to assess the spatial reference learning and memory in the 3×Tg model found deficits at 4-m, 11-m, or 12-m of age [2,5,6]. These studies did not utilize the probe phase for measuring cognitive deficits. The one study in which deficits were found at 4-m of age was reported by the LaFerla group, who found that measures of latency showed progressive impairment with age but measures of error did not [2]. Frazer et al., who reported deficits at 11-m of age, did not detect deficits at 2-m or 6-m of age. In their study, all the animals were injected with a herpes simplex virus amplicon vaccine, thus a completely naïve control was only available for the 2-m group [5]. A study by Banaceur et al., in which deficits were found at 12-m of age, used only one age group, male mice, and only reported the measure of latency for training trials [6]. Potentially, the differences in Barnes maze protocols utilized in the above studies may have contributed to the different age of deficit onset observed.

Here I present an improved protocol, which allows testing learning and memory in the 3×Tg mouse model of AD using a short training paradigm at a young age, resulting in substantial saving of cost and time. To cut down the high costs, I constructed a homemade Barnes maze (<$300), devised a shortened training protocol consisting of only two training days, and used manual analysis of time and HS on only the probe day. Using this method, I found memory deficits in the 3×Tg model not only at 15-m of age but also at 4-m of age.

It is also our goal here to present some of the idiosyncrasies involved with this method. As I have been developing our protocol, I often encountered situations that either are not addressed in the literature or are not described in enough detail, and thus had to use our own judgment. I hope to lead by example by including our observations, such as the value of examining the range or median of data, which may not be directly results-related, but provide valuable insight and hope that these details are of value to other groups.

5.3 Materials and Methods

Animals

All procedures were compliant with the National Research Council Guide for the Care and Use of Laboratory Animals, and approved by the UCLA Institutional Animal Care Use Committee. 3×Tg and WT mice were bred at UCLA. Mice were housed 2–4 per cage under standard conditions, maintained on a 12-h dark and 12-h light cycle with *ad libitum* access to rodent chow and water, randomized, and handled under the same conditions by two investigators. Mixed-gender mice were tested at 4-m- and 15-m of age with n=14–32 mice per group and a minimum of n=7 of each gender per group.

Barnes Maze

Barnes maze was administered to assess cognitive deficits in learning and memory of 3×Tg mice compared to the WT group. The maze was made from a circular, 13-mm thick slab of white polyvinyl chloride with a diameter of 48” (Figure 5.1). Twenty holes with a diameter of 1.75” were made on the perimeter at a distance of 1” from the

edge. This circular platform was then mounted on top of a rotating stool, 35” above the ground and balanced.

The escape cage was made by using a mouse cage and assembling a platform and ramp 1.25” below the surface of the maze. The platform, made of a square petri dish, and ramp, made of laminated cardboard, were made out of plastic to be easily cleanable with 70% ethanol. The outside of the walls of the cage was covered with black paper to make the inside of the cage dark and thus attractive to the mice. The maze was placed in the center of a dedicated room and two 120 W lights were placed on the edges of the room facing towards the ceiling about 3/4 of the way up from the floor and about 3–5 feet away from the maze. Eight simple colored-paper shapes (squares, triangles, circles) were mounted

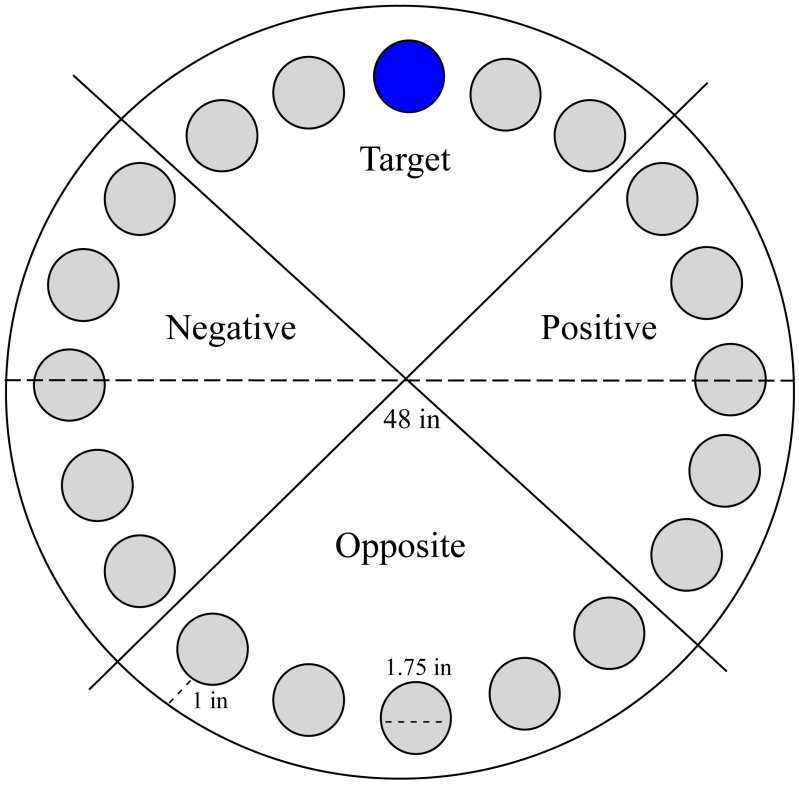

Figure 5.1: Barnes maze diagram with quadrants
The Barnes maze is made up of a circular platform, 48” in diameter, with 20 equally spaced holes around the periphery. The holes are 1” away from the edge and have a 1.75” diameter. The maze is divided into 4 quadrants labeled Target, Positive, Opposite, and Negative with the escape hole being in the center of the Target quadrant.

around the room as visual cues, in addition to the asymmetry of the room itself. After testing each mouse, the cleaning of the quadrant of the maze around the target hole was alternated with cleaning the whole maze, using 70% ethanol. The maze was rotated clockwise after every 3 mice to avoid intra-maze odor or visual cues. All sessions were recorded using COP Security Monochrome CCD Camera (Model 15-CC20) and MyTV/x software (Eskape Labs).

The animals interacted with the Barnes maze in three phases: habituation (1 day), training (2–4 days in the short or long training paradigms, respectively; Table 5.1), and probe (1 day). Before starting each experiment, mice were acclimated to the testing room for 1 h. Then all mice (n=2–4) from one cage were placed in individual holding cages where they remained until the end of their testing sessions. Holding cages were used during the experiment to control for potential artifacts that could result from housing some mice only two per cage, where one mouse remained alone while the other mouse was being tested, compared to other mice that were housed four per cage and therefore never were left on their own. Additionally, using holding cages prevented potential influence by mice that had already completed the test on the mice waiting for their turn. After all mice from one home cage completed testing for the day, they were placed back

Table 5.1: Comparison of short and long training paradigms

	Training duration (min)	Probe trial duration (min)	# of training trials	# of training days	Total protocol time (days)*
Short paradigm	2	2	5	2	4
Long paradigm	2	2	15	4	6

* Total time does not include the day of rest between training and probe phases.

in their home cage together, the holding cages were cleaned, and the next set of mice was separated into individual holding cages.

On the habituation day, the mice were placed in the center of the maze underneath a clear 3,500-ml glass beaker for 30 s while white noise was played through a sound system. Then, the mice were guided slowly by moving the glass beaker, over 10–15 s to the target hole that leads to the escape cage. The mice were then given 3 min to independently enter through the target hole into the escape cage. If they did not enter on their own during that time, they were nudged with the beaker to enter. Getting the mice to enter the escape cage is key in "showing" them that the escape cage exists and gives them practice in stepping down to the platform in the cage. The mice were allowed to stay in the escape cage for 1 min before being returned to the holding cage. Once all animals had completed the 1-session habituation, they were all returned to their home cage.

In the training phase, mice were placed inside an opaque cardboard cylinder, 10" tall and 7" in diameter, in the center of the Barnes maze for 15 s. This allowed the mice to be facing a random direction when the cylinder was lifted and the trial began. At the end of the holding period, a buzzer was turned on, the cylinder was removed, and the mice were allowed to explore the maze for 2 min (Table 5.1). If a mouse found the target hole, the end-point of the trial, and entered the escape cage during that time, it was allowed to stay in the escape cage for 1 min before being returned to the holding cage. If it did not find the target hole, the mouse was guided to the escape hole using the glass beaker and allowed to enter the escape cage independently. If it did not enter the escape cage within 3 min, it was nudged with the beaker until it did. If a mouse still did not enter the escape cage after 1 min of nudging, it was picked up and manually put on the

platform in the escape cage. Then it was allowed 1 min inside the escape cage before being returned to the holding cage. In all cases, the buzzer was turned off once the mouse entered the escape cage. This process typically took 5–7 min per mouse and was done with four mice at a time, providing a 20–30 min inter-trial interval. The total number of trials used was 5 for short training, 3 trials on training day 1 and 2 trials on training day 2, or 15 for long training with 3 trials on day 1 and 4 trials for days 2−4 (Table 5.1). During the training phase, measures of primary latency and primary HS were recorded. Primary latency was defined as the time to identify the target hole the first time, as mice did not always enter the hole upon first identifying it. HS was defined as nose pokes and head deflections over any hole. Primary HS was defined as the HS before identifying the target hole for the first time. Parameters were assessed by blinded observers. About 70% of the measures were randomly reassessed by a second blinded observer to identify potential inaccuracies. Differences between the two observers were insignificant in all cases. In all the cases in which two observers scored the raw data, their scores were averaged.

On the probe day, 48 h after the last training day, the escape cage was removed, mice were placed inside the opaque cylinder in the center of the maze for 15 s, the buzzer was turned on and the cylinder removed. Each mouse was given 2 min to explore the maze, at the end of which, the buzzer was turned off and the mouse was returned to its holding cage. During the probe phase, measures of time spent per quadrant and HS per quadrant were recorded. For these analyses, the maze was divided into quadrants consisting of 5 holes with the target hole in the center of the target quadrant (Figure 5.1). The other quadrants going clockwise from the target quadrant were labeled: positive, opposite, and negative.

An observation of potential value is that 8 mice at 15-m of age and 2 mice at 4-m of age fell off the Barnes table during the training trials on the first day of training. Typically, they fell through one of the holes by attempting to extend their view and not off the edge. Initially, they were placed back in the center of the maze and the study continued. However, these mice were excluded from data analysis. It remains to be determined what this observation may signify.

Statistics

Data are shown as means ± standard error of the mean. Statistical analysis was performed using Prism 6.0c (GraphPad, La Jolla, CA). Student's unpaired *t*-test and 2-way repeated measures ANOVA followed by Fisher's Least Significant Difference *post-hoc* analysis were used for probe day and training trials data, respectively. The level of significance was set at $p < 0.05$.

5.4 Results

5.4.1 Training trials – Comparison of 15 trials versus 5 trials

I began our use of the Barnes maze because I was interested in assessing the cognitive benefits of small molecule aggregation inhibitors for AD therapy [33]. Based on our extensive literature search on the Barnes maze in AD models, I developed a 15-training trial protocol and following its execution, found that either our 3×Tg mice did not have cognitive deficits compared to WT mice or the test was not sensitive enough to detect the deficits.

Our analysis of the training day latencies in the initial long-training paradigm, which included 15 training trials showed that consistent differences in latency between

the WT and 3×Tg groups existed only in the first 4 trials followed by stochastic values in the remaining trials, especially for the 3×Tg group (Figure 5.2A). Repeated-measures ANOVA with *post-hoc* analysis showed significant differences on trials 2, 4, and 12, yet examination of the entire trend suggested that the difference observed on trial 12 likely was coincidental. Thus, I hypothesized that much of the training after trial 4 was redundant and leading to elimination of cognitive difference between the groups. Thus, I developed a shortened Barnes maze paradigm to test this hypothesis.

Short training, consisting of 5 trials, of 15-m old mice showed significant differences between WT and 3×Tg mice on trials 2 and 5 (Figure 5.2B). Latency measures in 4-m old mice administered short training showed a significant difference between groups on trial 2 (Figure 5.2C). Based on these data, I argue that latency data from training days is not robust enough to establish meaningful differences and is greatly influenced by the high variability of the system, resulting in potentially false positive data. Many studies examine, or even only examine, differences in latency or HS between groups on training days. Though these measures can illuminate differences between groups, the differences often occur on only one or two of many training trials. Our study suggests that relative to the value gained, the time and effort required for analysis of training days is not an efficient use of resources.

Because in the long-training paradigm the latency means for trials 5–15 were highly variable within each group, I asked whether the range of latencies might offer additional information. The range of latencies for WT and 3×Tg mice in trials 5–15 was 34–58 s and 18–64 s, respectively. This suggested that the 3×Tg mice actually reached a

shorter average latency (on trial 12) than the WT mice, which seemed counterintuitive. However, when the raw latency values for the mice were evaluated, it became evident that this observation was due to an artifact created by using the arithmetic mean population descriptor (i.e., the average of the population). This causes larger numbers to have a larger weight even though a more reasonable analysis would give each animal's latency value the same weight. Thus, I posit that the median is a better population descriptor in this situation. Comparison of the

Figure 2: Training Trials Latency

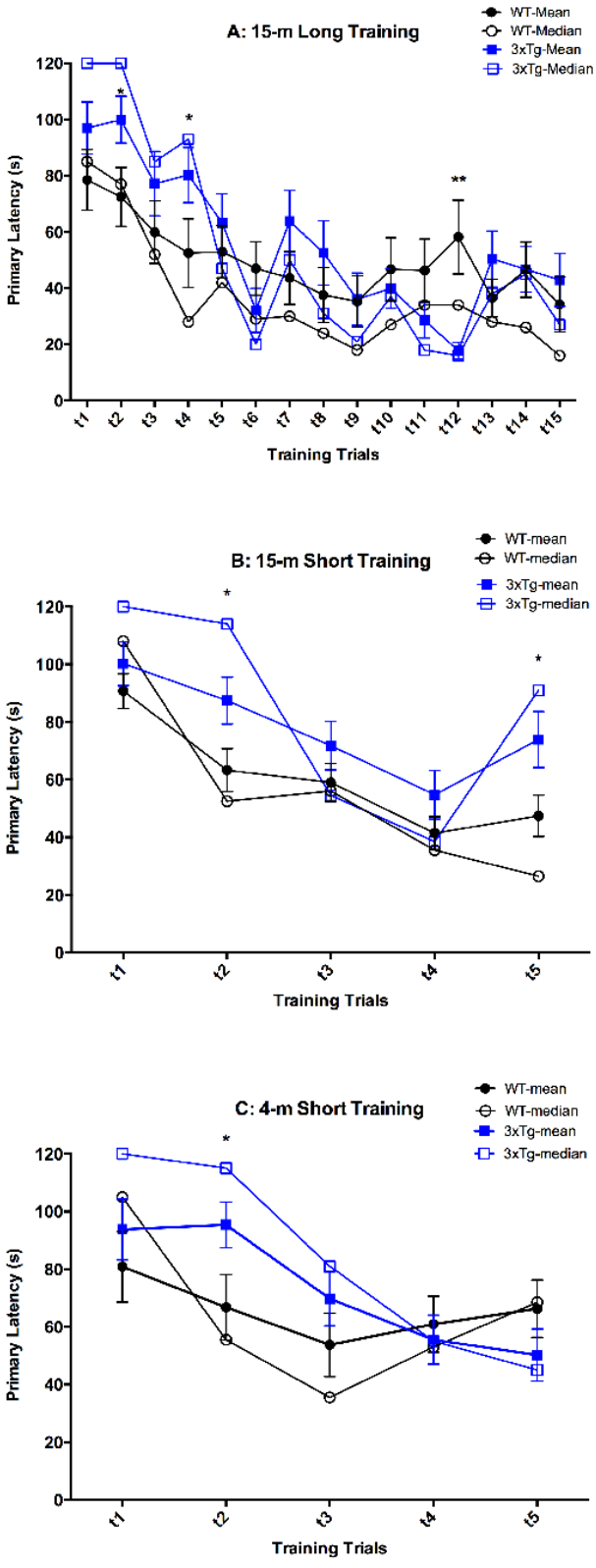

Figure 5.2: Primary latency of training trials shows group differences only in first 4 trials
A) Primary latency, out of 120 s, for 15-m old WT or 3×Tg mice receiving 15 training trials (WT n=32, 3×Tg n=24). Mean and median values given for comparison. Primary latency over 5 training trials for 15-m old (B; WT n=15, 3×Tg n=15) and 4-m old (C; WT n=14, 3×Tg n=17) mice. * $p < 0.05$, ** $p < 0.01$ compare mean values of WT and 3×Tg.

3×Tg mean and median curves shows very similar results. Notably, the median latency values for trial 1 and 2 are increased relative to the mean values. Comparison of the WT mean and median curves shows a general drop in latencies on trials 4 and later. Thus, the range of median trial latencies for WT and 3×Tg mice in trials 5–15 changes to 16–42 s and 16–50 s, respectively, supporting the conclusion that the WT mice learned as well as the 3×Tg mice did.

5.4.2 Probe day – Comparison of long versus short training in 15-m old mice

Initially, I used the long training paradigm to compare 15-m old WT and 3×Tg mice. Using this paradigm, the differences between the 3×Tg mice and the WT mice in the number of HS and time spent in the target quadrant, which measure the ability of the mice to remember the general location of the escape hole on probe day, were small (Figure 5.3). Though the 3×Tg mice showed significantly lower percent HS in the target quadrant compared to the WT mice (WT 65.4 ± 4.9%, 3×Tg 48.6 ± 5.9%; $p < 0.05$, Figure 5.3A), the time spent in the target quadrant was not significantly different between groups (described below, Figure 5.3B). Moreover, the % HS in the target quadrant for both groups was prominently above a chance level of 25% (Figure 5.3B) indicating that learning and long-term memory were intact, albeit less efficient in the 3×Tg group.

To test if the results reflected over-training of the mice, I shortened the number of training sessions from 15 to 5. Using this short-training paradigm, a more pronounced difference was observed in % HS in the target quadrant between the WT and 3×Tg mice (WT: 37.3 ± 3.5%, 3×Tg: 21.6 ± 2.0%; $p < 0.001$; Figure 5.3A). Importantly, 3×Tg mice

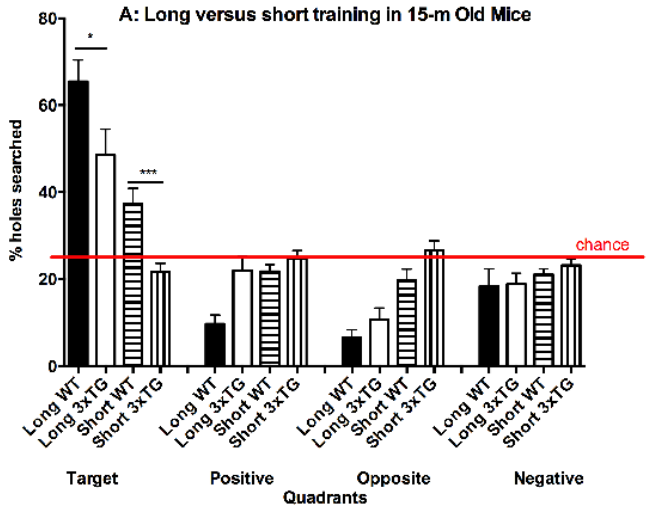

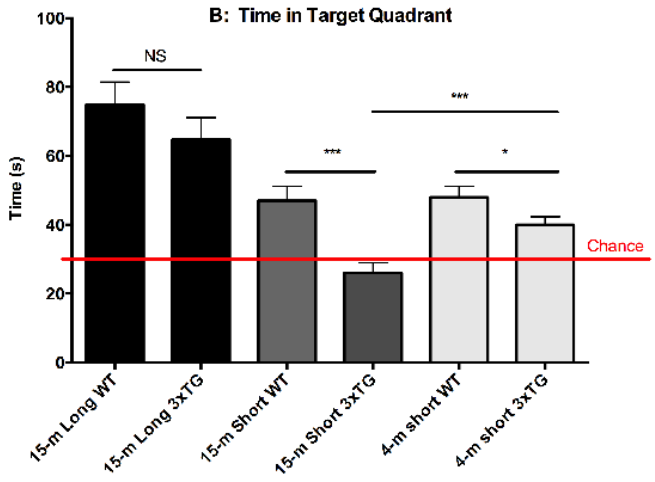

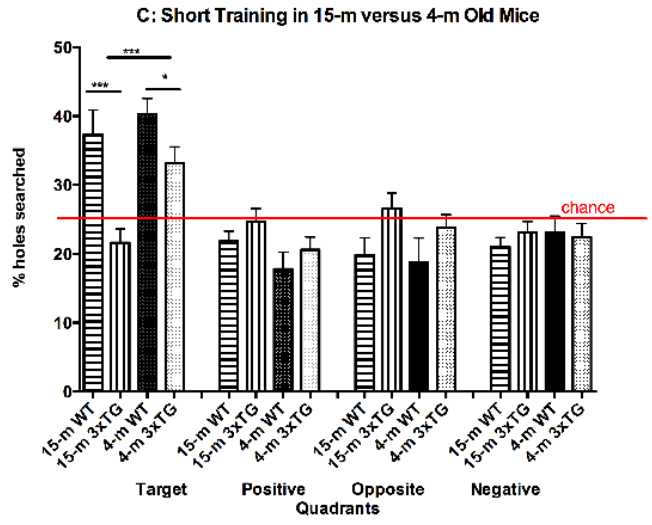

receiving short training did not search in any quadrant at levels higher than chance suggesting that they did not remember which quadrant contained the escape cage. The difference between the WT and 3×Tg in % HS on probe day indicated a deficit in memory retrieval rather than in learning for both the long and short training paradigms because all groups demonstrated learning, by a decrease in latency, of the target hole on training days (Figure 5.2).

Similar results were observed

Figure 5.3: Percent holes searched and time in target quadrant show short training can resolve cognitive deficits
A) Percent holes searched, on probe day, in each of four quadrants by 15-m old WT or 3×Tg mice receiving either short or long training. Chance level of holes searched in each quadrant is 25%. B) Time (s) spent in the Target quadrant by all 6 groups of mice. Chance amount of time spent per quadrant is 30 s out of 120 s. C) Percent holes searched in each of four quadrants by WT or 3×Tg and 15-m or 4-m old mice receiving short training. * $p < 0.05$, *** $p \leqq 0.001$ compare WT and 3×Tg.

using measures of time (Figure 5.3B) or % time (data not shown) spent in each quadrant on probe day. Long training of 15-m old mice resulted in similar values, which were significantly above chance (30 s) for both WT and 3×Tg mice. In contrast, short training resulted in highly significant differences between the WT and 3×Tg groups. The 3×Tg spent near chance levels of the time in each quadrant. Previous studies have shown that the 3×Tg mouse model presents not only with gender differences in brain pathology [33,34], but also in behavior [4,32]. Thus, I evaluated the effect of gender on the behavior of the different groups. I did not find significant differences in % HS in the target quadrant on probe day between males and females of either genotype with either training paradigm (data not shown).

5.4.3 Probe day – Comparison of young (4-m) versus old (15-m) mice in the short-training paradigm

Age is a highly important factor in studies related to AD. Not only is age a major determinant of phenotype and disease progression, but also in studies of animal models, the age of the animals has a substantial effect on the study cost. Following the development of an improved, short paradigm allowing observation of robust, significant differences between old (15-m of age) WT and 3×Tg mice, I asked whether such differences also could be observed in young mice. To answer the question, I trained and tested 4-m old WT and 3×Tg mice using the short-training paradigm.

Following short-training, both 4-m old WT and 3×Tg mice performed above chance levels in the % HS in the target quadrant on the probe day (Figure 5.3C). The % HS in the target quadrant by the 4-m old WT mice (40.2 ± 2.3%) was similar to that of

the 15-m old WT mice (37.3 ± 3.5%), suggesting that the age difference was not a significant determinant of memory retention in the WT group. In contrast, the 4-m old 3×Tg mice displayed 54% better ability to remember the target quadrant than their 15-m old counterparts (4-m 33.2 ± 2.4%, 15-m 21.6 ± 2.0%; $p < 0.001$), suggesting that in the presence of the transgenes, age was an important contributor to memory decline. Despite the improved memory of the young 3×Tg relative to the old 3×Tg mice, the difference between the 4-m old WT and 3×Tg groups still was statistically significant (WT 40.2 ± 2.3%, 3×Tg 33.2 ± 2.4%; $p < 0.05$; Figure 5.3C). Comparison of the time spent in the target quadrant between the WT mice at 15-m (47.0 ± 4.2 s) and 4-m (48.0 ± 3.2 s) showed similar values, whereas the 3×Tg mice show a larger difference of 35% with increasing age (15-m 26.0 ± 2.9 s vs 4-m 40.0 ± 2.4 s; $p = 0.001$). No effects of gender were found in the 4-m old WT or 3×Tg mice.

5.4.4 The 'Motivation' factor

The motivating stimuli for any behavioral task often are of great importance. Many studies use food or water deprivation, or survival instinct (in the case of the MWM), to instigate the mice to perform the task. Other tasks use natural tendencies such as object- or environment-exploration and thus do not add stress on the animals, with the cost of a decrease in the task-instituted motivation. One potential weakness of the Barnes maze test may be the relatively mild aversive stimuli used to motivate the mice to find the escape cage.

Our data suggest that the total number of HS on probe day, regardless of quadrant, may be an indication of motivation. Fifteen-m old mice receiving long training,

regardless of genotype, and 4-m old WT mice receiving short training, searched on average in 16–17 holes with a similar range — 1–37 holes and 8–35 holes for 15-m WT and 3×Tg, respectively, and 5–36 holes for 4-m WT mice. Interestingly, 15-m old mice receiving short training, regardless of genotype, and 4-m old 3×Tg mice receiving short training searched on average in 22–23 holes. The range of hole searched was substantially higher for these groups — 2–58 holes and 0–51 holes for 15-m old WT and 3×Tg, respectively and 8–48 holes for 4-m 3×Tg mice. One interpretation of these results is that the long training, and thus more experience with the task where no major threats are felt, in the 15-m old mice and the WT genotype in the 4-m old mice confers a feeling that the mouse is safe and decreases the anxiety and motivation to search for escape on the probe day.

Motivation also can be measured by the number of mice who needed to be guided to the escape hole during training days because they did not enter the escape hole on their own in the allowed time (Figure 5.4). Notably, this does not suggest that the mice did not identify the escape hole on training days, only that they did not go into the escape hole. Typically, the measure of primary HS, rather than total holes searched before entering the hole, can be used to overcome the effect of low motivation to enter the escape cage on evaluation of learning. Fifteen-m-old mice receiving long training needed to be guided to the escape hole at the end of their allotted time on average for the first five trials 56% and 83% of the time for WT and 3×Tg, respectively. This value decreases to 51% and 73% for trials 6–10 and to 29% and 60% for trials 11–15 for the WT and 3×Tg mice, respectively. Fifteen-m-old mice receiving short training needed guidance to the escape hole on average for the total five trials 64% and 91% for WT and 3×Tg, respectively, and

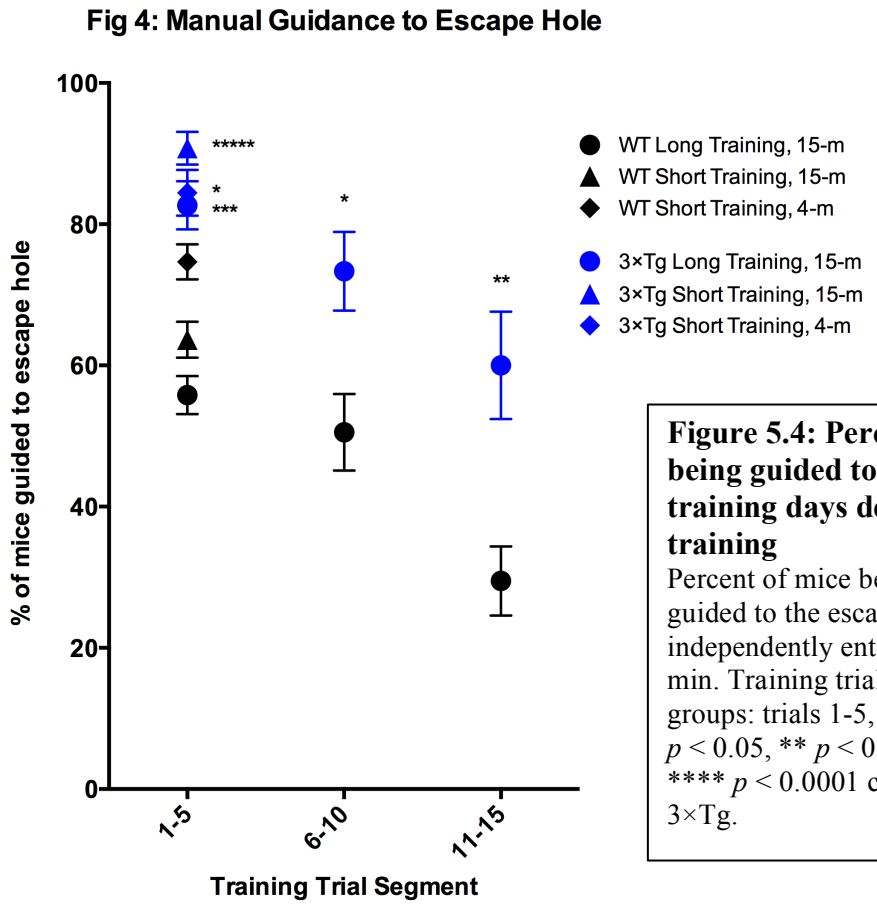

Figure 5.4: Percent of mice being guided to escape hole on training days decreased with training
Percent of mice being manually guided to the escape hole that did not independently enter in the allotted 2 min. Training trials divided into 3 groups: trials 1-5, 6-10, and 11-15. * $p < 0.05$, ** $p < 0.01$, *** $p < 0.001$, **** $p < 0.0001$ compare WT and 3×Tg.

4-m old mice receiving short training needed guidance 75% and 84% of the time for WT and 3×Tg, respectively. Three conclusions can be gleaned from these data. First, 3×Tg mice enter the escape cage on their own less often than WT mice, potentially indicating hypoactivity akin to AD-like apathy, as reported by Filali et. al. [35]. However, our analysis of total HS does not show a difference between 15-m old WT and 3×Tg mice when compared between similar training lengths. The difference seen between the 4-m old WT and 3×Tg also is not statistically significant. Second, the percentage of mice that entered the escape cage voluntarily increased with added training trials, indicating increased motivation to enter the escape cage. Lastly, age did not affect motivation to enter the escape cage in the 3×Tg mouse model. Thus, motivation in the

Barnes maze task potentially can be separated from changes in cognitive function. Though these results regarding manual guidance of mice do not directly affect measures of learning, as the end-point is hole identification and not entering hole, analysis of percent of mice guided to the escape hole suggests that motivation to enter the escape cage is low in early trials, especially for 3×Tg mice.

5.5 Discussion

5.5.1 Data from probe day is superior to data from training days

Our study illuminates the higher value of probe-day measures over training-day measures by demonstrating a correlation between performance and age, amount of training, and presence of transgenes. Inspection of HS or time spent in the target quadrant (Figure 5.3) shows the effects of extra training sessions on memory retrieval, the changes in cognition as a result of aging or the presence of transgenes, and several combinations thereof. These results are robust and are detectable following analysis of one 2-min trial per animal rather than the substantially longer and labor-intensive training-day analyses of 5 or 15 trials per animal. The decrease in data processing allows for a more accurate manual analysis, compared to tracking-software analysis, which is prone to recognition biases, such as different or sufficient body parts present in the target zone for a sufficient amount of time [36].

Comparisons of Figure 5.2 panels A–C show that 3×Tg mice started with 120 s median latency in the first two trials, whereas WT mice started with 85–110 s median latency in the first trial and often improved by the second trial. All groups of mice showed shorter latencies over the next few trials and converged at either trial 4 or 5. The

reduction in escape latency during the training trials is similar to learning curves in the hidden-platform MWM test. However, similar decreases in escape latencies have been observed in visible-platform MWM trials and cued Barnes maze studies [13,36]. When the mice can see the platform, a decrease in latency likely is not due to spatial learning, but rather due to habituation to the environment eventuating in decreased anxiety and increased motivation to escape over repeated trials [36]. This theory is supported by our observation of a decrease in the number of HS on probe day with long training and the decrease in the need for manual guidance of mice to the escape hole during the last 10 training trials in the long-training paradigm (Figure 5.4). A putative high level of anxiety at the start of the study seems to be especially prominent in the 3×Tg mice, which, compared to the WT mice, always started at a higher latency on trial 1. In addition, the 3×Tg mice showed significantly larger latencies on training-trial 2, compared to WT mice, regardless of age or training length (Figure 5.2).

Increased anxiety in this model has been identified previously [37,38]. Possibly, the consistent significant difference on trial 2 between the 3×Tg and WT mice suggests that the 3×Tg mice not only have higher anxiety levels, but also take longer to habituate to their environment. Our protocol consisted of a 30 s habituation phase and guidance to the escape hole to "show" the mice that escape existed. This habituation could be extended to potentially mitigate some of the initial anxiety due to the novel environment. Possibly, if both 3×Tg and WT mice had an extended habituation time, both groups might start at a lower initial latency and might still be different from each other or the extended habituation could serve to close the starting gap between the 3×Tg and WT groups. I theorize that a combination of both scenarios may be the most likely because of

the elimination of observable cognitive deficits found with overtraining, as discussed in the next section. As the longer training closed the gap in performance between the WT and 3×Tg mice and did not just increase both groups' time in the target quadrant (Figure 5.3B), it is probable that additional habituation would both decrease initial latency values for both groups and close the gap between them.

Significant differences in latency between WT and 3×Tg mice also were observed following the convergence, on trial 5 in the 15-m short training group (Figure 5.2B) and on trial 12 in the 15-m long training group (Figure 5.2A). However, considering the global trends of the data, specifically, the variability of the individual trial mean values and values for trials 10, 11, 13, and 14 in Fig. 2A, the high significance found on trial 12 appears to be a mere coincidence.

5.5.2 Observing cognitive deficits depends on the difficulty of the task

Comparison of the long- and short-training paradigms (Figure 5.3B) reveals that the number of training sessions affects directly the time spent in the target quadrant on the probe day, which indicates the ability of the mice to remember the location of the target hole. Importantly, our study shows that overtraining makes the probe day task too easy and results in elimination of observable cognitive deficits between WT and 3×Tg mice. Strong evidence for the high impact of overtraining is the fact that 4-m-old WT mice who received short training had less % HS in the target quadrant (40%, Figure 5.3C) than old 3×Tg who received long training (49%, Figure 5.3A), indicating that with sufficient training, the memory impairment caused by age and presence of the three dementia-causing transgenes can be overcome. Similar results are seen with time spent in

the target quadrant measure (Figure 5.3B). An additional difference between our Barnes maze protocol and typical published protocols that may increase the difficulty of the task is that I allowed for a 48 h delay between the training trials and the probe day. This assumes that the amount of delay is related to the difficulty of the task by requiring more neural processing for consolidated learning and long-term memory.

Ideally, the number of training trials and delay time would be calibrated to result in a difficulty level that leads animals with expected memory deficits to spend only chance levels of time or of % HS in the target quadrant as was achieved in the 15-m 3×Tg group receiving short training (Figure 5.3A, C). Chance-level behavior can be a useful additional indication of the difference between groups and can help reduce the probability that a particular measure, e.g., % HS in the target quadrant would show a difference whereas another measure, e.g., time in target quadrant, would not show a difference between the 3×Tg and WT groups, as was the case for the 15-m old mice receiving long training. The possibility to carefully adjust the number of training trials and delay time and thus the difficulty of the task is an advantage of the Barnes maze and other learning tasks relative to tasks that solely rely on exploratory behavior.

To our knowledge, this is the first study other than those by LaFerla's group, to show cognitive deficits in the 3×Tg mouse model at 4-m of age. Presumably, this was achieved thanks to our optimization of the Barnes-maze training paradigm. Frazer et al. who showed deficits in the 3×Tg mice at 11-m of age, but not at 2-m or 6-m of age, using the Barnes maze used 3 training trials for 1 day at 2-m, 6-m, and 11-m [5]. They reported measures of distance, errors, and latency averaged over the 3 trials during the training day yet did not perform a probe trial. A trend in the data of Frazer et al. suggested that latency

was higher at 6-m than at 2-m. However, high variability, possibly due to a relatively small number of animals (n=6) per group, might have prevented reaching statistical significance in that study. It is possible that Frazer et al. did not detect deficits at a younger age because they only tested learning, not long-term memory, and the 3×Tg mice show learning over the training trials in most studies. In addition, the values over the 3 trials were averaged together, which can mask an initial deficit. LaFerla and colleagues [2], who showed deficits in the 3×Tg mice at 4-m of age used 4 training trials per day for 4 days. They performed a long-term memory trial at 24-h and 7-d after the fourth day of training. However, the escape cage was present during these retention trials. Their study reported higher latency values for 3×Tg mice compared to WT mice on training days starting at 2-m of age. In addition, they found significantly longer escape latency at the 24-h memory retention test but not at the 7-d retention test in the 2-m old 3×Tg mice. The average number of HS in the target quadrant was not significantly different between 3×Tg and WT mice at 2-m of age. Thus, not all measures showed deficits at 2-m of age. The differences between 3×Tg and WT mice, by measures of training trial escape latency, 24-h and 7-d retention trial escape latencies, and HS in the target quadrant became significantly different at 4-m of age. Our data suggest that Clinton et al. might have been able to detect consistent significant differences between the 3×Tg and WT groups at 2-m if less training had been used.

5.5.3 More versatile models are necessary to break the cycle of failed drugs

The ability to identify cognitive deficits and to evaluate therapeutic means for rescuing or preventing these deficits is a fundamental tool needed for therapy

development in the AD field. Having this ability in young mice has several advantages. First, little time needs to be spent aging mice leading to cost reduction and allowing for a shorter experiment-planning time resulting in more possible leads being tested. Second, being able to test the cognition of animal models of AD before amyloid plaque deposition in the brain allows testing prevention, which likely will be more advantageous than treatment approaches as actual therapy for AD. For example, Das et al. treated Tg2576 mice, a mouse model of AD, with a γ-secretase inhibitor from 4−7-m of age, prior to the onset of the exponential increase in Aβ deposition. A much larger decrease in Aβ levels (60%) was observed in this group compared to treatment from 7−10-m (34%) or 12−15-m (no effect) of age. Importantly, in all cases, the mice were sacrificed and their brains analyzed when they reached age 15-m [39]. Clinical trials of Aβ lowering drugs, such as γ-secretase inhibitors or immunotherapeutics, in symptomatic patients have been unsuccessful, prompting concerns that such strategies may be of limited efficacy when used in symptomatic patients with AD compared to prevention at pre-symptomatic stages [40]. On the other hand, prophylactic administration of drugs without a good screening procedure for AD, which begins 10–20 years before the onset of symptoms [41,42], may be cost-prohibitive. A reasonable compromise is a hypothetical treatment paradigm, in which people may be treated preventatively, for example, for several months every 5 years beginning at age 40. If human data were to echo the findings by Das et al. [39], such a strategy could result in a delay of pathology progression and potentially the onset of disease by years. I recognize that transgenic mouse models are not perfect proxies for human disease, as they lack neurodegeneration and timing of appearance of biological and functional pathology cannot always be directly translated. Though human AD

patients present with lots of brain Aβ pathology prior to cognitive deficits, opposite to the mouse models, detecting cognitive deficits at the earliest age in mice can be thought of as dysfunction in neurotransmission and translated to the initial appearance of human cognitive deficits as Aβ pathology load is not correlated with cognitive deficits. Treatments that can prevent the loss of functional synapses during prodromal or early stages of the disease may complement the brain's innate compensatory defense mechanisms and significantly forestall additional AD-related cognitive symptoms and models of early disease are required for this approach. Thus, these models are essential for identification of leads and detection of early memory deficits offers the benefits of testing multiple leads with time and cost savings, as discussed above.

Several studies have examined shortened training paradigms in the MWM [36,43]. In contrast, to our knowledge, this is the first systematic analysis of the effect of the number of training trials, and comparison of training versus probe days, on the sensitivity of the Barnes maze to detect cognitive deficits, and its validation in young transgenic AD mice. Our study provides compelling evidence for using a short-training paradigm and for inclusion of a probe trial that can produce robust distinctions between 3×Tg and WT mice. These factors and the validation of cognitive deficits in 4-m old 3×Tg provide the framework for analysis of CLR01's influence on the memory component of AD in the 3×Tg model and thus bring us one step closer to finding a disease-modifying therapy for AD.

5.6 References

1. Barnes CA (1979) Memory deficits associated with senescence: a neurophysiological and behavioral study in the rat. J Comp Physiol Psychol 93: 74-104.

2. Clinton LK, Blurton-Jones M, Myczek K, Trojanowski JQ, LaFerla FM (2010) Synergistic Interactions between Aβ, tau, and α-synuclein: acceleration of neuropathology and cognitive decline. Journal of Neuroscience 30: 7281-7289.

3. O'Leary TP, Brown RE (2009) Visuo-spatial learning and memory deficits on the Barnes maze in the 16-month-old APPswe/PS1dE9 mouse model of Alzheimer's disease. Behavioural Brain Research 201: 120-127.

4. Clinton LK, Billings LM, Green KN, Caccamo A, Ngo J, et al. (2007) Age-dependent sexual dimorphism in cognition and stress response in the 3xTg-AD mice. Neurobiology of Disease 28: 76-82.

5. Frazer ME, Hughes JE, Mastrangelo MA, Tibbens JL, Federoff HJ, et al. (2008) Reduced pathology and improved behavioral performance in Alzheimer's disease mice vaccinated with HSV amplicons expressing amyloid-β and interleukin-4. Molecular Therapy: the Journal of the American Society of Gene Therapy 16: 845-853.

6. Banaceur S, Banasr S, Sakly M, Abdelmelek H (2013) Whole body exposure to 2.4 GHz WIFI signals: effects on cognitive impairment in adult triple transgenic mouse models of Alzheimer's disease (3xTg-AD). Behavioural Brain Research 240: 197-201.

7. Davis KE, Easton A, Eacott MJ, Gigg J (2013) Episodic-like memory for what-where-which occasion is selectively impaired in the 3xTgAD mouse model of Alzheimer's disease. Journal of Alzheimer's disease : JAD 33: 681-698.

8. Oddo S, Caccamo A, Shepherd JD, Murphy MP, Golde TE, et al. (2003) Triple-transgenic model of Alzheimer's disease with plaques and tangles: intracellular Aβ and synaptic dysfunction. Neuron 39: 409-421.

9. Peng Y, Sun J, Hon S, Nylander AN, Xia W, et al. (2010) L-3-n-butylphthalide improves cognitive impairment and reduces amyloid-β in a transgenic model of Alzheimer's disease. Journal of Neuroscience 30: 8180-8189.

10. Guzman-Ramos K, Moreno-Castilla P, Castro-Cruz M, McGaugh JL, Martinez-Coria H, et al. (2012) Restoration of dopamine release deficits during object recognition memory acquisition attenuates cognitive impairment in a triple transgenic mice model of Alzheimer's disease. Learning & memory 19: 453-460.

11. Medina DX, Caccamo A, Oddo S (2011) Methylene blue reduces Aβ levels and rescues early cognitive deficit by increasing proteasome activity. Brain Pathology 21: 140-149.

12. Morris R (1984) Developments of a water-maze procedure for studying spatial learning in the rat. Journal of Neuroscience Methods 11: 47-60.

13. Pompl PN, Mullan MJ, Bjugstad K, Arendash GW (1999) Adaptation of the circular platform spatial memory task for mice: use in detecting cognitive impairment in the APP(SW) transgenic mouse model for Alzheimer's disease. Journal of Neuroscience Methods 87: 87-95.

14. Ingram DK, Spangler EL, Iijima S, Ikari H, Kuo H, et al. (1994) Rodent models of memory dysfunction in Alzheimer's disease and normal aging: moving beyond the cholinergic hypothesis. Life Sciences 55: 2037-2049.

15. Moscovitch M, Rosenbaum RS, Gilboa A, Addis DR, Westmacott R, et al. (2005) Functional neuroanatomy of remote episodic, semantic and spatial memory: a unified account based on multiple trace theory. Journal of Anatomy 207: 35-66.

16. Sunyer B, Patil S, Höger H, Lubec G (2007) Barnes maze, a useful task to assess spatial reference memory in the mice. Nature protocols 390.

17. Schulz D, Huston JP, Buddenberg T, Topic B (2007) "Despair" induced by extinction trials in the water maze: relationship with measures of anxiety in aged and adult rats. Neurobiology of Learning and Memory 87: 309-323.

18. Holscher C (1999) Stress impairs performance in spatial water maze learning tasks. Behavioural Brain Research 100: 225-235.

19. Sun MK, Alkon DL (2004) Induced depressive behavior impairs learning and memory in rats. Neuroscience 129: 129-139.

20. Rodriguez GA, Burns MP, Weeber EJ, Rebeck GW (2013) Young APOE4 targeted replacement mice exhibit poor spatial learning and memory, with reduced dendritic spine density in the medial entorhinal cortex. Learning & Memory 20: 256-266.

21. Larson ME, Sherman MA, Greimel S, Kuskowski M, Schneider JA, et al. (2012) Soluble α-synuclein is a novel modulator of Alzheimer's disease pathophysiology. Journal of Neuroscience 32: 10253-10266.

22. Walker JM, Fowler SW, Miller DK, Sun AY, Weisman GA, et al. (2011) Spatial learning and memory impairment and increased locomotion in a transgenic amyloid precursor protein mouse model of Alzheimer's disease. Behavioural Brain Research 222: 169-175.

23. Ambree O, Richter H, Sachser N, Lewejohann L, Dere E, et al. (2009) Levodopa ameliorates learning and memory deficits in a murine model of Alzheimer's disease. Neurobiology of Aging 30: 1192-1204.

24. Rojanathammanee L, Puig KL, Combs CK (2013) Pomegranate polyphenols and extract inhibit nuclear factor of activated T-cell activity and microglial activation in vitro and in a transgenic mouse model of Alzheimer disease. The Journal of Nutrition 143: 597-605.

25. Oddo S, Caccamo A, Kitazawa M, Tseng BP, LaFerla FM (2003) Amyloid deposition precedes tangle formation in a triple transgenic model of Alzheimer's disease. Neurobiology of Aging 24: 1063-1070.

26. Oddo S, Caccamo A, Tran L, Lambert MP, Glabe CG, et al. (2006) Temporal profile of amyloid-β (Aβ) oligomerization in an in vivo model of Alzheimer disease. A link between Aβ and tau pathology. Journal of Biological Chemistry 281: 1599-1604.

27. Billings LM, Oddo S, Green KN, McGaugh JL, LaFerla FM (2005) Intraneuronal Aβ causes the onset of early Alzheimer's disease-related cognitive deficits in transgenic mice. Neuron 45: 675-688.

28. Oddo S, Caccamo A, Smith IF, Green KN, LaFerla FM (2006) A dynamic relationship between intracellular and extracellular pools of Aβ. Am J Pathol 168: 184-194.

29. Blurton-Jones M, Kitazawa M, Martinez-Coria H, Castello NA, Muller FJ, et al. (2009) Neural stem cells improve cognition via BDNF in a transgenic model of Alzheimer disease. Proc Natl Acad Sci USA 106: 13594-13599.

30. McKee AC, Carreras I, Hossain L, Ryu H, Klein WL, et al. (2008) Ibuprofen reduces Aβ, hyperphosphorylated tau and memory deficits in Alzheimer mice. Brain Research 1207: 225-236.

31. Chen Y, Liang Z, Blanchard J, Dai CL, Sun S, et al. (2013) A non-transgenic mouse model (icv-STZ mouse) of Alzheimer's disease: similarities to and differences from the transgenic model (3xTg-AD mouse). Molecular Neurobiology 47: 711-725.

32. Torres-Lista V, Gimenez-Llort L (2013) Impairment of nesting behaviour in 3xTg-AD mice. Behavioural Brain Research 247: 153-157.

33. Attar A, Ripoli C, Riccardi E, Maiti P, Li Puma DD, et al. (2012) Protection of primary neurons and mouse brain from Alzheimer's pathology by molecular tweezers. Brain 135: 3735-3748.

34. Hirata-Fukae C, Li HF, Hoe HS, Gray AJ, Minami SS, et al. (2008) Females exhibit more extensive amyloid, but not tau, pathology in an Alzheimer transgenic model. Brain Research 1216: 92-103.

35. Filali M, Lalonde R, Theriault P, Julien C, Calon F, et al. (2012) Cognitive and non-cognitive behaviors in the triple transgenic mouse model of Alzheimer's disease expressing mutated APP, PS1, and Mapt (3xTg-AD). Behavioural Brain Research 234: 334-342.

36. Gulinello M, Gertner M, Mendoza G, Schoenfeld BP, Oddo S, et al. (2009) Validation of a 2-day water maze protocol in mice. Behavioural Brain Research 196: 220-227.

37. Sterniczuk R, Antle MC, Laferla FM, Dyck RH (2010) Characterization of the 3xTg-AD mouse model of Alzheimer's disease: part 2. Behavioral and cognitive changes. Brain Research 1348: 149-155.

38. Hebda-Bauer EK, Simmons TA, Sugg A, Ural E, Stewart JA, et al. (2013) 3xTg-AD mice exhibit an activated central stress axis during early-stage pathology. Journal of Alzheimer's disease : JAD 33: 407-422.

39. Das P, Verbeeck C, Minter L, Chakrabarty P, Felsenstein K, et al. (2012) Transient pharmacologic lowering of Aβ production prior to deposition results in sustained reduction of amyloid plaque pathology. Molecular Neurodegeneration 7: 39.

40. Golde TE, Borchelt DR, Giasson BI, Lewis J (2013) Thinking laterally about neurodegenerative proteinopathies. Journal of Clinical Investigation 123: 1847-1855.

41. Reiman EM, Quiroz YT, Fleisher AS, Chen K, Velez-Pardo C, et al. (2012) Brain imaging and fluid biomarker analysis in young adults at genetic risk for autosomal dominant Alzheimer's disease in the presenilin 1 E280A kindred: a case-control study. Lancet Neurology 11: 1048-1056.

42. Fleisher AS, Chen K, Quiroz YT, Jakimovich LJ, Gomez MG, et al. (2012) Florβpir PET analysis of amyloid-β deposition in the presenilin 1 E280A autosomal dominant Alzheimer's disease kindred: a cross-sectional study. Lancet Neurology 11: 1057-1065.

43. Kraemer PJ, Brown RW, Baldwin SA, Scheff SW (1996) Validation of a single-day Morris Water Maze procedure used to assess cognitive deficits associated with brain damage. Brain Research Bulletin 39: 17-22.

Chapter 6

Conclusions

The studies in this dissertation used a mouse model of Alzheimer's disease (AD) to investigate whether an *in vitro*-validated protein-aggregation inhibitor, CLR01, which acts by a novel and unique mechanism also could exert its beneficial effects in complex *in vivo* environments without consequential toxicity. The findings suggest that indeed, the innovative approach of using molecular tweezers as protein assembly modulators is viable and promising for development of therapy for AD and other amyloidoses.

With the exception of one drug that has not been approved in the US (tafamidis for familial amyloidotic polyneuropathy) currently, there are no disease-modifying therapies for amyloidoses. As AD is estimated to affect over 5 million people in the US and expected to cost the American healthcare system over $200 billion in 2013 alone, disease characterization and new therapeutics are urgent, unmet public health needs. A promising strategy for prevention and/or treatment of amyloidoses is inhibition or modulation of the aggregation process to reduce the level of toxic protein assemblies. However, achieving this goal has been highly challenging due to the nature of the toxic oligomers, which have unfavorable structural characteristics for disruption by small molecules. Prior to the initiation of the studies in this dissertation, our group identified and evaluated *in vitro* a small molecule, designed as an artificial K receptor, for its aggregation-inhibition potential with encouraging results. CLR01, the current lead molecular tweezer, was characterized *in vitro* and found to be a process-specific, rather

than protein-specific, assembly and toxicity inhibitor that remodeled oligomers into non-toxic structures and dissociated pre-formed fibrils.

The studies in this dissertation extended the *in vitro* findings by evaluating their significance *in vivo*. First, treatment of a triple-transgenic mouse model of AD with microgram-per-day doses of CLR01 for one month demonstrated that CLR01 reduced the brain levels of the two pathological hallmarks of AD, amyloid plaques and neurofibrillary tangles, and decreased levels of microglia found in transgenic but not wild-type mouse brains. This finding is vital as a proof-of-concept and supports future study of CLR01 as an AD therapeutic lead. Second, the blood-brain barrier penetration of a single dose of CLR01 was established to be ~1−3% of blood levels in multiple combinations of different ages and transgenic profiles of mice. The absolute brain CLR01 level was found to be persistent over 72 h and was increased by additional doses or higher administered concentration. Third, toxicity studies established that the unique K-binding mechanism of CLR01 was not itself toxic at >250-fold the therapeutic dose. Because of the unique mechanism by which CLR01 and other molecular tweezers work, toxicity resulting from binding to off-target proteins was a great concern. Studies conducted in the context of this thesis have screened for and not detected any overt toxicity and thus provide the basis for more fine-tuned toxicity experiments. Studies of toxicity not only are fundamental for development of CLR01 as a treatment for AD, but also for several other protein-aggregation diseases where CLR01 currently is being explored as a therapy. Finally, the Barnes maze test of learning and memory deficits in mice was optimized for time, cost, and sensitivity. This optimization allowed for illumination of deficits in the

triple-transgenic mouse model of AD at 4-months of age, which had not previously been successful by groups external to the one that developed the model.

These studies provide the framework for better understanding AD therapeutics *in vivo*, and specifically lay the groundwork for development of CLR01 and molecular tweezers as therapeutic drugs for multiple diseases. Obviously, additional questions must be answered for successfully exploiting the therapeutic potential of molecular tweezers. Of high importance for AD would be the study of CLR01's effects on the memory deficits found in animal models because reduction in brain pathology does not necessarily reveal functional effects. This future study could readily combine the CLR01 efficacy study and the optimized Barnes maze method discussed here in both young mice, to assess prevention, and in old mice to assess therapy. Another area of future study will be further exploration of the pharmacokinetics of CLR01. Specifically, the fate of CLR01 in the brain should be explored to address concerns of potentially unwanted tissue accumulation, in addition to CLR01's metabolism and excretion. These studies will require optimization of methods for extraction of CLR01 from tissues and liquid chromatography-mass spectrometry for improved detection sensitivity.

The ambition of this PhD project was to advance the development of a cure for AD. The findings obtained in the project as a whole, advance the development of CLR01 for therapy of AD in particular and amyloidoses in general by providing proof-of-concept of the compound's *in vivo* efficacy in a mammalian model of disease and by providing a framework for the initiation of the next phase − clinical trials. It has been a privilege and an honor to play a role in this endeavor.